Self-consistent-field theory for chain molecules: extensions, computational aspects, and applications

Promotor: prof. dr. G. J. Fleer,
persoonlijk hoogleraar bij het laboratorium voor
Fysische Chemie en Kolloïdkunde

Co-promotor: dr. ir. F. A. M. Leermakers,
universitair hoofddocent bij de leerstoelgroep
Fysische Chemie en Kolloïdkunde

Promotiecommissie: prof. dr. A. M. Skvortsov, Chemical-Pharmaceutical
Academy, St. Petersburg

prof. dr. G. ten Brinke, Rijksuniversiteit Groningen

dr. E. M. Blokhuis, Universiteit Leiden

prof. dr. E. van der Linden, Wageningen Universiteit

Self-consistent-field theory for chain molecules: extensions, computational aspects, and applications

J. van Male

Proefschrift
ter verkrijging van de graad van doctor
op gezag van de rector magnificus
van Wageningen Universiteit,
prof. dr. ir. L. Speelman
in het openbaar te verdedigen
op vrijdag 14 maart 2003
des namiddags te vier uur in de Aula.

ISBN 90 5808 779 4

Contents

Stellingen

1. Adsorptie van polymeren op de kopgroepen van een zelf-associerend membraan maakt dit membraan stijver als de kopgroepen groot zijn en minder stijf als de kopgroepen klein zijn.

   —Dit proefschrift, hoofdstuk 4.

2. Bij het toepassen van de numerieke zelf-consistente veld theorie is het zaak om niet in hokjes te denken.

   —Dit proefschrift, appendix B.

3. In tegenstelling tot wat Currie et al. beweren is het wel mogelijk om een uitdrukking voor de oppervlaktedruk van verankerde ketens te geven binnen de self-consistente veldtheorie.

   —Macromolecules **32**, 487 – 498, 1999, Dit proefschrift, hoofdstuk 2.

4. De numerieke zelf-consistente veldtheorie is een waardevol gereedschap om de haalbaarheid van een analytische theorie te voorspellen, danwel om de correctheid hiervan aan te tonen.

5. Het feit dat veel barpersoneel in uitgaansgeledenheden gehoorbescherming draagt is geen geruststelling voor het publiek.

6. De Euro is te snel ingevoerd.

7. Iedere democratie kent slachtoffers van de dictatuur van de meerderheid.

8. De meest gehoorde zin in de trein is: "ik zit in de trein".

Stellingen behorende bij het proefschrift
'Self-consistent-field theory for chain molecules:
extensions, computational aspects, and applications',
J. van Male, Wageningen, 14 maart 2003.

1 Introduction

1.1 Thermodynamics

Molecules consist of atoms, the basic building blocks from the well-known periodic table of elements. Atoms may be linked to each other, forming molecules. The number of ways in which atoms may form molecules is almost limitless. All matter consists of molecules. Water, plastic, air, paint, peanut butter but also living beings are (as far as we know) merely a collection of molecules.

Until the beginning of the 20th century, however, the existence of molecules and atoms as basic building blocks for all matter was still heavily debated. Great scientists like Carnot, Joule, Kelvin, and Clausius laid the foundations of a branch of physics which is known as *thermodynamics*, without the assumption that atoms exist as separate particles. Thermodynamics therefore gives relations between macroscopic quantities like energy, heat, temperature, and work.

The first law of thermodynamics may be formulated simply as [1]

> **1th Law**: Energy is always conserved.

This definition may look simple, since energy is a term which is commonly used nowadays. However, it proves to be a difficult task to give a precise definition of the term energy. For a discussion about the issues involved see ref. [2].

A thermodynamical quantity that is not commonly used outside the scientific community is called *entropy*. The second law of thermodynamics may be formulated as [1]

> **2nd law**: Spontaneous processes increase the entropy of the universe.

Where the first law may look understandable at first sight, in contrast this second law seems a complete mystery. Although the term 'entropy' has not gained any popularity in everyday speech, it turns out to be easier to define than notions like 'energy' or 'temperature'.

A less precise rephrase of the second law is that anything that happens spontaneously increases the total chaos of the universe. The second law states that this order may be formed locally (e.g. a human being or a bike) but that this necessarily means that even more disorder has been created at the same time in the remainder of the universe. Boltzmann discovered the equation that enables us, in principle, to count this disorder. It was Boltzmann who quantified the term 'entropy' in the second half of the 19th century in terms of molecules. Before that time, the second law of thermodynamics was merely an observation, like the first law. His equation is[1]

$$S = k \log W \tag{1.1}$$

The symbol S denotes entropy, k is the Boltzmann constant, and W is a measure for the chaos of the system at hand. A more scientific term for W is the 'degeneracy' of the system. To be even more precise: W is the number of realisations for a given system when we fix the volume, the number of molecules, and the energy of the system [3].

In order to be able to count the number of realisations W we need to introduce the concept of molecules. One can envision that it is possible to 'count' the number of ways we can place, say, 5 identical molecules in a container. Eq. 1.1 therefore gives a relation between the macroscopic description of the world as given by thermodynamics and the microscopic world of molecules.

As stated in the first law of thermodynamics, the total energy of the universe is conserved. Mostly, however, we are not interested in the universe as a whole but only a small sub-system. This sub-system may exchange energy or molecules with its environment or it may not have a constant volume. Then it doesn't suffice to apply eq. 1.1 directly. Instead of a constant energy, volume, and number of molecules, the system under study may have a constant pressure and temperature, which is far more common. Theoretical methods to deal with these more common constraints have been developed systematically by Gibbs.

We will use these methods to derive equations that describe the equilibrium behaviour of different types of polymers in solution and near interfaces. Due to the complexity of the systems under study we will introduce several approximations and solve the resulting equations numerically.

1.2 Polymers in solution and near interfaces

The most simple type of polymer is a homopolymer: a linear string of interconnected equal monomers. Usually, this string is flexible and will form a coil in solution when the interaction with the solvent is not too unfavourable. Upon increasing the concentration of polymer, the coils will start to interpenetrate, the solution is then called semi-dilute. A further increase of polymer concentration leads to a concentrated solution or even a pure polymer phase: a melt. When the interaction of the homopolymer with the solvent is made more unfavourable, for example by changing the temperature, the polymers will phase separate. The result will be a dense polymer phase coexisting with a solvent phase.

The polymers do not have to be homopolymers. More complex chain architectures exist. Examples are block copolymers, where two or more blocks of identical segments are covalently linked into one chain. Block copolymers generally exhibit more complex behaviour than homopolymers. When one block is soluble and the

---

[1] This is the formula as it appears on Boltzmann's tombstone. In the main text of this thesis we will replace W by Ω and 'log' by 'ln'.

other block hardly so, they may form self-assembling aggregates in solution. The insoluble blocks will lump together in an aggregate that may be, for example, spherical or cylindrical. The soluble blocks will protrude into the solution, shielding the unfavourable interactions of the insoluble blocks with the solution. Different types of such aggregates exist.

This thesis deals with polymers in the liquid phase and near interfaces. This interface may be either a solid wall or a more diffuse one resulting from phase separation or self-assembling of molecules, as described above. The polymers will adsorb onto these interfaces when the interaction between the polymer and the interface is favourable. It is of interest to be able to predict to what extent this adsorption takes place and how the properties of the interfaces are altered when the polymers adsorb onto them.

1.3 Overview of theoretical approaches

Theoretical investigation of polymers can be done in a number of different ways. Each technique has its own merits and drawbacks. This section gives a short overview of the main theoretical methods that can be used to predict or explain the experimental behaviour of polymers. The classification used below is necessarily rather arbitrary, as many efforts have been made to integrate different techniques.

1.3.1 Simulations

Simulations start from a few fundamental equations and compute the time evolution of the system at hand. Within the limits of the (necessary) assumptions made in the simulation the results can be considered exact. Therefore, simulations are often referred to as 'computer experiments' and provide a good reference point for other theoretical approaches. Depending on the approximations made, simulations can be divided into different categories.

Ab-initio quantum mechanics makes use of our most fundamental knowledge of the behaviour of molecules: quantum mechanics. Only very few molecular systems are known for which exact solutions exist. Due to the complex mathematical nature of the equations of quantum mechanics, these exact solutions hardly surpass the realm of a single hydrogen atom. However, the introduction of computers and suitable approximations to the exact equations has lead to considerable progress. For example, the reaction pathway of an enzyme catalysed reaction is feasible through focusing only at the active center of the enzyme and its interactions with the reactants.

Molecular dynamics (MD) makes use of the fact that for many practical applications the quantum mechanical treatment is not necessary. Instead, the behaviour of the molecules are governed by the classical equations of motion as formulated by Newton. The quantum mechanical nature of mutual forces between atoms is replaced by so-called 'force fields'. When the position and velocity of all atoms together with the forces that act on each atom are known, the equations of motion can be numerically solved by brute force to obtain the time dependence of the system [4].

Brownian dynamics is in a way comparable to Molecular dynamics. The main difference is that it is usually applied for either large molecules or particles in solution. The large molecules or particles move far more slowly than the solvent molecules. In Brownian dynamics the solvent molecules are therefore not explicitly taken into account. Instead, use is made of the fact that that the solvent causes on the one hand random displacements of the large particles due to thermal noise and on the other hand give rise to a certain friction on the large molecules or particles. On top of this a systematic force, stemming from e.g. electrostatic interactions between the polymers or particles may be imposed to describe the time evolution of the system.

In the Monte Carlo method molecules are moved using other strategies. A trial move is made by switching the position of two (nearby) molecules (or atoms). When this lowers the total energy of the system, the move is accepted. When this increases the energy, a random number (between 0 and 1) is generated. This random number is compared to $\exp(-U/kT)$, where U/kT is the (dimensionless) energy increase. Only when the random number is lower than $\exp(-U/kT)$, the move is accepted. This method was originally devised to study the equilibrium state. However, when the two molecules are always chosen to be close to each other one can also study the diffusion dynamics of the system at hand.

A relatively new simulation technique is Dissipative Particle Dynamics (DPD) [5]. This technique resembles Molecular Dynamics (MD): the particles move according to Newton's laws. However, in DPD the interparticle interactions are chosen such that they allow for much larger time steps. The forces between DPD particles (which represent clusters of microscopic particles) are soft-repulsive: the particles are allowed to interpenetrate to some degree. Furthermore, the DPD particles are subject to a dissipative force which slows down the particles and to random force which adds energy to the particles. These two forces are chosen such that momentum is locally conserved. This allows for the study of physical behaviour on time scales many orders of magnitude greater than possible with MD.

The main drawback shared among all simulations is that it is hard to obtain the equilibrium or the long time-scale behaviour of polymers in solution, especially for large system sizes. The coarse-graining used in DPD solves this problem partially.

1.3.2 Field theories

A number of different approaches try to circumvent solving the many-body problem as is done in simulations. The focus is not on the position of every particle in the system, rather it is on the average density at a given position. At each position in space, a given particle interacts with the local average of all other particles, instead of interacting with different individual molecules. Especially for polymer systems in which the exact molecular details are not essential for the overall behaviour, this turns out to work rather well.

This thesis deals with one such theory, the self-consistent-field (SCF) theory, originally developed to study homopolymer adsorption onto a solid surface by Scheutjens and Fleer [6]. Historically, the continuum notation of the SCF equations dates back to 1965, when Edwards [7] analytically solved the equations describing an isolated homopolymer chain, which was grafted to the centre of a coordinate system of spherical geometry. Later this work was extended by Helfand and Tagami [8] to describe the demixing of polymer blends. In these seminal papers and a lot of work following them, a continuum notation was used for the chain propagators. However, it was soon noted that for non-trivial problems the equations had to be solved numerically. When solving the SCF equations numerically, space needs to be discretised.

Independently, DiMarzio and Rubin [9] used a discrete notation to describe the behaviour of homopolymers in solution in between two solid walls. This work was extended by Scheutjens and Fleer [6] in 1979 to incorporate excluded volume, a feature also present in the theories of Edwards and Helfand. Due to the different background of the researchers involved and the different notation of the equations it took several years before it was realised that the theory of Scheutjens and Fleer is in principle equal to that of Edwards, although they were originally constructed to solve a different problem.

The self-consistent-field (SCF) theory deals with the equilibrium distribution in space of (chain) molecules and the resulting thermodynamical quantities of the system at hand. The theory is formulated in terms of volume fractions of molecules and a molecular field, which is associated with the monomers. The volume fractions of the molecules are a function of their molecular fields and *vice-versa*. In equilibrium the volume fractions and molecular fields should be self-consistent. Typically, the molecular fields are varied numerically until an SCF solution is found.

Recently, the self-consistent-field theory has been generalised towards dynamical processes [10]. Here, one does not vary the fields as efficient as possible to obtain the SCF solution. Instead, the change in the fields is governed by a diffusion equation. The diffusion of molecules is directed by gradients in the fields and an additional noise term. This dynamic density functional theory enables the calculation of the time evolution of the density of polymers.

In a recent review, Fredrickson et al. [11] connected the SCF theory and the dynamic density functional theory in a common framework. As an extension, their partition function contains complex arguments, which account for fluctuations in the equilibrium state, which gives more exact results for the phase separation of polymer melts. They argue that the inclusion of a noise term in the dynamic density functional theory does not achieve the same goal.

1.3.3 Scaling and analytical theories

The scaling approach has proved to be very successful for polymers. The standard reference is the excellent book by de Gennes [12]. The underlying assumption is that, since polymers are large, atomistic detail is hardly of any influence on the overall large-scale behaviour. Scaling relations may predict for example the relative effect of a change in the volume fraction on the osmotic pressure, expressed as a power law. Finding the exact osmotic pressure for a given polymer and volume fraction is beyond the scope of scaling. This approximate nature is more or less comparable to the SCF theory: exact results are not to be expected due to the coarse-graining of the model. Moreover, the power laws resulting from the SCF theory may be wrong due to the mean-field approximation. In contrast, scaling arguments usually *do* result in the correct power laws.

The SCF theory is exact within the mean-field approximation. This means that it does not suffer from any mathematical approximations as usually applied in analytical theories. In fact, it is common to test the mathematical approximations in analytical mean-field theories by comparing with SF-SCF results. This comparison can easily detect a serious error in the analytical theory at hand. In contrast, a result from numerical theory that can be described by a simple analytical equation may suggest that an analytical theory for the problem at hand is feasible; at any rate such an analytical theory may provide the limiting behaviour for very long chains where numerical computations run into problems.

1.4 Numerical self-consistent-field theory

1.4.1 Approximations

As already stated in sec. 1.3.2 the SCF theory makes use of the mean-field approximation. This has the consequence of neglecting the fluctuations in the system. Furthermore, space is discretised in layers. Within these layers all volume fractions are averaged; no inhomogeneities within a layer are accounted for. Typically, the shape of an interface is imposed on the system by discretising the equations in a given geometry: planar, cylindrical, or spherical. The geometry that is imposed on the the system may not be that of the equilibrium state. This deficiency is not present in a system which is discretised in all three dimensions of space.

When considering a linear polymer chain in solution, all monomers of the chain will have a different position in space. When we would take a walk along the chain from the one end to the other, we would never pass the same position in space twice. A walk which satisfies this requirement is called a self-avoiding walk (SAW). It seems quite natural that any theory dealing with polymers should use these self-avoiding walks. Mathematically, however, the generation of SAWs is demanding, even when using a computer. Therefore, an approximation is used: the (weighted) random walk. The chains are described as a random walk through the average force field, where a given position in space *can* be occupied by more than one monomer. All possible conformations of the chains are generated in the mean field to predict the spatial distribution of the molecules.

Another mean-field approach was introduced by Ben-Shaul et al. [13]: the single chain mean-field (SCMF) theory. In the SCMF theory a sub-set of all possible conformations of the chains is generated as self-avoiding walks. This set is then weighted in the mean-field. This approach avoids the random-walk statistics used in the SCF theory. The theory of ref. [13] has many similarities to the SCF model: it is also a mean-field model which is numerically solved to a self-consistent solution. So, although the intra-molecular interactions can be treated 'exactly', the intermolecular interactions are still treated on a mean-field level. The SCMF theory has been successfully applied to amphiphilic aggregates and tethered polymer layers [14].

The exact treatment of the chain statistics does have some drawbacks. Firstly, the generation of self-avoiding walks (SAWs) is rather time consuming. This is overcome by generating a set of SAWs only once in the absence of any intermolecular interactions. For chains of 100 segments typically 10^6–10^7 different SAWs are generated [15]. This may seem a lot but when one considers that a chain of 100 segments has 10^{77} different random walk conformations on a six-choice lattice it is clear that only a tiny fraction of all real conformations is sampled. The problem at hand, e.g. a polymer brush in a collapsed state or at high grafting density, may have a strong preference for only a few or none of the conformations that are initially generated in zero field conditions. To successfully model these types of systems it is necessary to regenerate the conformations in the field they experience or to use shorter chains where almost all possible conformations can be generated. Additionally, the computational cost of considering bulk chains is very high.

1.4.2 Discrete versus continuous notation

Whether one uses a discrete or continuous notation is, in principle, immaterial: the basic ideas behind the theory remain the same. In this thesis the discretised notation is retained for three reasons. Firstly, the implementation of the theory is (necessarily) discretised. When implementing the theory it is easier to deal with discretised equations. Furthermore it seems more 'fair' to write discretised equations in the same way as they are implemented: the assumptions are clear from the start. The last reason can be summarized as local common practice: the laboratory at which this thesis was constructed has ample experience with the discretised notation.

Often the equations used in publications do not reflect the actual implementation. Therefore one may encounter mistakes in the literature while the actual calculated results are still correct, or *vice versa*. In fact, it is known that the discretisation of continuous equations is often not trivial and may lead to errors when done too naively. It can therefore be argued that the discrete notation is less susceptible to errors in the implementation. Some of the pitfalls are discussed in chapter 2 and in appendix B.

1.4.3 Numerical implementation

All of the results presented in this thesis were computed using a single computer program, called 'sfbox', which was designed to be as general as possible [16]. There are in principle no restrictions on the number of different molecules in the system, which means that many types of problems can be dealt with. Examples include adsorption of weak polyacids, self-assembly of surfactants, and wetting studies. Indeed it may solve SCF problems which one cannot think of today. This program is freely available for academic use.

The calculations are fast. The computer time needed on a modern personal computer varies from a few seconds (e.g. uncharged brushes) to a few days (e.g. when calculating a highly charged brush of chains with a length of about 1000 segments in a zero salt solution). This makes it easy apply the SCF theory; a new idea can be tested fast. Systematic variation of parameters can be done in very small steps, to ensure that no features of the calculated curve are lost.

1.5 Applications of the self-consistent-field theory

Polymers and surfactants in solution are present in many industrial and biological products. Examples are paint, milk, oil, and pesticides. Theory dealing with polymers and surfactants in solution therefore has potential applications in a many areas. A legitimate question therefore is: can we indeed apply SCF theory in these areas? The answer is twofold: yes and no.

No, because most practical problems are simply beyond the scope of the present theory. If, for example, one wanted to improve the adhesion of a paint by using predictions of the SCF theory the outcome would be rather disappointing. Paint contains a lot of ingredients, some of them are not even well characterised, others may have properties that cannot be well captured within the SCF theory. The adhesion process itself is a dynamical process instead of an equilibrium one. In short, most practical systems are so hopelessly complicated that applying the SCF theory seems pointless.

One may also have a more positive view. To improve the understanding of the fundamental processes involved in complicated mixtures like paint, a physical chemist will typically focus on a small subset of the ingredients. Academic research is mainly focused on well-characterised model systems. The self-consistent-field theory can be used to calculate the equilibrium properties of some of these model systems and further enhance the knowledge about them. These calculations are often performed by researches which are not theoreticians *per se*. When simulations are out of reach due to the nature of the system and analytical or scaling theories are too complicated then the self-consistent-field theory may give answers which may not be quantitatively correct due to its approximations but which nevertheless result in the right trends.

1.6 Outline of this thesis

The remainder of this thesis consists of several chapters dealing with extensions of the SCF theory and some applications. Three appendices deal with numerical aspects of the SCF theory.

In chapter 2 the SCF theory is described in detail and extended to segments which differ in dielectric permittivity and are subject to equilibrium reactions like acid-base, redox, and complexation equilibria. It is shown that both extensions have significant consequences for the formulation of the statistical thermodynamical quantities.

Chapter 3 deals with the bending rigidity of homopolymer layers adsorbed onto a (mathematically flat) solid surface. Both reversible and irreversible adsorption is considered. The results from the SCF theory are compared to those found from an analytical theory by Clement and Joanny [17], and qualitative agreement is obtained.

In chapter 4 the bending rigidity of homopolymers is again considered but from a different view point. Instead of adsorbing onto a solid surface, the polymers adsorb onto the head groups of a self-assembling bilayer, which forms a more diffuse adsorbing interface. The influence of the adsorbing polymers on the bending moduli of the vesicles is calculated for a varying size of the head groups.

Chapter 5 gives an efficient scheme to calculate the SCF volume fraction profiles of polydisperse copolymers, and may be seen as an extension of similar work on polydisperse homopolymers by Roefs et al. [18].

In chapter 6 the intramolecular excluded volume of homopolymers in solution is calculated within the mean-field approximation, using a chain which is anchored to the centre of a spherical coordinate system. The results are compared to known scaling relations. Furthermore, an attempt is made to correct for the neglect of the swelling of bulk homopolymers in the original theory of Scheutjens and Fleer. The influence of the correction on the volume fraction profiles of adsorbed homopolymers is calculated.

Appendix A deals with two computational aspects of the chain propagators which are needed to compute the volume fractions in the SCF theory. Firstly, a scheme is presented to avoid over- and underflows in the chain propagators. Secondly, a scheme is proposed to drastically reduce the computer memory needed to calculate the volume fractions of extremely long polymers.

Appendix B discusses the different ways to discretise space in the self-consistent-field theory. It describes common pitfalls in discretising the equations. Furthermore, the artefacts that may arise due to the discretisation are described. A new way to avoid artefacts due to the position of an interface on the layers is presented.

Lastly, in appendix C the numerical algorithm is described that has been used to solve the self-consistent-field equations. Some numerical tricks, developed during this investigation, are described that reduce the computational time needed to achieve convergence of the equations.

2 Theory for multicomponent mixtures of polyelectrolytes with state equilibria in inhomogeneous systems

ABSTRACT

A generalisation of the self-consistent-field (SCF) theory of Scheutjens and Fleer towards linear charged polymers subject to equilibrium reactions is presented. Any type of reaction can be dealt with, except for reactions that alter the chain architecture. Common examples of reactions that can be modelled are acid-base equilibria and complexation of ions. A statistical thermodynamical analysis leads to expressions for the spatial distribution of the molecules and several fundamental thermodynamical quantities like the surface tension and chemical potential. The influence of electrostatic polarisation on the chain statistics and thermodynamic quantities is explicitly taken into account. With our mean-field theory it is possible to study phenomena such as adsorption, self-assembly, and wetting of macromolecules in planar, cylindrical, and spherical geometry. The chains can also be grafted onto a surface. A distinction is made between mobile (as in Langmuir-Blodgett layers) or immobile (chemically linked) grafted molecules. The consequences for the surface pressure and the chemical potential of the grafted chains are derived.

2.1 Introduction

Most naturally occurring polymers are polyelectrolytes of which the segments have a charge that depends on the local environment and the pH [19]. Mostly, the charges can be described using acid-base equilibria. A polymer segment may also form a complex with an ion or be subject to redox equilibria. A thorough description of these equilibria is therefore important for determining the charge on biopolymers. Evidently, the same applies to synthetic polymers with a variable charge.

In most systems, the distribution of the molecules in space is inhomogeneous. At low and moderate salt concentrations, the charges on the molecules have a pronounced effect on their distribution in space. In this chapter we present a self-consistent-field (SCF) theory that predicts the spatial distribution of polymers with a charge that may depend on an arbitrary number of local equilibria with an arbitrary complexity. Furthermore, fundamental thermodynamic quantities like the surface tension and chemical potential are derived for such inhomogeneous systems.

Apart from the generalised treatment of reaction equilibria, the SCF theory is extended at two other levels in this chapter. Firstly, the influence of induced polarisation charges on the spatial distribution of the molecules and the thermodynamical quantities is taken into account correctly for the first time. Secondly, for the case of molecules that are grafted to a surface we distinguish mobile (as in Langmuir-Blodgett layers) and immobile (chemically linked) grafting in a way similar to that proposed by Carignano and Szleifer [20].

SCF theories for polymers were initially formulated by Edwards [7] and Helfand and Tagami [8], who modelled an isolated homopolymer and the interface between two homopolymer blends, respectively. In principle, both theories can be generalised to more complex systems like copolymers or multi-component mixtures. However, it was soon noted that, even for a moderately complex system, numerical evaluation of the continuum equations is necessary [21]. Independently, Scheutjens and Fleer [6] developed a numerical SCF theory to calculate the adsorption of homopolymers on a solid wall. The Scheutjens-Fleer (SF) theory was extended to calculate the adsorption of copolymers [22], branched molecules [23], and polydisperse mixtures of homopolymers [18]. The SF theory was also applied to describe self-assembling systems like micelles [24], vesicles [25], and membranes [23]. The original theory dealt with fully flexible homopolymers, but generalisations to include the rotational isomeric state (RIS) model [23] and anisotropic phases [26] of the chains have also been developed.

An important extension to the SCF model is the multi-state theory by Linse and Björling [27]. In this theory, segments of a chain may occur in two or more *states*. The local ratio between the different states of a segment is determined by their internal free energies and local contact interactions. The general form of the corresponding reaction equation reads

$$\mathtt{A} \rightleftarrows \mathtt{B} \tag{2.1}$$

$\mathtt{A}$ and $\mathtt{B}$ are, necessarily, states of the same segment. The internal free energies $\mu^*_{\mathtt{A}}$ and $\mu^*_{\mathtt{B}}$ determine the corresponding equilibrium constant, the local concentration ratio of $\mathtt{A}$ and $\mathtt{B}$ is determined by local contact interactions. This theory was developed to explain the temperature dependence of the adsorption and self-assembly of pluronics. In this theory, expressions for thermodynamical functions have been derived [27].

The polyelectrolyte theory of Israëls et al. [28] is in many aspects comparable. A noteworthy difference is that the states can be charged and the local equilibrium between the states is determined by the local electrostatic potential and the local proton concentration. The local proton concentration is assumed to be only a function of the local potential, since the protons do not take up any volume in the system. Their theory enabled the modelling of acid-base equilibria in an inhomogeneous system. However, within this framework expressions for thermodynamical functions like the surface tension are lacking so far.

Vincze et al. [29] considered complexation reactions. The general equation reads

$$\mathtt{A} + \mathtt{B} \rightleftarrows \mathtt{AB} \tag{2.2}$$

where $\mathtt{A}$ and $\mathtt{B}$ denote states of different molecules. Only one of the states $\mathtt{A}$ and $\mathtt{B}$ can belong to a chain molecule. This means that the state equilibria do not alter the chain architecture. If A is part of a chain molecule, obviously AB is too. For simplicity, the volume of the AB complex was taken to be equal to that of A and thus all segments and states have an equal volume. Vincze et al. used this theory to study the interface of two immiscible electrolyte solutions.

Recently, Shi and Noolandi [30] generalised an earlier density functional theory [31] to describe weakly charged polyelectrolytes. Their theory is in many ways comparable to that of Israëls et al. [28]. Only one type of acid-base equilibrium is dealt with. However, they *do* derive thermodynamical functions. They apply their theory to predict the phase separation of aqueous polyelectrolyte mixtures.

In this chapter, a more general approach is taken towards internal state equilibria. The number of states on the left and right hand side of the reaction equations is not restricted. However, similar to previous models, the same limitation applies as for the complexation reactions: linkage of two chain molecules is excluded. As an approximation the reaction equilibria are considered at a segment level only. The local equilibrium of a chain segment is not directly linked with the other segments of the chain. Instead, only the local mean field potentials influence the local equilibrium constants. In sec. 2.2.10 we elaborate on this aspect of the theory.

Using the proposed theory, acid-base equilibria, redox equilibria, and complexation can be investigated in a unified approach. Our theory is based on actual equilibrium constants, so that measurements of these equilibrium constants can be directly translated into dimensionless parameters needed for calculations. The necessary translations will be discussed in appendix B.8.

Generally, molecules have a polarisability which is finite: an electric field $\vec{E}$ induces polarisation charges on the molecules [32]. This results in a relative dielectric permittivity ϵ_r which exceeds unity. In this chapter the polarisation of the states is explicitly taken in to account, a feature which was neglected in previous formulations of the SCF theory [33]. The polarisation influences the volume fractions and the expressions for thermodynamical quantities, as elaborated in sec. 2.2.5.

Our model can also cope with molecules of which a given segment (e.g., an end segment) is attached to a surface. Two types of grafting mechanisms are distinguished: mobile and immobile grafting. Mobile grafting is experimentally found in Langmuir-Blodgett layers where the chains can not leave the surface but are free to wander around in two dimensions. Immobile grafting is experimentally accomplished by chemically attaching the molecules, e.g. to a solid surface. We will show that the *volume fractions* for both types of grafting are the same within the mean-field approximation, as long as the grafting plane is subject to the mean-field approximation. In contrast, the *thermodynamical properties* of the system differ for the two grafting mechanisms. Explicit expressions for the chemical potential of grafted molecules are derived in sec. 2.2.8.

We are interested in thermodynamical quantities such as the surface tension and the free energy of inhomogeneous systems. These are derived in sec. 2.2.9. Since general reaction equations are considered, the resulting expressions for thermodynamical quantities differ from those found in ref. [27]; the latter are, however, recovered as special cases of our general formulation. Also the polarisation charges and the type of grafting of molecules affect the thermodynamical quantities.

2.2 Theory

2.2.1 General aspects

We consider a system with an arbitrary number of molecules. The molecule type is labelled i. These molecules consist of one or more types of segments labelled A. Each type of segment A may assume different states, denoted by k. An example of a segment with different states is a weak acid, where the protonated and deprotonated states are distinguished. Polymer molecules are of special interest. For simplicity, we will consider linear chains only (extensions towards branched chains are possible, see e.g. ref. [23]). The segments in a chain have a ranking number $s = 1, 2, \ldots N_i$, where N_i is the chain length. When more than one segment of a polymer molecule may assume different states, the different states of the *molecule* need to be distinguished as well. We use the symbol t for the different states of the molecule. All possible combinations of segment states k are counted as a different molecular state t. For example: an oligomer of $N = 10$ segments for which each segment has 2 distinct states $k = 1, 2$ results in $2^{10} = 1024$ different molecular states t.

The equilibrium between different states t is described using equilibrium constants. These equilibrium constants are defined on a segment level. In general, the equilibrium constants depend on the states of the other segments along the chain. In a mean-field approximation, it is common to neglect this dependency [34]. As an approximation, the equilibrium only depends on the position of the segment in space. The equilibrium is independent of the fact whether a segment belongs to a chain or not. In sec. 2.2.10 we elaborate on this approximation.

In the numerical evaluation of the theory, space will be discretised. Instead of writing out the inhomogeneous equations using a general space coordinate $\vec{r}$, as is done in continuum theories, the discretisation will be made from the start. When considering systems with only one gradient in the volume fractions, space will be divided into layers (for a planar geometry) or shells (for a cylindrical or spherical geometry). We will use the term 'layers' for both cases. The layers are numbered $z = 1, 2, \ldots, M$. Note that the equations in this chapter also apply to a discretisation of more than one gradient. The only exceptions are the equations for the polarisation contribution to the segment potential which are derived in sec. 2.2.5.

The layers are filled up with segments which all have an equal volume ℓ^3, where ℓ is the spacing between layers. The (dimensionless) volume of a layer is denoted by $L(z)$, which is equal to the (not necessarily integer) number of segments that is needed to fill the entire layer z.

Within each layer a mean-field approximation is used. The volume fraction of segments A in state k of molecule i in layer z is denoted as $\varphi_{i,Ak}(z)$. The overall volume fraction profile for molecules of type i is then given by

$$\varphi_i(z) = \sum_{A,k} \varphi_{i,Ak}(z) \tag{2.3}$$

Likewise, the overall volume fraction segments of type A, irrespective in which type of molecule they occur, reads $\varphi_A(z) = \sum_{i,k} \varphi_{i,Ak}(z)$. A similar definition for segments of type A in state k is $\varphi_{Ak}(z) = \sum_i \varphi_{i,Ak}(z)$.

Both local contact interactions and electric contributions change the local equilibrium within each layer z and therefore affect the volume fractions $\varphi_{i,Ak}(z)$. The different conformations of the chains also affect the local volume fractions. In the following sections the partition function of the theory will be derived and its maximum term will be used as the equilibrium value for which the volume fractions are calculated.

2.2.2 Partition function

Scheutjens and Fleer [6] have given a detailed derivation of the micro-canonical partition function Ω for a homopolymer and a monomeric solvent in an inhomogeneous system, using the mean-field approximation. Evers et al. [22] generalised this approach to an inhomogeneous phase of multicomponent copolymers. They distinguish different conformations c of chain molecules, where a conformation is defined by a set of layers: $(z,s)_c$, the layer z where the segment with ranking number s finds itself in conformation c. After counting all possible conformations in space and applying Stirling's approximation $\ln n! = n \ln n - n$, they arrived at the micro-canonical partition function Ω describing the mixing and conformational entropy of the system. The generalisation to curved geometries reads [24]

$$\ln \Omega = \sum_{i,c} n_i^c \ln \frac{\omega^c}{N_i n_i^c} \tag{2.4}$$

In eq. 2.4 n_i^c denotes the number of molecules i in conformation c, N_i is the chain length of molecule i, and ω^c is a measure for the degeneration of conformation c. This quantity is most easily explained when space is discretised in only one direction, i.e. a system with only one gradient in the volume fractions. In a (curved) geometry with only one gradient the *a priori* step probability for a step from layer z to $z+1$ is denoted as $\lambda_1(z)$, the step probability from layer z to $z-1$ is $\lambda_{-1}(z)$, and that for a step within the same layer z $\lambda_0(z)$, such that $\lambda_{-1}(z) + \lambda_0(z) + \lambda_1(z) = 1$. The parameter ω^c is the product N_i of *a priori* step probabilities between layers that are encountered when walking from segment $s = 1$ to segment $s = N_i$ (in the order prescribed by conformation c), multiplied by $L(z^c)$, where $L(z^c)$ is the (dimensionless) volume of the layer where the first segment ($s = 1$) of conformation c is positioned. Note that the definition for ω^c needs to be independent on the direction of the walk through the layers, i.e. its value should not change if the walk starts at segment $s = N_i$ and ends in $s = 1$ or *vice versa*. For a system with one gradient this boils down to the requirement $\lambda_1(z)L(z) = \lambda_{-1}(z+1)L(z+1)$ [24]. Similar arguments can easily be constructed when more than one volume fraction gradient is considered. The exact expression for ω^c only affects the equations for computing the volume fractions (see sec. 2.2.4). When two or more gradients are considered care should be taken to make sure that the chains are isotropic in the absence of a field [35].

Noting that we have to distinguish between the different states t of a given molecule i, the generalisation of eq. 2.4 towards state equilibria is trivial:

$$\ln \Omega = \sum_{i,c,t} n_{i,t}^{c} \ln \frac{\omega^{c}}{N_i n_{i,t}^{c}} + \sum_{i} n_i^{\dagger} \ln \frac{n_i^{\dagger}}{L(z_i^{\dagger})} \tag{2.5}$$

In this equation the first term represents the generalisation of the partition function for multistate molecules. The second term only applies when component i is chemically grafted molecules, as discussed below.

The formulation of the first term for multi-state molecules differs from the equation given in Linse and Björling [27], where the mixing entropy of different states was introduced at the segment level rather than at the molecule level. This 'hides' the fact that all different states t of the molecule have their own contribution to the mixing entropy. The results are unaffected by this change in formulation.

The second term in eq. 2.5 accounts for molecules which are chemically attached to the surface, denoted by the superscript $\dagger$. It represents a correction to the parameter ω^c which is a measure for the *a priori* probability of placing a chain in conformation c in an empty system. When the first segment of a chain i is chemically attached to layer $z_i^{\dagger}$, the first segment does not have $L(z_i^{\dagger})$ possible positions but only $n_i^{\dagger}$, which is the number of chemically anchored molecules. Note that the chemical grafting points are still indistinguishable in the mean field.

When the second term is omitted for grafted molecules, *mobile* grafted chains are considered, as for example found in Langmuir-Blodgett layers. Due to the mean-field approximation the volume fraction profiles of chemically anchored (immobile) molecules is exactly equal to that of the mobile grafted chains. However, a difference between immobile and mobile grafted chains turns up in the thermodynamical quantities (see secs. 2.2.6, 2.2.8, and 2.2.9).

Grafted chains only assume those conformations which satisfy the grafting condition. So, when segment $s = 1$ is grafted to layer $z = 1$ the sum over c in eq. 2.5 runs only over those conformations which have segment $s = 1$ in layer $z = 1$. In contrast, free (i.e. non-grafted) chains may assume all possible conformations in space.

Eq. 2.4 was derived for non-dissociating copolymers using reference phases, one for each type i of molecule consisting of a pure phase of this molecule [22]. With multiple states, two obvious choices for the reference phase of one molecule type i come to mind. The reference phase for one type of molecule may consist of either n_i molecules in state $t = 0$, a state we are free to choose, or t different reference phases, each consisting of $n_{i,t}$ molecules in state t. The former choice was made by Linse and Björling [27]. The latter choice, which we adopt, implies $\Omega_i^* = \prod_t \Omega_{i,t}^*$, where the superscript $*$ denotes the reference phase. It turns out that after applying the Stirling approximation the logarithm of the partition function $\ln \Omega_i^*$ does not depend on the actual choice for a reference phase of a molecule. Hence, eq. 2.5 is unaffected by this choice.

The (contact) interactions in the reference phases have been explicitly included in various papers [6, 22–27]. While this is formally correct, the resulting equations become unnecessarily complicated. Additionally, in the case of pure reference phases for each type of molecule the question may arise how to account for electrostatic interactions. An easy solution is to omit all interactions in the reference phases. In the remainder of this chapter we will implicitly use pure reference phases for each state t of each molecule type i. The interactions in the reference phase are all set to zero. This is valid since the actual choice for a reference phase is arbitrary.

It is customary to let the micro-canonical partition function include all entropic effects. Weighting with the total energy U then yields the canonical partition function Q, which equals $\sum_U \Omega(U)\exp(-U/k_BT)$. In this chapter, Ω merely denotes the mixing and conformational entropy of the system. However, as we will show next, Q contains additional entropic contributions. Therefore, we replace the energy U by a Helmholtz energy F_x containing those additional contributions (but not the mixing and conformational entropy). These contributions are due to the nearest-neighbour contact interactions and the electrostatic interactions. The contact interactions are accounted for using Flory-Huggins parameters χ, which may have an entropic component. As we will see, the electrostatic interactions also have an entropic component due to polarisation of the segments. Therefore we use the symbol F_x, where x denotes the type of interactions, instead of U_x. The contribution of the contact interactions is denoted as F_c, and given by

$$F_c = \frac{1}{2}k_BT \sum_{z,A,k,B,l} L(z)\varphi_{Ak}(z)\chi_{Ak,Bl}\langle\varphi_{Bl}(z)\rangle \tag{2.6}$$

where $\varphi_{Ak}(z)$ is the volume fraction of segment A in state k at coordinate z. The Flory-Huggins parameter $\chi_{Ak,Bl}$ denotes the change in contact interactions in units k_BT when exchanging one segment A in state k from a pure phase of segments A in state k to a pure phase consisting of segments B in state l. Because of the double summation over all states, the factor $\frac{1}{2}$ comes in to correct for the double counting of contact interactions. The angular brackets define a local contact fraction through $\langle\varphi(z)\rangle = \sum_{z'} \lambda_{z-z'}(z)\varphi(z')$. For a system with one gradient $\lambda_{z-z'}(z)$ can be written out as $\langle\varphi(z)\rangle = \lambda_{-1}(z)\varphi(z-1) + \lambda_0(z)\varphi(z) + \lambda_1(z)\varphi(z+1)$, where the values for λ may, for example, be chosen equal to those used for the degeneration ω_c (see eqs. 2.4 and 2.5). Generalisations of $\lambda_{z-z'}(z)$ are possible, for example to include longer range interactions. In this case χ loses its usual meaning where it describes contact interactions only.

The electrostatic contribution to the free energy has been the subject of some debate [36]. To our knowledge, no general equation for the electrostatic contribution to the Helmholtz energy exists. Using the assumptions that will be introduced in sec. 2.2.5, it can be shown that [32, 36]

$$F_e = \frac{1}{2}\sum_{z,A,k} L(z)ev_{Ak}\varphi_{Ak}(z)\Psi(z) \tag{2.7}$$

where e is the elementary unit of charge, $\Psi(z)$ is the electrostatic potential (in Volts) in layer z, and v_{Ak} is the valence of state k of segment A. The polarisation of the segments is included in eq. 2.7, as will be elaborated on in sec. 2.2.5.

In principle, we could include a contribution to Q of internal free energies as was done by Linse and Björling [27]. However, when each state t of molecule i has its own reference phase, as in this chapter, the term representing internal free energies is zero.

Combining equations 2.5–2.7, we arrive at the following expression for the canonical partition function Q:

$$Q(\{n_{i,t}\},T) = \sum_{\{n^c_{i,t}\}} \Omega(\{n^c_{i,t}\}) \exp\left[-\frac{F_c(\{n^c_{i,t}\})}{k_BT} - \frac{F_e(\{n^c_{i,t}\})}{k_BT}\right] \tag{2.8}$$

where $n_{i,t}$ represents the number of molecules of type i in state t and $\{n_{i,t}\}$ represent a possible set of these numbers that satisfies the volume filling constraint. Because of the volume filling constraint, the volume V does not enter the equations. The sum runs over all sets $\{n^c_{i,t}\}$ of conformations c which are a realisation of the set $\{n_{i,t}\}$.

The grand canonical partition function Ξ is found from weighting the canonical partition function Q with the appropriate Boltzmann factors

$$\Xi(\{\mu_{i,t}\},T) = \sum_{\mathrm{all}\{n^c_{i,t}\}} Q(\{n^c_{i,t}\}) \exp\left[\sum_{i,t} \frac{n_{i,t}\mu_{i,t}}{k_BT}\right] \tag{2.9}$$

where $\mu_{i,t}$ is the chemical potential of molecule i in state t and $\{\mu_{i,t}\}$ represents a given set of chemical potentials of all molecules. Note that the chemical potentials are related through the reaction equations, as discussed in more detail in sec. 2.2.10.

2.2.3 Equilibrium

In the previous section we arrived at the appropriate expression for the grand canonical partition function Ξ. The next step is to define equilibrium. We will adopt the usual approximation of replacing the sum in the right hand side of eq. 2.9 by its maximum term, which has the effect of ignoring the fluctuations in the system. It is convenient to use Lagrange multipliers for the constraints and to define an unconstrained function f as

$$f = \ln Q + \sum_{i,t} \frac{n_{i,t}\mu_{i,t}}{k_BT} + \sum_z \beta(z)\left(L(z) - \sum_{i,t,c} n^c_{i,t} N^c_i(z)\right) \tag{2.10}$$

where $N^c_i(z)$ is the number of segments molecule i in conformation c has in layer z. The Lagrange multipliers $\beta(z)$ ensure that the volume is filled in each layer z. This does not necessarily make the system incompressible: an extra type of molecule representing 'vacuum' may be defined to consider a compressible system, like was done in the equation-of-state theory of Sanchez and Lacombe [37]. The SCF theory has been extended along these lines by Theodorou [38]. The introduction of 'vacuum' molecules leads to some formal differences in the thermodynamical quantities, see e.g. ref. [39]. Here we will avoid these formal differences by considering an incompressible system only.

It is not necessary to incorporate the reaction equilibria as constraints throughout the system in eq. 2.10 as was done by Linse and Björling [27]. The equilibria represent a relation between the values of $\mu_{i,t}$, as is shown in sec. 2.2.10. In equilibrium, the chemical potential $\mu_{i,t}$ for a given molecule i in state t is necessarily the same throughout the system. Therefore, the local equilibria are always obeyed.

Note that the M Lagrange multipliers in eq. 2.10 are not independent, because the volume filling constraint constitutes one relation between all chemical potentials. Once the chemical potentials of all molecules minus one are specified, the last chemical potential is fixed by the volume filling constraint. This will be dealt with in sec. 2.2.7 by setting β for the bulk phase to a fixed value, which in principle is arbitrary.

The maximum value of f is found from

$$\frac{\partial f}{\partial n^c_{i,t}} = \frac{\partial \ln Q}{\partial n^c_{i,t}} + \frac{\mu_{i,t}}{k_B T} - \sum_z \beta(z) N^c_i(z) = 0 \qquad \forall \quad n^c_{i,t} \tag{2.11}$$

The differentiation is easily performed using

$$\frac{\partial f}{\partial n^c_{i,t}} = \sum_{z,A,k} \frac{\partial f}{\partial n_{Ak}(z)} \frac{\partial n_{Ak}(z)}{\partial n^c_{i,t}(z)} = \sum_{z,A,k} \frac{\partial f}{\partial n_{Ak}(z)} N^c_{i,t,Ak}(z) \tag{2.12}$$

where $N^c_{i,t,Ak}(z)$ is the number of segments A in state k that a molecule i in state t and conformation c has in layer z and $n_{Ak}(z)$ is the number of segments A in state k in layer z. For other intricacies involving the differentiation we refer to the literature [22, 27]. The resulting equation is

$$\begin{aligned} &\ln \frac{\omega^c}{N_i n^c_{i,t}} - 1 + \frac{\mu_{i,t}}{k_B T} + \ln \sigma^\dagger_i + \delta_i(\dagger) \\ &- \sum_{z,A,k} N^c_{i,t,Ak}(z) \left[\beta(z) + \frac{\partial F_e / k_B T}{\partial n_{Ak}(z)} + \sum_{Bl} \chi_{Ak,Bl} \langle \varphi_{Bl}(z) \rangle \right] = 0 \end{aligned} \tag{2.13}$$

where $\sigma^\dagger_i = n^\dagger_i / L(z^\dagger_i)$ and $\delta_i(\dagger)$ is unity when molecule i is chemically grafted and zero otherwise. The differentiation $\partial F_e / \partial n_{Ak}(z)$ is not trivial: it introduces a contribution due to polarisation charges that was neglected before [40, 41]. This is discussed in sec. 2.2.5. Eq. 2.13 can be rearranged as

$$n^c_{i,t} = C_{i,t} \omega^c \prod_{z,A,k} G_{Ak}(z)^{N^c_{i,t,Ak}(z)} \tag{2.14}$$

where the state weighting factor $G_{Ak}(z)$ and the dimensionless state potential $u_{Ak}(z)$ are defined as

$$G_{Ak}(z) = \exp(-u_{Ak}(z)) \tag{2.15}$$

$$u_{Ak}(z) = \beta(z) + \frac{\partial F_{\bullet}/k_BT}{\partial n_{Ak}(z)} + \sum_{Bl} \chi_{AkBl} \langle \varphi_{Bl}(z) \rangle + u^{\mathrm{ref}}_{Ak} \tag{2.16}$$

The normalisation constant in eq. 2.14 $C_{i,t}$ is defined through

$$\ln C_{i,t} = -\ln N_i - 1 + \ln \sigma_i^{\dagger} + \delta_i(\dagger) + \frac{\mu_{i,t}}{k_BT} + \sum_{Ak} N_{i,t,Ak} u^{\mathrm{ref}}_{Ak} \tag{2.17}$$

where u^{ref}_{Ak} is an arbitrary reference potential. To evaluate the volume fractions (see sec. 2.2.4) it turns out to be convenient to choose u^{ref}_{Ak}, β, and Ψ for the bulk phase such that G_{Ak} is unity in the bulk. This will be done in sec. 2.2.7.

In principle, the volume fraction of molecule i in layer z can be computed from these equations as $\varphi_i(z) = \sum_{t,c,A,k} N^c_{i,t,Ak}(z) n^c_{i,t}/L(z)$. However, the number of different conformations c and different states t of molecule i is extremely large and generally the interest is not in their individual contributions. Therefore, in the following section we will rewrite eq. 2.14 to allow for an efficient evaluation of the sum over all states t and conformations c, resulting in the volume fraction $\varphi_i(z)$ of molecule i in layer z.

2.2.4 Volume fractions

In order to make the numerical evaluation of $\varphi_i(z)$ from eq. 2.14 feasible we first rewrite it as

$$n^c_{i,t} = C_{i,t} \omega^c \prod_{s=1}^{N_i} G^c_{i,t}(s) \tag{2.18}$$

where $G^c_{i,t}(s)$ is the analogon of eq. 2.15; it denotes the state weighting factor of segment number s for molecule i in state t and in conformation c. The following definition is introduced

$$C_{i,t} = C_i \prod_{s=1}^{N_i} \alpha^b_{i,t}(s) = C_i \prod_{z,A,k} \left(\alpha^b_{Ak}\right)^{N^c_{i,t,Ak}(z)} \tag{2.19}$$

where the α parameters need some explanation. The fraction of segments A that is in state k in the bulk is denoted by α^b_{Ak} so that $\sum_k \alpha^b_{Ak} = 1$. The parameter $\alpha^b_{i,t}(s)$ is the fraction of segments s of molecules i in molecular state t. Consequently, $\sum_t \alpha^b_{i,t}(s) = 1$ and $\sum_t \prod_{s=1}^{N_i} \alpha^b_{i,t}(s) = 1$. Substituting eq. 2.19 into 2.18, summing over t, and taking out segment $s = s'$ from the product yields

$$n^c_i = C_i \omega^c \sum_t \alpha^b_{i,t}(s') G^c_{i,t}(s') \prod_{s \neq s'}^{N_i} \alpha^b_{i,t}(s) G^c_{i,t}(s) \tag{2.20}$$

It is convenient to introduce the chain composition operator $\delta^A_{i,s}$ which is unity when segment s of molecule i is of type A and zero otherwise. Likewise, the conformation operator $\delta^z_{i,s,c}$ is unity when segment s of molecule i in conformation c resides in layer z and zero otherwise. These two delta functions enable us to rewrite the former equation as

$$n^c_i = C_i \omega^c \sum_{z,A,k} \alpha^b_{Ak} G_{Ak}(z) \delta^z_{i,s',c} \delta^A_{i,s'} \sum_t \prod_{s \neq s'}^{N_i} \alpha^b_{i,t}(s) G^c_{i,t}(s) \tag{2.21}$$

Note that eq. 2.21 is a valid replacement of eq. 2.20 since the reaction equilibria are considered at a segment level only. In this assumption, the relative dissociation α^b_{Ak} of a given segment does not explicitely depend on the states of the other segments in the chain. The relative dissociation of other segments is only incorporated through the mean-field potential. When repeating the procedure of eqs. 2.20 and 2.21 for all segments s, eventually the sum over t drops out. The result reads

$$n^c_i = C_i \omega^c \prod_{s=1}^{N_i} \sum_{z,A,k} \alpha^b_{Ak} G_{Ak}(z) \delta^z_{i,s,c} \delta^A_{i,s} = C_i \omega^c \prod_{s=1}^{N_i} \sum_{z,A} G_A(z) \delta^z_{i,s,c} \delta^A_{i,s} \tag{2.22}$$

where in the last identity the following definition was used

$$G_A(z) = \sum_k \alpha^b_{Ak} G_{Ak}(z) \tag{2.23}$$

where $G_A(z)$ is the segment weighting factor. It is a measure for the probability to find a segment of type A of molecule in layer z. Eq. 2.22 is essentially the same result as Hurter et al. [42] obtained from a simplification of the theory of Linse and Björling [27]. So, although our formulation of the partition function (eq. 2.5) is different, we arrive at the same expression for n^c_i.

In principle, eq. 2.22 permits the evaluation of the statistical weight of self-avoiding walks (SAWs). However, no efficient algorithm is available that generates all SAWs. A subset of all SAWs could be used instead, as done by Carignano and Szleifer [20]. Since in their theory each SAW is generated separately, the *intra*molecular interactions of the conformations can be treated exactly. The *inter*molecular interaction are solved self-consistently in their theory, i.e. through a mean-field approximation, as is done here as well. Obviously, the generation of the subset of SAWs is computationally demanding, so this is done only once: i.e. in the absence of a field [20]. This implies a loss of generality: when the spatial or intermolecular interactions on the chain conformations become large, only a few (or none) of the SAWs in the subset will dominate the real equilibrium set of chain conformations.

In our approach, the Markov approximation is used, which implies that direct backfolding of the chain is allowed. So, contrary to the theory by Carignano and Szleifer [20], the *intra*molecular interactions are approximated. However, *all* possible random walks are included, weighted with the proper Boltzmann factor, which depends on the local mean-field potential acting on the segments of the chain. This leads to a greatly simplified numerical evaluation of the volume fraction profiles.

Above we elaborated on eq. 2.14 to handle the large number of states t. The Markov approximation is used subsequently to deal with the large number of conformations c. This is done in a similar way as in Evers et al. [22]. Summing eq. 2.22 over all conformations c and dividing by the (dimensionless) volume $L(z)$ of coordinate z, we may rewrite eq. 2.22 as

$$\varphi_i(z,s) = C_i \frac{G_i(z,s|1)G_i(z,s|N_i)}{G_i(z,s)} \tag{2.24}$$

where $G_i(z,s)$ is the segment weighting factor of segment s of molecule i in layer z, defined as:

$$G_i(z,s) = \sum_A G_A(z)\delta^A_{i,s} \tag{2.25}$$

The end-segment weighting factors $G_i(z,s|1)$ are defined as

$$G_i(z,s|1) = G_i(z,s)\big\langle G_i(z,s-1|1)\big\rangle \tag{2.26a}$$

$$G_i(z,s|N_i) = G_i(z,s)\big\langle G_i(z,s+1|N_i)\big\rangle \tag{2.26b}$$

where $G_i(z,s|1)$ is proportional to the probability to find segment s of molecule i in layer z in a weighted random walk starting from segment $s = 1$. The equivalent starting from $s = N_i$ is denoted as $G_i(z,s|N_i)$. Their product, divided by $G_i(z,s)$ to prevent double counting of segment s, is proportional to the probability of finding segment s in layer z, cf. eq. 2.24. The angular brackets in eq. 2.26 denote a weighted average over neighbouring layers similar to that used in eq. 2.6. A common approach is to use the same weighted average in eq. 2.26 and eq. 2.6, however, we are free to use different values for λ in both equations.

The starting values of the propagators 2.26 are given by $G_i(z,1|1) = G_i(z,1)$ and $G_i(z,1|N_i) = G_i(z,N_i)$. It has been shown [43, 44], that the propagators 2.26 are the discrete version of the Edwards diffusion equation [7].

The evaluation of the normalisation constant C_i depends on the restriction posed on the molecule in the system. When the volume fraction in the bulk φ_i^b is fixed the most convenient way of finding C_i is by setting $u_{Ak} = 0$ in the bulk. The method to achieve this is discussed in sec. 2.2.7. From an evaluation of eq. 2.24 in the bulk phase it then follows that

$$C_i = \frac{\varphi_i^b}{N_i} \tag{2.27}$$

Alternatively, the total amount θ_i of monomers in molecule i in the system can be fixed. This total amount is defined as

$$\theta_i = \sum_z L(z)\varphi_i(z) \tag{2.28}$$

When θ_i for molecule i in the system is fixed the normalisation constant follows immediately from $\theta_i = N_i \sum_z L(z)\varphi(z,N)$ and from eq. 2.24 for $s = N$: $\varphi(z,N) = C_i G_i(z,N|1)$. Hence,

$$C_i = \frac{\theta_i}{N_i \sum_z L(z) G_i(z,1|N)} \tag{2.29}$$

The volume fraction φ_i^b in the bulk phase of molecules with a fixed θ_i is easily computed by equating this expression for C_i with that of eq. 2.27. Necessarily, u_{Ak} in the bulk should be set to zero for this relation to hold.

Eq. 2.29 is also the natural normalisation for chains grafted to e.g. a surface. Obviously, the number of different possible conformations c for a grafted chain is less than that for a free chain. Typically, a given segment of a grafted chain is only present in one layer or coordinate. However, multiple grafting points can also be considered. For example, grafting one end of a chain to a surface and the other end at a given layer enables the computation of the force needed to pull a grafted chain off an adsorbing surface. For each grafted segment the segment weighting factor $G_i(z,s)$ is set to zero outside the grafting layer(s). Other than that, the propagator procedure to compute the volume fractions remains unaltered.

There is no difference in the volume fraction of laterally mobile and laterally immobile grafted chains, since the distinction does not show up in the resulting equations for the volume fractions. Note that grafted molecules have a bulk volume fraction of zero by definition. Therefore, equating eq. 2.29 (the proper normalisation for grafted chains) with 2.27 is not a valid operation to compute φ^b for grafted molecules.

Often, the interest is in the interaction free energy between surfaces. When the ratio between the surface area and the total system volume is (close to) zero, the bulk composition does not change as the surfaces approach each other and eq. 2.27 can be used. When the ratio between the surface area and the total system volume is finite rather than zero (which is true for most practical systems), the bulk composition usually changes upon approach of the surfaces. The total (dimensionless) volume of the system is the volume between the two surfaces, given by $\sum_z L(z)$, augmented by the volume of the bulk phase, denoted by L^b. A slightly modified version of eq. 2.29 has to be used in this case:

$$C_i = \frac{\theta_i}{N_i \left[L^b + \sum_z L(z) G_i(z,1|N)\right]} \tag{2.30}$$

The total amount of monomers in molecules i in the system θ_i is usually given. It can be computed from $\sum_z L(z)\varphi_i(z) + L^b\varphi^b$. The term L^b in the denominator of eq. 2.30 originates from the fact that $G_i(z,1|N)$ is unity in the bulk phase.

The chemical potential of a given state t of molecule i can also be fixed. This then fixes the chemical potentials of all other states t of molecule i through the reaction equilibria. The normalisation C_i follows immediately from eqs. 2.17 and 2.19

$$\ln C_i = -\ln N_i - 1 + \ln \sigma_i^\dagger + \delta_i(\dagger) + \frac{\mu_{i,t}}{k_B T} + \sum_{Ak} N_{i,t,Ak}\left[u_{Ak}^{\mathrm{ref}} - \ln \alpha_{Ak}^b\right] \tag{2.31}$$

which needs to be evaluated for an arbitrary molecular state t.

For some applications we may want to fix the volume fraction of molecules at one layer or the average volume fraction at a number of layers. This is done by using the normalisation

$$C_i = \frac{\widetilde{\varphi}_i \sum_{z^\circ} L(z^\circ)}{\sum_{z^\circ,s} L(z^\circ) G_i(z^\circ, s|1) G_i(z^\circ, s|N)/G_i(z^\circ, s)} \tag{2.32}$$

where $\widetilde{\varphi}_i$ is the (average) fixed volume fraction and the layers over which it is imposed are denoted by the superscript $\circ$. The volume fraction φ_i^b of the bulk phase is found by equating eqs. 2.32 and 2.27. Besseling and Cohen Stuart [45] used this normalisation to study the nucleation of amphiphilic molecules into micelles. The normalisation enables the computation of the (off-equilibrium) transition states in the formation and breakdown of micelles.

2.2.5 The electrostatic contribution to the state potential

The state weighting factor eq. 2.16 contains the term

$$\frac{\partial F_e/k_B T}{\partial n_{Ak}(z)} \tag{2.33}$$

which needs to be determined. It is not always equal to $v_{Ak} e \Psi(z)/k_B T$ as was assumed before [33]. This is only true when all relative dielectric permittivities $\epsilon_{r,Ak}$ are equal to unity. When $\epsilon_{r,Ak}$ exceeds unity, polarisation charges are induced by the electric field $\vec{E} = -\nabla \Psi$; this electric field $\vec{E}$ gives rise to a local separation of charge within the segments. In this section first some general equations describing electrostatics are reviewed. Then the derivative in eq. 2.33 is taken for the special case of a system with only one gradient in the volume fraction profiles. Finally, the exact expressions for eq. 2.33 on planar and curved geometries are derived.

The fundamental equation describing electrostatics reads

$$\rho_t = \epsilon_0 \nabla \cdot \vec{E} \tag{2.34}$$

where ρ_t is the total charge density and $\vec{E}$ is the field strength. Integrating this equation, using Gauss' theorem, over a given volume V yields

$$\int_V \rho_t \mathrm{d}\vec{r} = \epsilon_0 \int_S \vec{E} \cdot \vec{n} \mathrm{d}\vec{r} \tag{2.35}$$

where S is an arbitrary closed surface, V is the volume inside this surface, and $\vec{n}$ represents the unit vector normal to the surface pointing outward of the volume. The electrostatic potential $\Psi(\vec{r}_1)$ at coordinate $\vec{r}_1$ is given by

$$\Psi(\vec{r}_1) = \int_{\vec{r}_2 \neq \vec{r}_1} \frac{\rho_t(\vec{r}_2)}{r(1,2)} \mathrm{d}\vec{r}_2 \tag{2.36}$$

where $r(1,2)$ is the distance between the coordinates $\vec{r}_1$ and $\vec{r}_2$.

The total charge density ρ_t contains two contributions: the *free* charge density ρ_f and the polarisation charge density ρ_p:

$$\rho_t \equiv \rho_f + \rho_p \tag{2.37}$$

In principle it is possible to account for dipole charges. However this would require that the orientation of segments is taken into account. We do not pursue this point here.

The polarisation charge density ρ_p can be described by [46]

$$\rho_p = -\epsilon_0 \nabla \cdot (\epsilon_r - 1)\vec{E} \tag{2.38}$$

where for simplicity we use the approximation that the dielectric permittivities of states are additive, leading to

$$\epsilon_r(\vec{r}) = \sum_{Ak} \epsilon_{r,Ak} \varphi_{Ak}(\vec{r}) \tag{2.39}$$

Other choices can be made. Most notably, the polarisability of a molecule can be related to the dielectric permittivity by the Clausius-Mossotti equation [32]. Again, we do not pursue this point here. Using $\rho_t = \rho_f + \rho_p$ with eqs. 2.34 and 2.38 immediately results in

$$\rho_f = \epsilon_0 \nabla \cdot \epsilon_r \vec{E} \tag{2.40}$$

which is Poisson's equation. This equation is not exact: it assumes a linear dependence of the polarisation charge on E [46]. In our theory $\epsilon_{r,Ak}$ does not depend on the field strength, which boils down to the same assumption.

The electrostatic contribution to the energy U_e is defined as [46]

$$U_e = \frac{1}{2} \iint_{\vec{r}_2 \neq \vec{r}_1} \frac{\rho_t(\vec{r}_1)\rho_t(\vec{r}_2)}{r(1,2)} \mathrm{d}\vec{r}_2 \mathrm{d}\vec{r}_1 = \frac{1}{2}\epsilon_0 \int \vec{E}^2 \mathrm{d}\vec{r} \tag{2.41}$$

where the last equality is found using eq. 2.34 and eq. 2.36. As was already remarked above eq. 2.7, there is no general formulation of the electrostatic contribution to the Helmholtz energy. However, using the same assumption as was needed to arrive at eq. 2.40, it is possible to derive the following expression [32, 36]:

$$F_e = \frac{1}{2} \iint_{\vec{r}_2 \neq \vec{r}_1} \frac{\rho_f(\vec{r}_1)[\rho_f(\vec{r}_2) + \rho_p(\vec{r}_2)]}{r(1,2)} \mathrm{d}\vec{r}_2 \mathrm{d}\vec{r}_1 = \frac{1}{2}\epsilon_0 \int \epsilon_r \vec{E}^2 \mathrm{d}\vec{r} \tag{2.42}$$

where the last equality is found using eq. 2.40 and eq. 2.36. The difference between eqs. 2.41 and 2.42 should be attributed to the entropy arising from polarisation charges. Polarisation charges represent a charge separation, which results in an entropic contribution to the free energy.

In order to find an expression for the derivative in eq. 2.33, the charge densities ρ_f and ρ_p need to be expressed as a function of the local state volume fractions. In

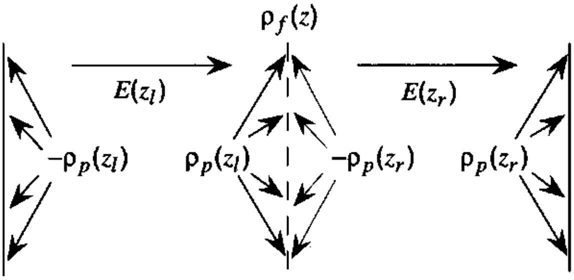

FIGURE 2.1: The capacitor model. The free charges $\rho_f(z)$ are positioned in the middle of the layer, denoted by a dashed line. In each half of the layer, denoted by z_l and z_r, a different field strength E is present. Due to the electric field the segments are polarised resulting in a positive and a negative contribution which placed at the surfaces of the half layer.

order to simplify the arguments, a system with only one gradient in volume fractions is considered.

When a system with only one density gradient is considered, space reduces to a system of layers. The discretisation of the electrostatic equations is done using a capacitor model as depicted in fig. 2.1. This is the same model Barneveld et al. [41] used to discretise the Poisson equation. Within this model, the free charges reside in the middle of the layers.

Eq. 2.42 is equal to eq. 2.7 as can be derived by inserting eq. 2.36 and using the following equation

$$\rho_f(r) = \frac{\sum_{Ak} L(z) e\nu_{Ak}\varphi_{Ak}(z)}{A(r)} = \frac{\sum_{Ak} e\nu_{Ak} n_{Ak}(z)}{A(r)} \tag{2.43}$$

where r is the distance from the centre of the (curved) system of layers to the middle of layer z: $r = (z - 0.5)\ell$ where ℓ is the distance between two layers. The area of the sphere or cylinder is denoted by $A(r)$. For a planar system of layers we can use $L(z) = 1$ and $A(r) = \ell^2$. Note that z has no dimension, whereas both ℓ and r are expressed in meters.

Since the free charges only reside in the middle of the layers, $\nabla \cdot \epsilon_r \vec{E}$ is zero in between two middle planes of neighbouring layers. However, ϵ_r is generally different between two layers which results in a finite value of $\nabla \cdot \vec{E}$ at the plane separating two neighbouring layers. This value is equal to the net polarisation charge density ρ_p at this plane (cf. eq. 2.38). At the middle of the layer $\nabla \cdot \vec{E}$ is also finite, since the free charges reside there, which results in a discontinuity in $\vec{E}$. The polarisation charges at this middle plane are given by

$$\begin{aligned}\rho_p(r)A(r) &= \sum_{Ak} L(z)\left[p_{Ak}(z_l)\varphi_{Ak}(z) + p_{Ak}(z_r)\varphi_{Ak}(z)\right] \\ &= -\int_{S_z} \epsilon_0(\epsilon_r(r)-1)\vec{E}\cdot\vec{n}\mathrm{d}a\end{aligned} \tag{2.44}$$

where $A(r)$ is the area of the midplane at layer z and $p_{Ak}(z)$ is the polarisation charge at position z due to segments A in state k. The integral represents Gauss' law: S_z is a closed surface *inside* layer z. Within this surface all the polarisation charges on the left hand side of eq. 2.44 reside. It turns out to be convenient to split up the polarisation charge in two contributions: one arising from the left part of the layer and one from the right part. The polarisation charge $p_{Ak}(z_r)$ is necessarily also present at the upper boundary of layer z, but with a different sign since the total polarisation charge in the system equals zero. A likewise argument holds for $p_{Ak}(z_l)$ at the lower boundary of the layer. Explicit expressions for $p_{Ak}(z_l)$ and $p_{Ak}(z_r)$ will be given below.

The derivative to $n_{Ak}(z)$ in eq. 2.33 is split-up in two parts: the derivative with respect to the free charges and the derivative with respect to the polarisation charges.

$$\frac{\partial F_e}{\partial n_{Ak}(z)} = \left(\frac{\partial F_e}{\partial n_{Ak}(z)}\right)_f + \left(\frac{\partial F_e}{\partial n_{Ak}(z)}\right)_p \tag{2.45}$$

The derivative with respect to the free charges yields

$$\left(\frac{\partial F_e}{\partial n_{Ak}(z)}\right)_f = \frac{1}{2}v_{Ak}e\Psi(z) + \frac{1}{2}v_{Ak}e\Psi_f(z) + \frac{1}{2}\iint_{\vec{r}_2\neq\vec{r}_1} \frac{\rho_f(z_1)\left(\frac{\partial\rho_p(z_2)}{\partial n_{Ak}(z)}\right)_f}{r(1,2)}\mathrm{d}\vec{r}_2\mathrm{d}\vec{r}_1 \tag{2.46}$$

The different terms in this equation stem from applying the chain rule when differentiating eq. 2.42. Note that the second term contains $\Psi_f(z)$ which is defined analogous to eq. 2.36 but now for free charges. The third term expresses the change in polarisation charges due to the change in the free charges in layer z. It is well known that bringing an unpolarisable charge e from infinity to z in a potential field Ψ should yield an energy of $e\Psi(z)$, so

$$\left(\frac{\partial F_e}{\partial n_{Ak}(z)}\right)_f = v_{Ak}e\Psi(z) \tag{2.47}$$

Therefore, the last term in eq. 2.46 can be written as

$$\iint_{\vec{r}_2\neq\vec{r}_1} \frac{\rho_f(z_1)\left(\frac{\partial\rho_p(z_2)}{\partial n_{Ak}(z)}\right)_f}{r(1,2)}\mathrm{d}\vec{r}_2\mathrm{d}\vec{r}_1 = v_{Ak}e\Psi_p(z) \tag{2.48}$$

where $\Psi_p(z) = \Psi(z) - \Psi_f(z)$ and is defined analogous to eq. 2.36 for polarisation charges. It is customary to refer to Ψ_p as the reaction potential [32]. The reaction potential Ψ_p is a measure for the change in the potential due to the system wide change in the polarisation charges when adding/removing a charge locally.

The derivative eq. 2.33 with respect to the polarisation charge can also be viewed as consisting of two contributions.

$$\left(\frac{\partial F_e}{\partial n_{Ak}(z)}\right)_p = \left(\frac{\partial F_e}{\partial n_{Ak}(z)}\right)_{p,L} + \left(\frac{\partial F_e}{\partial n_{Ak}(z)}\right)_{p,R} \tag{2.49}$$

Firstly, the removal/addition of a segment changes ρ_p locally (denoted by a subscript L), since the segment carries polarisation charge. Secondly, the local change in polarisation results in a change in polarisation charges (affecting the entire system), which may be expressed in the reaction potential $\Psi_p(z)$. This contribution is labelled with subscript R. The first (local) contribution reads

$$\begin{aligned}\left(\frac{\partial F_e}{\partial n_{Ak}(z)}\right)_{p,L} = \frac{1}{2}\big[&- p_{Ak}(z_l)\Psi_f(z-1/2) + p_{Ak}(z_l)\Psi_f(z) \\ &+ p_{Ak}(z_r)\Psi_f(z) - p_{Ak}(z_r)\Psi_f(z+1/2)\big]\end{aligned} \tag{2.50}$$

which is most easily seen from differentiating eq. 2.44 with respect to $n_{Ak}(z)$

$$\left(\frac{\partial \rho_p(r)A(r)}{\partial n_{Ak}(z)}\right)_p = p_{Ak}(z_l) + p_{Ak}(z_r) \tag{2.51}$$

where $p_{Ak}(z_l)$ denotes the polarisation charge on state k of segment A in the left half of layer z, as given by eq. 2.44. Likewise, $p_{Ak}(z_r)$ denotes the polarisation charge in the right half of layer z.

The second (non-local) term of the right hand side of eq. 2.49 resembles eq. 2.50: the only difference is that Ψ_f is replaced by Ψ_p. The sum of both contributions can be written using the total potential $\Psi = \Psi_f + \Psi_p$:

$$\begin{aligned}\left(\frac{\partial F_e}{\partial n_{Ak}(z)}\right)_p = -\frac{1}{2}\big[&p_{Ak}(z_l)\Psi(z-1/2) - p_{Ak}(z_l)\Psi(z) \\ &- p_{Ak}(z_r)\Psi(z) + p_{Ak}(z_r)\Psi(z+1/2)\big]\end{aligned} \tag{2.52}$$

The negative sign at the right hand side of this equation expresses that , the polarisation of state Ak represents a relaxation in the system, hence it gives a negative contribution to the state potential $u_{Ak}(z)$. The signs in front of $p_{Ak}(z_l)$ and $p_{Ak}(z_r)$ follow from eq. 2.44. The expressions for $p_{Ak}(z_l)$ and $p_{Ak}(z_r)$ will turn out to have a form such that the term in between the square brackets is positive. The expressions for $p_{Ak}(z_l)$ and $p_{Ak}(z_r)$ depend on the chosen geometry of space, which affects the discretisation. Next, we will therefore distinguish between planar, cylindrical, and spherical geometry of a system with one gradient.

Planar geometry

In a planar geometry the Poisson equation 2.40 can written as

$$\epsilon_0 \frac{\partial}{\partial r} \epsilon_r(r) \frac{\partial}{\partial r} \Psi(r) = -\rho_f(r) \tag{2.53}$$

Since all free charges are positioned in the middle of the layers, $\rho(r) = 0$ in between planes positioned at the middle of two subsequent layers. Integrating in between those planes yields

$$E(r) = -\frac{\partial \Psi(r)}{\partial r} = -\frac{C(z, z+1)}{\epsilon_r(r)} \tag{2.54}$$

where the first equality is true by definition and $C(z, z+1)$ (in V/m) is an integration constant, which depends on the actual layers that are considered. Integrating this expression from r to $r + 1/2$ and from $r + 1/2$ to $r + 1$ yields

$$\Psi(z + 1/2) - \Psi(z) = \frac{\ell C(z, z+1)}{2\epsilon_r(z)} \tag{2.55a}$$

$$\Psi(z + 1) - \Psi(z + 1/2) = \frac{\ell C(z, z+1)}{2\epsilon_r(z+1)} \tag{2.55b}$$

where ℓ is the spacing between two neighbouring layers (in meters). Equating $\Psi(z + 1/2)$ in the above equations yields

$$C(z, z+1) = \frac{2}{\ell} \frac{\epsilon_r(z)\epsilon_r(z+1)(\Psi(z+1) - \Psi(z))}{\epsilon_r(z) + \epsilon_r(z+1)} \tag{2.56}$$

which enables us to write $\Psi(z + 1/2)$ as a function of $\Psi(z)$, $\Psi(z + 1)$, $\epsilon_r(z)$, and $\epsilon_r(z + 1)$:

$$\Psi(z + 1/2) = \frac{\epsilon_r(z)\Psi(z) + \epsilon_r(z+1)\Psi(z+1)}{\epsilon_r(z) + \epsilon_r(z+1)} \tag{2.57}$$

Next, eq. 2.44 is evaluated for an arbitrary closed volume inside layer z, using eq. 2.54. In eq. 2.44 the product $\vec{E} \cdot \vec{n}$ equals $E(r)$ of eq. 2.54 in the right (positive) half of layer z, and it is $-E(r)$ in the left (negative) half of layer z. Note that $L(z)$ can be taken unity for the planar geometry and that the volume of a monomer is ℓ^3. The integral over the closed surface consists of two parts: one in the negative half layer, the other in the positive half. It seems justified to assign the polarisation charges in the same fashion.

$$\sum_{Ak} p_{Ak}(z_l)\varphi_{Ak}(z) = -\ell^2 \epsilon_0 (\epsilon_r(z) - 1) \frac{C(z-1, z)}{\epsilon_r(z)} \tag{2.58a}$$

$$\sum_{Ak} p_{Ak}(z_r)\varphi_{Ak}(z) = \ell^2 \epsilon_0 (\epsilon_r(z) - 1) \frac{C(z, z+1)}{\epsilon_r(z)} \tag{2.58b}$$

The right hand side of these equations is split up into the separate contributions for the states Ak using the approximation of eq. 2.39.

$$p_{Ak}(z_l) = -\ell^2\epsilon_0(\epsilon_{r,Ak} - 1)\frac{C(z-1,z)}{\epsilon_r(z)} \tag{2.59a}$$

$$p_{Ak}(z_r) = \ell^2\epsilon_0(\epsilon_{r,Ak} - 1)\frac{C(z,z+1)}{\epsilon_r(z)} \tag{2.59b}$$

Substituting eqs. 2.55, we find

$$p_{Ak}(z_l) = 2\ell\epsilon_0(\epsilon_{r,Ak} - 1)(\Psi(z-1/2) - \Psi(z)) \tag{2.60a}$$

$$p_{Ak}(z_r) = 2\ell\epsilon_0(\epsilon_{r,Ak} - 1)(\Psi(z+1/2) - \Psi(z)) \tag{2.60b}$$

Eq. 2.45 can be rewritten using eq. 2.52 and the above equation as

$$\frac{\partial F_e}{\partial n_{Ak}(z)} = v_{Ak}e\Psi(z) - \frac{1}{2}\epsilon_0(\epsilon_{r,Ak} - 1)P(z) \tag{2.61}$$

where $P(z)$ is defined as

$$P(z) = 2\ell[\Psi(z-1/2) - \Psi(z)]^2 + 2\ell[\Psi(z) - \Psi(z+1/2)]^2 \tag{2.62}$$

where $P(z)$ is easily identified as the average of the square of the electric field over the two half-layers. For curved geometries we will show that $P(z)$ does not correspond to the electric field squared, hence the separate symbol. Eq. 2.61 represents the general formulation of the derivative in eq. 2.16: it is independent of the discretisation of space. In contrast, eq. 2.62 is not general: it only applies to a planar system of layers with one gradient in the volume fractions.

Cylindrical geometry

For the cylindrical case the Poisson equation is written as

$$\epsilon_0\frac{1}{r}\frac{\partial}{\partial r}r\epsilon_r(r)\frac{\partial}{\partial r}\Psi(r) = -\rho_f(r) \tag{2.63}$$

Integrating between the midplane of two adjacent layers, as done for the planar case, yields

$$E(r) = -\frac{\partial\Psi(r)}{\partial r} = -\frac{C(z,z+1)}{r\epsilon_r(r)} \tag{2.64}$$

For $C(z,z+1)$ we find

$$C(z,z+1) = \frac{\Psi(z+1) - \Psi(z)}{\ln(\frac{z}{z-0.5})/\epsilon(z) + \ln(\frac{z+0.5}{z})/\epsilon(z+1)} \tag{2.65}$$

which results in

$$\Psi(z+1/2) = \frac{\ln(\frac{z+0.5}{z})\epsilon(z)\Psi(z) + \ln(\frac{z}{z-0.5})\epsilon(z+1)\Psi(z+1)}{\ln(\frac{z+0.5}{z})\epsilon(z) + \ln(\frac{z}{z-0.5})\epsilon(z+1)} \tag{2.66}$$

Integrating eq. 2.44 over layer z results in the separate contributions for the polarisation of state Ak, which read

$$p_{Ak}(z_l) = -2\pi\ell\epsilon_0(\epsilon_{r,Ak} - 1)\frac{C(z-1,z)}{L(z)\epsilon_r(z)} \tag{2.67a}$$

$$p_{Ak}(z_r) = 2\pi\ell\epsilon_0(\epsilon_{r,Ak} - 1)\frac{C(z,z+1)}{L(z)\epsilon_r(z)} \tag{2.67b}$$

Again we can rewrite eq. 2.33 as eq. 2.61. However, the expression for $P(z)$ is different from eq. 2.62:

$$P(z) = 2\pi\ell\frac{C(z-1,z)}{L(z)\epsilon_r(z)}(\Psi(z) - \Psi(z-1/2)) + 2\pi\ell\frac{C(z,z+1)}{L(z)\epsilon_r(z)}(\Psi(z+1/2) - \Psi(z)) \tag{2.68}$$

Using eq. 2.65 for the C's this can be rewritten in a form containing the square of the electric field in the two half-layers. The result does not differ much from eq. 2.62. However, using eq. 2.62 for cylindrical geometry results in a small but systematic thermodynamical inconsistency. Most notably, Gibbs' adsorption law (eq. 2.94) is no longer obeyed: a difference of order 0.1% is observed between the left and right hand side of eq. 2.94. In contrast, eq. 2.68 yields results which are exact within the numerical accuracy.

Spherical geometry

The preceding procedure can also be applied to a spherical geometry. The field strength E reads

$$E(r) = -\frac{\partial\Psi(r)}{\partial r} = -\frac{C(z,z+1)}{r^2\epsilon_r(r)} \tag{2.69}$$

and for $C(z, z+1)$ we find

$$C(z,z+1) = 2\ell\frac{\Psi(z+1) - \Psi(z)}{1/[z(z-0.5)\epsilon(z)] + 1/[z(z+0.5)\epsilon(z+1)]} \tag{2.70}$$

which results in

$$\Psi(z+1/2) = \frac{(z-0.5)\epsilon(z)\Psi(z) + (z+0.5)\epsilon(z+1)\Psi(z+1)}{(z-0.5)\epsilon(z) + (z+0.5)\epsilon(z+1)} \tag{2.71}$$

The polarisation charges on the individual states are given by

$$p_{Ak}(z_l) = -4\pi\epsilon_0(\epsilon_{r,Ak} - 1)\frac{C(z-1,z)}{L(z)\epsilon_r(z)} \tag{2.72a}$$

$$p_{Ak}(z_r) = 4\pi\epsilon_0(\epsilon_{r,Ak} - 1)\frac{C(z,z+1)}{L(z)\epsilon_r(z)} \tag{2.72b}$$

The resulting expression for $P(z)$ reads

$$P(z) = 4\pi\frac{C(z-1,z)}{L(z)\epsilon_r(z)}(\Psi(z)-\Psi(z-1/2)) + 4\pi\frac{C(z,z+1)}{L(z)\epsilon_r(z)}(\Psi(z+1/2)-\Psi(z)) \tag{2.73}$$

Again, as in the cylindrical case, it is not exact to replace eq. 2.73 by eq. 2.62.

2.2.6 Chemical potential

The chemical potential $\mu_{i,t}$ of molecule i in state t is defined as

$$\mu_{i,t} = \left(\frac{\partial F}{\partial n_{i,t}}\right)_{\{n_{j\neq i,u\neq t}\}} \tag{2.74}$$

where F is the Helmholtz energy of the system. The physical process corresponding to the derivative in eq. 2.74 is transferring a molecule i in state t from its reference phase to the system or *vice versa*, while the number of all other molecules ($j \neq i$) and states ($u \neq t$) is fixed. The evaluation of the chemical potential for (end-)grafted molecules has lead to some confusion in the past [47] since their bulk volume fraction is zero. Their chemical potential will be discussed separately in section 2.2.8.

The derivative of eq. 2.74 is most easily evaluated for a bulk phase, since it has no gradients and an analytical expression for the free energy is available as soon as we know the bulk volume fractions φ_i^b of each molecule i and the relative amounts α_{Ak}^b of each state k for each segment A from which the number $n_{i,t}$ of molecules i in molecular state t follows.

The Helmholtz energy F of a bulk phase reads

$$\frac{F}{k_BT} = \sum_{i,t} n_{i,t}^b \ln \varphi_{i,t}^b + \frac{1}{2}\sum_{i,t,A,k} n_{i,t}^b N_{i,t,Ak} \sum_{B,l} \chi_{Ak,Bl}\varphi_{Bl}^b \tag{2.75}$$

Note that no electrostatic contributions are present in eq. 2.75 because the electrostatic potential Ψ is set to zero in the bulk.

When taking the derivative of eq. 2.75 to $n_{i,t}^b$ to evaluate eq. 2.74 we should be aware of the incompressibility constraint: placing an extra molecule i in the bulk phase changes the volume and therefore the volume fractions φ_j^b of all components j, even though n_j^b is constant for $j \neq i$. If we replace $\varphi_{i,t}^b$ by $n_{i,t}^b N_i / \sum_{i,t} n_{i,t}^b N_i$ the differentiation of $\varphi_{i,t}^b$ to $n_{i,t}^b$ is easily performed

$$\frac{\partial \varphi_{j,u}^b}{\partial n_{i,t}^b} = \frac{N_i(1-\varphi_{i,t}^b)}{\sum_i n_i^b N_i} \qquad \text{for} \quad i = j \quad \text{and} \quad t = u \tag{2.76a}$$

$$\frac{\partial \varphi_{j,u}^b}{\partial n_{i,t}^b} = -\frac{N_i \varphi_{j,u}^b}{\sum_i n_i^b N_i} \qquad \text{for} \quad i \neq j \quad \text{or} \quad t \neq u \tag{2.76b}$$

A similar approach is needed for the differentiation of φ_{Bl}^b with respect to $n_{i,t}^b$. The result of eq. 2.74 then reads

$$\begin{aligned}\frac{\mu_{i,t}}{k_BT} &= \ln \varphi_{i,t}^b + 1 - N_i \sum_j \varphi_j^b / N_j \\ &\quad + \sum_{A,k,B,l} N_{i,t,Ak}\chi_{Ak,Bl}\varphi_{Bl}^b - \frac{1}{2} N_i \sum_{A,k,B,l} \varphi_{Ak}^b \chi_{Ak,Bl}\varphi_{Bl}^b\end{aligned} \tag{2.77}$$

Linse and Björling [27] defined the chemical potential as

$$\mu_i = \left(\frac{\partial F}{\partial n_i}\right)_{n_j \neq n_i} \tag{2.78}$$

This yields correct results since all states t of a molecule i have the same chemical potential in their theory due to the fact that the state equilibria are all of the simple type given by eq. 2.1. When more complex state reactions are considered this approach breaks down since all states t of a molecule i may have different chemical potentials.

One might have some worries about contributions to the derivative 2.74 due to charges on the molecules. In principle, transferring a charged molecule from its reference phase to the bulk introduces a charge and consequently a non-zero electrostatic potential in the bulk. However, in a mean-field theory this potential would be equal throughout the bulk phase so that the chemical potential would depend on the size of the bulk phase. When measuring a chemical potential or activity in practice, the bulk phase remains electroneutral. No net charge occurs. This means that the derivative of eq. 2.74 is not operational in practice for charged molecules. If we take the example of the salt `NaCl`, we might define the chemical potential of single ionic species as

$$\mu_{\mathtt{Na}^+} = \mu^*_{\mathtt{Na}^+} + k_B T \ln a_{\mathtt{Na}^+} \tag{2.79a}$$

$$\mu_{\mathtt{Cl}^-} = \mu^*_{\mathtt{Cl}^-} + k_B T \ln a_{\mathtt{Cl}^-} \tag{2.79b}$$

However these definitions only contain non-operational terms, none of the terms represent a measurable quantity. Instead, the chemical potential of a neutral combination of ions is operational:

$$\mu_{\mathtt{NaCl}} = \mu^*_{\mathtt{NaCl}} + k_B T \ln a_{\mathtt{Na}^+} a_{\mathtt{Cl}^-} \tag{2.80}$$

For simplicity we do not pursue this point here and (as stated above) ignore any electric contributions to the chemical potential. We note that our chemical potentials are formally wrong for single charged species, since strictly speaking they are undefined. However, the chemical potentials for neutral combinations of charged species are correct. Since all systems under consideration are by definition electroneutral in equilibrium, this does not pose a problem. For more details see for example Lyklema [48].

2.2.7 State weighting factor and local dissociation

In sec. 2.2.5 the contribution to $u_{Ak}(z)$ due to electrostatics was derived. The only two undefined quantities in eq. 2.16 for the state potential are the reference potential u^{ref}_{Ak} and the value for β in the bulk. They are defined in such a way that $u^b_{Ak} = 0$. The same condition was used to derive eq. 2.27. Using eq. 2.19 we can rewrite eq. 2.27 as $C_{i,t} = \varphi^b_{i,t}/N_i$. Substituting this result in eq. 2.17 with the help of eq. 2.77 immediately leads to

$$u^{\mathrm{ref}}_{Ak} = \sum_i \frac{\varphi^b_i}{N_i} + \frac{1}{2} \sum_{Bl,Cm} \varphi^b_{Bl} \chi_{Bl,Cm} \varphi^b_{Cm} - \sum_{Bl} \chi_{Ak,Bl} \varphi^b_{Bl} \tag{2.81}$$

Substituting eq. 2.81 in eq. 2.16, setting both $u_{Ak}(z)$ and the electric potential Ψ to zero for the bulk, and realising that 2.61 is zero in the bulk enables us to write:

$$\beta^b = -\sum_i \frac{\varphi^b_i}{N_i} - \frac{1}{2} \sum_{Bl,Cm} \varphi^b_{Bl} \chi_{Bl,Cm} \varphi^b_{Cm} \tag{2.82}$$

Now we can rewrite eq. 2.16 in the following simple form:

$$\begin{aligned} u_{Ak}(z) = \beta(z) - \beta^b + \sum_{Bl} \chi_{Ak,Bl} \left(\langle \varphi_{Bl}(z) \rangle - \varphi^b_{Bl} \right) \\ + v_{Ak} e \frac{\Psi(z)}{k_B T} - \frac{1}{2} \epsilon_0 (\epsilon_{r,Ak} - 1) \frac{P(z)}{k_B T} \end{aligned} \tag{2.83}$$

The various terms in eq. 2.83 represent the volume filling constraint $(\beta(z) - \beta^b)$ and the contribution to the state potential due to contact interactions, free charges, and polarisation charges, respectively.

In order to obtain the volume fractions of states we have to revisit eq. 2.24. Summing over all segments s that are of type A and over all molecule types i yields the volume fraction $\varphi_A(z)$ of A. The relative dissociation of state k of segment A is found from

$$\alpha_{Ak}(z) = \frac{\alpha^b_{Ak} G_{Ak}(z)}{G_A(z)} \tag{2.84}$$

from which the volume fraction of state k is easily calculated as

$$\varphi_{Ak}(z) = \alpha_{Ak}(z) \varphi_A(z) \tag{2.85}$$

2.2.8 Chemical potential of grafted molecules

The chemical potential for molecules which are not grafted is given in sec. 2.2.6. When the molecules are grafted, e.g. to a surface, the bulk volume fraction φ^b_i is zero and the derivative of eq. 2.75 is undefined. However, changing the grafting density at a fixed amount of surface area does lead to a change in the Helmholtz energy of the inhomogeneous system. When the amount of all other molecules in the system is fixed, this change in the free energy is a measure for the chemical potential. However, in general the amount of all other molecules is not easily fixed in the system. Therefore, the following Legendre transformation is convenient

$$X = F - \sum_{\mu_{i,t}=\mathtt{fixed}} \frac{\theta_{i,t}}{N_i} \mu_{i,t} \tag{2.86}$$

where $\theta_{i,t}$ is defined by eq. 2.28. The number $n_{i,t}$ of molecules i in state t present in the system equals $n_{i,t} = \theta_{i,t}/N_i$. The chemical potential can be defined as following from

$$\mu_{i,t} = \frac{\partial X}{\partial(\theta_{i,t}/N_i)} \tag{2.87}$$

This is a generalisation of the procedure followed by Currie et al. [47] to determine the chemical potential of end-grafted homopolymers. The sum in eq. 2.86 runs over all molecules i and their state t for which the system is open or, equivalently, for which the chemical potential is fixed upon differentiating. For all other states t of molecules (except of course the one that is differentiated), the total amount θ should be constant upon differentiating.

Note that this procedure is numerically quite expensive. It involves solving the full set of self-consistent-field equations for at least two values of $\theta_{i,t}$. The number of computations depend on the desired accuracy. Numerical procedures are available that take all computations of X for different $\theta_{i,t}$ into account to obtain a good estimate of both $\mu_{i,t}$ and the numerical error in this value [49].

In general, the above procedure cannot be followed for grafted molecules with state equilibria. All states t of molecule i may have a different chemical potential and upon adding a grafted molecule i in state t both μ and n of all other states of the molecule will change. This means that the Legendre transformation cannot be used.

As we mentioned earlier, eq. 2.77 cannot be used for grafted molecules directly, since $\varphi^b_{i,t}$ is zero in this case, so the equation is undetermined. However, eq. 2.77 was derived for the special case of a bulk phase, whereas eq. 2.17 is more general. An expression for $\mu_{i,t}$ is found by substituting eqs. 2.19 and 2.81 in eq. 2.17

$$\begin{aligned}\frac{\mu_{i,t}}{k_BT} &= \ln N_iC_i + \sum_{A,k} N_{i,t,Ak}\ln\alpha_{Ak} + 1 - \ln\sigma_i^\dagger - \delta(\dagger) - N_i\sum_j \varphi_j/N_j \\ &+ \sum_{A,k,B,l} N_{i,t,Ak}\chi_{Ak,Bl}\varphi_{Bl} - \frac{1}{2}N_i\sum_{A,k,B,l}\varphi_{Ak}\chi_{Ak,Bl}\varphi_{Bl}\end{aligned} \tag{2.88}$$

where the terms $\ln\sigma^\dagger$ and $\delta(\dagger)$ only apply for a chemically grafted (immobile) molecule; their meaning is explained below eq. 2.13. For mobile grafted molecules, e.g. interfacial molecules in a Langmuir-Blodgett layer, these terms are zero. For a molecule that is also present in the bulk $C_i = \varphi_i^b/N_i$ so that eq. 2.77 is recovered from 2.88. In other words eq. 2.88 is a more general version of eq. 2.77. We checked numerically that the results for μ_i from eqs. 2.88 and 2.87 are identical, also for charged molecules. Note that through the use of eq. 2.81 in the derivation of eq. 2.88 we implicitly used eq. 2.77 for the chemical potential of the bulk phase and the condition that $u_{Ak} = 0$ in the bulk phase.

2.2.9 Other thermodynamic quantities

The Helmholtz energy F of the inhomogeneous system is given by

$$F = -k_BT\ln Q \tag{2.89}$$

Substituting eq. 2.14 in the logarithmic term of eq. 2.5 and summing over c and i yields an expression for the conformational and mixing entropy

$$
\begin{aligned}
S^{\text{conf,mix}}/k_B = \ln\Omega = -\sum_{i,t}\frac{\theta_{i,t}}{N_i}\ln N_i C_{i,t} \\
+\sum_{i,t}\frac{\theta_i^\dagger}{N_i}\ln\sigma_i^\dagger - \sum_z{}' \sum_{A,k} L(z)\varphi_{Ak}(z)\ln G_{Ak}(z)
\end{aligned}
\tag{2.90}
$$

where the prime in the last term denotes that the sum is *not* taken over the surfaces. The dagger (†) indicates again immobile grafted chains. The term which contains $\ln\sigma_i^\dagger$ corrects for the fact that these chains do not have a mixing entropy.

After substituting eqs. 2.6, 2.7, and 2.90 into eq. 2.8 and using eq. 2.15, the Helmholtz energy eq. 2.89 can be written as

$$
\begin{aligned}
\frac{F}{k_BT} &= \sum_i \frac{\theta_i}{N_i}\ln N_iC_i - \sum_i\frac{\theta_i^\dagger}{N_i}\ln\sigma_i^\dagger \\
&+\sum_{A,k}\theta_{Ak}\ln\alpha_{Ak}^b - \sum_z{}'\sum_{A,k}L(z)\varphi_{Ak}(z)u_{Ak}(z) \\
&+\frac{1}{2}\sum_{z,A,k,B,l}L(z)\varphi_{Ak}(z)\chi_{Ak,Bl}\langle\varphi_{Bl}(z)\rangle + \frac{1}{2}\sum_{z,A,k}L(z)ev_{Ak}\varphi_{Ak}(z)\frac{\Psi(z)}{k_BT}
\end{aligned}
\tag{2.91}
$$

Note that when computing interaction curves with the normalisation given by eq. 2.30 the sums over z include the bulk phase with a dimensionless volume of L^b.

The grand potential Δ is found from $\Delta = -k_BT\ln\Xi = F - \sum_{i,t} n_{i,t}\mu_{i,t}$ where the sum over the chemical potentials of states t is found from summing eq. 2.88 over all states:

$$
\begin{aligned}
\sum_t n_{i,t}\frac{\mu_{i,t}}{k_BT} = \frac{\theta_i}{N_i}\ln N_iC_i + \frac{\theta_i}{N_i} - \theta_i\sum_j\frac{\varphi_j^b}{N_j} - \frac{\theta_i^\dagger}{N_i}(1+\ln\sigma_i^\dagger) + \sum_{A,k}\theta_{i,Ak}\ln\alpha_{Ak}^b \\
+\sum_{A,k,B,l}\theta_{i,Ak}\chi_{AkBl}\varphi_{Bl}^b - \frac{1}{2}\theta_i\sum_{A,k,B,l}\varphi_{Ak}^b\chi_{AkBl}\varphi_{Bl}^b
\end{aligned}
\tag{2.92}
$$

Summing this equation over all molecules i and subtracting the result from eq. 2.91, using eq. 2.83 we end up with

$$\begin{aligned}\frac{\Delta}{k_BT} = &\sum_i \frac{\theta_i^\dagger}{N_i} - \sum_i \frac{\theta_i}{N_i} + \sum_z{}' \sum_i \frac{L(z)\varphi_i^b}{N_i} - \sum_z L(z)(\beta(z) - \beta^b) \\ &- \frac{1}{2}\sum_z{}' \sum_{A,k,B,l} L(z)\left[\varphi_{Ak}(z)\chi_{Ak,Bl}\langle\varphi_{Bl}(z)\rangle - \varphi_{Ak}^b\chi_{AkBl}\varphi_{Bl}^b\right] \\ &- \frac{1}{2}\sum_z{}' \sum_{A,k} L(z)ev_{Ak}\varphi_{Ak}(z)\frac{\Psi(z)}{k_BT} + \frac{1}{2}\sum_z{}'' \sum_{A,k} L(z)ev_{Ak}\varphi_{Ak}(z)\frac{\Psi(z)}{k_BT} \\ &+ \frac{1}{2}\sum_z{}' \sum_{A,k} L(z)\varphi_{Ak}(z)\epsilon_0(\epsilon_{r,Ak} - 1)\frac{P(z)}{k_BT}\end{aligned} \tag{2.93}$$

where the prime denotes again that the sum over z is not over the surfaces. Note that this also affects the sitefraction $\langle\ldots\rangle$ operator. The double prime denotes that the sum is *only* over the surfaces. It is easily verified that the contribution of the bulk phase to $\ln\Xi$ is zero, since the electrostatic potential Ψ and the electric field E are zero in the bulk. The term θ_i/N_i is the ideal gas pressure which is absent for chemically attached molecules, since it cancels against the first term in eq. 2.93.

For grafted (non-dissociating) homopolymers, eq. 2.93 reduces to eq. 19 of Carignano and Szleifer [15], both for mobile and immobile grafted chains. This fact is an illustration of the similarities between their theory and ours. Some differences have been discussed in sec. 2.2.4.

In the case of a system with only one planar interface the function $\ln\Xi = -\Delta/k_BT$ represents γA, where γ is the surface tension and A the surface area. Then γ also denotes minus the surface pressure Π. Therefore, contrary to what was claimed in ref. [47], an explicit expression for Π can be given within the SCF theory for grafted molecules, which is a function of the way the molecules are grafted (mobile vs. immobile). In the absence of electrostatic interactions and reactions, this expression is similar to the expression derived in the theory of Carignano and Szleifer [15].

The theory presented here needs to be evaluated numerically. Due to the high computational demand of the equations in many applications, a dedicated computer program is mandatory. It should be clear that the implementation of the thermodynamical equations is rather prone to errors. A good test is based upon the Gibbs adsorption law. Evidently, this law should be obeyed in all cases. It can be written as

$$\left(\frac{\partial X}{\partial \mu_{i,t}}\right)_T = -\frac{\sum_z (\varphi_{i,t}(z) - \varphi_{i,t}^b)}{N_i} \tag{2.94}$$

where X follows from the Legendre transformation given by eq. 2.86. Also, the result from the numerical evaluation of $\mu_{i,t}$, i.e. eq. 2.87, should be equal to the result of eq. 2.88. Our implementation passes these tests consistently upto the highest attainable numerical accuracy, where the relative error lies in the order of 10^{-10}, showing the internal consistency of both the equations and their implementation.

2.2.10 Reaction equilibria

Generally, reaction equilibria can be written as:

$$\sum_x \nu_x S_x = 0 \tag{2.95}$$

where S denotes both products and reactants. The stoichiometric coefficients ν_x of products are positive and those of reactants negative. The thermodynamic equilibrium constant K is written as

$$K = \prod_x (a_x)^{\nu_x} \tag{2.96}$$

where a_x is the activity of the component x. The definition of the chemical potential gives the relationship of K with thermodynamic quantities

$$\mu_x = \mu_x^* + k_B T \ln a_x = \mu_x^* + k_B T \ln \gamma_x \varphi_x^b \tag{2.97}$$

where μ, γ, and φ^b are the chemical potential, activity coefficient, and bulk volume fraction, respectively. The superscript $*$ denotes the reference state consisting of the pure component x. In equilibrium

$$\sum_x \nu_x \mu_x = 0 \tag{2.98}$$

so that the equilibrium constant K can be rewritten as

$$\ln K = -\frac{1}{k_B T} \sum_x \nu_x \mu_x^* = \sum_x \nu_x \ln \gamma_x \varphi_x^b \tag{2.99}$$

An alternative way to write the reaction constant is to decompose the internal free energy μ^* of the components involved into an enthalpic and entropic part as was done in Linse and Björling [27].

$$\ln K = -\frac{1}{k_B T} \sum_x \nu_x \mu_x^* = -\frac{1}{k_B T} \sum_x \nu_x \left(U_x^* - k_B T \ln g_x^*\right) \tag{2.100}$$

where U_x^* and g_x^* denote the internal energy and degeneration of component x, respectively. This formulation can be used to model the temperature dependence of the state equilibria [27].

Since in our theory the reference phases are incorporated in the chemical potentials, eq. 2.97 simplifies to

$$\mu_{i,t} = k_B T \ln a_x = k_B T \ln \gamma_{i,t} \varphi_{i,t}^b \tag{2.101}$$

A comparison with eq. 2.77 leads to an expression for the activity coefficient $\gamma_{i,t}$. With the help of eqs. 2.77, 2.82, 2.96, and 2.101 it is straightforward to derive

$$\begin{aligned} \ln K^R &= \frac{1}{k_B T} \sum_{i,t} \nu_{i,t}^R \mu_{i,t} \\ &= \sum_{i,t} \nu_{i,t}^R \left(\ln \varphi_{i,t}^b + N_i (1 + \beta^b) + N_{i,t,A,k} \sum_{Bl} \chi_{Ak,Bl} \varphi_{Bl}^b \right) \end{aligned} \tag{2.102}$$

Here, R is a label for the particular reaction at hand $\nu_{i,t}^{R}$ is the stoichiometric reaction coefficient of molecule i in state t for reaction R. This equation is quite general: it allows for different equilibrium constants K for each state t of any molecule i.

However, in secs. 2.2.1 and 2.2.4 we have made the approximation that the reactions are considered at a segment level only. This means for example that the reactions

$$\mathrm{(HA)_2 + H_2O \rightleftarrows HAA^- + H_3O^+} \tag{2.103a}$$

$$\mathrm{HAA^- + H_2O \rightleftarrows A_2^{2-} + H_3O^+} \tag{2.103b}$$

have the same equilibrium constant. In the particular example at hand, this seems a rather severe approximation. However, when the interest is in dissociating polymers it is numerically impossible to account for all different states t of the molecules and their corresponding reaction constants. In principle, it is possible to assign a different reaction constant for dissociation of a segment which is linked to an already dissociated segment in the polymer. This approach has proven successful for calculations in the bulk [34]. In our theory such an approach requires a more complex handling of the chain propagators. Another approach for this particular example is to distinguish between the two HA segments and assign two different dissociation constants.

Note that for grafted polymers the current approximation should work rather well. As the first segment dissociates, an electrostatic potential is built up which affects the dissociation of subsequent segments; this potential is computed self-consistently. In contrast, in the bulk phase the electrostatic potential is zero, and the mean-field approximation does not work well: the intra-molecular swelling of chains is neglected. To model the dissociation of a bulk chain one could graft it to the centre of a spherical geometry so that its dissociation is affected by its own electrostatic potential [50].

For equilibria that have an equal amount of states t on the left and right hand side of the reaction equation for each molecule type i, the term $N_i(1+\beta^b)$ drops out of eq. 2.102. When the reactions are considered at a segment level only, as is done here, eq. 2.102 can be simplified to

$$\ln K^R = \sum_{Ak} \nu_{Ak}^{R}(\ln \varphi_{Ak}^{b} + \delta_{Ak}(\text{comp.})(1+\beta^b) + \sum_{Bl} \chi_{AkBl}\varphi_{Bl}^{b}) \tag{2.104}$$

where δ(comp.) is unity when the state Ak may complex with a (chain) segment (as is the case for segment B in eq. 2.2) and zero otherwise (i.e. the chain segment states A and AB in eq. 2.2. Note that in the formulation of eq. 2.104 only monomers may complex with a (chain) segment. Also, the volume of the complexed segment is again equal to ℓ^3.

Since the reaction equations may be of arbitrary complexity, a numerical scheme is needed to compute the values for α^b. This numerical scheme is described in appendix 2.A.

2.3 Concluding remarks

A general self-consistent field theory for polyelectrolytes with dissociating segments (or more generally, polymers subject to complexation reactions) has been put forward. We have shown that within this framework the volume fraction profiles of chain molecules in inhomogeneous systems can be obtained. Also expressions for thermodynamical functions like the chemical potential and the surface tension have been derived. These thermodynamical expressions pass all known tests for internal consistency.

The contribution to the state potential $u_{Ak}(z)$ in eq. 2.16 due to the electrostatic interactions is given by eq. 2.61. The last term in this equation has been neglected before [40, 41]. This omission has no consequences when the the relative dielectric permittivity $\epsilon_r(z)$ is equal for all segment states Ak. This is because the error in $u_{Ak}(z)$ is equal for all states Ak and cancels when evaluating the volume fraction profiles. However, when gradients in $\epsilon_r(z)$ are present in the system, as in refs. [40, 41], this omission leads to different volume fraction profiles and inconsistent values for the thermodynamic functions.

As we have seen in sec. 2.2.5 the precise formulation of the contribution to the segment potential of polarisation charges in curved geometries is not straightforward. This is due to the (necessary) discretisation of the equations. When eq. 2.62 (which is strictly valid only for planar geometry) is used for a curved geometry instead of the curved variants eqs. 2.68 and 2.73, an error in the Gibbs equation 2.94 is introduced of about 0.1%. Although the error is small, the thermodynamical inconsistency introduced this way is not always negligible and may lead to physically unrealistic results. For example, the mechanical properties of a lipid bilayer can be calculated using a second order expansion of the surface tension in the curvature. It is clear that a small systematic error in the surface tension may have a large effect on the coefficients of this expansion.

The discretisation of the electrostatic equations was done using a capacitor model. Although we have shown that the discretisation of the equations is exact within this model, it is unclear whether a capacitor model is the suitable one. The discretisation is done at a molecular/atomic length scale whereas a capacitor is macroscopic in nature. Furthermore, the resulting equations of the capacitor model are rather complex. Work is in progress to simplify the formulation of these equations, abandoning the capacitor model.

Throughout this chapter, the approximation of equal volume for each segment was used. For segments that may form complexes we have used the approximation that the complex has the same volume as the non-complexed segment. This influences the equilibria of complex formation in inhomogeneous systems. A more realistic approach would be to assign a double volume for the complex. In principle, it should be possible to assign more or less arbitrary volumes to segments. However, the equations would become more complex.

In this chapter only the theory was discussed, without applying it to a real (physical) problem. Due to the numerical nature of the theory, evaluation of the equations is done with a dedicated software package `sfbox` [16]. The key design goals of this software package have been ease of use and flexibility. The ease of use was achieved by introducing a simple user interface which checks for subtle errors in the input parameters. Flexibility means that a great deal of different problems can be dealt with. Partly, this is a numerical problem. The SCF equations are essentially a system of coupled highly non-linear equations. They are solved using the method outlined in appendix C. The chain propagators may cause numerical over- or underflows, especially in charged systems. Furthermore, the propagators may require an excessive amount of computer memory for long chains. A solution to both problems is presented in appendix A.

2.A Numerical procedure

The values for the relative dissociation rates in the bulk α^b_{Ak} need to be determined numerically, as we know of no general analytical scheme. The α values are in the range from 0 to 1, but it is convenient to transform them to unbounded variables while linearising the equations as much as possible.

The first iteration variable is $x_1 = \log\left[\varphi^b_s/(1-\varphi^b_s)\right]$, where φ^b_s is the bulk volume fraction of solvent (s) molecules, which is adjusted to ensure

$$\sum_i \varphi^b_i = 1 \tag{2.105}$$

so that in the bulk the constraint of volume filling is obeyed.

The second iteration variable is $x_2 = \log\left[\varphi^b_n/(1-\varphi^b_n)\right]$, where φ^b_n is the bulk volume fraction of neutraliser (n), which is adjusted to ensure

$$\sum_i \varphi^b_i N_{i,Ak} v_{Ak} = 0 \tag{2.106}$$

which guarantees the electroneutrality of the bulk. This condition is not needed when the amount θ_i of all charged molecules in the system is fixed and their charges add up to zero. In this case there is no neutraliser present in the system.

It proved convenient to introduce *ratios* of α, when two states of the same segment type are present in the left and right hand side of the reaction equation. In this case the volume fraction φ^b_A drops out of the equation and the ratio between α^b values of the corresponding states at the left and right hand side is taken. The logarithm of these ratios are used as unconstrained iteration variables. In the case of complexation the volume fraction is again transformed into an unconstrained variable as $x = \log\left[\varphi^b/(1-\varphi^b)\right]$. The reaction equations 2.104 together with equations that may fix either a certain α^b or a given φ^b of a state in the bulk complete the set of equations.

In the case of a molecule with different states that is present in the system with a fixed amount, the bulk volume fraction φ^b is not known *a priori*: it is found from equating eqs. 2.29 and 2.27 *after* the self-consistent-field (SCF) solution is found. This means that the values for α^b are not known at the start of the numerical procedure to find the SCF solution. Updating the α^b values at each step in the SCF iteration does not work because it leads to large, undamped oscillations in the iteration variables for subsequent iterations. Instead, the values for α^b are fixed to a certain value and the corresponding SCF solution is computed. Then the α^b values are recomputed. With these new values for α^b, a new SCF solution is computed. This procedure is repeated until the α^b values have converged. To obtain a precision in the α^b values of 14 significant digits the procedure needs to be repeated about 10 times.

3 Bending moduli for adsorbed homopolymer layers

ABSTRACT

The influence of adsorbing homopolymers on the bending moduli of surfactant membranes is analysed theoretically. An impenetrable surface is used as a model for the membrane. The homopolymers are either reversibly or irreversibly adsorbed. When changing from reversible to irreversible adsorption the bending rigidity k_c increases, whereas both the Tolman length and the saddle-splay modulus are unaffected. A general proof for these findings is presented, independent of a molecular model. Numerical Self-Consistent-Field theory is used to calculate the bending moduli. Two adsorption mechanisms are considered. The first one is called 'adsorption on sites'. Here the adsorption energy per segment is constant upon bending. The second one is adsorption through contact interactions, where the adsorption energy per segment changes upon curving the interface. Both methods give qualitatively different results: the sign of the polymer contribution to the bending constants may depend on the method used. The numerical results are compared to an analytical mean-field theory.

3.1 Introduction

Self-assembly of surfactant molecules may lead to a number of different types of aggregates. One of them is a bilayer where the head groups of the surfactants are on the outside of the membrane, protecting the tails from an (unfavourable) interaction with the solution. These bilayers may form lamellar phases or vesicles.

The stability of a lamellar phase or vesicle is determined in part by the bending properties of the bilayer. In particular when the membranes are flexible, i.e. when there is a low bending rigidity, relatively large shape fluctuations are permitted and consequently a large spacing is found between bilayers of a lamellar phase.

Several theoretical attempts have been made to predict the influence of an adsorbing polymer layer on the flexibility of a membrane [17, 51, 52]. The general trend found from those theories is that the influence of the polymer layer is relatively weak. This may explain the lack of experimental data in the literature. However, the rigidity of the membrane has a significant effect on phase behaviour when it is small so even a small polymer contribution may become important in this case.

The flexibility of interfaces is generally expressed by the bending moduli k_c and $\bar{k}$. The bending modulus k_c is a measure for the rigidity of the membrane. The saddle-splay modulus $\bar{k}$ expresses the resistance of the interface to assume a saddle shape.

The influence of polymer adsorption on the bending moduli was first discussed by de Gennes [51]. However, his scaling approach did not yield the sign of the contribution of the polymer layer to the bending moduli. Using a mean-field model, Brooks et al. [52] found the surprising result that adsorption of polymer makes the membrane less stiff. Clement and Joanny [17] also used a mean field theory and found the same result.

In this work we use a numerical Self-Consistent-Field (SCF) theory to revisit this problem. We will compare our results with those of Clement and Joanny [17]. Within our model, the bending modulus turns out to be *not* always negative. Most notably, when the polymer layer is irreversibly adsorbed, we predict a positive contribution from the polymer layer for a range of adsorption energies. The system under consideration is not only of practical interest but is also very suitable to illustrate some pitfalls in the calculation of bending moduli from excess pressure profiles.

In the following we will first recapitulate the Helfrich equation. Then the influence of reversible and irreversible adsorption on the bending constants is derived, independent of a molecular model. The bending moments are also written as a function of $\mathcal{P}$, the excess local tangential pressure. After this general treatment, the focus is on homopolymer adsorption. The fundamentals of the numerical SCF mean-field theory are explained followed by some analytical results from a ground-state approximation.

3.2 Curvature thermodynamics

In this section we will not yet focus on polymers but derive a general framework to obtain the bending constants, both for reversible and irreversible adsorption, and explain how these bending constants are derived from the excess tangential pressure profile.

3.2.1 The Helfrich equation

Uniformly curved interfaces are characterised by the curvatures J and K defined by

$$J = \frac{1}{R_1} + \frac{1}{R_2} \tag{3.1}$$

$$K = \frac{1}{R_1 R_2} \tag{3.2}$$

where R_1 and R_2 are the two radii of curvature which, at each point at the surface, define the local shape of it. Upon bending an initially planar interface the surface tension will change. For uniformly curved interfaces this change is described by the Helfrich equation [53]. The Helfrich equation (3.3) is a second order expansion in inverse curvature radii R_1 and R_2 of the surface tension around a planar interface. So this equation is valid for small curvatures ($J \ll 1$ and $K \ll 1$). It is given by

$$\gamma(J,K) = \gamma^0 - k_c J_0 J + \frac{1}{2} k_c J^2 + \bar{k} K \tag{3.3}$$

where γ^0 is the surface tension of the planar interface. Eq. 3.3 defines the bending modulus k_c, the saddle splay modulus $\bar{k}$, and the parameter J_0, often referred to as the spontaneous curvature. As we will show below, J_0 does not generally correspond to the spontaneous curvature. However, for simplicity we will retain this name. The Tolman length is defined to be the distance between the Gibbs dividing plane and the surface of tension of the planar interface. It can be calculated as $k_c J_0/\gamma^0$ [54, 55].

To obtain values for the spontaneous curvature J_0 and the bending moduli k_c and $\bar{k}$, the surface tension γ should be explicitly expressed in the curvatures J and K. Or, if an explicit expression cannot be derived, the surface tension should be fitted to eq. 3.3. For most molecular models it is convenient to make use of homogeneously curved geometries, in particular cylindrical and spherical surfaces. For a cylindrical geometry ($K = 0$) eq. 3.3 reduces to

$$\gamma(J) = \gamma^0 - k_c J_0 J + \frac{1}{2} k_c J^2 \tag{3.4}$$

So, from the evaluation of $\gamma(J)$ in a cylindrical geometry we get values (or expressions) for k_c and J_0. In a spherical geometry ($K = \frac{1}{4} J^2$) eq. 3.3 reduces to

$$\gamma(J) = \gamma^0 - k_c J_0 J + \frac{1}{2}\left(k_c + \frac{1}{2}\bar{k}\right) J^2 \tag{3.5}$$

which shows that $\bar{k}$ can be obtained from an evaluation of $\gamma(J)$ in a spherical geometry once k_c is available from the analysis in a cylindrical geometry.

3.2.2 Reversible and irreversible adsorption

The general expression for the differential of the surface tension for a curved surface reads [56]

$$\mathrm{d}\gamma = -s^s \mathrm{d}T + C_1 \mathrm{d}J + C_2 \mathrm{d}K - \sum_i \Gamma_i \mathrm{d}\mu_i \tag{3.6}$$

where s^s is the excess entropy per unit area, Γ_i the excess number of molecules of type i per unit area and μ_i is the chemical potential of molecule i. The coefficients C_1 and C_2 are the so-called bending stress and torsion stress, respectively [57].

Let us first consider a solid wall. Interactions between the wall and the molecules lead to adsorption phenomena. Here we will consider the wall to be inert, adsorption of molecules does not change the properties of the wall. If the wall models a bilayer membrane, this is a simplifying assumption since generally adsorption will lead to changes in the structure of the membrane.

When the adsorption and desorption processes are fast compared to the shape fluctuations of the interface, one may consider the adsorption to be reversible. Then the amount of molecules that adsorb onto the interface is fully controlled by the chemical potentials and adsorption energies.

The bending constants for reversible adsorption are readily obtained in this system. Since the bulk phase is assumed to be infinite, all chemical potentials are constant upon bending the interface. Comparing eq. 3.3 and eq. 3.6 leads to

$$-k_c J_0 = \left(\frac{\partial \gamma}{\partial J}\right)^0_{K,T,\{\mu_i\}} = (C_1)^0 \tag{3.7a}$$

$$k_c = \left(\frac{\partial^2 \gamma}{\partial J^2}\right)^0_{K,T,\{\mu_i\}} = \left(\frac{\partial C_1}{\partial J}\right)^0_{K,T,\{\mu_i\}} \tag{3.7b}$$

$$\bar{k} = \left(\frac{\partial \gamma}{\partial K}\right)^0_{J,T,\{\mu_i\}} = (C_2)^0 \tag{3.7c}$$

where as usual the subscripts denote the variables that are kept constant upon differentiating and the superscript 0 denotes evaluation at the planar interface. These results are consistent with the more general equations that have been derived before [55].

Alternatively, when the adsorption and desorption rates are much lower than the rate of shape changes, we should consider the irreversible case. Irreversible adsorption is defined as follows: upon bending the interface the adsorbed amount per unit area is constant. The adsorbed amount per unit area is calculated at the planar interface at full equilibrium. When considering the irreversible adsorption of, say, molecule type p the population of p needs to be split up into an adsorbed (denoted by a superscript a) and a free (denoted by a superscript f) part.

The new state variable corresponding to the irreversible adsorption case is found from a Legendre transformation.

$$X = \gamma + \Gamma^a_p(\mu^a_p - \mu^f_p) \tag{3.8}$$

The subtraction of μ^f_p ensures that X equals γ at the planar interface. For a planar interface $\mu^a_p = \mu^f_p$ because the planar interface is defined to be in equilibrium. Upon bending the interface the chemical potential μ^f_p of the free molecules is taken to be constant. When the molecules p are irreversibly adsorbed the chemical potential μ^a_p of the adsorbed part of the population is not constant.

The split-up of molecules p in adsorbed and free species means that $\Gamma_p \mathrm{d}\mu_p$ in eq. 3.6 has to be replaced by $\Gamma^a_p \mathrm{d}\mu^a_p + \Gamma^f_p \mathrm{d}\mu^f_p$. The differential of X now reads

$$\mathrm{d}X = -s^s \mathrm{d}T + C_1 \mathrm{d}J + C_2 \mathrm{d}K - \Gamma_p \mathrm{d}\mu^f_p + \mu^a_p \mathrm{d}\Gamma^a_p - \mu^f_p \mathrm{d}\Gamma^a_p - \sum_{i \neq p} \Gamma_i \mathrm{d}\mu_i \tag{3.9}$$

The bending constants are calculated in a way similar to that for the reversible case. In contrast to the reversible case $X(J, K)$ is computed and, instead of the chemical potential μ^a_p of the adsorbed molecules, the adsorbed amount Γ^a_p is kept constant.

$$-k_c^{\,\mathrm{irr}} J_0^{\,\mathrm{irr}} = \left(\frac{\partial X}{\partial J}\right)^0_{K,T,\{\mu_{i\neq p}\},\mu_p^f,\Gamma_p^a} = (C_1)^0 \tag{3.10a}$$

$$k_c^{\,\mathrm{irr}} = \left(\frac{\partial^2 X}{\partial J^2}\right)^0_{K,T,\{\mu_{i\neq p}\},\mu_p^f,\Gamma_p^a} = \left(\frac{\partial C_1}{\partial J}\right)^0_{K,T,\{\mu_{i\neq p}\},\mu_p^f,\Gamma_p^a} \tag{3.10b}$$

$$\bar{k}^{\,\mathrm{irr}} = \left(\frac{\partial X}{\partial K}\right)^0_{J,T,\{\mu_{i\neq p}\},\mu_p^f,\Gamma_p^a} = (C_2)^0 \tag{3.10c}$$

It is trivial to see that the product $k_c^{\,\mathrm{irr}} J_0^{\,\mathrm{irr}}$ and $\bar{k}^{\,\mathrm{irr}}$ for the irreversible adsorption are identical to the reversible case. The equation for the bending modulus k_c^{irr} is comparable to that of the reversible case but it has different constraints on the derivative. The different constraints for the irreversible case lead to a different value for k_c, whereby it is expected that k_c is higher for the irreversible case. This is due to the fact that a constraint is added. Upon bending, the phase space is restricted which leads to higher values for γ compared to the equilibrium case. As can be seen from eq. 3.8 and comparing eqs. 3.7 and 3.10, γ for the irreversible case is equal to γ for the reversible case up to first order in curvature. Therefore, irreversible adsorption necessarily leads to an increase of k_c.

3.2.3 The local tangential pressure

It is possible to write the grand potential Ω as a function of the local tangential pressure $p_T(\vec{r})$.

$$\Omega = -\int_V p_T(\vec{r})\mathrm{d}\vec{r} \tag{3.11}$$

When the bulk tangential pressure in the bulk phase is denoted by p^b it follows that the excess grand potential Ω^s, defined by $\Omega^s = \Omega - \Omega^b$, is given by

$$\Omega^s = -\int_V p_T(\vec{r})\mathrm{d}\vec{r} + \int_V p^b \mathrm{d}\vec{r} \tag{3.12}$$

Introducing the excess tangential pressure profile $\mathcal{P}(\vec{r})$ as

$$\mathcal{P}(\vec{r}) = p_T(\vec{r}) - p^b(\vec{r}) \tag{3.13}$$

then gives with eqs. 3.12 and 3.13 $\gamma A = \Omega^s$ as a function of $\mathcal{P}$

$$\gamma A = -\int_V \mathcal{P}(\vec{r})\mathrm{d}\vec{r} \tag{3.14}$$

For uniformly curved interfaces the volume integral of eq. 3.14 is replaced by

$$\gamma A = -\int A(R)\mathcal{P}(R)\mathrm{d}R \tag{3.15}$$

where $A(R)$ is the area at radius R and $\mathcal{P}(R)$ equals the excess tangential pressure profile. If we take an arbitrary dividing plane at R_s to define the curvature and the area A of the interface, it can be shown that for an arbitrary function $f(R)$ and an uniformly curved interface

$$\int A(R)f(R)\mathrm{d}R = A(R_s)\int f(R)\left[1+(R-R_s)J+(R-R_s)^2K\right]\mathrm{d}R \tag{3.16}$$

We define $\mathbb{P}_n$ to be the n-th moment of the excess pressure profile:

$$\mathbb{P}_0 = \int \mathcal{P}(R)\mathrm{d}R \tag{3.17a}$$

$$\mathbb{P}_1 = \int (R-R_s)\mathcal{P}(R)\mathrm{d}R \tag{3.17b}$$

$$\mathbb{P}_2 = \int (R-R_s)^2\mathcal{P}(R)\mathrm{d}R \tag{3.17c}$$

so eq. 3.15 can be rewritten as

$$\gamma = -\mathbb{P}_0 - \mathbb{P}_1 J - \mathbb{P}_2 K \tag{3.18}$$

where γ is defined at R_s. Below we will use R_s equal to the radius of a solid sphere or cylinder.

3.2.4 Bending moduli in terms of pressure profiles

The Taylor expansion of the surface tension to second order in inverse curvature radii reads

$$\gamma = \gamma^0 + \left(\frac{\partial\gamma}{\partial J}\right)_K^0 J + \frac{1}{2}\left(\frac{\partial^2\gamma}{\partial J^2}\right)_K^0 J^2 + \left(\frac{\partial\gamma}{\partial K}\right)_J^0 K \tag{3.19}$$

where again the subscripts denote constant variables upon differentiating and the superscript 0 means that the expression is evaluated at the planar interface. When the derivatives in eq. 3.19 are rewritten using the exact relation (3.18), we have

$$\gamma = \gamma^0 - \left(\mathbb{P}_1 + \frac{\partial\mathbb{P}_0}{\partial J}\right)^0 J - \left(\frac{\partial\mathbb{P}_1}{\partial J} + \frac{1}{2}\frac{\partial^2\mathbb{P}_0}{\partial J^2}\right)^0 J^2 - \left(\mathbb{P}_2 + \frac{\partial\mathbb{P}_0}{\partial K}\right)^0 K \tag{3.20}$$

Mapping eq. 3.20 on the Helfrich equation (3.3) is a valid operation since they are both expansions in γ up to second order in curvature. This yields one of the central results of Oversteegen and Blokhuis [55]

$$-k_c J_0 = -\left(\mathbb{P}_1 + \frac{\partial\mathbb{P}_0}{\partial J}\right)^0 \tag{3.21a}$$

$$k_c = -\left(2\frac{\partial\mathbb{P}_1}{\partial J} + \frac{\partial^2\mathbb{P}_0}{\partial J^2}\right)^0 \tag{3.21b}$$

$$\bar{k} = -\left(\mathbb{P}_2 + \frac{\partial\mathbb{P}_0}{\partial K}\right)^0 \tag{3.21c}$$

These expressions differ from the ones we arrive at using the equations for C_1 and C_2 suggested in the literature [58].

$$-k_c J_0 = -\left(\mathbb{P}_1\right)^0 \tag{3.22a}$$

$$k_c = -\left(\frac{\partial \mathbb{P}_1}{\partial J}\right)^0 \tag{3.22b}$$

$$\bar{k} = -\left(\mathbb{P}_2\right)^0 \tag{3.22c}$$

These equations can be obtained by making the (wrong) assumption that the excess tangential pressure profile does not change upon bending [55]. However, likewise expressions result from a ground-state analysis of an adsorbed homopolymer layer [17]. This is a motivation to investigate whether these expressions are valid.

3.3 Mean field theory for homopolymer adsorption

Experimental and theoretical aspects of homopolymer adsorption from (semi-)dilute solution have been discussed extensively in literature. In this section we will briefly outline the most important features of the mean-field theory by Scheutjens and Fleer, generalised for adsorption on curved interfaces. Except for (necessary) discetisation effects, this theory is exact within the mean-field approximations. We will compare this theory to the approximate analytical theory which features the so-called ground-state approximation. The focus will be on comparing the bending moduli obtained from both approaches.

3.3.1 Numerical SCF theory

For numerical evaluation of polymer adsorption it is convenient to consider a infinite half space, bound on one side by a surface. Parallel to the surface we identify layers. If the surface is curved, the layers are curved as well. The curved space has either a cylindrical or spherical geometry. The distance from the center of the cylinder or sphere to the surface is denoted by the radius R which defines the radius of curvature of the interface. The layers are denoted by z and run from $z = 0$ for the surface, $z = 1$ for the first layer adjacent to the outside of the surface, up to $z = M$, the last layer of the system, which is in the bulk solution.

We will consider homopolymers p in a monomeric solvent s. For each component $i = p, s$ a dimensionless mean field $u_i(z)$, to be specified later, is present. The volume fraction of monomeric solvent $\varphi_s(z)$ follows directly from Boltzmann's law

$$\varphi_s(z) = \varphi_s^b \exp(-u_s(z)) \tag{3.23}$$

where the bulk volume fraction of solvent φ_s^b is the proper normalisation constant since the field $u_s = 0$ in the bulk phase far away from the surface.

When computing the volume fraction profile $\varphi_p(z)$ of polymers we have to take into account that the segments along the chain are connected. To do this it is convenient to introduce a free segment weighting factor $G(z)$

$$G(z) = \exp(-u_p(z)) \tag{3.24}$$

and an end segment weighting factor $G(z, s|1)$ which is a measure for the probability of finding the end segment of a polymer fragment with length s in layer z, given that the first segment $s = 1$ can be anywhere in space. The end segment weighting factor is obtained from the following recurrence relation

$$G(z, s|1) = G(z)\langle G(z, s-1|1)\rangle \tag{3.25}$$

This recurrence relation or propagator links segment s to the walks that start from segment 1 and end at $s - 1$. The propagator is initiated by $G(z, 1|1) = G(z)$. The angular brackets denote a weighted average over the neighbouring layers, also called the site fraction, according to

$$\langle f(z)\rangle = \lambda_{-1}(z)f(z-1) + \lambda_0(z)f(z) + \lambda_1(z)f(z+1) \tag{3.26}$$

The site fraction features the *a priori* step probabilities $\lambda_{-1}(z)$, $\lambda_0(z)$, and $\lambda_1(z)$, which depend the distance from the center of the cylinder or sphere. The curvature dependence is obtained by considering $L(z)$, the dimensionless volume of layer z, and $S(z)$, the contact area between layers z and $z+1$. The step probabilities are defined as $\lambda_{-1}(z) = S(z-1)/6L(z)$ for a step from layer z to $z-1$ and $\lambda_1(z) = S(z)/6L(z)$ for a step from layer z to $z+1$. A step within the same layer z has a probability $\lambda_0(z) = 1 - \lambda_{-1}(z) - \lambda_1(z)$.

The complementary end segment weighting factor of $G(z, s|1)$ is defined by considering a chain fragment starting from the other end of the chain $s = N$, where N is the chain length, i.e. $G(z, s|N)$. This quantity obeys the propagator equation

$$G(z, s|N) = G(z)\langle G(z, s+1|N)\rangle \tag{3.27}$$

where the corresponding starting condition reads $G(z, N|N) = G(z)$. The volume fraction profile of polymer is computed as

$$\varphi_p(z) = \frac{\varphi_p^b}{N}\sum_{s=1}^{N}\frac{G(z, s|1)G(z, s|N)}{G(z)} \tag{3.28}$$

The division by $G(z)$ is necessary to correct for the double counting of segment s in the product of both end segment weighting factors. Since in the bulk all weighting factors G are equal to unity, it is easily seen that φ_p^b/N normalises the profile.

Eqs. 3.23 – 3.28 give the volume fractions of solvent s and polymer p from the potential fields $\{u_i(z)\}$. These fields are in turn a function of the densities $\{\varphi_i(z)\}$ according to

$$u_s(z) = u'(z) \tag{3.29a}$$

$$u_p(z) = u'(z) - \chi_s\delta(z-1) \tag{3.29b}$$

where the volume filling potential $u'(z)$ is a Lagrange multiplier that ensures that each layer z is exactly filled.

The Silberberg adsorption parameter χ_s denotes the energy change when substituting a solvent monomer next to the surface with a polymer segment. The Kronecker delta function $\delta(z-1)$ ensures that the adsorption energy is only counted in layer $z = 1$. For curved surfaces χ_s may be defined in two ways. One method keeps the adsorption energy per segment χ_s constant upon curving, which corresponds to adsorption on sites, e.g. y hydrogen bonding. This method is consistent with the definition of Silberberg, each contact with the surface yields an equal energy change.

Another method to define χ_s is to allow for curvature dependence of the adsorption energy. A suitable definition is to weight the adsorption energy with the average number of contacts with the surface.

$$\chi_s^c = 6\lambda_{-1}(1)\chi_s \tag{3.30}$$

where the superscript c denotes the curvature dependence through contacts with the interface. The weighting of χ_s with the ratio $6\lambda_{-1}(1)$ accounts for the curvature dependence, note that $\lambda_{-1}(1) = 1/6$ for a planar interface. In this chapter we will use both methods and compare the results.

To evaluate the bending constants we need an expression for the surface tension. A straightforward generalisation to curvature of the expression given in Fleer et al. [43] yields

$$\frac{\gamma A}{k_B T} = \sum_z L(z)\left[(\varphi_p(z) - \varphi_p^b)(1 - \frac{1}{N}) + \ln\frac{\varphi_s(z)}{\varphi_s^b}\right] \tag{3.31}$$

When curving an interface with irreversibly adsorbed polymers the adsorbed amount per unit area Γ^a remains constant upon bending. This effectively corresponds to the limiting case where the ad- and desorption rates are low as compared to the rate of curving the interface. Indeed, polymer desorption is known to be a relatively slow process. We assume that the non-adsorbed polymers are still in equilibrium with the bulk solution, so that their chemical potential remains constant. The adsorbed chains are free to re-equilibrate their conformations. The state variable X for the irreversible case is found as

$$XA = F - n_s\mu_s - n_p^f\mu_p^f - A\left(\Gamma^a\mu_p^a\right)^0 \tag{3.32}$$

where n_p^f is the number of free (non-adsorbed) polymers in the system, F is the Helmholtz energy as given by eq. 2.91, and the superscript 0 again denotes evaluation at the planar interface.

Upon bending, the adsorbed amount is kept constant. This is accomplished by splitting the volume fraction of polymer in an adsorbed and free part [22, 59]

$$G^a(1,s|1) = G(1)\langle G^a(1,s-1|1) + G^f(1,s-1|1)\rangle \tag{3.33a}$$

$$G^a(z,s|1) = G(z)\langle G^a(z,s-1|1)\rangle \quad \text{for} \quad z > 1 \tag{3.33b}$$

$$G^f(1,s|1) = 0 \tag{3.33c}$$

$$G^f(z,s|1) = G(z)\langle G^f(z,s-1|1)\rangle \quad \text{for} \quad z > 1 \tag{3.33d}$$

and calculating the adsorbed volume fraction profile as

$$\varphi^a(z) = \frac{A\Gamma^a}{\sum_z L(z)G^a(z,N|1)} \frac{(2G^f(z,s|1) + G^a(z,s|1))G^a(z,s|N)}{G(z)} \tag{3.34}$$

where the normalisation ensures that the adsorbed amount is fixed to Γ^a at the interface. In principle, eq. 3.34 can be used to fix any adsorbed amount Γ^a at the surface. In this chapter Γ^a is calculated from the equilibrium adsorption at the planar interface. The volume fraction of free chains is obtained from eq. 3.28 where $G(z,s|1)$ and $G(z,s|N)$ are replaced by $G^f(z,s|1)$ and $G^f(z,s|N)$, respectively.

3.3.2 Analytical ground state approximation

An analytical theory for polymers adsorbing from semi-dilute solution has been considered by Clement and Joanny [17]. These authors start from the following expression for the surface tension

$$\frac{\gamma A}{k_B T} = -\frac{A\varphi_s}{6p} + \int_R^\infty [\frac{1}{6}(\nabla\psi)^2 + G(\psi)]\mathrm{d}\vec{r} \tag{3.35}$$

where ψ is the order parameter of the problem, defined through $\varphi_p = \psi^2$, p is the (dimensionless) extrapolation length which is a function of the adsorption strength, φ_s is the volume fraction at the surface, A is the (dimensionless) area of the surface, and $G(\psi)$ in an athermal solvent is defined by

$$G(\psi) = \frac{1}{2}(\psi^2 - \varphi_p^b)^2 \tag{3.36}$$

in the case of homopolymer adsorption. Eq. 3.35 is the equivalent of eq. 3.31 as has been shown before for planar interfaces [43, 44]. For high adsorption energies $1/p = -6(\chi_s - \ln 6/5)$ [44].

Eq. 3.35 is expanded up to second order in curvature. The expansion in curvature of eq. 3.35 and the mapping to the Helfrich equation is written out in detail in the appendix also for the case of irreversible adsorption. The results for the reversible case read

$$\gamma^0 = -\frac{\varphi_s}{p} + 2\int_0^\infty G(\psi_0)\mathrm{d}z \tag{3.37a}$$

$$k_c J_0 = -2\int_0^\infty G(\psi_0) z\mathrm{d}z \tag{3.37b}$$

$$k_c = -\frac{1}{3}\int_0^\infty \psi_1 \psi_0' \mathrm{d}z \tag{3.37c}$$

$$\bar{k} = 2\int_0^\infty G(\psi_0) z^2 \mathrm{d}z \tag{3.37d}$$

where ψ_1 is equal to $\psi_{c,1}$ from the appendix. The parameter ψ_1 represents the first-order correction to the order parameter profile due to curvature: $\psi = \psi_0 + \psi_1 J$. For convenience, $k_B T$ is set to unity.

The irreversible adsorption case is derived in appendix 3.A (eqs. 3.50, 3.53, and 3.59). The results are identical to eq. 3.37, in contrast to the findings of Clement and Joanny [17]. This discrepancy is discussed in the appendix. As was already derived in sec. 3.2.2 only k_c is sensitive to the reversibility of the adsorbed chains. This is because ψ_1 is different in the reversible and irreversible adsorption cases.

It is striking to see that in eq. 3.37 the product of the bending modulus and the spontaneous curvature $k_c J_0$ but also the saddle-splay modulus $\bar{k}$ are obtained from an evaluation of the volume fraction profiles at the planar interface only, whereas in the general eq. 3.21 derivatives are required. It seems that the planar interface contains information of the curved interface. We will return to this point in the discussion.

3.4 Results

The numerical and analytical mean-field theories as described in the theory section are used to analyse the bending constants as given by the Helfrich equation (3.3). Throughout this chapter we use a chain length $N = 1000$ and a bulk volume fraction $\varphi_p^b = 0.01$ for the polymer, i.e. well above the overlap concentration so that adsorption from semi-dilute solution is considered. The adsorption strength will be accounted for in two ways, using adsorption on 'sites' where the adsorption energy is equal for each segment in contact with the surface and through 'contact' interactions, where the adsorption energy is weighted with the available contact area of the surface, calculated with eq. 3.30.

The influence of the adsorption strength on the product of the bending modulus k_c and J_0 is shown in fig. 3.1. The numerical results are found from fitting eq. 3.3 to eq. 3.31. The way in which the adsorption interactions are accounted for has clearly a mayor impact on $k_c J_0$: fig. 3.1 shows a sign reversal between $k_c J_0$ calculated with adsorption on sites and that calculated with contact interactions. Adsorption on sites gives a positive value for $k_c J_0$ which increases monotonically

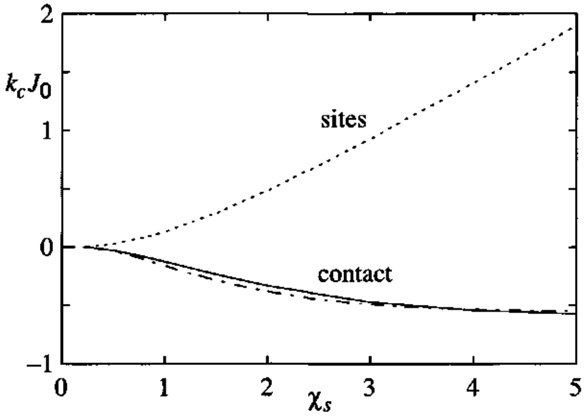

FIGURE 3.1: The influence of the adsorption strength χ_s on k_cJ_0 for polymers with chain length $N = 1000$ in an athermal solvent, $\varphi^b = 0.01$. Adsorption on sites is given by a dotted line, contact interactions by a solid line. The dashed-dotted curve is the prediction from the analytical eqs. 3.36 and 3.37, where the numerical result for φ_p is used as input. Both reversible and irreversible adsorption give identical results.

upon increasing χ_s. Adsorption with contact interactions yields a monotonically decreasing, negative value for k_cJ_0 upon increasing χ_s. Below the critical adsorption energy $\chi_s = 0.18$, k_cJ_0 is close to zero. Depletion of polymers does not affect the bending properties of the interface. For the contact interactions, a saturation effect is seen; k_cJ_0 hardly decreases for high values of χ_s. In contrast, k_cJ_0 continues to increase with increasing χ_s for adsorption on sites.

The product k_cJ_0 represents the first-order correction to the surface tension due to curvature. Our results show that even the sign of this first order correction depends on the actual boundary condition at the surface. Obviously, the same conclusion holds for the contribution of adsorbed polymers to the Tolman length k_cJ_0/γ^0, since γ^0 is unaffected by the actual boundary condition.

Some insight in the strong dependence of k_cJ_0 on the boundary condition is gained from considering the curvature dependence of the excess adsorbed amount of polymer per unit area Γ and the volume fraction of chains at the surface $\varphi(1)$. These parameters are plotted against the curvature J in fig. 3.2 for the typical case of $N = 1000$, $\varphi^b = 0.01$, and $\chi_s = 1$ in an athermal solvent. The excess amount per unit area Γ increases upon increasing curvature J. This is explained from a geometrical argument. Upon increasing curvature more space becomes available to the chains on the outside of the adsorbed layer, hence the increased excess amount. The adsorption on sites gives a slightly higher amount upon bending the interface.

In contrast, the volume fraction of the first layer $\varphi(1)$ shows different trends for both adsorption mechanisms. Adsorption on sites gives a slight increase in volume

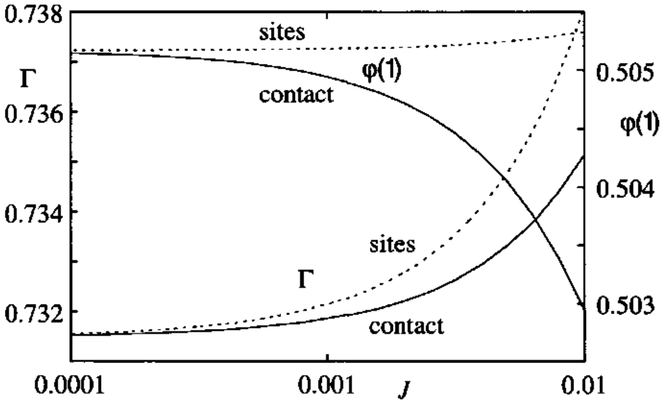

FIGURE 3.2: Dependence of the excess adsorbed amount Γ of chains per unit area and volume fraction near the surface $\varphi(1)$ on the curvature J in a cylindrical geometry for $\chi_s = 1$. Other parameters equal to those of fig. 3.1

fraction upon bending. The adsorption energy per adsorbing segment is constant but the overall increase in adsorption leads to the slight increase in $\varphi(1)$. When the adsorption energy stems from contact interactions a decrease in $\varphi(1)$ is observed. This is due to the fact that effectively the adsorption energy per segment decreases upon bending.

The surface tension γ is dominated by the region next to the surface. The negative value for k_cJ_0 for contact interactions corresponds to a increase in γ upon bending (see eq. 3.3). This is explained from the decrease of $\varphi(1)$ upon bending . A corresponding (reversed) argument holds for adsorption on sites.

Reversible and irreversible adsorption give numerically identical results for k_cJ_0, as expected from the analysis given in sec. 3.2.2. This does not mean that both k_c and J_0 separately are identical, since k_c is higher for irreversible adsorption, as explained in sec. 3.2.2.

The prediction for the contact interaction case is in nearly quantitative agreement with the analytical theory, shown by the dashed-dotted line in fig. 3.1, k_cJ_0 is negative and decreases upon increasing the adsorption strength. The dashed-dotted line was calculated with eq. 3.36 where the numerical results for φ_p where used.

The influence of the adsorption strength on the bending modulus k_c is shown in fig. 3.3 both for the two adsorption mechanisms as well as for the reversible and irreversible adsorption case. For reversible adsorption k_c is found to be negative for both boundary conditions. Adsorption of polymer makes the membrane less stiff, which is in agreement with the literature [17, 52]. Adsorption on sites leads to a monotonically decreasing small value for k_c. In contrast, when the the adsorption energy is accounted for through contact interactions, the bending modulus k_c is more negative and shows a minimum around $\chi_s = 2$. Again a large influence on

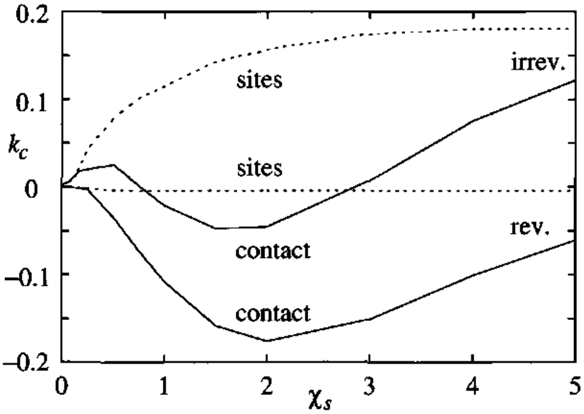

FIGURE 3.3: The influence of the adsorption strength χ_s on the bending modulus k_c for polymers with chain length $N = 1000$ in an athermal solvent, $\varphi^b = 0.01$. Adsorption on sites is given by a dotted curve, contact interactions by a solid curve.

the exact treatment of the boundary condition is observed. Unfortunately, there is no obvious way to unravel the physics similar to the analysis for $k_c J_0$. This is due to the fact that k_c is a second-order correction on the surface tension. There is no simple way to obtain ψ_1 from the numerical data, therefore a comparison with the analytical theory is omitted from fig. 3.3.

Irreversible adsorption leads to a higher value for k_c, i.e. the polymer layer becomes stiffer, as was expected. The effect of irreversible adsorption is large, it may lead to a sign reversal in the contribution of the polymer layer to k_c. This is in contrast to the findings of Clement and Joanny [17], who found only a minor influence of irreversibly adsorbed polymers.

For low values of χ_s the bending modulus k_c is positive for irreversible adsorbed polymers. In practice, we expect that at low χ_s the adsorption can always be considered reversible; desorption is easy at low adsorption strengths.

Now that k_c has been determined, J_0 is obtained from the product $k_c J_0$, shown in fig. 3.1. Since k_c is negative in many instances, J_0 looses its usual meaning of spontaneous curvature, referring to a minimum in the surface tension γ. Instead, when k_c is negative, J_0 represents a prediction for the *maximum* of γ. The system will avoid this curvature. However, the surface also gives a contribution to k_c, which is not explicitly taken into account here. A stable system has a positive overall k_c, so that J_0 is well defined.

The influence of χ_s on the saddle-splay modulus $\bar{k}$ is shown in fig. 3.4. Again, a large influence on the mechanism to account for the adsorption energy is observed. For adsorption on sites, $\bar{k}$ is negative and decreasing upon increasing adsorption strength. When the adsorption energy is accounted for through contact interactions,

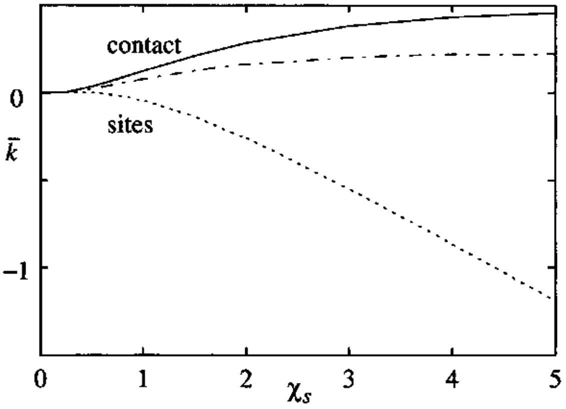

FIGURE 3.4: The influence of the adsorption strength χ_s on the saddle-splay modulus $\bar{k}$ for polymers with chain length $N = 1000$ in an athermal solvent, $\varphi^b = 0.01$. Adsorption on sites is given by a dotted curve, contact interactions by a solid curve. The dashed-dotted curve is the prediction from eq. 3.37 using φ_p from the numerical calculation. Reversible and irreversible adsorption give identical results.

$\bar{k}$ is positive and increases with increasing adsorption strength.

Irreversible adsorption gives exactly the same results for $\bar{k}$ as the reversible case. This is expected from the theory in sec. 3.2.2 and is confirmed numerically.

The result from eq. 3.37 shows reasonable agreement with the calculation for adsorption through contact interactions. The same trend is observed although the results are about a factor of two lower than the numerical results.

The bending moduli were also evaluated using eqs. 3.21. In fig. 3.5 the results are shown for a constant χ_s upon bending (site interactions). The values (symbols) for k_cJ_0, k_c, and $\bar{k}$ resulting from eqs. 3.21 are (within the numerical accuracy) identical to those we obtained in fig. 3.1, 3.3, and 3.4, as they should be. The curves in fig. 3.5 test eqs. 3.22. For k_cJ_0 the agreement between eq. 3.21a and 3.22a looks excellent. However, a difference of less than 1% between the results of the two equations is still observed. Likewise, a small but graphically visible difference in the values for $\bar{k}$ is present resulting from comparing eq. 3.21c and eq. 3.22c. In contrast, the values for k_c found from eq.3.21b and 3.22b even have a different sign.

3.5 Discussion

The theoretically predicted values for the bending constants of homopolymers at a surface are highly affected by the treatment of the boundary layer. Large differences in their values are obtained when comparing adsorption on sites and through contact interactions. This is not surprising when it is realised that the dominant

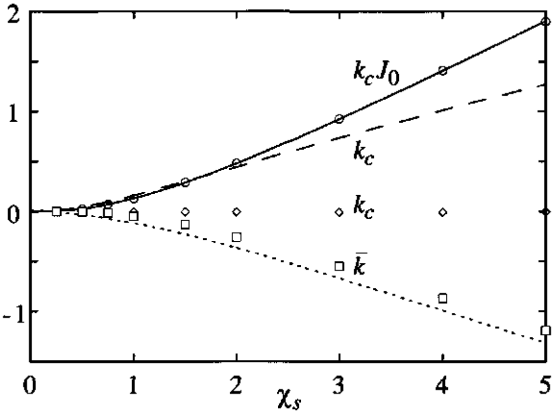

FIGURE 3.5: The bending constants $k_c J_0$, k_c and $\bar{k}$ as a function of χ_s (site interactions), other parameters equal to that of fig. 3.1. Two results are given, the symbols correspond to eq. 3.21. The curves denote the results given by eq. 3.22

contribution to the surface tension stems from the contacts with the surface. The bending constants are obtained through a second order expansion in curvature of the surface tension. Any change in the exact treatment of the surface contacts is bound to lead to large differences in the bending constants.

The large influence of the treatment of the boundary condition near the surface on the results also explains why the comparison of the numerical results with those from the analytical theory of sec. 3.3.2 has its problems. The numerical and analytical theory differ in the treatment of the boundary condition. Most notably, in the analytical theory the interaction of polymers is of infinitely short range. In contrast, the numerical theory has a finite range of interaction with the surface due to the discretisation of space. As has been shown before for planar interfaces [60, 61], a quantitatively correct mapping of continuum models and the discrete theory is feasible.

When the adsorption energy is accounted for through a contact fraction with the surface a remarkable resemblance is found between the numerical results and the analytical theory. In order to make the comparison, numerical data were used as input for analytical equations, this was done to circumvent the major differences in the treatment of the boundary layer between the analytical and numerical theory. The numerical theory explicitly takes the finite volume of the polymer segments near the surface into account [60]. The numerical treatment is comparable to the Stern-layer, known from electric double layer theory. In the analytical theory the finite segment volume is not accounted for, resulting in volume fractions which exceed unity next to the surface. In principle it should be possible to reformulate the analytical theory in terms of such a 'Stern' layer.

Hence, the resemblance between the numerical data and the analytical theory seems a coincidence resulting from cancellation of errors. Both numerical methods used to account for the adsorption energy differ from the analytical theory. In the analytical theory the surface interaction energy is of infinitely short range, in the numerical theory the interaction has a finite range. Furthermore, the finite volume of segments near the surface is not incorporated in the analytical theory.

The analytical theory predicts expressions for $k_c J_0$ and $\bar{k}$ which can be evaluated from a planar interface. This is a useful result since it makes the evaluation of these bending constants much easier. This result also seems to indicate that some bending information is 'stored' in the planar interface. It would seem as if the planar interface is 'clairvoyant' and knows what is going to happen upon bending. However, the exact treatment of the boundary layer upon bending is not stored in the planar interface. The bending constants depend strongly on the treatment of the boundary layer. This means that the analytical result is only valid for the particular boundary condition that was considered, namely an infinitely short range interaction.

The eqs. 3.22 where derived from equations for C_1 and C_2 as proposed by Markin et al. [58]. Fig. 3.5 shows that they do not yield the exact values for the bending moduli of an adsorbed polymer with site interactions. Furthermore, for contact interactions the values of the bending moduli are completely different so that even the reasonable agreement that was found for $k_c J_0$ and $\bar{k}$ is lost. Similar results have been shown for a liquid-vapor interface [56] where one needs the full expressions given by eqs. 3.21 instead of eqs. 3.22.

However, when considering *monomer* adsorption, one *does* obtain exactly the same values from eqs. 3.22 and a direct fitting of the surface tension (not shown). We have derived expressions resembling eqs. 3.22 for $k_c J_0$ and $\bar{k}$ where the values for both these parameters are obtained from a planar interface alone. The resulting expressions for $k_c J_0$ and $\bar{k}$ depend on the adsorption mechanism (contact or site interactions) but are always evaluated from the planar interface alone. The difference between the expressions for contact or site interactions boils down to a shift in the position in space of some local tangential pressure contributions.

For polymer adsorption, preliminary results show that it is possible to come up with variants of eqs. 3.22 also for contact interactions. However, the resulting values are again not identical to those resulting from a direct fit of the curvature dependence of the surface tension. This is in contrast with the monomer case, where these expressions yield exact results. Thus it remains an open question whether it is possible to come up with general equations for $k_c J_0$ and $\bar{k}$ which can be evaluated from the planar interface alone.

When comparing reversible and irreversible adsorption, exactly the same results are obtained for $k_c J_0$ and $\bar{k}$, both numerically and from fundamental considerations, as shown in sec. 3.2.2. The exact nature of the restriction that is imposed on the polymer layer upon bending is immaterial for this conclusion. In this chapter, the adsorbed amount per unit area upon bending was fixed. Additionally, a fixed length distribution of loops, a fixed average length of tails, or some other additional restriction could be applied. The saddle-splay modulus $\bar{k}$ and the product k_cJ_0 both remain unaltered when such alternatives are used.

Clement and Joanny [17] did find different values for k_cJ_0 and $\bar{k}$ when comparing reversible and irreversible adsorption. This is due to the way they impose the restriction on the adsorption layer. For the irreversible case they ignore the free polymers in solution, which leads to a different order parameter (and therefore a different volume fraction profile) than in the reversible case, even for a planar interface. As shown in the appendix, when going from reversible to irreversible adsorption the total adsorbed amount decreases in their treatment.

In contrast to the results for k_cJ_0 and $\bar{k}$, treating the adsorbed polymer layer as irreversibly adsorbed does qualitatively affect the bending modulus k_c. Contrary to Clement and Joanny [17] we see a significant effect on the overall polymer contribution to the bending modulus when the adsorbed amount is kept constant upon bending. Most notably, a sign reversal was found for relatively small and high adsorption energies (see fig. 3.3). At small adsorption energies desorption is probably relatively fast. It is questionable whether irreversible adsorption is then an appropriate mechanism.

The saddle-splay modulus $\bar{k}$ is found from the subtraction of two second order expansions in curvature of the surface tension γ: an expansion in spherical and cylindrical curvature. This places a high demand on the numerical accuracy. We found that we had to evaluate the volume fractions at a precision of 13 digits to obtain graphically identical results for $\bar{k}$ as found from eqs. 3.31 and 3.21. Nevertheless, this indicates that our numerical evaluation of the bending moduli is consistent.

In the present approach the membrane was treated as an adsorbent with an invariant structure. This is an approximation. In the next chapter we will take the membrane structure explicitly into account. When polymers adsorb onto the membrane we expect that the membrane will change. Therefore, there is not only a polymer contribution to the bending modulus but also an additional membrane contribution. Furthermore, a real membrane is to some extent diffuse which leads to a different boundary condition. Preliminary results show that the bending constants of polymer layers adsorbing onto a membrane differ significantly from those of polymers adsorbing onto a solid wall.

3.A The bending constants from an analytical expression for the surface tension

In the following the derivation of the bending constants as given by Clement and Joanny [17] (CJ) is written out in more detail than in the original paper. In addition, a different result is derived for the irreversible case. A noteworthy difference in this appendix compared to CJ is that we choose the (dimensionless) segment length a as the unit length instead of $a/\sqrt{6}$.

For the irreversible adsorption case, the appropriate thermodynamical function to minimise is the state variable X, defined by eq. 3.8

$$XA = -\frac{A\varphi(0)}{6p} + \int_R^\infty [\frac{1}{6}(\nabla\psi)^2 + G(\psi) + \varphi_a(\psi)\Delta\mu]\mathrm{d}\vec{r} \qquad (3.38)$$

where A is the surface area, $\varphi(0)$ is the volume fraction next to the surface, p is the proximal (extrapolation) length, ψ is the order parameter or ground state eigenfunction related to the volume fraction φ by $\varphi = \psi^2$, $\varphi_a(\psi)$ is the volume fraction of adsorbed polymers, $G(\psi)$ describes the interactions between solvent and polymer, and $\Delta\mu$ is the difference in chemical potential of adsorbed chains that stems from bending the interface. Note that we do not specify the exact nature of the irreversibility.

We define $\Delta\mu = \mu_p^a - \mu_p^f$, which retrieves the full equilibrium case in planar geometry. The reversible adsorption case is recovered when $\Delta\mu$ is omitted from the equations, then X reduces to γ.

The equilibrium order parameter profile ψ is found by minimisation of X. This profile obeys the following Euler-Lagrange equation

$$\nabla^2\psi = 3\frac{\partial G}{\partial\psi} + 3\frac{\partial\varphi_a\Delta\mu}{\partial\psi} \qquad (3.39)$$

with boundary condition

$$\mathbf{n}\nabla\psi = -\frac{\psi}{p} \qquad (3.40)$$

where $\mathbf{n}$ is the unit vector normal to the surface.

We first take a cylindrical surface of radius R and expand X in powers of the curvature $1/R$. The order parameter for the cylindrical geometry, ψ_c, is expanded up to second order in curvature as

$$\psi_c = \psi_0 + \frac{\psi_{c,1}}{R} + \frac{\psi_{c,2}}{R^2} \qquad (3.41)$$

where R is again dimensionless. Since $\nabla^2\psi_c = \frac{1}{r}\frac{\partial\psi_c}{\partial r} + \frac{\partial^2\psi_c}{\partial r^2}$, where $r = R + z$ and z is the distance from the surface, it follows that

$$\nabla^2\psi_c = \frac{1}{r}\frac{\partial\psi_0}{\partial r} + \frac{\partial^2\psi_0}{\partial r^2} + \frac{1}{rR}\frac{\partial\psi_{c,1}}{\partial r} + \frac{1}{R}\frac{\partial^2\psi_{c,1}}{\partial r^2} + \frac{1}{rR^2}\frac{\partial\psi_{c,2}}{\partial r} + \frac{1}{R^2}\frac{\partial^2\psi_{c,2}}{\partial r^2} \qquad (3.42)$$

A series expansion of the right hand side of eq. 3.39 in ψ, around ψ_0, yields

$$\frac{\partial G}{\partial\psi} = \frac{\partial G}{\partial\psi_0} + \left(\frac{\psi_{c,1}}{R} + \frac{\psi_{c,2}}{R^2}\right)\frac{\partial^2 G}{\partial\psi_0^2} + \frac{1}{2}\left(\frac{\psi_{c,1}}{R} + \frac{\psi_{c,2}}{R^2}\right)^2\frac{\partial^3 G}{\partial\psi_0^3} \qquad (3.43)$$

where $\partial G/\partial\psi_0$ is a shorthand for $\partial G/\partial\psi$ evaluated at $\psi = \psi_0$. Substituting eqs. 3.42 and 3.43 in eq. 3.39 and requiring that all coefficients in the expansion to second order on both sides of the equation are equal to each other, we find

$$\frac{\partial^2\psi_0}{\partial z^2} = 3\frac{\partial(G+\varphi_a\Delta\mu)}{\partial\psi_0} \tag{3.44a}$$

$$\frac{\partial^2\psi_{c,1}}{\partial z^2} + \frac{\partial\psi_0}{\partial z} = 3\psi_{c,1}\frac{\partial^2(G+\varphi_a\Delta\mu)}{\partial\psi_0^2} \tag{3.44b}$$

$$\frac{\partial^2\psi_{c,2}}{\partial z^2} + \frac{\partial\psi_{c,1}}{\partial z} = 3\psi_{c,2}\frac{\partial^2(G+\varphi_a\Delta\mu)}{\partial\psi_0^2} + \frac{3\psi_{c,1}^2}{2}\frac{\partial^3(G+\varphi_a\Delta\mu)}{\partial\psi_0^3} \tag{3.44c}$$

where we made use of the fact that a derivative with respect to r is equal to a derivative with respect to z and we substituted $r = R$ for r outside the derivatives, which is valid if $z \ll R$, so for small curvatures. Rewriting eq. 3.38 for a cylinder, substituting $\varphi_s = \psi(0)^2$, eq. 3.41, and expanding of both G and $\varphi_a\Delta\mu$ in ψ around ψ_0, we find

$$\begin{aligned} XA = &-\frac{A}{6p}\left(\psi_0(0)^2 + \frac{2}{R}\psi_0(0)\psi_{c,1}(0) + \frac{2}{R^2}\psi_0(0)\psi_{c,2}(0) + \frac{1}{R^2}\psi_{c,1}(0)^2\right) + \\ &+\frac{\pi}{3}\int_0^\infty \left[(\psi_0')^2 + \frac{2}{R}\psi_0'\psi_{c,1}' + \frac{2}{R^2}\psi_0'\psi_{c,2}' + \frac{1}{R^2}(\psi_{c,1}')^2\right](R+z)\mathrm{d}z \\ &+2\pi\int_0^\infty \left[G(\psi_0) + \frac{\psi_{c,1}}{R}\frac{\partial G}{\partial\psi_0} + \frac{\psi_{c,2}}{R^2}\frac{\partial G}{\partial\psi_0} + \frac{\psi_{c,1}^2}{2R^2}\frac{\partial^2 G}{\partial\psi_0^2}\right](R+z)\mathrm{d}z \\ &+2\pi\int_0^\infty \left[\frac{\psi_{c,1}}{R}\frac{\partial\varphi_a\Delta\mu}{\partial\psi_0} + \frac{\psi_{c,2}}{R^2}\frac{\partial\varphi_a\Delta\mu}{\partial\psi_0} + \frac{\psi_{c,1}^2}{2R^2}\frac{\partial^2\varphi_a\Delta\mu}{\partial\psi_0^2}\right](R+z)\mathrm{d}z \end{aligned} \tag{3.45}$$

where we made use of $\nabla f = \partial f/\partial z$ and $d^3r = 2\pi(R+z)dz$ in cylindrical geometry. All derivatives with respect to z are abbreviated as $\partial f/\partial z = f'$ and all third and higher order terms are omitted. Now we divide both sides by the area $A = 2\pi R$, collect all terms with the same order of curvature, and compare these with eq. 3.4 with $J = 1/R$ and γ replaced by X for the irreversible case. The zero-order term reads

$$\gamma^0 = -\frac{\varphi_0(0)}{6p} + \int_0^\infty [\frac{1}{6}(\psi_0')^2 + G(\psi_0)]\mathrm{d}z \tag{3.46}$$

Using eq. 3.44a the first-order terms $(-k_c J_0)$ are

$$\begin{aligned} -\frac{\psi_0(0)\psi_{c,1}(0)}{3p} + \frac{1}{6}\int_0^\infty (\psi_0')^2 z\mathrm{d}z + \frac{1}{3}\int_0^\infty \psi_0'\psi_{c,1}'\mathrm{d}z + \\ \int_0^\infty G(\psi_0)z\mathrm{d}z + \frac{1}{3}\int_0^\infty \psi_{c,1}\psi_0''\mathrm{d}z \end{aligned} \tag{3.47}$$

The first integral can be rewritten using eq. 3.44a. Multiplying eq. 3.44a by ψ_0' and integrating once gives

$$G(\psi_0) = \frac{1}{6}(\psi_0')^2 + \text{constant} \tag{3.48}$$

In the bulk phase ψ_0 is constant and $G(\psi_0) = 0$ for $z \to \infty$ since the contribution of the bulk phase to the excess free energy is zero. As a consequence, the constant in eq. 3.48 equals zero. Using eq. 3.48, the first and third integral of eq. 3.47 are identical. The second and fourth integral of eq. 3.47 can be reduced through integration by parts of the latter integral

$$\frac{1}{3}\int_0^\infty \psi_0'\psi_{c,1}'\mathrm{d}z + \frac{1}{3}\int_0^\infty \psi_{c,1}\psi_0''\mathrm{d}z = \frac{1}{3}\left[\psi_{c,1}\psi_0'\right]_0^\infty = -\frac{1}{3}\psi_0(0)'\psi_{c,1}(0) \tag{3.49}$$

We rewrite this result using eq. 3.40 which now reads $\psi'(0) = -\psi(0)/p$. If we then combine all first-order terms the following expression is found

$$k_c J_0 = -2\int_0^\infty G(\psi_0) z \mathrm{d}z \tag{3.50}$$

which is equal to the expression found by CJ for the equilibrium case except for the factor 2, a misprint in CJ. Since $\Delta\mu$ does not occur in eq. 3.50, the Tolman length $k_c J_0/\gamma^0$ is unaltered when the polymers are irreversibly adsorbed. CJ arrived at $k_c J_0 = -2\int_0^\infty (G(\psi_0) + \mu_0\varphi_a) z \mathrm{d}z$ for irreversibly adsorbed polymers, which is not equal to our result. They used μ instead of $\Delta\mu$ in eq. 3.38. Also they changed order parameter compared to the equilibrium case, omitting the free polymers. When one then solves the planar case, a starved layer is found.

Using eqs. 3.44a and 3.44b, the second-order terms $(k_c/2)$ are given by

$$\begin{gathered}\frac{1}{3}\int_0^\infty \psi_0''\psi_{c,1} z\mathrm{d}z + \frac{1}{3}\int_0^\infty \psi_0'\psi_{c,1}' z\mathrm{d}z \\ -\frac{\psi_{c,1}(0)^2}{6p} + \frac{1}{6}\int_0^\infty \psi_{c,1}\psi_{c,1}''\mathrm{d}z + \frac{1}{6}\int_0^\infty \psi_{c,1}\psi_0'\mathrm{d}z + \frac{1}{6}\int_0^\infty (\psi_{c,1}')^2\mathrm{d}z \\ -\frac{1}{3}\frac{\psi_{c,0}(0)\psi_{c,2}(0)}{p} + \frac{1}{3}\int_0^\infty \psi_0'\psi_{c,2}'\mathrm{d}z + \frac{1}{3}\int_0^\infty \psi_0''\psi_{c,2}\mathrm{d}z\end{gathered} \tag{3.51}$$

The first integral is integrated by parts and the result cancels against the second integral in eq. 3.51. The fifth integral, upon integration by parts, gives

$$\frac{1}{6}[\psi_{c,1}\psi_{c,1}']_0^\infty - \frac{1}{6}\int_0^\infty \psi_{c,1}\psi_{c,1}''\mathrm{d}z = \frac{\psi_{c,1}(0)^2}{6p} - \frac{1}{6}\int_0^\infty \psi_{c,1}\psi_{c,1}''\mathrm{d}z \tag{3.52}$$

where eq. 3.40 was used. This result cancels against the third and fourth terms in eq. 3.51. After integrating the last integral of eq. 3.51 by parts, the two preceding terms cancel. The final result for k_c is

$$k_c = -\frac{1}{3}\int_0^\infty \psi_{c,1}\psi_0'\mathrm{d}z \tag{3.53}$$

Again, this expression is the same as found by CJ for the equilibrium case. However, for irreversible adsorption $\psi_{c,1}$ is (necessarily) different from the equilibrium case, so that the resulting k_c is sensitive to the reversibility of adsorption.

The same procedure can be applied for a spherical geometry. The equivalents of eqs. 3.44a and 3.44b are

$$\frac{\partial^2\psi_0}{\partial z^2} = 3\frac{\partial(G+\varphi_a\Delta\mu)}{\partial\psi_0} \tag{3.54a}$$

$$\frac{\partial^2\psi_{s,1}}{\partial z^2} + 2\frac{\partial\psi_0}{\partial z} = \frac{3\psi_{s,1}}{2}\frac{\partial^2(G+\varphi_a\Delta\mu)}{\partial\psi_0^2} \tag{3.54b}$$

where we used $\nabla^2\psi_s = \frac{2}{r}\frac{\partial\psi_s}{\partial r} + \frac{\partial^2\psi_s}{\partial r^2}$. Rewriting eq. 3.38 yields

$$\begin{aligned} XA = &-\frac{A}{6p}\left(\psi_0(0)^2 + \frac{2}{R}\psi_0(0)\psi_{s,1}(0) + \frac{2}{R^2}\psi_0(0)\psi_{s,2}(0) + \frac{1}{R^2}\psi_{s,1}(0)^2\right) \\ &+ \frac{2\pi}{3}\int\left[(\psi_0')^2 + \frac{2}{R}\psi_0'\psi_{s,1}' + \frac{2}{R^2}\psi_0'\psi_{s,2}' + \frac{1}{R^2}(\psi_{s,1}')^2\right](R+z)^2\mathrm{d}z \\ &+ 4\pi\int\left[G(\psi_0) + \frac{\psi_{s,1}}{R}\frac{\partial G}{\partial\psi_0} + \frac{\psi_{s,2}}{R^2}\frac{\partial G}{\partial\psi_0} + \frac{\psi_{s,1}^2}{2R^2}\frac{\partial^2 G}{\partial\psi_0^2}\right](R+z)^2\mathrm{d}z \\ &+ 4\pi\int\left[\frac{\psi_{s,1}}{R}\frac{\partial\varphi_a\Delta\mu}{\partial\psi_0} + \frac{\psi_{s,2}}{R^2}\frac{\partial\varphi_a\Delta\mu}{\partial\psi_0} + \frac{\psi_{s,1}^2}{2R^2}\frac{\partial^2\varphi_a\Delta\mu}{\partial\psi_0^2}\right](R+z)^2\mathrm{d}z \end{aligned} \tag{3.55}$$

Again, we divide by the area $A = 4\pi R^2$ and collect the terms of equal order in $1/R$. The results for γ^0 and k_cJ_0 are identical to eqs. 3.46 and 3.50, as they should be. However, a difference turns up in the second-order terms which are equal to

$$\begin{aligned} &2\int_0^\infty G(\psi_0)z^2\mathrm{d}z + \frac{2}{3}\int_0^\infty \psi_0'\psi_{s,1}'z\mathrm{d}z + \frac{2}{3}\int_0^\infty \psi_0''\psi_{s,1}z\mathrm{d}z \\ &-\frac{\psi_{s,1}(0)^2}{6p} + \frac{1}{6}\int_0^\infty \psi_{s,1}\psi_{s,1}''\mathrm{d}z + \frac{1}{3}\int_0^\infty \psi_{s,1}\psi_0'\mathrm{d}z + \frac{1}{6}\int_0^\infty (\psi_{s,1}')^2\mathrm{d}z \\ &-\frac{\psi_0(0)\psi_{s,2}(0)}{3p} + \frac{1}{3}\int_0^\infty \psi_0'\psi_{s,2}'\mathrm{d}z + \frac{1}{3}\int_0^\infty \psi_0''\psi_{s,2}\mathrm{d}z \end{aligned} \tag{3.56}$$

Simplifying some terms as was done before and comparing the result to eq. 3.5, realising that $J = 2/R$, we find

$$k_c + \frac{1}{2}\bar{k} = -\frac{1}{6}\int_0^\infty \psi_{s,1}\psi_0'\mathrm{d}z + \int_0^\infty G(\psi_0)z^2dz \tag{3.57}$$

Comparing eqs. 3.44b and 3.54b we arrive at

$$\psi_{s,1} = 2\psi_{c,1} \tag{3.58}$$

Substituting this in eq. 3.57 and subtracting eq. 3.53, we end up with

$$\bar{k} = 2\int_0^\infty G(\psi_0)z^2\mathrm{d}z \tag{3.59}$$

which is again identical to the expression for the equilibrium case found by CJ. Like the Tolman length, also the saddle-splay modulus $\bar{k}$ remains unchanged as compared to the equilibrium case when the polymers are irreversibly adsorbed upon bending. For irreversible adsorption CJ found the second moment over $G + \mu_0\varphi_a$, which is consistent with their result for k_cJ_0 but again not equal to our findings. The probable reasons for this discrepancy are explained below eq. 3.50.

4 Bending moduli for vesicles with adsorbed homopolymers

ABSTRACT

We have computed the bending moduli for vesicles with a homopolymer layer adsorbed onto the head groups of the surfactants using a mean-field self-consistent-field theory. In our calculations the self-assembly of $C_{12}E_6$ and $C_{12}A_nC_{12}$ surfactants into vesicles is explicitly taken into account. When adsorbing polymers are introduced the bending moduli of the membranes change. The magnitude and the sign of the change in bending moduli is shown to depend on the size n of the head groups. The bending moduli of adsorbed polymer layers onto a solid surface with a hairy layer are used as a model for a membrane whose composition does not change upon adsorption of homopolymers. This model system is able to reproduce the sign reversal of the polymer contribution on the bending rigidity of the $C_{12}A_nC_{12}$ vesicles. However, this model is unable to reproduce the sign reversal found for the contribution to the saddle-splay modulus.

4.1 Introduction

The stability of a phase of bilayer membranes is determined largely by the bending moduli of the membranes [62, 63]. Several authors have discussed the magnitude of the bending moduli of bilayer membranes [53, 62–64]. A relatively new topic is the influence of polymers which adsorb onto the bilayer. From theoretical considerations it is generally found that the influence of adsorbing polymers on the bending moduli is relatively low, of the order of one k_BT or less [17, 51, 52].

Helfrich has developed a framework to describe the rigidity of interfaces [53]. The Helfrich equation is a second order expansion of the surface tension as a function of curvature. This Helfrich equation features three parameters: the spontaneous curvature J_0, the bending rigidity k_c, and the saddle-splay modulus $\bar{k}$.

In this chapter we use the numerical mean-field theory in the formulation of Scheutjens and Fleer [43]. This method was generalised by Oversteegen and Leermakers [64] to evaluate the bending rigidity of surfactant bilayers. Here, a similar approach will be used, taking into account simultaneously the bilayer, the adsorbing polymer, and their mutual interactions upon bending.

For bilayer membranes of only one component the spontaneous curvature J_0 is usually zero due to the symmetry of the membrane. A noteworthy exception is a bilayer of an asymmetric triblock copolymer [65]. Here, only bilayers with a spontaneous curvature will be considered. When polymers adsorb on both sides the symmetry is preserved.

The main focus will be on the difference in bending moduli caused by the adsorbing polymers

$$\Delta k_c = k_c^{\mathrm{ads}} - k_c^{\mathrm{free}} \tag{4.1a}$$

$$\Delta \bar{k} = \bar{k}^{\mathrm{ads}} - \bar{k}^{\mathrm{free}} \tag{4.1b}$$

where k_c^{ads} is the total bending rigidity of the membrane in the presence of adsorbing polymers and k_c^{free} that without adsorbing polymers.

In chapter 3 the bending moduli of homopolymers adsorbing onto a solid wall was studied using an adsorption interaction with a length scale equal to the statistical length of a polymer bead. It was shown that the exact nature of the adsorbing boundary condition has a large effect on the bending moduli. Both a curvature-dependent adsorption energy per bead and a constant adsorption energy per bead were considered. It was found that, depending on this choice, Δk_c is either negative or negligible small, and $\Delta \bar{k}$ changes sign. The surface of a vesicle forms a different boundary as compared to a solid wall. When polymers adsorb onto the head groups the adsorption interaction is of a longer range than at a solid wall. Furthermore, it is unclear whether the vesicle itself remains unaltered as polymers adsorb onto it. This motivated the current investigation, which takes the structure of the vesicles explicitly into account.

An additional motivation stems from the results found for membranes of charged surfactants. The electrostatic contribution to k_c is always positive: electrostatics makes the membranes stiffer. The electrostatic contribution to $\bar{k}$ is negative. The same results were found for electric double layers on solid cylinders. However, on solid cylinders, the bending rigidity k_c was found to decrease upon increasing the salt concentration [41, 66, 67]. This effect was found to be reversed for membranes. The reverse in trend was explained as stemming from a decrease in electric repulsion between surfactant for higher salt concentrations, leading to the formation of thicker bilayers [41]. Thicker bilayers generally have a higher bending rigidity.

Due to the numerical nature of our theory, space needs to be discretised. However, the discretisation of space may lead to artefacts in the results. In most cases, these artefacts are negligible. Volume fraction profiles, for example, are seldom affected by these artefacts, as far as can be seen from a graphical representation of these profiles. However, thermodynamical quantities like the surface tension may suffer from a discretisation artefact. In the case of a vesicle these artefacts show up as oscillations of the surface tension as a function of the vesicle radius. When fitting the surface tension to the curvature up to second order in curvature, these artefacts need to be carefully controlled.

Several methods have been presented in the past to either fully eliminate the discretisation artefacts for certain applications or to greatly reduce them. In appendix B.5 we review these methods in detail and we present a new method to reduce the discretisation artefacts. Typically, the artefacts increase in magnitude when the calculated membranes become more stiff. Until now the membranes calculated with the numerical SCF theory had to be rather flexible in order to obtain reliable values for the bending moduli. The new method does not completely remove the discretisation artefacts. However, as shown in appendix B.5 our method is reliable for membranes with a rigidity which is more than an order of magnitude higher than could be dealt with before.

4.2 Theory

The numerical SCF theory has been described in detail in chapter 2. Here we give only a short summary of the main principles. Space is divided in layers parallel to each other. The calculations are performed in cylindrical and spherical layer geometry. The layers are numbered $z = 1, 2, \ldots, M$. We are interested in the volume fractions $\varphi_i(z)$ in each layer, where i stands for the type of molecule. In this case surfactants, polymers and solvent. The polymer and the solvent consist of one type of segment only. The copolymer (or surfactant) has a head and tail group of consisting of different segment types. A segment type is distinguished by its interactions with other segments. Only nearest neighbour interactions are accounted for, using Flory-Huggins interaction parameters, χ_{AB}, where A and B denote the type of segment. Together with the Lagrange field $u'(z)$ resulting from the incompressibility constraint, $\sum_i \varphi_i = 1$, this leads to a dimensionless potential field $u_A(z)$ [22]

$$u_A(z) = u'(z) + \sum_B \chi_{AB} \left(\langle \varphi_B(z) \rangle - \varphi_B^b \right) \tag{4.2}$$

Where φ_B^b denotes the bulk volume fraction of segment type B. The angular brackets denote a local average over the layers, defined by eq. 3.26. The mean-field averaging in the layer leads to one dimensional volume fraction gradients in the z-direction perpendicular to the layers.

The volume fraction of monomers is directly found from eq. 3.23. To compute the volume fractions of the chain molecules it is convenient to introduce the free segment weighting factor $G_A(z)$, using Boltzmann statistics.

$$G_A(z) = \exp(-u_A(z)) \tag{4.3}$$

where A again denotes the segment type. The volume fractions are found from two complementary end-segment distribution functions $G_i(z, s|1)$ and $G_i(z, s|N_i)$:

$$\varphi_i(z) = C_i \sum_{s=1}^{N_i} \frac{G_i(z, s|1) G_i(z, s|N_i)}{G_i(z, s)} \tag{4.4}$$

where $G_i(z, s)$ equals $G_A(z)$ if segment s is of type A. The division by $G_i(z, s)$ corrects the double counting of segment s. The normalisation constant C_p for the polymer is given by $C_p = \varphi_p^b/N_p$. For the surfactant a fixed total amount is used

$$C_s = \frac{\sum_z L(z)\varphi(z)}{N_s \sum_z L(z)G(z,N_s|1)} \tag{4.5}$$

The amount of surfactant will be used to vary the curvature of the membrane.

We now have equations relating the volume fractions to the potential field (eq. 4.2) and vice-versa (eq. 4.4). These equations are solved numerically to arrive at the self-consistent solution.

To evaluate the bending constants, the parameter of interest is the surface tension of the membrane-polymer system. The bending constants are defined by the Helfrich equation [53]

$$\gamma(J,K) = \gamma_0 - k_c J_0 J + \frac{1}{2} k_c J^2 + \bar{k} K \tag{4.6}$$

This expression defines the bending modulus k_c, the saddle-splay modulus $\bar{k}$, and the spontaneous curvature J_0. The Helfrich equation is a second-order expansion in curvature of the surface tension around a planar interface. The expansion is done in terms of the inverse curvature radii $1/R_1$ and $1/R_2$, where $J = 1/R_1 + 1/R_2$ and $K = 1/(R_1 R_2)$.

One way to obtain the bending moduli is to compute the surface tension γ for several radii R in both a cylindrical and a spherical geometry. Subsequently, we fit two second order polynomials through the results. The coefficients of the fit in the cylindrical geometry ($J = 1/R$, $K = 0$) give values for $k_c J_0$ and k_c. The coefficients resulting from a calculation in the spherical geometry ($J = 2/R$, $K = 1/R^2$) give values for both $k_c J_0$ and $k_c + \bar{k}/2$. This method will be used in sec. 4.3.2 to compute the bending moduli for polymers adsorbed on hairy layers.

For vesicles, the Helfrich equation can be simplified. The surface tension γ_0 of a planar membrane is zero, and the system is symmetrical so that the spontaneous curvature J_0 should be zero. Given these conditions, the bending rigidity k_c is found from a calculation in a cylindrical geometry ($J = 1/R$ and $K = 0$) as $k_c = 2\gamma/J^2 = \gamma A R/\pi$, where $A = 2\pi R$ is the area of the cylinder per unit length. We may rewrite this as

$$k_c = -k_B T \frac{\ln(\Xi) R}{\pi} \tag{4.7}$$

where the radius R is calculated as the first moment of the excess volume fraction profile of lipids, $\varphi_i(z) - \varphi^b$, and Ξ is the grand canonical partition function which defines the surface tension γ as

$$\gamma = \frac{-k_B T \ln(\Xi)}{A} \tag{4.8}$$

In a spherical geometry ($J = 2/R$ and $K = 1/R^2$) we can write in a similar way

$$\left(k_c + \frac{1}{2}\bar{k}\right) = -k_B T \frac{\ln(\Xi)}{8\pi} \tag{4.9}$$

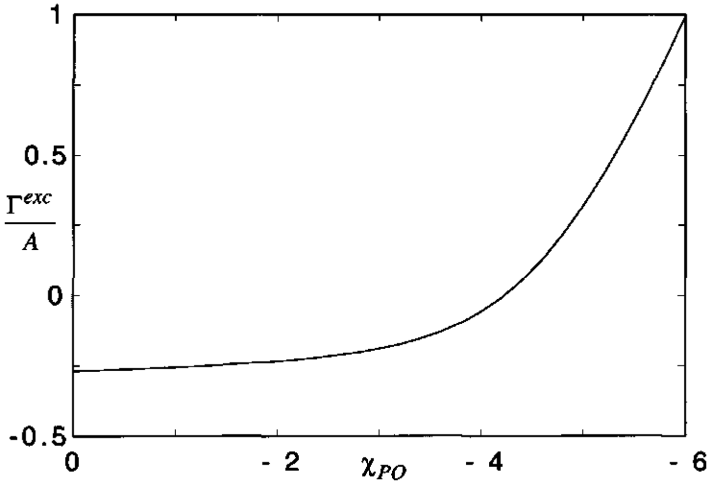

FIGURE 4.1: The excess adsorbed amount Γ^{exc} of homopolymers P_{100} divided by the area A on a $C_{12}E_5$ vesicle, upon increasing the adsorption strength $-\chi_{PO}$. Parameters: $\chi_{CW} = \chi_{CO} = \chi_{PC} = 1.6$, $\chi_{OW} = -0.3$. The bulk volume fraction of polymers is 0.01.

which shows that $\bar{k}$ can be obtained once k_c is calculated in a cylindrical geometry. When eqs. 4.7 and 4.9 are valid (i.e. $\gamma_0 = 0$ and $k_c J_0 = 0$) they greatly reduce the computational demand for finding the bending moduli. Instead of fitting through the results of calculations for multiple radii, it suffices to perform one calculation with a given radius. No terms of third order in curvature should be found since they are zero due to the symmetry of the membrane. Care should be taken to use a large enough radius R so that also fourth and higher order terms vanish.

4.3 Results

4.3.1 The $C_{12}E_5$ surfactant

The surfactant $C_{12}E_5$ is modelled as $C_{12}O(C_2O)_5$ where each C and O is taken to be one segment (of equal size). The solvent consists of monomers denoted W. This is the same system as studied by Oversteegen and Leermakers [64]. Using the approach outlined in appendix B.5 to reduce the discretisation artefact, we were able to reproduce their results by fitting numerical results for the surface tension for different radii of the vesicle to the Helfrich equation. Numerically, we find $\gamma_0 \approx 0$ and $k_c J_0 \approx 0$. Calculating cylindrical and spherical vesicles with a radius of $R \approx 150$ was sufficient to use eqs. 4.7 and 4.9 directly and yielded graphically identical results as found by the fitting procedure. This indicates that for $R \approx 150$ third and higher order terms in curvature are absent.

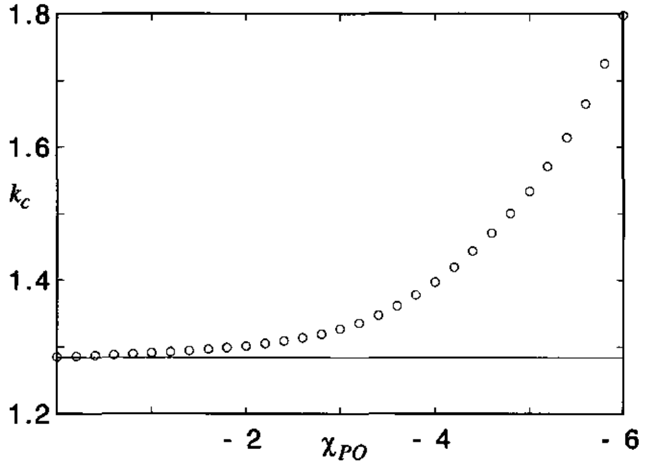

FIGURE 4.2: The bending rigidity k_c of a $C_{12}E_5$ vesicle with adsorbing homopolymers P_{100}, as a function of the adsorption strength (symbols). The horizontal line is the bending rigidity in the absence of polymer.

The adsorption energy of the polymer on the vesicle is controlled by varying χ_{OP}, the interaction between oxygen (O) and polymer (P). The excess adsorbed amount of polymer per (dimensionless) unit area is defined by:

$$\frac{\Gamma^{exc}}{A} = \frac{\sum_z L(z)(\varphi_p - \varphi_p^b)}{A} \tag{4.10}$$

where the area depends on the geometry considered. An example of Γ^{exc}/A for a $C_{12}E_5$ vesicle is shown in fig. 4.1. As the adsorption interaction χ_{OP} becomes more negative, the adsorbed amount on the vesicles increases. The slightly negative values at small $|\chi_{OP}|$ result from both depletion and the fact that the interior of the membrane is repulsive for the polymers.

The results for the bending rigidity are given in fig. 4.2. It can be seen that the influence of the adsorbed polymer layer on the bending modulus k_c is positive. From calculations done in chapter 3 for a polymer layer on a solid surface it was found that the contribution is negative. The contribution of polymers to the bending modulus of a vesicle becomes more positive as the adsorption energy is increased, whereas it is more negative when using a solid substrate.

Similar observations can be made for the saddle splay modulus (fig. 4.3) although the overall picture is less clear. Upon introduction of the polymer, the saddle-splay modulus $\bar{k}$ increases when no adsorption energy is present. We attribute this increase to the (slightly) decreased solubility of the surfactants in the solution, since the polymer volume fraction is 0.01. Upon increasing the adsorption strength the contribution $\Delta\bar{k}$ of the polymers to $\bar{k}$ changes sign: the saddle splay modulus of the

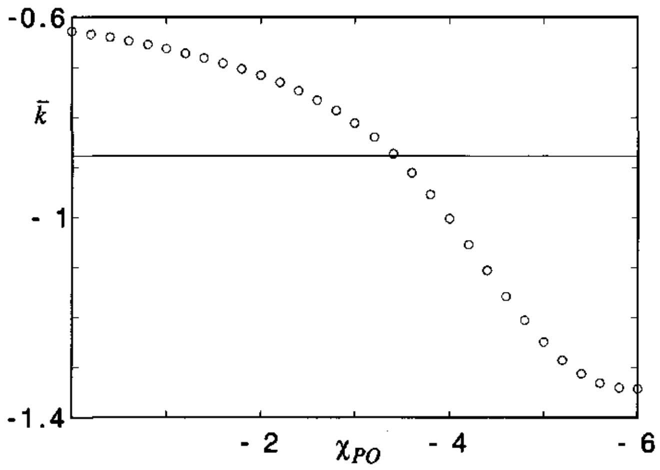

FIGURE 4.3: The saddle splay modulus plotted for the same system as fig. 4.2.

polymer layer becomes negative and increasingly so upon increasing the adsorption energy. Adsorption onto a solid surface gives a positive contribution to $\bar{k}$, increasing as the adsorption energy was higher as is shown in chapter 3.

4.3.2 Adsorption on hairy layers

In the previous section it was shown that for a relatively diffuse membrane the bending moduli are affected by introducing polymer which adsorbs onto the head-groups of the surfactant. The surprising result is that the contribution to the bending moduli generally has a different sign as compared to adsorption on a solid interface. Therefore, in this paragraph we investigate the contribution to the bending moduli of polymers adsorbing onto hairy layers, where the hairs are attached to a solid surface. This calculation is used as a model for an inert bilayer, i.e. a bilayer where the number of head groups per unit area is not affected by adsorbing polymer.

We consider relatively short hairs, at most 5 segments. The introduction of the hairs itself to the solid surface (without any added polymer) will also lead to finite values for the bending moduli. We have verified that (for long hairs) we can reproduce the mean-field results for the bending moduli of brushes [68], which read

$$k_c \sim \sigma^3 N^3 \tag{4.11a}$$

$$\bar{k} \sim -\sigma^3 N^3 \tag{4.11b}$$

where σ is the grafting density, expressed as the number of chains per unit area and N is the chain length of the anchored polymers. However, since the short hairs studied here are outside the brush regime these scaling relations break down.

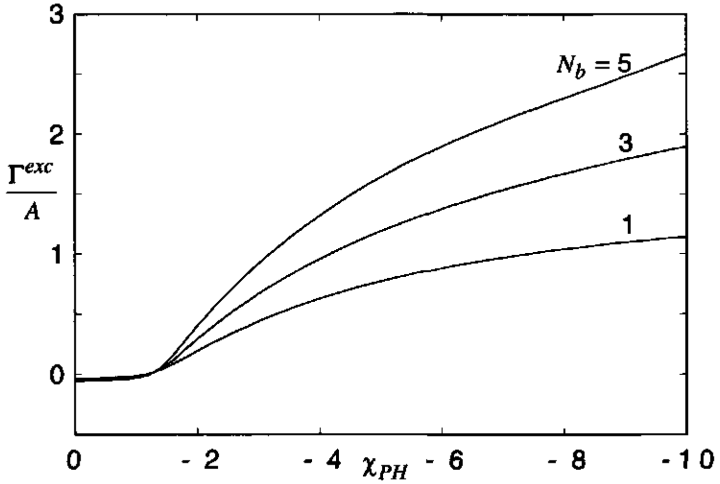

FIGURE 4.4: The excess adsorbed amount Γ^{exc} of homopolymers (P_{100} adsorbing on a hairy layer divided by the area A, upon increasing the adsorption strength $-\chi$. The bulk volume fraction of polymers is 0.01, the chain lengths of the hairs is indicated.

Here the focus is on the influence of the adsorbing polymers, therefore we will only consider the increments Δk_c and $\Delta \bar{k}$ and not the values of k_c and $\bar{k}$ themselves.

The volume fraction of head groups in the bilayer is about 0.2 for the $C_{12}E_5$ surfactant used in the previous section. Therefore the grafting density σ for the hairs is set to 0.2 as well. Both the surface and the hairs attract the polymer, which mimics a more or less smooth transition from a solid surface to a more diffuse adsorbing surface. The attraction to the surface is modelled through contact interactions, which gives a curvature dependence on the effective adsorption energy per adsorbed polymer segment, as described in the previous chapter (see eq. 3.30). The Flory-Huggins parameters for the interaction between the hairs and the polymer on the one hand and the interaction between the solid surface and the polymer on the other hand is taken to be equal and is denoted by χ_{PH}.

The excess adsorbed amount of polymer per unit area, Γ^{exc}/A as defined in eq. 4.10, on the hairy layers is plotted in fig. 4.4. As the adsorption strength is increased, the adsorbed amount increases as well. The critical adsorption energy can be estimated as $\chi_{PH} \approx -1.5$. As the hairs increase in length, more polymer is adsorbed, as expected.

The change in bending rigidity Δk_c of the hairy interface with adsorbing polymers as a function of the adsorption energy χ_{PH} is shown in fig. 4.5 for three different lengths of hairs: $N_b = 1$, 3, and 5. Again, the polymers have a length N of 100 and a bulk volume fraction of 0.01. For very short hairs, $N_b = 1$, the contribution to the bending rigidity is negative for moderate adsorption energies ($\chi \approx -2$ to

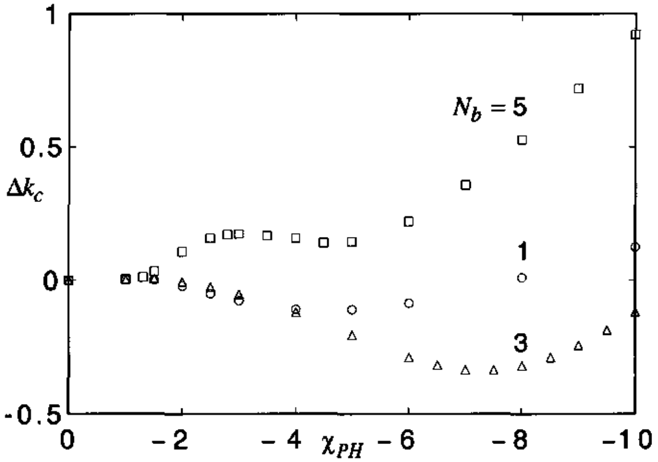

FIGURE 4.5: The change in bending rigidity Δk_c of a hairy layer with adsorbing homopolymers (P_{100}), upon increasing the adsorption strength $-\chi$ in a good solvent. The bulk volume fraction of polymers is 0.01.

$\chi \approx -7$), with a minimum around $\chi \approx -4$. For longer hairs ($N_b = 3$), Δk_c is more negative and the minimum is shifted to $\chi \approx -7$. When the hairs have a length N_b of 5 segments the contribution Δk_c of adsorbing polymers to the bending rigidity is positive over the whole range of χ_{PH}. Upon increasing the adsorption strength Δk_c first increases, has a maximum around $\chi \approx -3$ and minimum around $\chi \approx -5$, and it increases again as the adsorption strength $-\chi_{PH}$ is further increased.

The contribution of adsorbing polymer to the saddle-splay modulus is more straightforward than the contribution to the bending rigidity. The contribution $\Delta \bar{k}$ is always positive, increasingly so as the adsorption energy is increased. Upon increasing the length of the hairs $\Delta \bar{k}$ increases almost linearly, also for longer hairs (not shown).

4.3.3 Membranes with varying head-group size $C_{12}0_nC_{12}$

So far, we have seen that for a relatively diffuse membrane the influence of adsorbing polymer is to increase the bending rigidity k_c and (for high adsorption energy) to decrease $\bar{k}$. A comparison with adsorption on a hairy layer showed that the contribution to k_c indeed becomes positive for long hairs. This suggests that the change in bending rigity observed for adsorption onto a membrane of $C_{12}E_5$ surfactants is likely due to the length of the head groups. For the contribution of the adsorbing polymers to $\bar{k}$ the same reasoning does not apply. The adsorption of polymers onto a membrane of $C_{12}E_5$ surfactants showed a decrease in $\bar{k}$, whereas adsorption on hairy layers showed a positive contribution as the hairs become larger.

In this section we investigate the influence of a varying head-group size of the

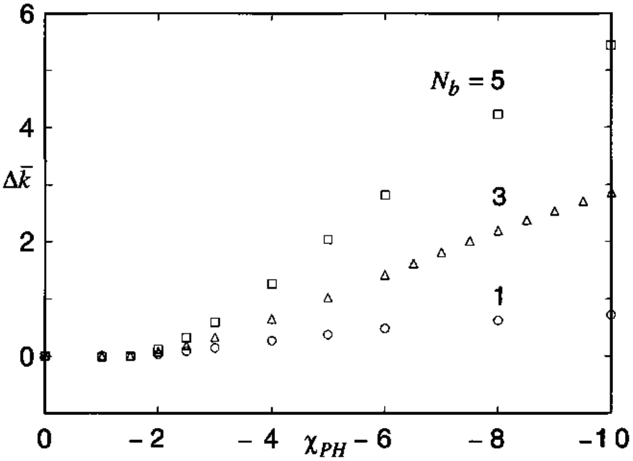

FIGURE 4.6: The change in the saddle-splay modulus Δk_c of a hairy layer with adsorbing homopolymers (P_{100}), upon increasing the adsorption strength $-\chi$ in a good solvent. The bulk volume fraction of polymers is 0.01.

surfactant. A more rigid membrane is used, to decrease the effect of the polymers on the solubility of the surfactants. A more rigid membrane will also allow us to decrease the size of the head group. Membranes with a small head group could be considered to act more like a solid adsorbing wall.

We have chosen a triblock surfactant $C_{12}O_nC_{12}$. The rationale behind this is that they will generate a more rigid membrane. This enables us to use a size of the head group as small as 3 segments ($n = 3$). The small middle block will be on the outside of the bilayer, with the triblock molecule resembling a hair-pin, which further reduces the effective size of the head-group.

The bending moduli k_c and $\bar{k}$ of membranes of $C_{12}O_nC_{12}$ without polymers are shown in fig. 4.7 as a function of the size n of the head group. When comparing with fig.4.2 it can be seen that these membranes are considerably more rigid than the membranes of $C_{12}E_5$ surfactants. As the size of the head group increases, the membranes become more rigid until a plateau of about 13 kT is reached. The saddle-splay modulus $\bar{k}$ shows a decrease as the head-groups become longer.

The excess adsorbed amount per unit area Γ^{exc}/A of homopolymer adsorbing onto the head group of the triblock surfactant is shown in fig. 4.8 as a function of the adsorption strength χ_{PO}, for different sizes of the head group. It can be seen that for small $-\chi_{PO}$ the same depletion effect is present as in fig. 4.1. In contrast with fig. 4.1 there is a more clearly defined critical adsorption energy $\chi_{PO} \approx -2.4$. The adsorption increases as the adsorption interaction becomes more favourable and as the size of the head groups increase.

The bending rigidity increment Δk_c of adsorbing polymer as a function of the

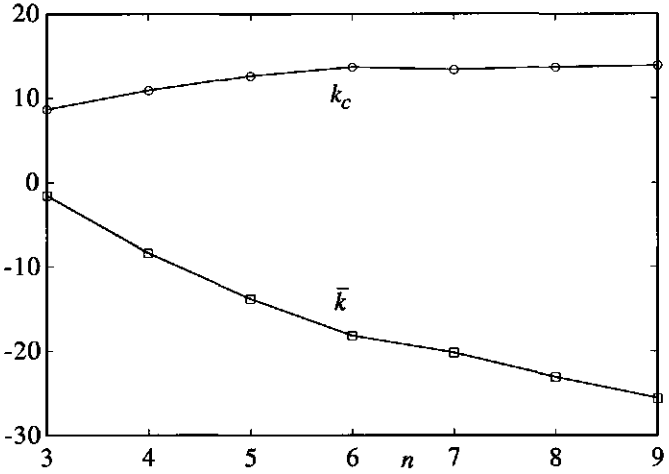

FIGURE 4.7: The bending rigidity k_c and the saddle-splay modulus $\bar{k}$ of $C_{12}E_nC_{12}$ membranes as a function of the head-group size n. Parameters: $\chi_{CW} = \chi_{CO} = 2.2$, $\chi_{WO} = -1.2$.

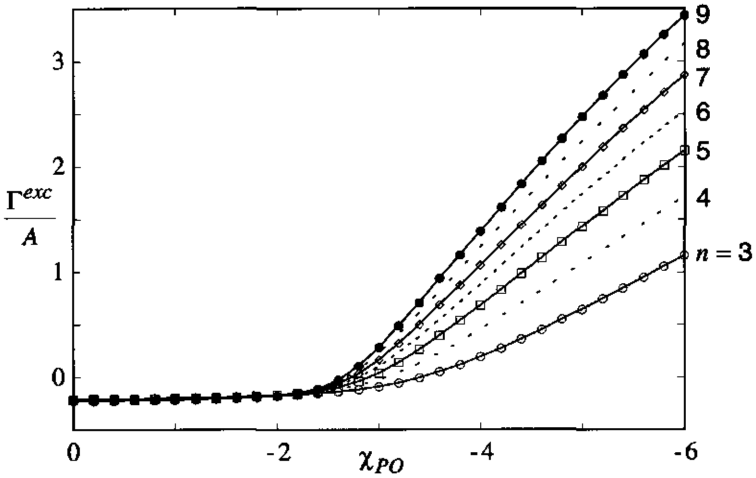

FIGURE 4.8: The excess adsorbed amount Γ^{exc}/A per unit area of homopolymers P_{100} adsorbing on vesicles upon increasing the adsorption strength $-\chi_{PO}$, for different sizes n of the head groups (indicated). The polymers are in good solvent ($\chi_{PW} = 0$), repel the tails of the surfactant ($\chi_{PC} = 1.6$), and have a volume fraction of 0.01. Other parameters as in fig. 4.7.

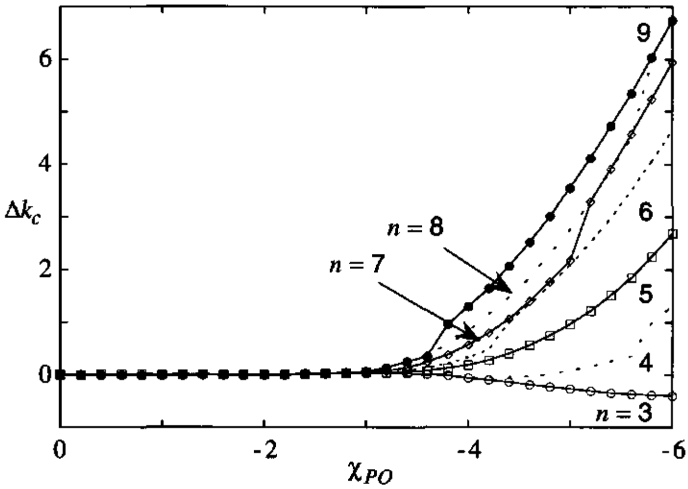

FIGURE 4.9: The increment in bending rigidity Δk_c of $C_{12}0_nC_{12}$ membranes due to adsorbing homopolymers P_{100}, as a function of the adsorption strength $-\chi_{PO}$. Parameters as in fig. 4.8.

adsorption energy is depicted in fig. 4.9 for different sizes n of the head group of a membrane consisting of $C_{12}0_nC_{12}$ surfactants. For relatively high adsorption energies we see indeed that the contribution of the adsorbing polymer becomes negative for a small head-group size ($n = 3$), as expected from calculations with an adsorbing solid wall. Upon increasing the head-group size n the contribution of the adsorbing polymers to the bending rigidity increases and becomes positive, as found from calculations on hairy layers.

The influence of the adsorbing polymer on the saddle-splay modulus $\Delta\bar{k}$ as a function of the adsorption energy is depicted in fig. 4.10. For relatively high adsorption energy $\Delta\bar{k}$ is positive when the head groups of the surfactants are small, as found for a solid wall. However, upon increasing the head-group size n the contribution of adsorbing polymer to $\bar{k}$ passes through a maximum and becomes it negative for head-group sizes above $n = 7$. This is in contradiction with the behaviour for hairy layers, where $\Delta\bar{k}$ continues to increase almost linearly as the hairs become longer, even for hairs with a length of 10 segments (not shown).

The scatter which is present in figs. 4.9 and 4.10 results from a small artefact still present in the current calculations. As explained in appendix B.5.4 the method to reduce the discretisation artefact results in a bulk volume fraction of polymers that is not exactly 0.01, although the difference is small (at most 0.5%). In principle, it should be possible to eliminate this artefact as well. The artefacts are more pronounced in the results for $\Delta\bar{k}$. This is due to two reasons. First, $\bar{k}$ results from comparing calculations in a spherical and cylindrical geometry so that the artefact

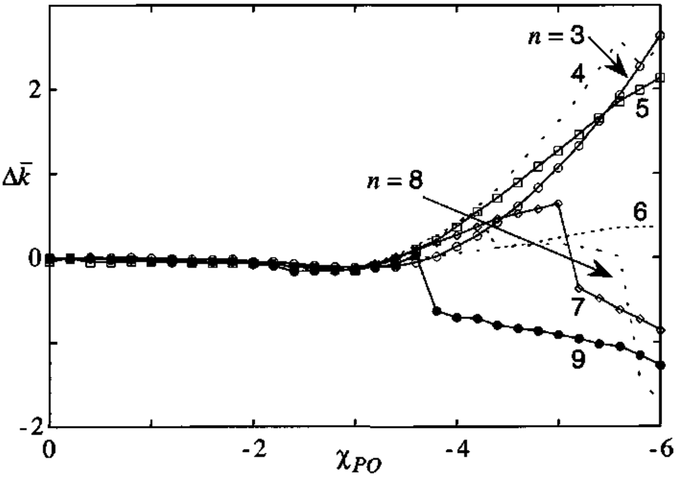

FIGURE 4.10: The contribution $\Delta\bar{k}$ of adsorbing polymer to the saddle splay modulus plotted for the same systems as fig. 4.9.

accumulates. Furthermore, the absolute values for $\bar{k}$ are relatively high. In fig. 4.10 only the increment (i.e., the difference between two large numbers) is given, which leads to more scatter.

4.4 Conclusions

Using a numerical mean-field theory we have investigated the influence of adsorbing homopolymer on the bending moduli of two types of surfactant bilayers. The polymer adsorbs onto the head groups of the surfactants. It is shown that for a relatively large head group the contribution Δk_c of the adsorbing polymer to the bending rigidity is positive, whereas the contribution $\Delta\bar{k}$ to the saddle-splay modulus is negative. In contrast, for smaller head groups Δk_c may become negative and $\Delta\bar{k}$ becomes positive.

The change in sign of Δk_c appears to be only due to the length scale of the adsorption interaction and not due to a change in the membrane, induced by the adsorbing polymers. This was checked by performing calculations on a hairy solid surface, where the polymer adsorbs both on the surface and on the hairs. Upon increasing the chain length of the hairs Δk_c increases, whereby it changes sign from negative to positive, in agreement with the findings for adsorption on surfactant bilayers with varying head-group size.

The change in sign of $\Delta\bar{k}$ upon increasing the head-group size of the surfactants could not be reproduced by the model calculations with hairy layers. For adsorption on hairy layers $\Delta\bar{k}$ increases almost linearly with the length of the hairs. In contrast, for adsorption on membranes a maximum in $\Delta\bar{k}$ is found as a function of the head-group size. The reason for this difference is still unresolved.

Overall, the values of the bending moduli turn out to be sensitive to the molecular detail of the membranes on which they adsorb. This is in agreement with findings in chapter 3 of bending moduli of polymer adsorbing on a solid wall, where it was found that the exact nature of the short range adsorption interaction has a large influence on the values found for k_c and $\bar{k}$. The latter parameter can even change sign, depending on the nature of the adsorption interactions.

It would be extremely helpful to be able to split up the bending rigidities into separate contributions from the polymer and from the membrane (or the hairy layer). This would enable to attribute the change in bending moduli to either of the polymer layer itself or to the induced changes in the membrane due to adsorption of polymer and/or changes in solubility of the surfactant. However, such a procedure is unavailable at the moment. One might attempt to split up the characteristic partition function into separate contributions from different molecules. However, at present it is unclear how this can be done unambiguously.

The current study has several limitations. Firstly, the stability of the membrane - polymer complex was not investigated in detail. It could very well be that the polymers and surfactants do not form a bilayer system spontaneously. Furthermore, if bilayers are formed from the triblock surfactant they could very well be in a stacked form, relatively close to each other. Preliminary calculations do indeed show an attractive well upon approach of two bilayers formed by the triblock $C_{12}O_nC_{12}$, with or without adsorbing polymers. For the $C_{12}E_6$ surfactant, the interaction is repulsive. The triblock surfactant is no longer resembles a hair-pin when two membranes approach each other. Instead, the hair-pin unfolds and forms an attractive bridge between the two bilayers. Lastly, this chapter, like chapter 3, shows that the bending moduli of adsorbing polymer are rather sensitive to details. The mean-field approximation is known to have deficiencies in the description of homopolymer adsorption. It could very well be that the whole picture emerging from this study is changed when a better approximation could be used.

Despite the limitations on the current results, we feel that it is safe to conclude that in general it is not allowed to use results generated for a solid wall in the presence of adsorbing polymer for making predictions for self-assembling vesicle systems with adsorbing polymer. Firstly, the membrane itself may change under the influence of polymers, as illustrated in fig. 4.3. In the present study this effect is not fully elucidated. Furthermore, length scale of the adsorption interaction plays a large role in the contributions to the bending moduli of the adsorbing polymers. Therefore, using a solid wall as a model for a membrane seems inappropriate to assess the bending moduli.

5 An efficient method to calculate volume fraction profiles for polydisperse block copolymers in self-consistent-field theory

ABSTRACT

An efficient procedure is described to calculate polydispersity effects in mean-field self-consistent-field (SCF) theory. The resulting volume fraction profiles are exactly equal to those generated by standard SCF theory, but they are calculated up to orders of magnitudes faster. Two conditions must be met for our efficient scheme to work. Firstly, the polymers need to be in equilibrium with an infinitely large bulk phase. Secondly, the length distributions in the bulk of different blocks cannot be correlated.

5.1 Introduction

In experiments most polymers are polydisperse. Polydispersity is known to have effects on for example phase diagrams of polymers and adsorption isotherms. The theory of Evers et al. [22] is suitable for multicomponent copolymer mixtures. However, the computational demand for a typical polydisperse copolymer is rather high. Let us consider for example a block copolymer consisting of two blocks with an average length of 50 segments: $A_{50}B_{50}$. A typical way of synthesis links two separably synthesized blocks together. When both blocks have a Flory like polydispersity the number of different molecules becomes of order 10000, where we have assumed that the number of different lengths of a single block is of order 100. As a result, the computational demand increases with about a factor of 10000 as compared to a homodisperse block copolymer. The computational demand diverges as the copolymers under consideration become increasingly complex, e.g. by adding more different blocks.

Roefs et al. [18] have proposed a method to deal with polydisperse homopolymers in a very efficient manner. In this chapter we propose a numerical method which is a generalisation of this efficient scheme towards block copolymers. This method has a computational demand which is about twice that of a monodisperse copolymer, irrespective of the complexity of the molecule. There are two restrictions which need to be met in order for this efficient scheme to work. Firstly, the polymers need to be in equilibrium with an infinitely large bulk phase. Secondly, the length distributions of different blocks cannot be correlated in the bulk, which may not always be the case in practice but is a rather common approximation.

5.2 Volume fraction profiles

For simplicity we will concentrate on diblock copolymers in a one dimensional mean field without curvature. In principle our method can be generalised towards arbitrary complex linear molecules where the lattice can have an arbitrary number of dimensions with added curvature. A generalisation towards branched molecules is also straightforward.

We consider a surface with an adjoining space that is divided into layers perpendicular to the surface. The layers are numbered with z running from $1, 2, \dots M$. Within each layer a mean field potential $u_A(z)$ is present, where the subscript A denotes the segment type. Here, segments will differ in their contact interactions, to be discussed later.

Consider a diblock copolymer consisting of two different segment types A and B. The length distribution of the A block is given by a probability $P_A(m)$ and N_{Am} denotes the length of the fraction m of A blocks. The maximum length of the A block is given by N_A. The total maximum chain length is given by $N = N_A + N_B$. The segment ranking number within the A block is s_A and runs from $1, 2, \dots, N_A$. We compute $G(z, s_A|1)$ from $s_A = 1$ to $s_A = N_A$, the same way we would do for a homodisperse block of length N_A.

$$G(z, s_A|1) = G_A(z) < G(z, s_A - 1|1) > \tag{5.1}$$

This propagator links the weight of segment s_A to all possible walks of segment $s_A - 1$ that end in a layer adjoining to z, while segment $s_A = 1$ can be anywhere on the lattice. The angular brackets denote a weighting over the adjoining layers defined through

$$< f(z) >= f(z) - \lambda(f(z-1) - 2f(z) + f(z+1)) \tag{5.2}$$

which is the discretisation of $f(z) - \partial^2 f(z)/\partial z^2$. The lattice constant λ is equal to $1/6$ on a cubic lattice. The starting condition of eq. 5.1 is

$$G(z, s_A = 1|1) = G_A(z) \tag{5.3}$$

Now we introduce the average end-segment weighting factor $G(z, \bar{s_A}|1)$ for the A block as

$$G(z, \bar{s_A}|1) = \sum_{s_A=1}^{N_A} P_A(s_A) G(z, s_A|1) \tag{5.4}$$

Next, we compute $G(z, s_B|1)$ for the B block. The starting equation is

$$G(z, s_B = 1|1) = G_B(z) < G(z, \bar{s_A}|1) > \tag{5.5}$$

the propagator towards the end of the chain is defined similar to eq. 5.1

$$G(z, s_B|1) = G_B(z) < G(z, s_B - 1|1) > \tag{5.6}$$

where $G(z, s_B|1)$ denotes the probability of finding segment s_B in layer z, while the first segment of the chain, $s_A = 1$, can be anywhere on the lattice. It should be clear that this procedure can be extended to more that 2 blocks rather easily by again applying an equation similar to eq. 5.4 on the result of eq. 5.6.

We also need probabilities for walks that start at the other end of the chain, at $s = N$. In principle the equations could be defined as the analog of the previously given walks forward. However, it turns out that the computation of the overall volume fractions is much more efficient when a different route is taken. This route is comparable to that given by Roefs et al. [18].

$$G(z, s_B|N_{Bm} \geq s_B) = G_B(z) < G(z, s_B + 1|N_{Bm} \geq s_B + 1) > + \\ P(s_B)G_B(z) \qquad (5.7)$$

where $G(z, s_B|N_{Bm} \geq s_B)$ denotes the statistical weight of all possible walks ending in segment s_B, while segment N_{Bm} can be anywhere on the lattice, *also* taking into account the length distribution of block B. That is, $G(z, s_B|N_{Bm} \geq s_B)$ denotes the weighted sum of walks that start at all end segments N_{Bm} that have a greater or equal length than the ranking number s_B. The starting condition reads

$$G(z, s_B = N_B|N_{Bm} \geq s_B) = G_B(z) \qquad (5.8)$$

Linking the A block can be done directly, without an averaging step as in eq. 5.4, since we have already averaged due to the rewriting of the propagator. So the starting condition for the A block reads

$$G(z, s_A = N_A|N_{Am} \geq s_A, N) = G_A(z)P(N_A) < G(z, 1|N_{Bm} \geq 1) > \qquad (5.9)$$

The propagator for block A towards the beginning of the chain is defined similar to eq. 5.7

$$G(z, s_A|N_{Am} \geq s_A, N) = G_A(z) < G(z, s_A + 1|N_{Am} \geq s_A + 1, N) > + \\ G_A(z)P(s_A) < G(z, 1|N_{Bm} \geq 1) > \qquad (5.10)$$

Again it should be clear that the number of blocks that can be linked in this way is easily extended.

Volume fractions can be calculated as follows

$$\varphi_A(z) = \frac{\varphi^b}{N^{av}} \frac{1}{G_A(z)} \sum_{s_A=1}^{N_A} G(z, s_A|1) G(z, s_A|N_{Am} \geq s_A, N) \qquad (5.11)$$

A similar equation is applied to block B. The normalization contains a factor N^{av} which is defined as

$$N^{av} = \sum_{m,n} P(m)P(n)N_{m,n} = \sum_{m=1}^{N_A} P(m)N_{Am} + \sum_{n=1}^{N_B} P(n)N_{Bn} \qquad (5.12)$$

The self-consistent field (SCF) solution can now be found exactly the same way as was done by Evers et al. [22]. Note that in our efficient scheme we have, temporarily, thrown away information on distribution of the volume fractions $\varphi_{m,n}(z)$ for the different chain lengths. This is a permitted operation since the SCF equations are written in terms of segment potentials and the total volume fraction in the system. As soon as the SCF solution is found we could do the computationally demanding task calculating the volume fractions of the individual components in the system.

$$\varphi_{m,n}(z, s_A) = \frac{\varphi^b_{m,n}}{N_{m,n}} \frac{G(z, s_A|1)G(z, s_A|N_{m,n})}{G_A(z)} \tag{5.13}$$

where $N_{m,n}$ equals $N_{Am} + N_{Bn}$ and $\varphi^b_{m,n}$ is the bulk volume fraction of chains containing N_{Am} segments A and N_{Bn} segments B. It is calculated as

$$\varphi^b_{m,n} = \frac{P(m)P(n)N_{m,n}}{\sum_{m,n} P(m)P(n)N_{m,n}} \varphi^b = \frac{P(m)P(n)N_{m,n}\varphi^b}{N^{av}} \tag{5.14}$$

Now it is also easily shown why this scheme works. The volume fraction of segment s_A of all chains, $\varphi(z, s_A)$, is the sum over m, n of eq. 5.13. Inserting eq. 5.14 we arrive at

$$\varphi_A(z, s_A) = \frac{\varphi^b}{N^{av}} \frac{G(z, s_A|1)}{G_A(z)} \sum_{m,n} P(m)P(n)G(z, s_A|N_{m,n}) \tag{5.15}$$

where the last sum is identified as $G(z, s_A|N_{Am} \geq s_A, N)$ in eq. 5.11

Note that computation of all $\varphi_{m,n}(z)$ for every m and n may become a computationally very demanding task when the number of different m and n becomes large or when more blocks are added. It usually suffices to compute $\varphi_m(z)$ and $\varphi_n(z)$, averaging over the other block(s).

6 Self-consistent-field theory for polymers with intramolecular excluded volume: bulk behaviour and effect on adsorption

ABSTRACT

Intramolecular excluded volume for polymers is considered on a mean-field level, using a simple extension of the standard Scheutjens-Fleer theory. We graft an average of all segments of one polymer to the centre of a spherical lattice, similar to the end-grafting as introduced by Edwards [7]. Our theory gives predictions for the properties of a single chain in solution which are in good agreement with scaling results. Satisfactory agreement with known results is obtained for a solution with a finite concentration of chains. The bulk solution shows relatively small oscillations in the density profile in the semi-dilute to concentrated regime. The dominant length scale in these oscillations is the chain length. The effect of intramolecular excluded volume on adsorption on to a solid wall is compared with known scaling results. It is our expectation that our theory may be generalised to study more complex systems as copolymer and polyelectrolyte adsorption.

6.1 Introduction

Homopolymer adsorption has been the topic of many theoretical and experimental studies over the past decades. Although some subtleties remain unsolved, general consensus seems to have been reached about the most important features of an adsorbed homopolymer layer. In this introduction we will briefly outline the main theoretical contributions to the understanding of homopolymer adsorption. In the following sections we proceed with one particular example of such a theory, that by Scheutjens and Fleer, and try to improve on its most important shortcoming within the mean-field approximation: the treatment of intramolecular excluded volume.

An important contribution to our present understanding of homopolymer adsorption from (semi-)dilute solution was made by the French school. Using arguments from both scaling theory and an analytical ground-state approximation, it was shown that an adsorbed homopolymer layer under experimentally accessible conditions, i.e. moderate adsorption energies and chain lengths, can be subdivided into three regions: the proximal, central, and distal region. The proximal region resides next to the surface and is dominated by the adsorption energy. Far away from the surface, the volume fraction φ shows an exponential decay as function of the distance r from the surface; this is the distal regime. In between the proximal and distal regions lies the central region, where the volume fraction scales as

$\varphi \sim r^{-4/3}$ in a good solvent and $\varphi \sim r^{-1}$ in a theta solvent as argued by de Gennes [12]. The scaling exponent in good solvent was recently confirmed by Monte Carlo simulations [69].

More advanced studies show that the simple subdivision as presented here is subject to all types of subtleties [70, 71]. However, for the present purpose and most practical applications the simple subdivision presented above suffices.

Another theoretical approach that has contributed greatly to our present understanding of homopolymer adsorption is due to Scheutjens and Fleer [6]. They used a numerical self-consistent-field (SCF) theory in which trains, loops, and tails were explicitly taking into account. A train is a walk of the chain along the surface, a loop connects two trains, and a tail is a chain end protruding into solution. The theory of Scheutjens and Fleer (SF-SCF) emphasised the importance of tails whereas earlier homopolymer adsorption theories neglected those. No explicit distinction is made in this model between the proximal, central and distal regions. However, in a recent contribution [60], dealing with analytical approximations of the SF-SCF theory these regions could be distinguished. The central region turned out to be relatively narrow and shows indeed a power law with, however, the wrong exponent -2 in a good solvent. As stated above, the correct exponent is $-4/3$.

An important drawback of the mean-field theory by Scheutjens and Fleer is its treatment of intramolecular excluded volume. In the bulk phase it is ignored completely and all chains are Gaussian, irrespective of the solvent strength or composition of the chain. In contrast, at the surface the chains swell due to accumulation of mass at the surface which results in intra- and intermolecular excluded volume. The neglect of the excluded volume of bulk chains has its repercussions on the adsorbed amount. For example, for homopolymers in good solution the adsorbed amount is systematically underestimated in the SF-SCF theory, due to the overestimation of the entropy of the bulk chains.

Another effect of the partial neglect of excluded volume is on the self-similar central regime of the adsorbed layer, as seen in the wrong exponent of the power law as discussed above. The mean-field exponent -2 for good solvents was predicted by several authors [60, 70, 72, 73]. As was shown numerically by Van der Linden and Leermakers [73], the SF-SCF model does indeed give this result in the limit of infinitely long chains. For finite chain lengths, a bulk volume fraction dependence on the exponent -2 is found which is also present on the exponent $-4/3$ as shown by Monte Carlo calculations [69].

As was noted earlier, the theoretical understanding of an adsorbed homopolymer layer is rather complete. This does not seem to justify an attempt to incorporate an description of excluded volume within the SF-SCF theory for homopolymers. However, the SF-SCF mean-field formalism which was originally put forward for homopolymer adsorption is more versatile. Generalisations towards copolymer and polyelectrolyte adsorption were formulated within the same framework. The SF-SCF theory has also been applied to study self-assembling and wetting. Therefore, an extension of the SF-SCF theory towards intramolecular excluded volume is expected to lead to an increased understanding of these more complex systems. The simple case of homopolymer adsorption is merely used as a test-case in this chapter. The results for the adsorbed amount and the scaling behaviour of the central regime will be used to test our theory.

This chapter is organised as follows. Firstly, the SF-SCF theory is extended to incorporate intramolecular excluded volume. Then, the properties of an isolated chain in solution are investigated and compared to well-known results. Secondly, a chain surrounded by bulk chains is considered. Again the results are compared to known scaling relations. Furthermore we observe (small) oscillations in the density profile when the polymer is surrounded by a semi-dilute to concentrated polymer solution. These oscillations have the interesting property that the dominating length scale is the chain length and are analysed in detail. Finally, polymers adsorbing onto a flat interface are considered and the central region of the adsorbed layer is analysed. The chemical potential of adsorbed polymer is set equal to that of a (swollen) chain in solution and the resulting adsorbed layer is analysed.

6.2 Theory

Space is discretised in layers, essentially in the way described in appendix B.2. The only difference is that the treatment is generalised to arbitrary dimensionality of space. The volume V of a 'sphere' with radius r in arbitrary dimension d reads

$$V(r) = \pi 2^{d-1} r^d / d \tag{6.1}$$

Two obvious special cases are a sphere ($d = 3$) and a cylinder ($d = 2$). In the latter case $V(r)$ is the volume per unit length of the cylinder. From eq. 6.1 the volume $L(r)$ of layer r is easily generated as $L(r) = V(r) - V(r-1)$. The surface S is given by

$$S(r) = \pi 2^{d-1} r^{d-1} \tag{6.2}$$

Again, for a cylinder ($d = 2$) $S(r)$ is the area per unit length. The *a priori* transition probabilities $\lambda(r)_{-1,0,1}$ are defined as

$$\lambda(r)_{-1} = \lambda S(r-1)/L(r) \tag{6.3a}$$

$$\lambda(r)_{1} = \lambda S(r)/L(r) \tag{6.3b}$$

$$\lambda(r)_{0} = 1 - \lambda_{-1} - \lambda_{1} \tag{6.3c}$$

The indices -1, 0, and 1 refer to to inward, parallel, and outward steps, respectively. These equations constitute all modifications needed to the standard SCF theory to incorporate different dimensionalities in a curved geometry. The dimensionality can be varied continuously and is not restricted to integer values.

We now consider a single chain grafted with an average of all segments at the centre of a curved geometry. A more precise description of the immobilisation mechanism is given at the end of this section, after we have discussed the equations that are needed. This central chain is surrounded by a bulk phase consisting of only solvent when the interest is in an isolated chain. The bulk phase may also contain polymers when the influence of the overall volume fraction of polymer on the conformations of the central chain is studied.

The segment weighting factor $G(r)$ of polymer is defined in the usual way:

$$G(r) = exp(-u'(r) + \chi(\langle\varphi_s(r)\rangle - \varphi_s^b)) \tag{6.4}$$

where $\varphi_s(r)$ is the volume fraction of solvent molecules, χ the Flory-Huggins interaction parameter, $u'(r)$ is the volume-filling potential or Lagrange multiplier resulting from the incompressibility constraint, and the angular brackets $\langle f(r)\rangle$ denote a layer average equal to $\lambda(r)_{-1}f(r-1) + \lambda(r)_0 f(r) + \lambda(r)_1 f(r+1)$.

When computing the volume fractions of polymer it is necessary to distinguish between walks, denoted by g (grafted), that pass the centre of the curved space and walks that do not, denoted by f (free). The chain propagators are written as usual [22, 59]:

$$G^g(1,s|1) = G(1)\langle G^g(1,s-1|1) + G^f(1,s-1|1)\rangle \tag{6.5a}$$
$$G^g(r,s|1) = G(r)\langle G^g(r,s-1|1)\rangle \quad \text{for} \quad r>1 \tag{6.5b}$$
$$G^f(1,s|1) = 0 \tag{6.5c}$$
$$G^f(r,s|1) = G(r)\langle G^f(r,s-1|1)\rangle \quad \text{for} \quad r>1 \tag{6.5d}$$

where the centre of the lattice is situated at $r = 1$. The end-segment weighting factors $G^g(r,s|1)$ and $G^f(r,s|1)$ for the grafted and free walks, respectively, are added in the centre ($r = 1$) as can be seen in the right-hand side of eq. 6.5a since any walk that passes through the centre is considered to be grafted.

The volume fractions are generated from the end-segment weighting factors as

$$\varphi^f(r) = C^f \sum_s \frac{G^f(r,s|1)G^f(r,N-s+1|1)}{G(r)} \tag{6.6a}$$
$$\varphi^g(r) = C^g \sum_s \frac{\left(G^f(r,s|1) + G^g(r,s|1)\right) G^g(r,N-s+1|1)}{G(r)} \tag{6.6b}$$

where C^f and C^g are the normalisation factors defined by

$$C^f = \varphi^b/N \tag{6.7a}$$
$$C^g = \frac{1}{\sum_r L(r)G^g(r,N|1)} \tag{6.7b}$$

The normalisation C^g ensures that exactly one chain walks through the centre. When calculating an isolated chain it suffices to set the bulk volume fraction φ^b to zero.

The above scheme immobilises the chain in a way that may seem peculiar at first. All walks of the chain through the centre are added and averaged. No segment is *a priori* excluded from being in the centre. In principle, the chain can be immobilised in a number of different ways. Edwards considered an end-attached chain. Alternatively, the middle segment can be grafted. We present comparisons between our method and these alternatives. It is to be expected that the differences are only minor. Nevertheless, we have a preference for the current immobilisation scheme for two reasons. Firstly, when we consider homopolymer adsorption onto a solid wall we will use the same immobilisation scheme at the surface. The volume fraction of the immobilised chains next to the surface will be renormalised such that their chemical potential is equal to that calculated for a (swollen) bulk chain. Clearly, when considering polymer adsorption one cannot simply end-graft a chain to a surface since this would correspond to a brush. However, to ensure that we can equate the chemical potentials for the bulk and surface chains, the same immobilisation scheme should be used at the surface as for the solution. Furthermore, in the current chapter, homopolymers are considered as a test case; we would like to generalise the current scheme to different polymer architectures. When considering different chain compositions different results can be expected. For example, a diblock copolymer with an insoluble block and a soluble block will shield its insoluble block from solution. Our method of immobilising the chain ensures that the chain has the degrees of freedom to assume the most favourable conformations.

In summary, the present theory presents a minor modification of the original theory by Edwards [7] to allow for the extension towards adsorption theory and more complicated chain architectures.

In the results section we are interested in the limit of infinite chain length. Obviously, this limit can not be reached using our numerical theory. Calculations for $N \approx 10^5$ become a computational burden on contemporary desktop computers. A special trick to save memory when evaluating the propagators is needed for these long chains (see appendix A.4). The combination of long chains and high χ values also leads to problems, as the values of the end-segment weighting factors $G(r, s|1)$ may become lower than the numerical representation of numbers (typically 10^{-300}). This problem is circumvented by using the scheme described in appendix A.3.

6.3 Results

6.3.1 Isolated chain

Firstly, an isolated chain anchored to the centre of a spherical geometry is considered. We will mainly present results for the radius of gyration R_g of the chain, which is defined as

$$R_g{}^2 = \frac{1}{N}\int_0^\infty L(r)\varphi^g(r)r^2\mathrm{d}r \tag{6.8}$$

The integral is discretised as described in appendix B.4.1. Fig. 6.1 shows the radius of gyration R_g as a function of the chain length for different solvent strengths on a lin-log scale. For all solvent strengths the radius of gyration increases with increasing chain length. For a given chain length the radius of gyration decreases as the solvent strength $-\chi$ is decreased. The curves for $\chi = 0.55$ and $\chi = 0.6$ show a

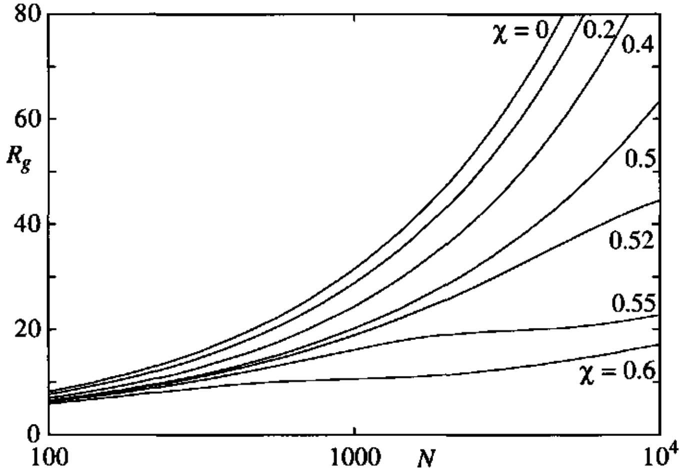

FIGURE 6.1: The radius of gyration R_g as a function of the chain length for different solvent strengths as indicated, plotted on a lin-log scale.

semi-plateau. For $\chi = 0.55$ the plateau in R_g is situated between about $N = 2000$ and $N = 5000$. We will elaborate on this plateau at the end of this section.

The remainder of this section will be split up in two parts. First, the swelling of the chain is investigated for conditions where the chain dissolves ($0 \le \chi \le 0.5$); the results are in figs. 6.2–6.5. Second, the collapse of the chain is studied in the bad solvent regime $\chi > 0.5$ (figs. 6.6–6.8). Our results will be compared to some well-known scaling results.

The relation between R_g and N is investigated by defining the apparent exponent ν_{app} as

$$\nu_{app} = \frac{\partial \ln R_g}{\partial \ln N} \tag{6.9}$$

This is the chain-length dependent equivalent of ν, the swelling exponent for infinite chain length. As ν_{app} increases, the chain swells more upon increasing the chain length.

Fig. 6.2 shows ν_{app} as a function of chain length N for different solvent strengths. For $\chi = 0$, ν_{app} increases for short chains and seems to reach a limiting value of about 0.59 for long chains. The limit of infinite chain length for $\chi = 0$ has received considerable theoretical attention. We will return to it shortly.

For $\chi = 0.2$, ν_{app} increases upon increasing chain length as well. However, as compared to $\chi = 0$ the limiting value is reached only at longer chain lengths. The same trend is observed for $\chi = 0.4$ and $\chi = 0.45$: the start of the plateau for ν_{app} is situated at a higher chain length upon decreasing the solvent strength. For $\chi = 0.5$ the well-known result $\nu = 0.5$ for a random coil is reproduced for long

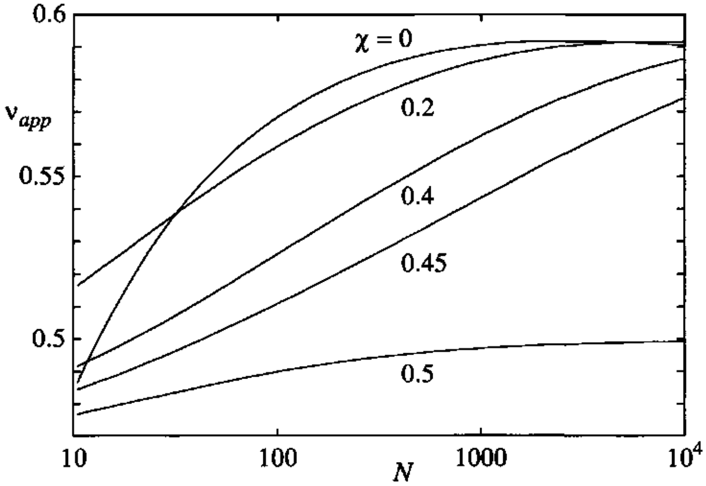

FIGURE 6.2: The apparent exponent ν_{app} for an isolated chain as a function of chain length for different solvent strengths as indicated.

enough chains.

In fig. 6.3 the apparent exponent ν_{app} for an isolated chain is plotted for a good solvent as a function of the chain length N, for $N > 1000$, and for three grafting methods. The first method is described in the theory section where an average of all segments is anchored in the centre (denoted by 'av-grafted'). In the second method the isolated chain is anchored by an end-point ('end-grafted') and in the third the chain is anchored by the middle segment ('mid-grafted'). It can be seen in fig. 6.3 that the latter two grafting methods result in a monotonically increasing apparent exponent. Instead, the results for the av-grafted chains show a maximum and a minimum as the chain length is increased. The maximum is positioned at $N = 2700$ and $\nu_{app} = 0.5917$. The minimum is positioned at $N = 38000$ and $\nu_{app} = 0.5895$. The occurrence of these extrema is not completely understood. For small chain lengths ($N < 100$), ν_{app} is close to the values found for the mid-grafting case (not shown). Apparently, these short chains have a preference for conformations with a middle segment in the centre. As the chains increase in length, the excluded volume forces more and more mass outside the centre of the lattice. Therefore, upon increasing the chain length, the conformations with an end-point in the centre will become more favourable. This leads to an extra increase in R_g, resulting in a higher apparent exponent ν_{app}. As soon as the number of conformations with a middle segment in the centre has dropped, the scaling of R_g will be more like the end-grafted case, leading to a decrease in ν_{app}. Finally, an increase is observed for long chains ($N > 40000$). We expect for the limit of infinite chain length that ν_{app} becomes exactly 0.6, as found from an analytical mean-field analysis [7, 74].

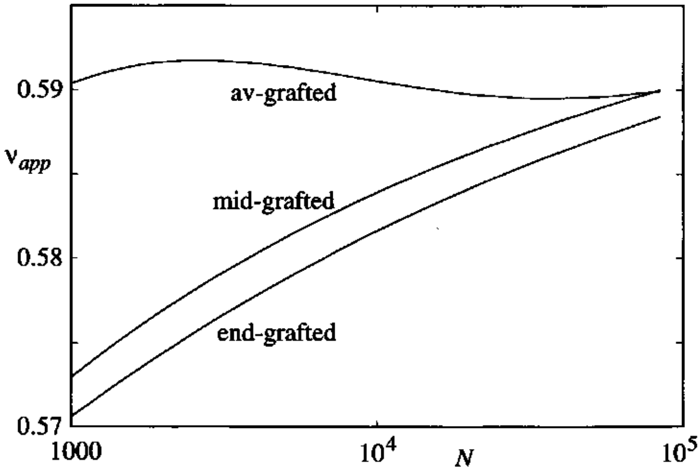

FIGURE 6.3: The apparent exponent ν_{app} for an isolated chain as a function of the chain length for three different grafting methods as indicated.

The analytical mean-field result of 0.6 for ν is equal to the value Flory [75] found from a surprisingly simple analysis of the excluded volume problem. More recent analyses have resulted in a slightly smaller value of ν for infinite chain lengths. It should be noted that no exact value for this exponent is available. Different techniques can be applied to calculate the value of ν [76]. The most noteworthy results are from the renormalisation group theory ($\nu = 0.588$) [74] and Monte Carlo simulations $\nu = 0.5877 \pm 0.0006$ [77]. Our apparent exponent matches the exact results for infinite chain lengths quite well over a broad range of chain lengths. However, our apparent exponent reaches its limiting value for infinite chain length from below, whereas Monte Carlo studies show that the limit should be reached from above. No exact limiting behaviour can be expected from a mean-field analysis as is argued by Des Cloizeaux and Jannink [74]. Therefore, we speculate that in the limit of infinite chain length ν_{app} is equal to 0.6 for the 'av-grafting' case.

Fig. 6.4 gives ν_{app} for a chain length N of 10000 segments as a function of the dimensionality of space for both a good ($\chi = 0$) and a theta solvent ($\chi = 0.5$). We can compare with the results of the Edwards approach for good solvent [74] and the scaling approach for a random walk (theta solvent).

$$\nu = 3/(d+2) \qquad \text{for} \qquad d \le 4, \qquad \chi = 0 \tag{6.10a}$$

$$\nu = 2/(d+1) \qquad \text{for} \qquad d \le 3, \qquad \chi = 0.5 \tag{6.10b}$$

As can be seen from fig. 6.4 the results for ν_{app} are in good agreement with these predictions. We attribute the remaining differences to the fact that the numerical results are for a finite chain length.

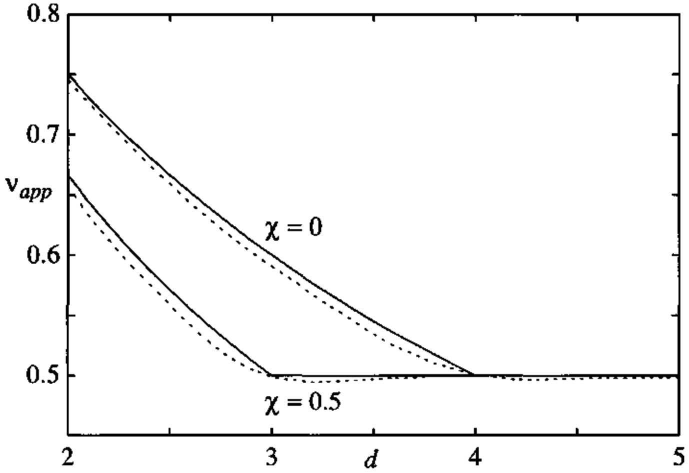

FIGURE 6.4: The apparent scaling exponent ν_{app} for an isolated chain of 10000 segments in a good and a theta solvent for different dimensionalities of space. The solid curves indicate the mean-field predictions for infinite chain length (eqs. 6.10), the dotted curves give the numerical results.

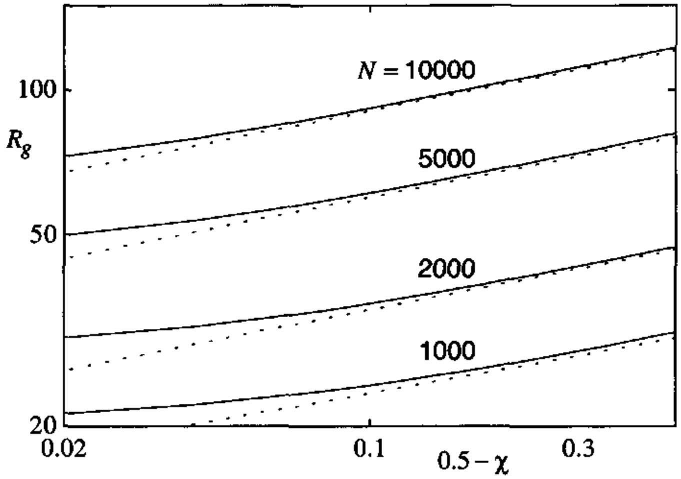

FIGURE 6.5: The radius of gyration of an isolated chain as a function of $0.5 - \chi$, plotted on a log-log scale for different chain lengths, as indicated (solid curves). The dotted lines represent the predicted scaling behaviour and have a slope of $2\nu - 1 = 0.180$.

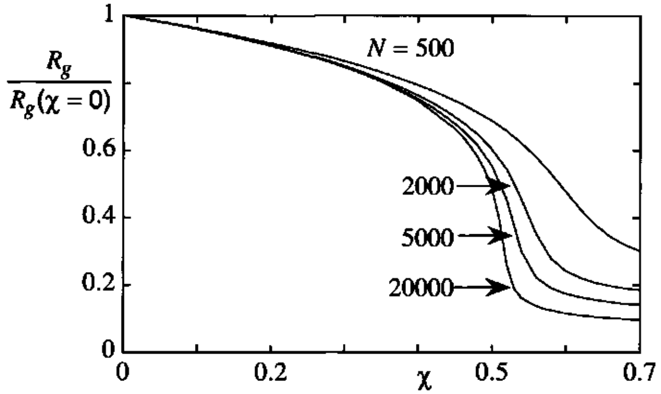

FIGURE 6.6: The radius of gyration R_g divided by R_g found for a good solvent ($\chi = 0$) as a function of the interaction parameter χ for an isolated chain

Upon increasing χ the radius of gyration goes down. The predicted scaling behaviour is $R_g \sim (0.5 - \chi)^{2\nu-1}$ [78]. As can be seen from fig. 6.5 our numerical calculations describe this behaviour very well. The agreement improves upon increasing the chain length, as expected.

We now turn to the chain collapse in a bad solvent ($\chi > 0.5$). Fig. 6.6 shows the coil-globule transition for different chain lengths. The radius of gyration R_g, normalised to that of $\chi = 0$, is given as a function of χ. Upon decreasing the solvent strength R_g decreases. For relatively high chain lengths ($N > 2000$) the coil-globule transition is clearly visible. As the chain length goes to infinity, an infinitely sharp transition is expected at $\chi = 0.5$), corresponding to a second-order phase transition.

In fig. 6.7 the relative fluctuations in the radius of gyration are given as a function of the solvent strength. The relative fluctuations are given by

$$\frac{{R_4}^4 - {R_g}^4}{{R_g}^4} \tag{6.11}$$

where R_4 is the fourth moment of the volume fraction profile, defined as

$${R_4}^4 = \frac{1}{N}\int_0^\infty L(r)\varphi(z)z^4 \mathrm{d}z \tag{6.12}$$

The relative fluctuations pass through a maximum at the transition between a coil and a globule, as is common for a phase transition. Clearly, the transition becomes narrower as the chain length is increased. Furthermore, the transition approaches $\chi = 0.5$ for infinite chain length. In the collapsed state, the relative fluctuations should approach zero upon decreasing solvent strength, which cannot be explicitly tested with our numerical theory.

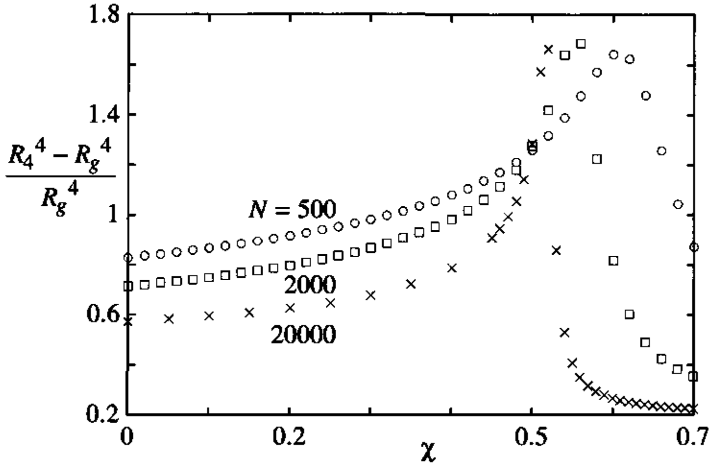

FIGURE 6.7: The relative fluctuations in the radius of gyration of an isolated chain as a function of solvent strength, for three chain lengths as indicated.

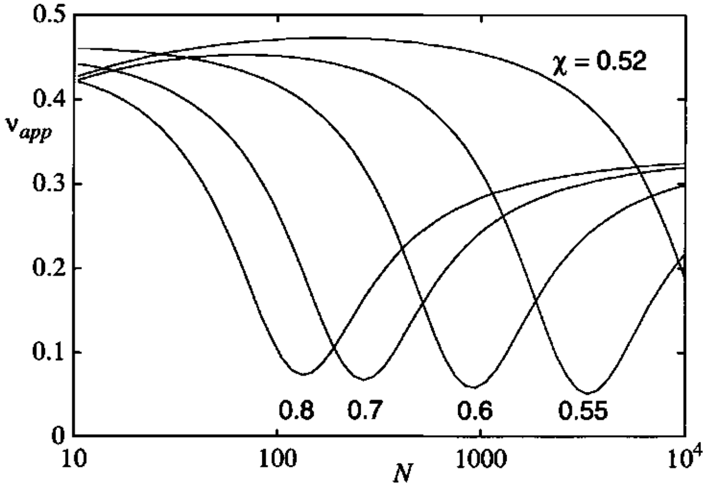

FIGURE 6.8: The apparent exponent ν_{app} for an isolated chain as a function of chain length for different solvent strengths as indicated.

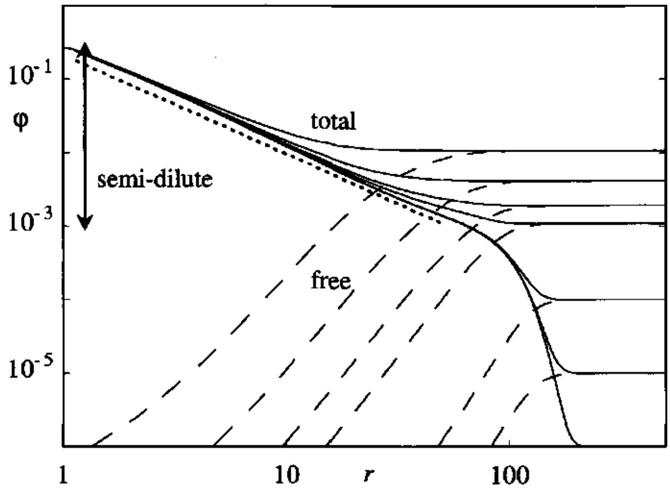

FIGURE 6.9: The volume fraction as a function of the distance r from the centre for a central chain with a length N of 5000 in good solvent, surrounded by different bulk volume fractions plotted on a log-log scale. The solid curves represent the total volume fraction, the dashed curves show the volume fraction of surrounding (free) chains. The dashed line has a slope of -4/3.

Fig. 6.8 shows the apparent scaling exponent ν_{app} as defined by eq. 6.9 as a function of chain length for different bad solvents as indicated. The most unfavourable solvent $\chi = 0.8$ shows a minimum of about $\nu_{app} \approx 0.07$ around $N = 110$, and reaches the limiting value of $\nu_{app} = 1/3$ for longer chains, as expected for a globule. For more favourable solvents the minimum in ν_{app} shifts to higher chain lengths. The minima of ν_{app} in fig. 6.8 correspond to the plateaus shown in fig. 6.1 where the radius of gyration R_g changes only very little as a function of N. The minima of ν_{app} are related to the collapse transition and are in the proximity of both the maxima in the relative fluctuations of R_g as given in fig. 6.7 and the inflection points in fig. 6.6. Increasing the chain length in this case does lead to an increase in R_g, since ν_{app} is positive. However, this increase almost cancels against the additional collapse caused by an increase in chain length for a given solvent strength.

6.3.2 Effect of volume fraction

In the previous section it was shown that we are able to reproduce known (mean-field) scaling relations for an isolated chain. Now we turn our attention to a central chain surrounded by a solution of both solvent and polymer of the same chain length.

The total volume fraction profiles $\varphi(r)$ and those of the surrounding chains are plotted on a log-log scale in fig. 6.9 for a chain length N of 5000 and good solvent

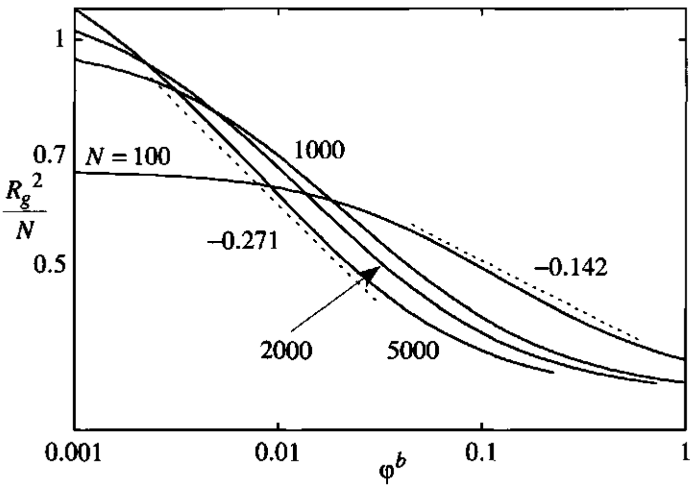

FIGURE 6.10: The scaled radius of gyration of a central chain as a function of the volume fraction of bulk chains in a good solvent, plotted on a log-log scale.

conditions ($\chi = 0$). As can be seen, the free chains penetrate the central chain further upon increasing the bulk volume fraction. The total volume fraction near the centre can be described with a power law which is predicted as $\varphi \sim r^{-(3\nu - 1/\nu)}$ [7]. For dilute solutions the power law holds up to the radius of gyration, which is 81 here. In the semi-dilute regime the power law holds approximately until the bulk volume fraction is reached where the power law crosses over to a constant. The power law has a scaling exponent of about $-4/3$ as indicated in fig. 6.9.

In fig. 6.10 the radius of gyration of the central chain in good solvent is shown as a function of the bulk volume fraction of the polymer solution. Upon increasing the bulk volume fraction the chains shrink, as expected. In the limit of a polymer melt, the intramolecular excluded volume is screened and the central polymer can be described as a random walk on the basis of the Flory theorem [75]. The scaling relation for the shrinking of the chain is $R_g^2 \sim (\varphi^b)^{-1/4}$ [12, 79]. The dotted lines in fig. 6.10 give the fitted slope over the interval shown. The resulting exponents are arbitrary to some degree: if the width of the fitting interval is changed, a different exponent results. Although for N = 1000–5000 the scaling relation is reasonably obeyed, it is observed that the correspondence between the numerical results and the scaling relation does not improve as we increase the chain length: the trend is away from the scaling relation.

In fig. 6.11 the excess volume fraction profile $\varphi(r) - \varphi^b$ is given for a solution of $\varphi^b = 0.3$ and $N = 100$. Upon magnification, one can clearly observe oscillations in the volume fraction profile. Recently, damped oscillations in the density profile of a concentrated polymer solution near a solid surface were reported [80]. These

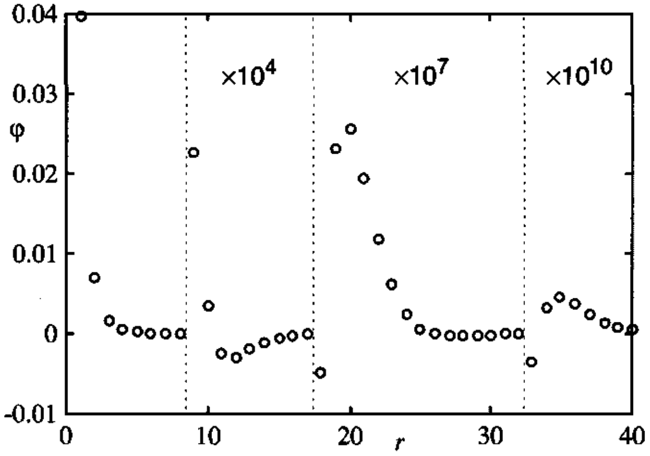

FIGURE 6.11: The excess volume fraction φ^{exc} as a function of the distance r from the centre. The dotted lines denote a change in scale of the values for φ^{exc}. The oscillations can hardly be seen without magnification. The magnification factors are indicated in the figure.

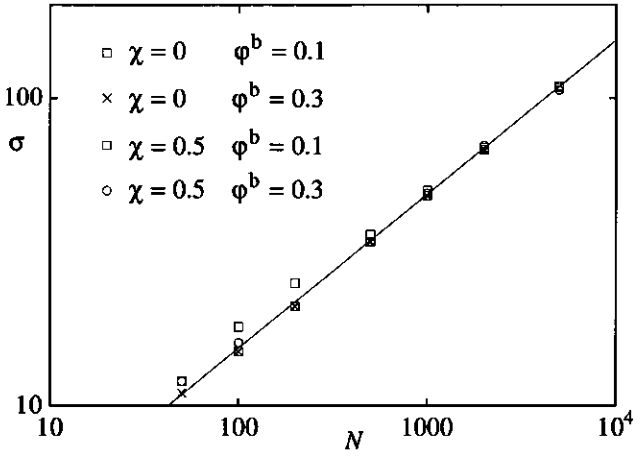

FIGURE 6.12: The wavelength σ of oscillations in volume fraction in the bulk phase surrounding a central chain as a function of the chain length N in a concentrated polymer solution. Concentrations and solvent conditions are as indicated in the legend.

damped oscillations can be described by

$$\varphi(r) - \varphi^b = B \exp(-\alpha r) \cos(2\pi r/\sigma) \tag{6.13}$$

Here we will use the same equation to describe the oscillations in the bulk solution. The parameters in eq. 6.13 describe the ordering in the solution. The wavelength of the ordering is given by σ, α is the inverse decay length of the oscillations, and B is the amplitude.

The oscillations present in fig. 6.11 have the same origin as those reported for a polymer solution near a solid wall. The polymer chains in solution behave like coils which slightly repel each other. When considering denser coils, like dendrimers, it is expected that the repulsion becomes more pronounced, ultimately leading to hard-sphere behaviour.

The parameters from eq. 6.13 can easily be obtained from the density profile. The wavelength σ is found by looking at the positions of the maxima and minima in the volume fraction profile. A semi-logarithmic plot of the magnitude of the successive extrema versus the distance from the centre of the spherical coordinate system gives a straight line from which α and B can be obtained.

We looked at the oscillations in the density profile for two bulk volume fractions $\varphi^b = 0.1$ and 0.3 in a good and in a θ solvent. Fig. 6.12 shows the wavelength σ as a function of the chain length N. It is clear from this figure that both the bulk volume fraction φ^b and the solvent strength have no influence on the wavelength σ, which obeys the equation $\sigma \approx 1.5N^{0.5}$. This result is identical to that found for polymers near a non-adsorbing wall [80]. For a θ solvent σ is comparable to the

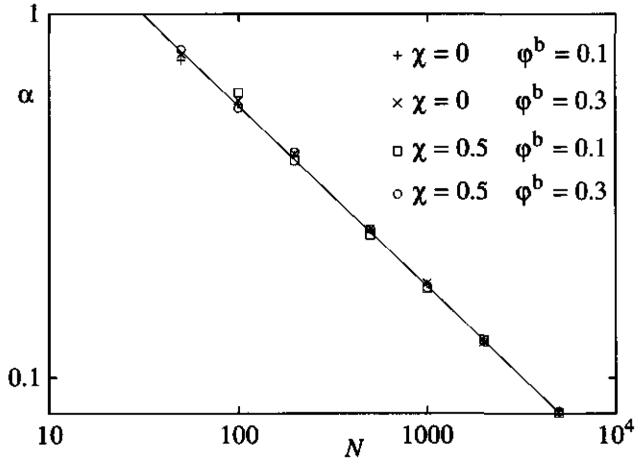

FIGURE 6.13: The inverse decay length of the oscillations in the volume fraction profile for the same system as fig. 6.12.

radius of gyration R_g of the chain. In a good solvent this is not the case, one would expect σ to scale as $N^{0.6}$. This is a manifestation of the fact that in our calculations only the central chain has intramolecular excluded volume. For the bulk chains the intramolecular excluded volume is neglected. Hence, for a simulation where also the bulk chains have excluded volume we expect that the results for $\chi = 0$ and $\chi = 0.5$ would not coincide, as they do in fig. 6.12.

Fig. 6.13 shows the inverse decay length α of the oscillations. Again no influence of either the bulk volume fraction or the solvent strength is observed. The decay length obeys the equation $\alpha^{-1} = 0.19N^{0.5}$. Again, this result is identical to that found for polymers near a non-adsorbing wall [80].

The amplitude B of the oscillations, shown in fig. 6.14, scales as $B \sim N^{-2.2}$. The scaling exponent does not depend on the solvent strength χ and the bulk volume fraction φ^b. The prefactor of the scaling relation does depend on these parameters. This can be explained as follows. The parameter B is a measure for the amount of ordering of the chains. A solid wall is expected to have a strong influence on the ordering. Therefore, B is higher for non-adsorbing polymers near a solid wall [80]. Upon increasing the bulk concentration the central chain is screened, which leads to a higher interpenetration of chains and hence to a lower ordering. This explains the differences found between $\varphi^b = 0.1$ and 0.3. The central chain in a good solvent is more strongly swollen than in θ solvent, leading to lower volume fraction within the chain, which in turn leads to less ordering. This effect is more pronounced for lower φ^b, since the central chain is less screened in this case.

Near the depletion region next to a solid wall B was found to scale as $N^{-1.8}$, whereas here we find a scaling of $N^{-2.2}$. The difference can be attributed to the

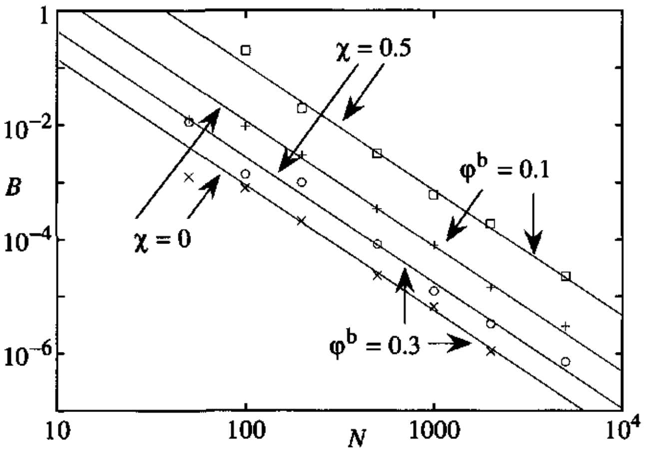

FIGURE 6.14: The amplitude of the oscillations in the volume fraction profile for the same system as fig. 6.12.

different geometry of the calculations: planar for a solid wall, spherical in this case.

For non-adsorbing polymer next to a solid wall, it was argued that for small chain lengths the scaling exponent is less negative, indicating a different regime. We do not find this result for the bulk case. Instead, scatter is observed for small chain lengths due to inaccuracies in the fitting procedure used to find B. The positions of the extrema in the density profile may have a deviation as large as half a segment diameter. This is due to the discretisation of space, which is divided into layers with a spacing of one segment diameter. A shift over one lattice layer of the extrema may lead to a difference in B of about 100%. This is especially important for small chain lengths were the wavelength σ of the oscillations is only a few lattice layers. This discretisation artefact results in the scatter in fig. 6.14.

6.3.3 Effect on polymer adsorption

As in the bulk case, we can treat the chains adsorbed onto the surface separately and renormalise their density to ensure a pre-imposed adsorbed amount. This is done by performing a calculation for a planar geometry, using eqs. 6.5 and renormalising the volume fraction in a way similar to eq. 6.7b. The only difference is that we want to be able to fix the adsorbed amount θ^a to a given value. The normalisation used for adsorbed chains is written as:

$$C^a = \frac{\theta^a}{N \sum_r G^g(r, N|1)} \tag{6.14}$$

which is a variant of eq. 6.7b, with θ^a being the adsorbed amount and $L(r)$ is set equal to 1 for the planar geometry.

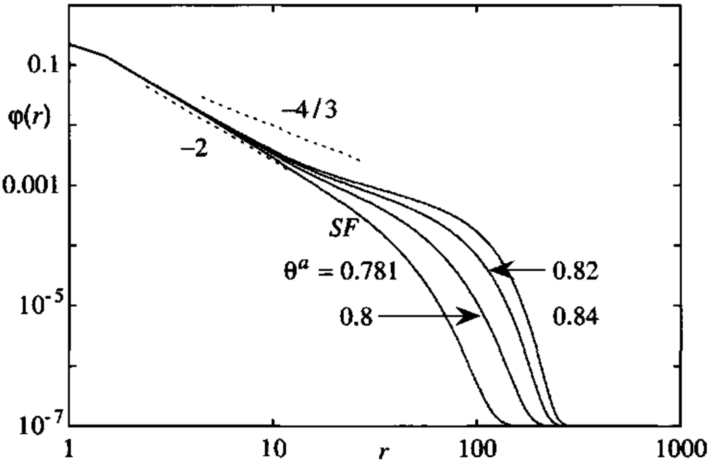

FIGURE 6.15: The volume fraction profile plotted on a log-log scale for adsorbing homopolymer with a chain length N of 10000 for different values of a imposed adsorbed amount. The volume fraction profile labelled 'SF' corresponds to a standard Scheutjens-Fleer equilibrium calculation.

Fig. 6.15 gives the structure of the adsorbed layer as a function of the amount of polymers, immobilised to an adsorbing surface, with a dimensionless attractive energy $\chi_s = 1$, which corresponds to 1 kT for each adsorbing segment. Apart from the immobilized chains a bulk solution of $\varphi^b = 10^{-7}$ is present. We have varied the adsorbed amount using the split-up of adsorbed and free chains as described in eqs. 6.5 and 6.14.

The curve in fig. 6.15 labelled '*SF*' corresponds to the SCF solution for the Scheutjens-Fleer theory. Upon increasing the adsorbed amount above this solution we see that the adsorbed chains start to swell. A self-similar region in the volume fraction is predicted to be present from $r \approx D$ to $r \approx R_g$, where D is the proximal length. The curve for $\theta^{ads} = 0.82$ has a power-law type behaviour $\varphi(r) \sim r^{-\alpha}$, where α is above -2: it appears to reach a value close to $-4/3$. Upon increasing the adsorbed amount even further, we overshoot the power of $-4/3$.

The power-law behaviour of the volume fraction profiles given in fig. 6.15 is investigated in detail in fig. 6.16. Here, the apparent exponent $\alpha_{app}(r)$ of the volume fraction profile is plotted, which is defined by:

$$\alpha_{app}(r) = \frac{\partial \log \varphi(r)}{\partial \log r} \tag{6.15}$$

This equation is discretised as

$$\alpha_{app}(r) = \frac{\log\left[\varphi(r)\right] - \log\left[\varphi(r-1)\right]}{\log\left(r-0.5\right) - \log\left(r-1.5\right)} \tag{6.16}$$

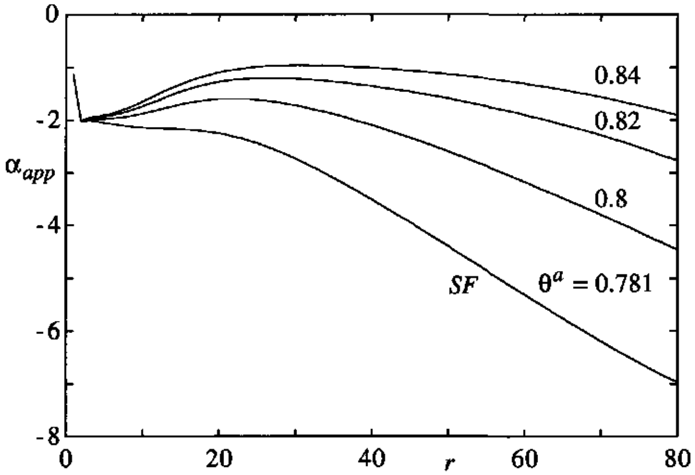

FIGURE 6.16: The apparent exponent α_{app} as a function of the distance from the interface for the volume fraction profiles of fig. 6.15. The volume fraction profile labelled '*SF*' corresponds to a standard Scheutjens-Fleer equilibrium calculation.

The shift over half a layer in the denominator of eq. 6.16 appears because the volume fraction $\varphi(r)$ in layer r is assigned to the middle of the layer.

Fig. 6.16 shows that the scaling regime is not clearly defined. Rather than a region with a constant value for α_{app} we see a continuous decreasing value of α_{app} for low adsorbed amounts. For higher adsorbed amounts, an oscillation in α_{app} is found. The curve indicated with 'SF' corresponds to the SCF solution of the Scheutjens-Fleer theory. Also in this case, a clear scaling region is not found. This effect is probably due to a finite chain-length effect combined with a dependence on the bulk volume fraction φ^b of the scaling exponent α. Monte Carlo calculations for chains of length 1000 show a similar dependence of the exponent in the self-similar region on the bulk volume fraction [69]. De Joannis et al. [69] also find that the self-similar region has a lower power law as the bulk volume fraction is decreased below the overlapping volume fraction.

6.3.4 Matching chemical potentials

The previous section showed that the scaling exponent of the volume fraction of the central region can be increased above the Scheutjens-Fleer mean-field value of -2 by increasing the adsorbed amount. For a certain adsorbed amount the exponent appears to become close to the value predicted from a scaling analysis. It is then of interest to calculate the chemical potential of the chains immobilized to the surface.

The chemical potential μ^a of the adsorbed chains is defined through:

$$\mu^a = \left(\frac{\partial (F - \sum_{i=\mathbf{free}} n_i \mu_i^{FH})}{\partial n^a} \right)_A \tag{6.17}$$

where F is the Helmholtz energy, μ^{FH} is the chemical potential following from Flory-Huggins theory, n^a is the number of adsorbed chains, and the sum runs over all components that are not immobilized on the surface, so all molecules except for the chains that are adsorbed onto the surface. The differential is taken at constant surface area A. In sec. 2.2.8 it is argued that the chemical potential μ^a from eq. 6.17 is equal to that in eq. 2.88, which in the absence of chemical equilibria and for a good solvent can be simplified to

$$\frac{\mu^a}{k_B T} = \ln (NC^a) + 1 - N(1 - \varphi^b) + \varphi^b \tag{6.18}$$

We verified the equivalence of eqs. 6.17 and 6.18 also numerically.

The chemical potential of the bulk chains, computed in a spherical geometry, will also be different from the Flory-Huggins value. The incorporation of intramolecular excluded volume for the chain in the bulk will lead to a change in chemical potential as compared to the expression from the Flory-Huggins theory. The chemical potential μ^b for the bulk chain is computed as

$$\mu^b = F - \sum_{i \neq g} n_i \mu_i^{FH} + kT \ln \varphi^b \tag{6.19}$$

where F is the Helmholtz energy of the system, μ_i^{FH} is the Flory-Huggins expression for the chemical potential, and the sum runs over all components which are present in the system except the chain which is anchored in the centre, denoted by g. Since the chain is immobile, the translational entropy needs to be added separately in the last term.

The effect on the adsorption to a solid wall is computed by ensuring that the adsorbed chains have the same chemical potential as that computed for the bulk chain. For the adsorption case we therefore perform two separate calculations. Firstly, a calculation in a spherical geometry to calculate the chemical potential of the chain with intramolecular excluded volume. Next we proceed with a calculation in a planar geometry. The chains of interest are those who are adsorbed onto the surface. The chemical potential of the (swollen) polymer in the bulk is known from eq. 6.19. The adsorbed amount is increased until the chemical potential of the adsorbed chains is equal to that of the swollen chain in the bulk phase. It turns out that an iteration based on the normalisation given by eq. 2.31 does not result in convergence of the SCF equations for relatively long chains. Instead, we vary the amount of molecules anchored to the surface, until their chemical potential equals that of the bulk chains.

In fig. 6.17 the difference between the chemical potential defined by eq. 6.19 and the Flory-Huggins chemical potential is plotted as a function of the bulk volume

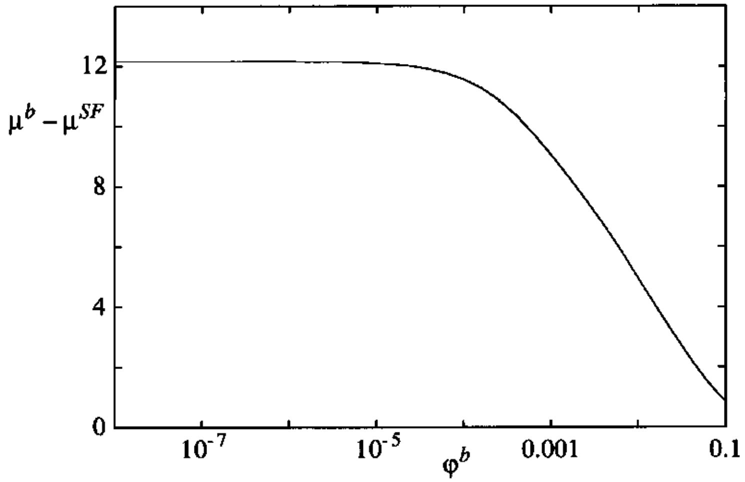

FIGURE 6.17: The difference between the chemical potential μ^b of a immobilised chain in the bulk and the Flory-Huggins chemical potential μ^{FH} as a function of the bulk volume fraction. Both immobilised and bulk chains have a chain length N of 10000 and are in good solvent ($\chi = 0$).

fraction. Upon decreasing the bulk volume fraction below the semi-dilute regime, the difference in both chemical potentials becomes constant. This is to be expected since the grafted chain does not swell any more upon lowering the bulk volume fraction. The chemical potential of a melt is not exactly equal to the Flory-Huggins chemical potential. This is due to the fact that the central lattice site has a radius of unity. It is possible to tune the volume of the central lattice site such that both chemical potentials exactly coincide (not shown).

The volume fraction profiles resulting from matching the chemical potential of the adsorbed chains to that of the (swollen) bulk chain are shown in fig. 6.18 on a log-log scale for $N = 10000$. For a bulk volume fraction φ^b of 10^{-13} to 10^{-7} the central region of the adsorbed layer follows more or less a power law, although for smaller φ^b the exponent of the power law slightly decreases. For $\varphi^b = 10^{-4}$ the resulting volume fraction profile resembles that of fig. 6.15 in the case of (too) high adsorbed amounts. For comparison, the volume fraction of the standard SCF theory are given in fig. 6.19. Here it is seen that the mean-field power law exponent of -2 is approximately found for $\varphi^b = 10^{-4}$.

Fitting power law exponents is a rather delicate procedure. Therefore, in figs. 6.20 and 6.21 the apparent exponent $\alpha_{app}(r)$ is plotted as a function of the distance from the surface for the volume fraction profiles given in figs. 6.18 and 6.19, respectively. In figs. 6.20 and 6.21 it can be seen that $\alpha_{app}(r)$ increases as the bulk volume fraction φ^b is increased. From both figures it can be concluded that it is hard to assign one

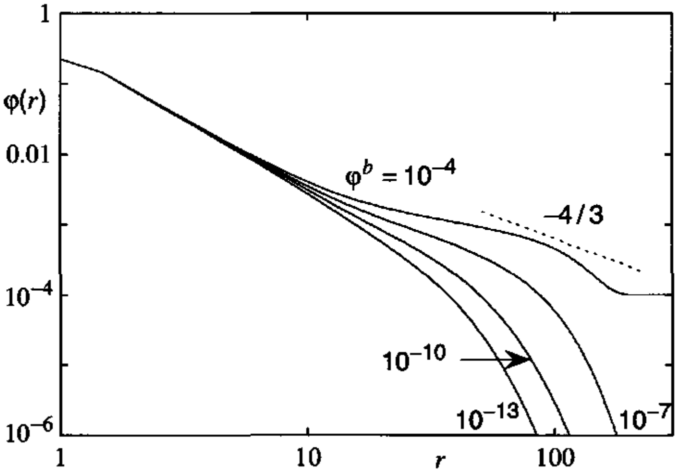

FIGURE 6.18: The volume fraction profiles plotted on a log-log scale for adsorbing homopolymers resulting from our method to incorporate intramolecular excluded volume for a chain length N of 10000, a good solvent ($\chi = 0$) and $\chi_s = 1$.

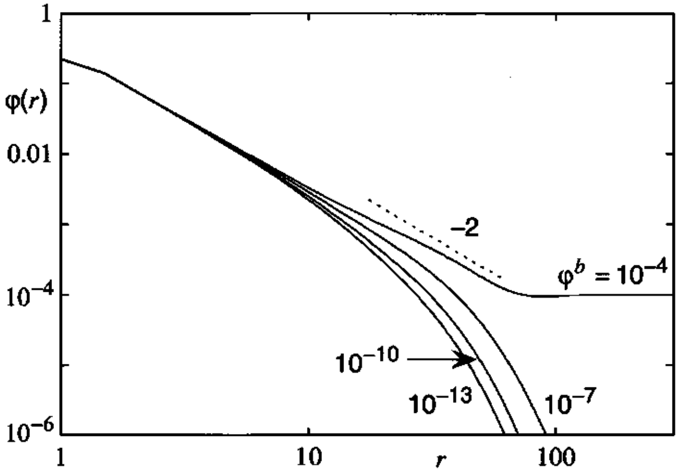

FIGURE 6.19: The volume fraction profiles plotted on a log-log scale for adsorbing homopolymers in the standard SCF theory, parameters equal to those of fig. 6.18.

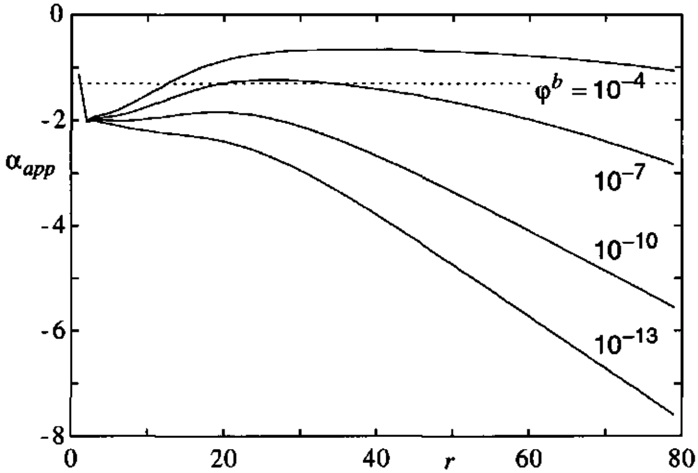

FIGURE 6.20: The apparent exponent $\alpha_{app}(r)$ as a function of the distance from the interface for the volume fraction profiles of fig. 6.18.

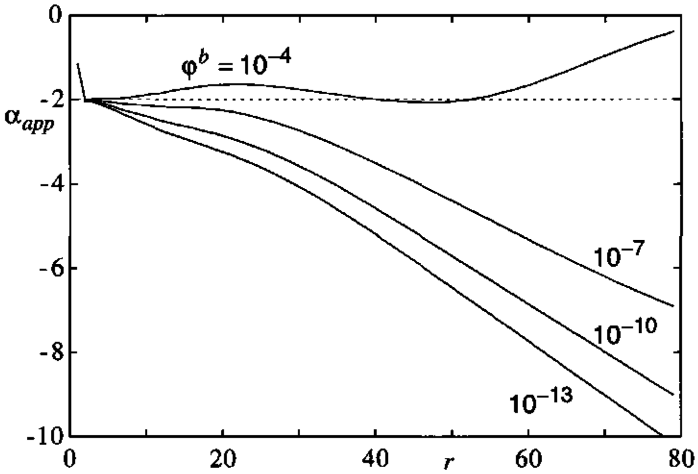

FIGURE 6.21: The apparent exponent $\alpha_{app}(r)$ as a function of the distance from the interface for the volume fraction profiles of fig. 6.19.

power law exponent to the volume fraction profiles: the apparent exponent is not constant as a function of the distance from the surface. This is not too surprising since in figs. 6.20 and 6.21 all three regions of the adsorbed layer are present. The proximal region is relatively small: a few layers. In this region, the volume fraction profile does not graphically depend on φ^b. The distal region has an exponential decay of the volume fraction profile: no power law behaviour is expected at all. The central region, where a power law for the volume fraction is expected lies in between the proximal and distal region. The overlap between the different regions is partly the cause for the variation in $\alpha_{app}(r)$ as a function of r. The central region ends where the volume fraction drops below the overlap concentration which is given by $N^{-4/5}$ [12]. For $N = 10000$ we find $\varphi(r) \approx 6 \cdot 10^{-4}$ as the lower limit for the central region.

In fig. 6.20 the apparent scaling exponent $\alpha_{app}(r)$ becomes larger than -2 for φ^b equal to 10^{-7} and 10^{-10}. For $\varphi^b = 10^{-7}$ the apparent exponent is approximately equal to $-4/3$ for a rather broad region. In contrast, for $\varphi^b = 10^{-4}$ the apparent exponent becomes even larger than -1, which is clearly unrealistic. In fig. 6.21 a similar, but less severe, overshoot of the apparent scaling exponent is seen for $\varphi^b = 10^{-4}$ for the standard SCF theory. Also, for φ^b equal to 10^{-10} and 10^{-13} no clear scaling region can be identified. The overshoot in fig. 6.21 can be slightly reduced by fitting to a different power law behaviour $\varphi \sim (r + D)^{-4/3}$, where D is the proximal length, which is about unity here.

6.4 Discussion

A first-order correction for the effect of intramolecular excluded volume in the self-consistent-field theory is presented. For individual chains in the bulk solution the results converge to those obtained from the analytical theory of Edwards [7] in the limit of long chains. Whereas Edwards' theory applies only for infinite chain length, we considered necessarily finite chains.

For such isolated chains many well-known scaling relations could be reproduced. The scaling of the radius of gyration R_g upon varying the chain length in a good solvent converges to the mean-field exponent 0.6. The scaling exponents for chains in an arbitrary dimensionality of space also show good agreement with known results. The scaling relation $R_g \sim (0.5 - \chi)^{2\nu-1}$ could be reproduced, as well

Upon decreasing the solvent strength the chain collapses. At the collapse transition the relative fluctuations in the radius of gyration are shown to increase. The globule has a radius of gyration R_g that scales as $R_g \sim N^{1/3}$, as expected.

Upon increasing the volume fraction φ^b of bulk chains in a good solvent, the bulk chains interpenetrate the central chain. The bulk chains suppress the swelling of this central chain. The scaling relation ${R_g}^2 \sim {\varphi^b}^{-1/4}$ is only approximately reproduced. The exponent is too small for short chains, whereas it becomes too large for long chains. The bulk chains screen the intramolecular excluded volume as is known from a scaling analysis. However, unlike for the scaling approach, the outside of the immobilised chain loses all intramolecular excluded volume as the bulk volume fraction is increased. This remains a deficiency in our approach.

When we consider even higher bulk volume fractions an interesting feature of the volume fraction profile emerges: it shows (very small) oscillations in the total volume fraction. These oscillations are very similar to those found for polymers near a non-adsorbing wall [80]. The oscillations have a wavelength which scales with the coil size. Scaling theory assumes that the only relevant length scale for semi-dilute to concentrated polymer solutions is the mesh-size, which does not depend on the chain length. Our calculations show that this is not strictly the case, the coil size plays a role as well, albeit small.

For isolated chains it was shown that many well-known scaling relations can be reproduced. The resulting power laws do not have the precise exponents predicted from calculations like Monte Carlo and renormalisation group theory. However, the exponents from our mean-field approach are close to the values found from these more exact theories. This was to be expected due to the remarkable cancellation of errors that is present in the mean-field theory [12]. Our theory suffers from the same defects as Edwards theory [7]. The excluded-volume interaction is overestimated due to the averaging of the volume fractions. On the other hand, the excluded-volume interaction is underestimated due to the neglect of correlations along the chain. As Des Cloizeaux and Jannink [74] put it: 'In brief, the self-consistent field method appears here as completely unrealistic'. We will certainly not argue against this point: for obtaining exact scaling exponents the mean-field theory is inappropriate.

However, within the mean-field description, the standard Scheutjens-Fleer theory entirely neglects the effect of intramolecular excluded volume on the bulk chains. In this chapter, it was attempted to partially correct for this deficiency and to calculate the equilibrium structure of the adsorbed layer by matching the chemical potential of a chain with intramolecular interactions in a bulk solution to the chemical potential of the adsorbed layer. This results in an increase of the adsorbed amount of about 2–10% compared to the Scheutjens-Fleer theory. Monte Carlo simulations show a two or three fold increase in the adsorbed amount compared to the SCF theory [69]. So, although in our approach the adsorbed amount is indeed higher than for the standard SCF theory, the increment is clearly too low compared to the Monte Carlo results.

The central region of the adsorbed layer shows a power law behaviour of the volume fraction profile $\varphi \sim r^{\alpha}$. For the standard mean-field calculations the scaling exponent is -2, although the power law behaviour is only approximate and the exponent is smaller for lower bulk volume fractions. When the adsorbed amount is adjusted such that the chemical potential of the adsorbed chains is equal to the chemical potential of a (swollen) bulk chain, we find an exponent higher than -2 for relatively small bulk volume fractions. For bulk volume fractions close to the overlap volume fraction the volume fraction profiles become unrealistic. A scaling exponent higher than -1 is found, which cannot be correct. We do believe that within the mean-field approximation, more realistic volume fraction profiles with a scaling exponent of $-4/3$ can in principle be attained. Apparently, the current approach is still too primitive. Below, we consider several possible options.

Since in our approach two separate calculations need to be performed, both are candidates for a possible error. Let us first consider the calculation in the bulk phase. The chemical potential of the swollen bulk chain is an obvious candidate. It could be that the chemical potential of the bulk chain is slightly overestimated. This leads to an overestimated adsorbed amount and, consequently, to the overshoot in the volume fraction profiles. One may argue that instead of eq. 6.19 we should use the equivalent of eq. 6.18, where we substitute C^g from eq. 6.7b for C^a. However, this only increases the chemical potential in the bulk and leads to the (undesired) effect that the total free energy of the bulk phase is not equal to the sum of the chemical potentials of all components: we are left with a (negative) excess value. Such an excess value is usually associated with a surface tension. However, a bulk phase cannot have a surface tension.

Another possible modification of the calculation in the bulk is to refrain from the special grafting scheme used here. We may choose to simply end-graft the chain to the centre of the spherical lattice. This also does not help much: again it leads to an even higher value for the chemical potential since end-grafting is an additional restriction on the bulk chain.

We believe that the most likely source of error is the matching of chemical potentials obtained from calculations in different spatial geometries (namely planar and spherical). The adsorbed chains only swell in the direction perpendicular to the surface, not parallel to the surface. When an adsorbed chain is considered that is immobilised in the centre of an additional spatial (cylindrical) gradient parallel to the surface, this would lead to qualitatively different results. In other words, the neglect of lateral inhomogeneities has an influence on the numerical results. In contrast, when an additional spatial gradient could be introduced in the spherical shells, the results would be exactly the same: on a mean-field level no inhomogeneities will be found within a spherical shell.

A possible solution would be to perform both the calculation for the surface and the calculation for the bulk chain in a cylindrical geometry with an additional spatial gradient along the axis of the cylinder. This would solve the inconsistency resulting from matching two chemical potentials resulting from different spatial geometries. However, the calculations would become more time consuming, especially for long chains.

Despite the remaining uncertainties and errors we believe that the current approach is promising. Using a relatively small modification to the original Scheutjens and Fleer theory, we can correct for the intramolecular excluded volume of bulk chains on a mean-field level. For polyelectrolytes it is known that the swelling of the chains in the bulk can be considerable. Hence, treating these chains as random walks in the bulk gives a large overestimation of their entropy. It is expected that using the simple approach outlined in this chapter for adsorbing polyelectrolytes leads to more realistic results for the adsorbed amount and the layer thickness.

A Computation of chain propagators in inhomogeneous systems: over- and underflow protection and reducing computer memory requirements

ABSTRACT

Two numerical procedures are described that solve common problems in the numerical evaluation of Green's functions. Their discrete variant is used to evaluate the volume fractions of chain molecules in Scheutjens-Fleer self-consistent-field calculations. The first procedure prevents over- and underflows. The main principle of the method is to rewrite the equations that compute the volume fraction distribution of the polymers in a logarithmic form. The second procedure deals with extremely long chains. The memory and CPU time needed to compute the volume fractions of a polymer chain from a given potential field normally scale both as MN, where M is the number of lattice coordinates and N is the chain length. We present an algorithm for which the memory consumption scales as $MN^{1/3}$ while the CPU time increases by at most a factor of two.

A.1 Introduction

Inhomogeneous polymer solutions can, on a mean-field level, be described by solving the Edwards diffusion equation [7]. Only for special cases are analytical solutions available. Usually, one has to apply numerical methods to solve the equation. A successful example of such a method is the Scheutjens-Fleer self-consistent-field (SCF) theory [6], which is a generalization of the Flory-Huggins theory for inhomogeneous systems. In this SCF model the system is discretised. The contour of the chain is split up into segments and space is divided into layers of equal spacing. The diffusion equation is replaced by a discrete chain propagator. Several authors have described similar theories which are formulated in continuous equations [21, 31, 81, 82]. In order to solve the equations the diffusion equation is also discretised in these theories.

Typically, in numerical SCF calculations the volume fractions of chain molecules are calculated in an inhomogeneous potential field. The numerical evaluation of the equations needed to compute the volume fractions, when used in the form that is generally given in literature [6, 22, 43], may give rise to floating point under- or overflows. An underflow occurs when a value is computed that is smaller than the minimal floating point number that can be handled by a computer, e.g., smaller than 10^{-300}. An overflow occurs when the values become too large, e.g., larger than 10^{300}. The problem of under- and overflows has been dealt with in the past specifically for brushes by Wijmans et al. [83].In this work the equations used to compute the volume fractions were rescaled to ensure that no under- or overflow occurs for the case that the amount of molecules in the system is fixed. A different, more general, procedure is implemented in the computer program `copel` [84] which has been used to study weak polyacid brushes [28], but this procedure has remained undocumented so far.

Another problem is computer memory shortage. This occurs when the chains are very long and the system consists of many space coordinates. The standard algorithm [6] requires considerable memory while the CPU time needed to perform the calculations is at its minimum. In the second part of this appendix we describe a method that uses several orders of magnitude less memory but the needed CPU time is at most doubled. This method was originally introduced by the late Jan Scheutjens, who also implemented it in the shareware program `polad` [85]. It has been used successfully, for example in homopolymer adsorption theory [73, 86], but also this procedure has never been documented. In the next section the literature equations to compute the volume fractions of a chain molecule are briefly recapitulated. In section A.3 it is shown how under- or overflows may occur when using the equations in their standard form. The procedure which avoids these problems rewrites the equations in a logarithmic form, as in the program `copel` [84]. The procedure is extended to ensure convergence of the equations in extreme cases. Finally, section A.4 describes the algorithm used to save memory for the propagators and gives an analysis of the computational demand.

All equations given in this appendix are suitable only for a simple case, i.e., linear (co)polymers. However, both computational schemes are easily generalized for branched molecules and may indeed be used simultaneously. Recent applications are, for example, weak polyacid brushes in incompatible liquids [87] and star-branched polyelectrolytes in solution [50].

A.2 Chain propagators for inhomogeneous systems

Let $\mathbf{r}$ be a generalized lattice coordinate. In the most common calculations only one gradient is considered; in this case space is divided in layers and $\mathbf{r}$ represents the lattice layer number. For convenience, the generalized lattice coordinates are numbered as $\mathbf{r} = 1, 2, \ldots, M$. The chains are linear polymer molecules consisting of N (possibly different) segments, indicated by the ranking number $s = 1, 2, \ldots, N$. We are interested in the volume fraction distribution $\varphi(\mathbf{r})$ of polymer when a given potential field $u(\mathbf{r}, s)$ acts on each segment. It is convenient to define segment weighting factors $G(\mathbf{r}, s)$ from the potential field $u(\mathbf{r}, s)$:

$$G(\mathbf{r}, s) = e^{-u(\mathbf{r},s)/kT} \tag{A.1}$$

Here it suffices to note that $u(\mathbf{r}, s)$ is a function of the volume fractions. The statistical weights of the full set of polymer chains are built up from these segment weighting factors by applying a propagator, which is the discrete version of the Edwards diffusion equation

$$G(\mathbf{r},s|1) = G(\mathbf{r},s)\sum_{\mathbf{r}'}\lambda(\mathbf{r},\mathbf{r}')G(\mathbf{r}',s-1|1) \tag{A.2a}$$

$$G(\mathbf{r},s|N) = G(\mathbf{r},s)\sum_{\mathbf{r}'}\lambda(\mathbf{r},\mathbf{r}')G(\mathbf{r}',s+1|N) \tag{A.2b}$$

where $\lambda(\mathbf{r},\mathbf{r}')$ is the *a priori* transition probability between coordinates r and $\mathbf{r}'$. The coordinates for which $\lambda(\mathbf{r},\mathbf{r}')$ is unequal to zero are spatially near each other; usually $\mathbf{r}$ and $\mathbf{r}'$ are neighbouring sites. The end segment weighting factor $G(\mathbf{r},s|1)$ is a measure for the probability of finding segment s in layer $\mathbf{r}$ when segment $s=1$ of the chain can be anywhere on the lattice. The starting condition is $G(\mathbf{r},1|1) = G(\mathbf{r},1)$. The end-segment weighting factor $G(\mathbf{r},s|N)$ is a measure for the probability to find segment s at coordinate $\mathbf{r}$, starting from the other end of the chain, at segment N. The starting condition is now $G(\mathbf{r},N|N) = G(\mathbf{r},N)$. The volume fraction of segment s at coordinate $\mathbf{r}$ is computed from the so-called composition law:

$$\varphi(\mathbf{r},s) = C\frac{G(\mathbf{r},s|1)G(\mathbf{r},s|N)}{G(\mathbf{r},s)} \tag{A.3}$$

where C is a normalization constant. The denominator $G(\mathbf{r},s)$ corrects for double counting of $G(\mathbf{r},s)$ in the product of the numerator. Obviously, the total volume fraction $\varphi(\mathbf{r})$ is simply the sum over all segments s:

$$\varphi(\mathbf{r}) = \sum_{s}\varphi(\mathbf{r},s) \tag{A.4}$$

The normalization constant is given by

$$C = \frac{\varphi^b}{N} \tag{A.5}$$

for molecules for which the system is open, i.e., when the bulk volume fraction φ^b (or, equivalently, the chemical potential) of the molecules is fixed. Alternatively, the normalization constant is given by

$$C = \frac{\theta}{NG(N|1)} \tag{A.6}$$

where

$$G(N|1) = \sum_{\mathbf{r}} G(\mathbf{r},N|1) \tag{A.7}$$

for molecules for which the system is closed, i.e., when a given fixed amount of molecules $\theta = \sum_{\mathbf{r}}\varphi(\mathbf{r})$ is present in the system.

A.3 Preventing overflows in the propagators

The equations from the previous section constitute the procedure to compute volume fractions of chain molecules as described in literature and used routinely for actual calculations. However, numerical under- or overflows may occur in this procedure as we will show below.

As a simplification we take a homopolymer in a field $u(\mathbf{r})$ without any gradient, therefore $G(\mathbf{r}, s) = G$ and equation A.3 simplifies to

$$\varphi(s) = CG^N \tag{A.8}$$

The chain length N may be of order 10000, so that quite normal values of 2 or 0.5 for G will cause G^N to exceed the numerical representation of a computer, resulting in an over- or underflow, respectively. One might argue that these values for G lead to an unrealistic volume fraction φ. However, the self-consistent field solution for φ is found by iterating the potential field u. In numerical procedures to find solutions to a large number of equations, it is generally difficult to put constraints on the variables while iterating. Therefore the field u may temporarily take any value. Furthermore, in 'closed' systems the normalization constant C, eq. A.6, may compensate for the (temporary) under- or overflow, so that the volume fraction φ does take a physically realistic value. This situation typically occurs in polyelectrolyte brushes of moderate length, say a few hundred segments, with a low volume fraction of electrolytes, i.e., when the Debye screening length is large. This results in high potential fields over relatively large distances. Here, the weighting factors G may easily take values as low as 0.01 for the SCF solution, in this case resulting in an underflow in the end-segment weighting factors.

The main principle of the procedure used to prevent overflows is to rewrite the propagator, eq. A.2, and the composition law, eq. A.3, in a logarithmic form. As a shorthand we denote the logarithmic forms by a tilde. First we introduce the logarithm of the segment weighting factor G

$$\tilde{G}(\mathbf{r}, s) = \ln G(\mathbf{r}, s) \tag{A.9}$$

The logarithm of zero is redefined to give a very large negative number ϵ, close to the minimum machine representation, say $\epsilon = -10^{300}$. This allows us to use $G(\mathbf{r}, s) = 0$, e.g. in the starting condition of eq. A.2 for the calculation of brushes. Now we rewrite eq. A.2 in a logarithmic form. We illustrate this for eq. A.2a In the sum of eq. A.2a we single out the term for lattice coordinate r^*, which is chosen such that $\lambda(\mathbf{r}, \mathbf{r}^*) > 0$ and $\tilde{G}(\mathbf{r}^*, s-1|1) > \epsilon$ (hence $\tilde{G}(\mathbf{r}^*, s-1|1) > \epsilon$), and this term is written as a prefactor outside the sum. Taking the logarithm, we get

$$\begin{aligned} \tilde{G}(\mathbf{r}, s|1) \;=\; & \tilde{G}(\mathbf{r}, s) + \ln\lambda(\mathbf{r}, \mathbf{r}^*) + \tilde{G}(\mathbf{r}^*, s-1|1) + \\ & \ln\left[1 + \sum_{\mathbf{r}' \neq \mathbf{r}^*} \frac{\lambda(\mathbf{r}, \mathbf{r}')}{\lambda(\mathbf{r}, \mathbf{r}^*)} \exp\left(\tilde{G}(\mathbf{r}', s-1|1) - \tilde{G}(\mathbf{r}^*, s-1|1)\right)\right] \end{aligned} \tag{A.10}$$

The sum over $\mathbf{r}'$ runs over all coordinates unequal to $\mathbf{r}^*$ and for which $\lambda(\mathbf{r},\mathbf{r}') \neq 0$. We can see why this procedure prevents under- and overflows. The difference in the exponent ensures that the exponent in eq. A.10 does not generate an under- or overflow. The values of $\tilde{G}(\mathbf{r}', s-1|1)$ and $\tilde{G}(\mathbf{r}^*, s-1|1)$ may both be very large or very small but the difference between the two remains small. This is because the distance on the lattice between $\mathbf{r}'$ and $\mathbf{r}^*$ is always small and gradients in the volume fractions never become extremely large.

The composition law (eq. A.3) is rewritten as

$$\tilde{\varphi}(\mathbf{r},s) = \tilde{C} + \tilde{G}(\mathbf{r},s|1) + \tilde{G}(\mathbf{r},s|N) - \tilde{G}(\mathbf{r},s) \tag{A.11}$$

where $\tilde{\varphi}(\mathbf{r},s) = \epsilon$ when either $\tilde{G}(\mathbf{r},s|1)$, $\tilde{G}(\mathbf{r},s|N)$, or $\tilde{G}(\mathbf{r},s)$ equals ϵ. The normalization $\tilde{C}$ is defined by either

$$\tilde{C} = \ln \frac{\varphi^b}{N} \tag{A.12}$$

for molecules with a given bulk volume fraction φ^b or

$$\tilde{C} = \ln(\frac{\theta}{N}) - \tilde{G}(N|1) \tag{A.13}$$

for molecules with a given fixed amount θ in the system. Eqs. A.4 and A.7 contain sums that for convenience are denoted as

$$F(y) = \sum_{x=1}^{x=y} f(x) \tag{A.14}$$

This sum may also be written as a recurrency relation:

$$F(y) = F(y-1) + f(y) = F(y-1)\left[1 + f(y)/F(y-1)\right] \tag{A.15}$$

with starting condition $F(1) = f(1)$. Taking the logarithm, we find $\tilde{F}$ from the following relation

$$\tilde{F}(y) = \tilde{F}(y-1) + \ln\left[1 + \exp\left(\tilde{f}(y) - \tilde{F}(y-1)\right)\right] \tag{A.16}$$

with starting condition $\tilde{F}(1) = \tilde{f}(1)$. When the exponent in eq. A.16 generates an overflow, so when $\tilde{F}(y-1) \ll \tilde{f}(y)$, we use $\tilde{F}(y) = \tilde{f}(y)$. The resulting volume fractions $\tilde{\varphi}(\mathbf{r})$ in logarithmic form can now be transformed back to the normal representation

$$\varphi(\mathbf{r}) = \exp(\tilde{\varphi}(\mathbf{r})) \quad \text{for} \quad \tilde{\varphi}(\mathbf{r}) < A \tag{A.17a}$$

$$\varphi(\mathbf{r}) = \exp\left[A + B\tanh(\frac{\tilde{\varphi}(\mathbf{r}) - A}{B})\right] \quad \text{for} \quad \tilde{\varphi}(\mathbf{r}) > A \tag{A.17b}$$

where the constant A is chosen such that $\exp(A)$ is well below the maximum value of the machine representation of a number. The constant B has a value such that

$\exp(A + B)$, which is the maximum allowed value for $\varphi(\mathbf{r})$, is also well below the maximum machine number. Typical values of A and B are 400 and 100 respectively. The transformation with the hyperbolic tangent done in eq. A.17b prevents an overflow in $\varphi(\mathbf{r})$ while keeping $\varphi(\mathbf{r})$ a continuous and differentiable function of $u(\mathbf{r})$, which is a demand for the numerical procedure to find the self-consistent field solution.

A.4 Saving memory for the propagators

Most analytical and scaling theories for polymers make use of an approximation for infinite chain length. To compare lattice results with this type of theories it is necessary to perform numerical calculations with very high chain lengths, for example $N = 10^4$ or $N = 10^5$. The propagator routine as previously described is unsuitable for such large chain lengths on contemporary desktop computers because of memory restrictions. More than ten years ago Jan Scheutjens came up with a scheme that reduces the memory usage of the propagator routine considerably. In this section we describe this method, which has never been published.

Inspection of the equations given in section A.2 shows that the evaluation of the volume fraction distribution $\varphi(\mathbf{r})$ for a given potential field has a CPU and memory demand which both scale as MN. Here M is the number of lattice coordinates in the system and N is the number of segments of the chain. This demand on computer capacity stems from eqs. A.2 – A.4. An important feature of Eq. A.3 is that $G(\mathbf{r}, s|1)$ is combined with $G(\mathbf{r}, s|N)$ for computing the volume fractions $\varphi(\mathbf{r}, s)$ of segment s. The standard way is to first compute $G(\mathbf{r}, s|1)$ for $s = 1 \dots N$ and store all N vectors; this we call the "forward" computation (eq. A.2a). After arriving at $s = N$, $G(\mathbf{r}, s|N)$ is computed from $s = N$ downward, which is the "backward" procedure (eq. A.2b). On this way back, there is no need to store the vectors $G(\mathbf{r}, s|N)$ since the result is immediately processed as a contribution to $\varphi(\mathbf{r})$, according to eqs. A.3 and A.4. Note that the stored vectors $G(\mathbf{r}, s|1)$ are needed in reverse order, from $s = N$ downward.

For "symmetric" molecules where $\varphi(\mathbf{r}, s) = \varphi(\mathbf{r}, N - s + 1)$, such as homopolymers, the relation $G(\mathbf{r}, s|N) = G(\mathbf{r}, N - s + 1|1)$ holds and it is possible to reduce the CPU-time and memory consumption by a factor of 2. Now it is sufficient to do only a "forward" computation, storing only the first $N/2$ vectors of $G(\mathbf{r}, s|1)$. In the following discussion, we describe the general asymmetric case, keeping in mind that for "symmetric" situations the memory consumption can be further reduced.

In order to save memory a very naive method could, in principle, be used. We could choose not to store the $G(\mathbf{r}, s|1)$ for different s and simply recompute this vector for any s when needed. This reduces the memory demand greatly: it would scale as M. However, the CPU-time now scales as MN^2, which makes this method unsuitable.

Another possible method would be to invert the propagator A.2a, computing $G(\mathbf{r}, s - 1|1)$ from $G(\mathbf{r}, s|1)$. On a lattice with one gradient this inversion procedure reduces to a tridiagonal system of equations which takes order M computations, see for example ref. [49]. Now the CPU time would still scale as MN and the memory usage as M. If, however $\lambda(\mathbf{r}, \mathbf{r}')$ is unequal to zero for many coordinates $\mathbf{r}'$, as is the case in lattices with more than one gradient [35, 88], the inversion takes more than order M computations so that this procedure is then not favorable.

The algorithm presented here is a compromise between memory consumption and CPU time. The vector $G(\mathbf{r}, s|1)$ is always recalculated from vectors with lower s which were stored on the forward route for a limited set of s. The increase in CPU-time for the recalculations is only a factor of two, whereas the memory consumption is reduced by a factor of order $N^{2/3}$.

In this algorithm, only n vectors $G(\mathbf{r}, s|1)$ are stored instead of the N vectors in the standard procedure. As we will show below, n is about $(6N)^{1/3}$. The scheme is illustrated in table A.1 for $n = 6$, which enables the computation for an arbitrary copolymer with a length of at most $N_{max} = 55$. A general relation between the number of vectors stored and the maximum chain length N_{max} may be obtained as follows. The N vectors $G(\mathbf{r}, s|1)$ computed in the forward calculation may be arranged in triangles, as shown in table A.1. Each triangle contains $m(m + 1)/2$ vectors, where $m = n$ for the upper triangle and $m = 2$ for the lower triangle. The maximum number of vectors N_{max} is found by the sum over all triangles:

$$N_{max} = \sum_{m=2}^{n} m(m+1)/2 = \frac{1}{6}\left\{(n+1)^3 - (n+7)\right\} \tag{A.18}$$

The main principle of the method is to store only the first vector (indicated in bold in table A.1) of each triangle on the forward route. During the backward procedure the other (non-stored) vectors are needed as well. All elements of each triangle are recomputed from the first (stored) vector but now only the diagonal elements (indicated in italics) are stored. When the remaining elements are needed, they are recomputed for the second (and last) time from the first (diagonal) element in each row. In this way, each vector is recomputed twice at most and never more than n vectors have to be stored.

The order of recomputations and the storing procedure is shown in table A.2, again for $n = 6$ but now for $N = 50$, which is slightly less than $N_{max} = 55$. In the forward computation the lower triangle in table A.1 is not needed. This space is used to store the diagonal element $s = 50$. The first row of table A.2 shows the vectors stored in the matrix at the start of the backward procedure. The following rows in table A.2 show what vectors are stored during the backward procedure and what vector is used to recompute these vectors (the source). The first recalculation is for $s = 48$ and 49, which are stored by overwriting vector $s = 50$, which is no longer needed. In step 2, vector $s = 37$ is used to recompute the vectors 38–46, but only the diagonal elements (41, 44, 46) are stored in this step; the others are recomputed again later, either from the stored diagonal elements (steps 3 and 4) or from using vector 37 for the second time (step 5). This procedure is repeated until in the final step only the vectors for $s = 1$–6 are stored.

TABLE A.1: Example of filling a storage matrix of 6 vectors for a calculation with the corresponding maximum chain length $N_{max} = 55$. The bold values **s** are stored in the forward calculation. In the backward calculation needed for $\varphi(\mathbf{r}, s)$, the other vectors are recalculated from the "bold" ones but only the diagonal elements s (italics) are then stored, overwriting vectors for higher s which are no longer needed. The vectors with s denoted in roman numbers are stored at their second recalculation from the "bold" or "italic" ones. The precise order of the recalculations in the backward calculation is given in table A.2

.

1	2	3	4	5	6
1	2	3	4	5	6
	7	8	9	10	11
		12	13	14	15
			16	17	18
				19	20
					21
	22	23	24	25	26
		27	28	29	30
			31	32	33
				34	35
					36
		37	38	39	40
			41	42	43
				44	45
					46
			47	48	49
				50	51
					52
				53	54
					55

TABLE A.2: Handling of the storage matrix for $n = 6$ and $N = 50$. At the end of the forward calculation the vectors in row 1 are available. In the second step vectors *48* and *49* are recomputed from vector **47**, thereby overwriting **50** which is no longer needed. In the third step **37** is used to obtain *41*, *44*, and *46*. This procedure is repeated for the other vectors. At the end of the computation only the vectors for $s = 1 \dots 6$ are available; all the others are already used and have been overwritten.

1	2	3	4	5	6	source
1	**22**	**37**	**47**	**50**	-	
				48	*49*	**47**
			41	*44*	*46*	**37**
					45	*44*
				42	43	*41*
			38	39	40	**37**
		27	*31*	*34*	*36*	**22**
					35	*34*
				32	33	*31*
			28	29	30	*27*
		23	24	25	26	**22**
	7	*12*	*16*	*19*	*21*	1
					20	*19*
				17	18	*16*
			13	14	15	*12*
		8	9	10	11	*7*
	2	3	4	5	6	**1**

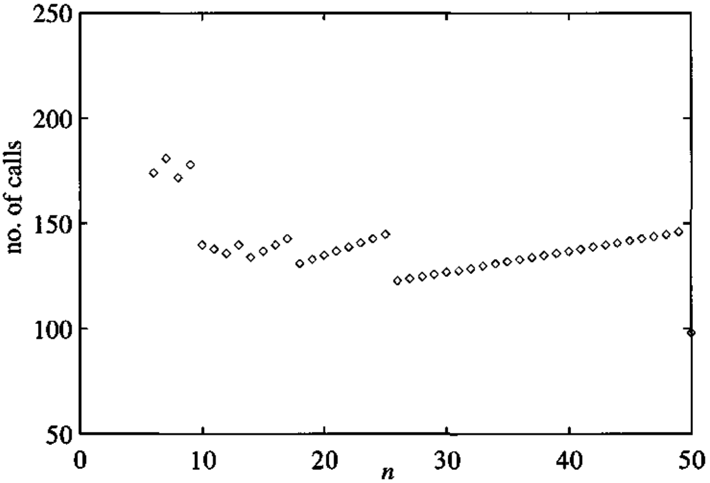

FIGURE A.1: The number of calls to the propagator function for a copolymer chain with chain length $N = 50$, as a function of the number of columns n

Hence, in this scheme much less storage space is needed: instead of N stored vectors $G(\mathbf{r}, s|1)$, only n vectors need to be stored. According to eq. A.18, n is of order $(6N)^{1/3}$. A more precise relation is obtained by solving, for given N, eq. A.18 for n. Defining

$$x = n + 1 \tag{A.19a}$$

$$X = 6(N + 1) \tag{A.19b}$$

we can rewrite eq. A.18 as a cubic equation $x^3 - x - X = 0$, which may be solved exactly. The non-imaginary solution reads $(1 + \sqrt{1-y})^(1/3) + (1 - \sqrt{1-y})^{1/3}$, where $y = 4/(27X^2)$. Since y is very small, the solution may be expanded in terms of y to lowest order. The result is

$$n = X^{1/3}\left(1 + \frac{1}{3}X^{-2/3}\right) - 1 \tag{A.20}$$

which is quite accurate even for n as low as 3 ($N = 9$). Obviously, for given N the result for n calculated with eq. A.20 should be rounded to the next higher integer.

Note that it would be possible to save a little extra memory by not storing the first vector $G(\mathbf{r}, 1|1)$ in table A.1. This would save one column in the matrix. However, this makes the algorithm more complex, while the advantage scales out as the chains increase in length.

We have investigated the efficiency of the algorithm in terms of the number of calls to the propagator (eq. A.2) as a function of the number of columns n for a fixed chain length $N = 50$. This is done because the propagator is computationally the most demanding step: the overhead of the algorithm is negligible. The results are shown in fig. A.1. The point at $n = 50$ corresponds to the standard procedure where all vectors $G(\mathrm{r}, s|1)$ for $s = 1 \ldots 50$ are stored: the propagator is then needed 98 times. Where one would expect a continuous decrease in the number of propagator steps needed as the number of columns n is increased, often the opposite is found as can be seen in fig. A.1. This is due to a suboptimal bookkeeping of what vectors need to be stored. This can also be seen from table A.2, where in principle it would be possible to store $s = 49$ in row 6. Optimizing the bookkeeping of the stored matrix is not worth the effort: it hardly makes a difference for low n, and it increases the complexity of the algorithm. The minimum number of calls to the propagator in the example of fig. A.1 is 98, the maximum number is 181, so indeed about a factor of two in efficiency loss is observed.

A.5 Acknowledgment

The numerical tricks discussed in this appendix were initiated by Jan Scheutjens who tragically died in 1992.

B On the discretisation of space in the self-consistent-field model

ABSTRACT

Numerical self-consistent-field (SCF) calculations for interfacial systems typically make use of discrete space co-ordinates, known as a lattice. In this appendix various types of lattices are discussed. The frequently used geometrical packing view of the lattice is critically examined. The discretisation of equations may lead to three types of possible problems. (i) The discretisation of derivatives can be done in a number of different ways. It is shown how physical arguments may favor one way over the other. (ii) Lattice artefacts may arise when the width of the interface is of the order of the lattice spacing. An overview of the methods that have been used in the past to correct for these artefacts is given. Also a new method to eliminate them is proposed. The central idea is to shift the lattice with respect to the interface at fixed molecular composition and system volume. (iii) The anisotropy of some lattices may lead to problems. A way to deal with this is reviewed. Furthermore, it is shown how the results of calculations with different lattice constants can be compared and how experimental data should be translated to parameters common in the lattice theory. Lastly, a Stern layer concept is used to show how a lattice theory may lead to more realistic results than a continuum model without such a Stern layer.

B.1 Introduction

The numerical evaluation of inhomogeneous self-consistent-field (SCF) equations typically makes use of discretised space, also named a lattice. The discretisation of space is needed because a computer is better able to evaluate discrete functions than continuous ones. Although the discretisation usually does not alter the physics in the problem, one should be aware of possible problems. In the following sections we will discuss a number of issues related to the discretisation.

The nature of the discretisation of space depends on the problem at hand. Most commonly used are lattices in which space is discretised in only one direction. This type of lattice is used when one is interested in only one gradient in the system. In addition, the geometry of the lattice may vary so we may have a planar, cylindrical or spherical lattice. A detailed description of the different geometries and their boundary conditions is given in sec. B.2. Lattices are often characterised as having a 'cubic', 'hexagonal', or other type of packing. Although this view may have its didactical merits, we argue in sec. B.3 that such a pictorial view is in principle incorrect.

A possible source of errors that directly follow from the discretisation of continuous equations is discussed in sec. B.4. It is shown that equations containing derivatives cannot be discretised unambiguously. However, physical arguments may favor one way of discretising over the other. As an example of this, the discretisation of the diffusion equation is discussed.

At the initial introduction of the SF-SCF theory in 1979 [6] some criticism was directed to the lattice approximation. Indeed, this approximation can lead to artefacts in the results as we will show. However most problems can be prevented. We distinguish two different types of discretisation artefacts. The most common type of artefact is due to the position of an interface relative to the layers. A shift in the position of the interface of less than one layer leads to a unphysical change in the thermodynamical quantities. In sec. B.5, an overview is given of the methods that have been used in the past to correct for this artefact. Also, a new method to correct for this artefact is proposed.

When more than one gradient in the volume fractions is considered then another type of discretisation artefact pops up: Gaussian chains may become anisotropic. This problem has been dealt with by Maurits et al. [35]. Their method is briefly discussed in sec. B.6.

Lattices with one gradient are characterised by an *a priori* transition probability between two neighbouring layers, denoted by λ. Varying λ while keeping all other parameters equal should yield, in principle, equivalent results. In practice, this means that the results have to be rescaled in a way dependent on the problem at hand. This is discussed in sec. B.7.

Often, it is of interest to compare experimental data with theoretical results, obtained by the SF-SCF theory. It turns out that the translation of experimental data to parameters used in the SCF theory is not entirely trivial. This subject is discussed in sec. B.8

Although, in general, continuous equations are more widely used, physical arguments may very well be in favour of a discrete variant of a given equation. This is illustrated by considering the Stern-layer concept in sec. B.9. We conclude by giving an overview of some open problems and possible future improvements in sec. B.10.

B.2 SCF theory and the lattice approximation

B.2.1 Planar lattice

The first application of the SF-SCF theory was polymer adsorption from solution onto a planar surface. The polymers are modelled as a string of equally sized beats, numbered $s = 1, \ldots, M$. The space is discretised in layers, parallel to the surface (see fig. B.1). Within each layer inhomogeneities in the densities of molecular components are averaged out, implying a mean-field approximation. The volume

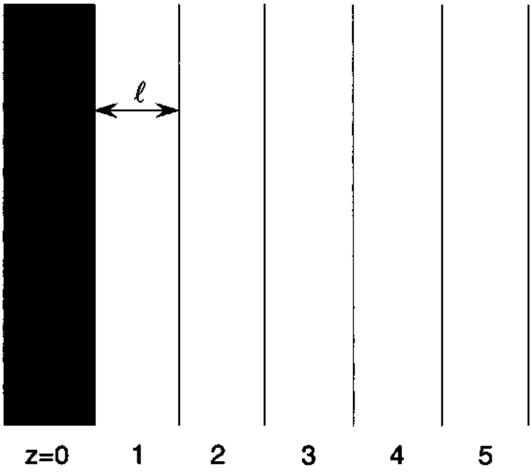

FIGURE B.1: The planar lattice. A solid interface is represented by the solid area. The first five lattice layers $z = 1, \ldots, 5$ and the lattice spacing ℓ are indicated

fraction of molecular components is allowed to vary between layers. The SF-SCF theory was soon known as a 'lattice' theory, where the term 'layer' theory is arguably more correct. However, we will retain the historical name.

The planar lattice with one gradient in the volume fractions is also useful to introduce some concepts that are used in the SF-SCF theory. The layers are numbered by $z = 1, 2, \ldots, M$, the width of a lattice layer is ℓ. When computing the volume fractions of molecules, the lattice constant λ comes in at two points: in the chain propagators (eqs. 2.26, 3.25, and 3.27) , and for counting the contact interactions 2.6. In the chain propagator, λ has the role of the *a priori* probability to find the next segment of the chain in an adjacent layer. When calculating the contact interactions, λ has the role of the fraction of contacts with neighboring lattice sites. Although not often done, it is of course possible to use values for λ in the chain propagator which are different than those used for the contact interactions.

Originally, the SF-SCF theory was constructed not by mapping continuous equations onto a lattice but from lattice considerations as formulated by DiMarzio and Rubin [9]. It is then tempting to associate for example $\lambda = 1/6$ with a cubic lattice. We argue against this view in section B.3.

B.2.2 Lattice boundaries

Special attention should be paid to the boundaries of the lattice. In this section we limit the discussion again to a planar lattice with one gradient. It proves useful to add boundary layers to the system. Instead of the layers $z = 1, 2, \ldots, M$, one extra layer is added on both sides of the lattice, i.e. $z = 0, 1, 2, \ldots, M, M + 1$. The various boundary conditions are implemented by special treatment of these outer layers.

Some different boundary conditions exist. The properties of the layer just outside the system ($z = 0$) can be equated to those of the layer at the boundary of the system ($z = 1$), this introduces a simple mirror boundary condition, also known as a absorbing boundary condition since it absorbs all walks of chains that pass the boundary. In the chain propagators (eqs. 2.26, 3.25, and 3.27) we use

$$G(0,s|1) = G(1,s|1) \tag{B.1a}$$

$$G(0,s|N) = G(1,s|N) \tag{B.1b}$$

to ensure that the propagators can also be used for $z = 1$. The volume fractions $\varphi(z)$ are treated likewise

$$\varphi(0) = \varphi(1) \tag{B.2}$$

This equation ensures that the contact interactions are calculated according to the mirror boundary condition. Note that the layers $z = 0$ and $z = M+1$ do not belong to the system. These layers are not included when calculating e.g. the total amount of molecules in the system or the free energy.

Another possible absorbing (or mirror) boundary condition equates properties of layer $z = 0$ to those of layer $z = 2$ in eqs. B.1b and B.1b. Here, the system is effectively reduced by half a lattice layer: the system extends from $z = 1/2$ onward. Also a periodic boundary condition can be used. Now, layer $z = M + 1$ is equated to layer $z = 1$ and layer $z = 0$ is equated to $z = M$. The equivalents of eqs. B.1b and B.2 are trivial to construct for these two boundary conditions.

A surface can be positioned outside the system, to calculate adsorption and depletion effects. This boundary condition is often addressed as a reflecting boundary condition, since no walk of the chain can leave the system, they are reflected by the surface. The most simple way of setting a surface at layer $z = 0$ is to set the segment weighting factor $G_A(0) = 0$ and $\varphi_{iA}(0) = 0$.

Using a mirror boundary condition at one boundary and a surface at the other boundary makes it possible to study the interaction as a function of the distance of two equal surfaces with adsorbing or depleting molecules. Simply reducing the number of lattice layers lets the one surface interact with its mirror image.

The original theory [6] was used to compute the volume fraction profile of polymers in solution adsorbing to a surface. The penetration of chains into the bulk phase was treated exactly: the propagators could also enter outside of layer $z = M$, where the potential field is zero. This is formally the exact way to calculate the volume fraction profile of the adsorbing polymers onto an isolated surface. However, the simple mirror boundary condition as discussed above yields identical results when the system is large enough.

B.2.3 Curved lattices

In the previous section the planar lattice was discussed. Also homogeneously curved lattices can be used: a cylindrical and spherical lattice. In curved lattices the transition probabilities λ depend on the distance from the center. Generally, the center of the cylinder or sphere does not need to be part of the system. Instead, the first layer starts at a distance R from the center.

The curvature dependence of λ is obtained by considering $L(z)$, the number of lattice layers in layer z, and $S(z)$, the outer area of layer z. The *a priori* step probabilities are defined as $\lambda_{-1}(z) = \lambda S(z-1)/L(z)$ for a step from layer z to $z-1$ and $\lambda_1(z) = \lambda S(z)/L(z)$ for a step from layer z to $z+1$. The probability for a step inside layer z is computed as $\lambda_0(z) = 1 - \lambda_{-1}(z) - \lambda_1(z)$. For a cylinder we find

$$\lambda_{-1}(z) = \lambda\frac{2(R+z-1)}{2(R+z)-1} \tag{B.3}$$

$$\lambda_{1}(z) = \lambda\frac{2(R+z)}{2(R+z)-1} \tag{B.4}$$

where it is easy to see that $\lambda_0(z) = 1 - 2\lambda$. For a sphere the result reads

$$\lambda_{-1}(z) = \lambda\frac{3(R+z-1)^2}{3(R+z)^2-3(R+z)+1} \tag{B.5}$$

$$\lambda_{1}(z) = \lambda\frac{3(R+z)^2}{3(R+z)^2-3(R+z)+1} \tag{B.6}$$

Both $\lambda_{-1}(z)$ and $\lambda_1(z)$ reduce to λ as $R + z \to \infty$ for both geometries.

B.2.4 Lattices with multiple gradients

In principle, there is no limit to the number of gradients that can be considered in a calculation. However, typically just one, two, or three gradients are used. Two common lattices with two gradients are in use, they both are refinements of the planar lattice with one gradient. In the first variant each lattice layer is subdivided into straight 'stripes', leading to two perpendicular gradients in the y,z directions and a mean-field approximation in the remaining x-direction. For the second variant in each lattice layer one introduces 'circles', with a common centre: each next circle has a radius ℓ larger than the former. The centres of successive layers all lay on a line perpendicular to the layers. This results in a combination of a 'planar' and 'cylindrical' lattice. In both lattices one can assign a 'λ' value to the diagonal direction on the lattice.

The lattice with three gradients is composed out of cubic cells, leading to three planar gradients. A value for λ can be assigned to the three principal next-neighbouring directions. This may help to overcome a common problem[35] in calculations with more than one gradient. We briefly discuss this problem and a way around it in sec. B.6.

B.3 The packing view of the lattice

Often, a physical meaning is attributed to the value of the lattice constant λ. In this section we would like to argue against this view. It is tempting to speak of a cubic planar lattice when $\lambda = 1/6$ due to the analogy with Monte Carlo lattices. Other types of lattices spring to mind easily, like a hexagonal or BCC lattice. The bond length b between two subsequent polymer segments on a chain necessarily cannot change when a different type of lattice is used. This leads to an adjustment in the lattice spacing, due to packing constraints in the different lattices, as is often argued [40].

The lattice constants can easily be overinterpreted. One could argue against a certain lattice constant since it does not correspond with a packing model. One could also choose a lattice that matches the physics most closely. The tetrahedral lattice seems appropriate for chains with a carbon backbone because of the 109.5° angle between three C atoms.

However, all above considerations are not valid. In the mean-field lattice with one gradient, all volume fractions within one layer are averaged and therefore the information on bond positions is lost. Furthermore, atomistic detail is rarely of interest, usually a polymer segment represents a Kuhn segment, so around 10 chemical monomers, depending on the type of monomer.

Although thinking about λ as originating from lattice packing constraints may be convenient didactically, in principle this view is incorrect. The parameter λ is merely a mathematical construct and no principal reason exists to restrict the value of λ to those that can be justified from packing constraints. Indeed, even *negative* λ values can not be rejected beforehand, they are used by Maurits et al. [35]. A more valuable approach is to choose values for λ and the lattice spacing ℓ depending on the problem at hand. The comparison between results obtained for different λ values will be discussed in section B.7.

B.4 Discretising equations on a lattice

B.4.1 Discretising integrals

The way to discretise integrals is rather straightforward. Here we will fix the boundaries of the integral to $z = 0$ and $z = M$, where M is the last layer of the system. A generalisation to different boundaries is straightforward.

Consider the following integral on a planar lattice

$$\int_0^M \varphi(z) z^2 \mathrm{d}z \tag{B.7}$$

where $\varphi(z)$ is the volume fraction in layer z, so the integral results in the second moment of the volume fraction profile. The volume fraction $\varphi(z)$ is constant within the layer. Its discrete analogon is

$$\sum_{z=1}^{M} \varphi(z) \int_{z-1}^{z} z\mathrm{d}z = \sum_{z=1}^{M} \varphi(z) \left[\frac{1}{3}(z)^3 - \frac{1}{3}(z-1)^3 \right] \tag{B.8}$$

where F is the integral of f. A commonly made approximation is

$$\sum_{z=1}^{M}\int_{z-1}^{z}\varphi(z)z^2\mathrm{d}z \approx \sum_{z=1}^{M} f(z)z^2 \tag{B.9}$$

or maybe

$$\sum_{z=1}^{M}\int_{z-1}^{z}\varphi(z)z^2\mathrm{d}z \approx \sum_{z=1}^{M} f(z)(z-0.5)^2 \tag{B.10}$$

which are both simpler to implement than eq. B.8 and will generally yield the correct trends. Application of these kinds of approximations is not generally recommended. This can be illustrated as follows. For a cylindrically curved space it can be mathematically shown that the following relation is exact for all functions $f(z)$.

$$\int_0^M f(z)A(z)\mathrm{d}z = A(R_s)\int_0^M f(z)\mathrm{d}z + \frac{A(R_s)}{R_s}\int_0^M (z-R_s)f(z)\mathrm{d}z \tag{B.11}$$

where R_s is an arbitrary dividing plane and $A(z) = 2\pi z$ is the corresponding surface area. When $f(z)$ is for example a volume fraction $\varphi(z)$ and therefore constant within the layer we obtain by using eq. B.8

$$\sum_{z=1}^{M}\varphi(z)L(z) = A(R_s)\sum_{z=1}^{M}\varphi(z) + \frac{A(R_s)}{R_s}\sum_{z=1}^{M}\varphi(z)\int_{z-1}^{z}(z-R_s)\mathrm{d}z \tag{B.12}$$

which is also exact, like eq. B.11. Using the approximations eqs. B.9 and B.10 both do not result in an exact relation.

B.4.2 Ambiguities in discretising derivatives

Discretising an equation which contains derivatives can not be done unambiguously in general. Consider for example the following derivative:

$$\frac{\partial g(f(z))}{\partial z} = \frac{\partial g(f(z))}{\partial f(z)}\frac{\partial f(z)}{\partial z} \tag{B.13}$$

where g is a function of $f(z)$. The central differentiation of this equation depends on whether one uses the left or right hand side.

$$\begin{gathered}\frac{g(f(z+\Delta z))-g(f(z-\Delta z))}{2\Delta z} \neq \\ \frac{g'(f(z+\Delta z))f(z+\Delta z)-g'(f(z-\Delta z))f(z-\Delta z)}{2\Delta z}\end{gathered} \tag{B.14}$$

Here, $g'(f(z))$ represents the derivative of g to f (we assume it is analytically available). Obviously, the left and right hand side of this equation become equal as Δz goes to zero. However, when z represents the distance on a lattice, the lattice spacing is the lower limit on Δz so the two methods will yield different results. In general there is no way to favour one way of discretising a derivative over the other. However, physical reasons may force the use of one method over the other. An example of this is the diffusion equation, which for simplicity will be evaluated in only one gradient.

$$\frac{\partial \varphi(z,t)}{\partial t} = \frac{\partial}{\partial z}\Lambda(z,t)\frac{\partial}{\partial z}\mu(z,t) \tag{B.15}$$

Here φ represents the volume fraction of molecules, z is the lattice coordinate, t represents time, Λ is the Onsager coefficient and μ is the local chemical potential which is the driving force for diffusion. Rewriting this equation yields

$$\frac{\partial \varphi(z,t)}{\partial t} = \Lambda'(z,t)\mu'(z,t) + \Lambda(z,t)\mu''(z,t) \tag{B.16}$$

where a prime indicates a derivative to z. Applying central differentiation on the right hand side yields

$$\begin{aligned}\frac{\partial \varphi(z,t)}{\partial t} = {} & \frac{\Lambda(z+1,t)-\Lambda(z-1,t)}{2}\frac{\mu(z+1,t)-\mu(z-1,t)}{2} \\ & +\Lambda(z,t)\left[\mu(z-1,t)-2\mu(z,t)+\mu(z+1,t)\right]\end{aligned} \tag{B.17}$$

While this differentiation scheme may seem good, it gives wrong physics as we will show below. A different route of differentiation starts with a central differentiation of the first derivative on the right hand side of eq. B.15.

$$\frac{\partial \varphi(z,t)}{\partial t} = \Lambda(z+1/2,t)\frac{\partial}{\partial z}\mu(z+1/2,t) - \Lambda(z-1/2,t)\frac{\partial}{\partial z}\mu(z-1/2,t) \tag{B.18}$$

Central differentiation of the last derivative and approximating $\Lambda(z+1/2,t)$ as $\{\Lambda(z,t)+\Lambda(z+1,t)\}/2$ yields

$$\begin{aligned}&\frac{1}{2}\left\{\left[\Lambda(z,t)+\Lambda(z+1,t)\right]\left[\mu(z+1,t)-\mu(z,t)\right]\right. \\ &\left.-\left[\Lambda(z-1,t)+\Lambda(z,t)\right]\left[\mu(z,t)-\mu(z-1,t)\right]\right\}\end{aligned} \tag{B.19}$$

This differentiation scheme is usable contrary to eq. B.17, which is leads to conflicts at the boundaries of the system. Eq. B.19 consists of two contributions, the transport of material between layers z and $z-1$ and a separate contribution from the transport between layers z and $z+1$. Eq. B.17 cannot be split up in this way and therefore does not hold when e.g. surface is present. In this case there should be no transport to and from the layer that contains the surface. Eq. B.17 cannot satisfy this condition and therefore is unusable due to a physical reason.

B.5 Artefacts due to the position of the interface

B.5.1 The Gibbs dividing plane

The position of a liquid-solid and gas-solid interface is readily assigned when the solid interface is considered to be perfectly smooth and chemically inert. When no solids are involved, e.g. a liquid-liquid interface, the position of the interface is arbitrary: there is a gradual change in the volume fractions in the interfacial region. We are free to choose a procedure to define the position of the interface. The physics of the system at hand is unaffected by our choice. Here we merely give some examples of choices that could be made. We will use the Gibbs convention where the interface is considered to be infinitely thin and both phases extend up to the interface. The excess amounts are attributed to the interface.

Consider two phases, α and β, separated by an interface. Say we have only two different molecules present in the system, A and B. Phase α consists mainly of molecules A, phase β mainly of molecules B. In this case we can use the Gibbs equimolar plane, to define the position of the interface. The equimolar plane z^{eq} of molecules A for a planar interface can be found from

$$\int_0^{z^{eq}} (\varphi_A(z) - \varphi_A^\alpha)\mathrm{d}z + \int_{z^{eq}}^{M} (\varphi_A(z) - \varphi_A^\beta)\mathrm{d}z = 0 \tag{B.20}$$

where $\varphi_A(z)$ is the volume fraction of monomers A in layer z and φ_A^α and φ_A^β are the bulk volume fractions of monomers A in phase α and β respectively.

When the bulk volume fractions φ_A^α and φ_A^β do not differ between the two phases, the Gibbs equimolar plane is undefined. This case occurs for example for a surfactant vesicle: the phase inside the vesicle has the same composition as the phase outside the vesicle. Then we may use, for example, the first moment of the excess volume fraction profile of the surfactants z^{fm}

$$z^{fm} = \frac{\int_0^M z\varphi^{exc}(z)\mathrm{d}z}{\int_0^M \varphi^{exc}(z)\mathrm{d}z} \tag{B.21}$$

where $\varphi^{exc}(z) = \varphi(z) - \varphi^b$ and φ^b is the bulk volume fraction.

B.5.2 Planar two component interfaces

In calculations where space is discretised in planar layers, the position of the interface with respect to the layers, may lead to an artefact in the results. In this section first the actual occurence of an artefact is shown. Then the method that has, in the past, been used to remove the artefact is reviewed. Finally, a new, more generally applicable method to remove the artefact is discussed.

Artefact in the dividing plane

Consider two phase separating molecules A_3 and B. Molecule A_3 has a length of 3 segments, molecule B is a monomer. This choice is made to make sure our arguments do not depend on the symmetry that arises from choosing two molecules of equal length. The Flory-Huggins interaction parameter is $\chi = 2.5$, resulting in a solubility gap so that at equal amounts of A_3 and B phase separation occurs. The SCF theory is used to analyse this system. We consider a system of 50 layers. This system is large enough to exclude effects from the system boundaries. The amount

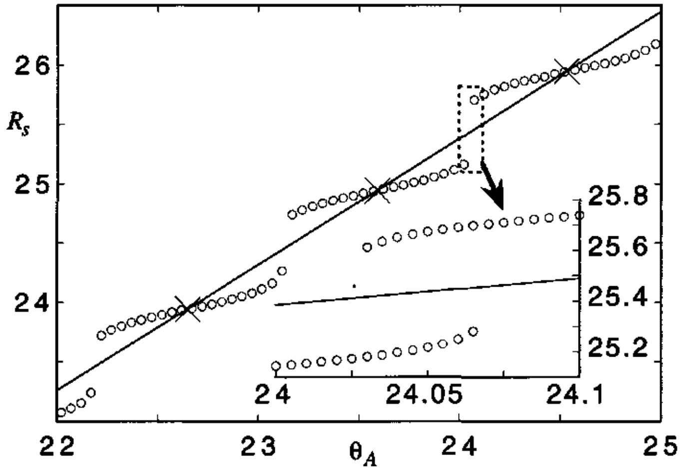

FIGURE B.2: The position of the Gibbs equimolar plane R_s (open symbols) as a function of the amount θ_A of A_3 in the bad solvent B ($\chi = 2.5$) for $\lambda = 1/6$. The discretisation artefact free points are denoted by crosses, the expected behaviour without artefact is shown as a straight line. In the enlarged region two solutions of the SCF equations are shown

$\theta_A = \sum_z \varphi(z)$ of molecules A_3 is gradually increased from 22 to 25. The position of the Gibbs dividing plane (open symbols), as calculated with eq. B.20 R_s, as a function of θ_A is shown in fig. B.2. It can be seen that R_s does not change linearly with θ_A. This is an indication of an artefact. The solid line is the result we get when removing the artefact with the procedure that will be outlined below. Around the artefact free points (denoted by crosses) R_s changes gradually, halfway between these points R_s changes discontinuous. This discontinuity is enlarged in the inset. It can be seen that two solutions of the SCF equation are found. A different value for R_s is found depending on whether one enlarges θ_A or decreases θ_A. This effect will be elaborated on when discussing fig. B.4.

Old method to eliminate the artefact

Fig. B.3 shows the surface tension as a function of the position of the dividing plane for the same system as fig. B.2. The surface tension oscillates with a period of exactly unity, equal to the spacing between subsequent layers. However, it should be clear that the surface tension cannot depend upon the amount of molecules present in this system. The same figure also shows the bulk pressure difference ΔP. As can be seen, ΔP is zero only in some distinct points. Physically, however, no pressure difference should be present. The non-zero pressure difference is identified as a discretisation pressure $\Delta P = \Delta P_{discr.}$ [89]. This pressure stems from the fact that the molecules are 'packed' at distinct layers. The artefact free points have a

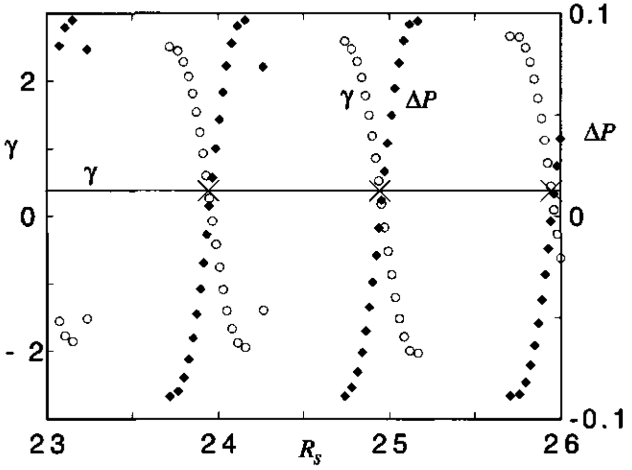

FIGURE B.3: The surface tension γ (diamonds) and the bulk pressure difference ΔP (circles) as a function of the position of the Gibbs equimolar plane. The crosses indicate the artefact-free surface tension ($\Delta P = 0$).The same system parameters as in fig. B.2 were used.

Gibbs equimolar plane R_s which is close to the boundary of a layer. The spacing between artefact free points is exactly one layer. In the symmetrical case of two phase separating molecules of equal length the Gibbs dividing plane of the artefact free point is exactly located at the boundary between two layers. The formation of an interface in the middle of a layer is opposed by a build-up of the discretisation pressure. This also explains the discontinuities in R_s in fig. B.2.

The chemical potentials of both molecules (not shown) oscillate as well when changing the amount θ_A of molecules A_3. In the artefact-free points the chemical potentials are equal to those predicted from Flory-Huggins theory. We conclude that the points where $\Delta P = \Delta P_{discr.} = 0$ are indeed artefact free points, which may be found by varying θ_A.

New method to eliminate the artefact

Changing the amount of one of the liquids changes the physics of the system and this may be unwanted for the problem at hand. Therefore, a different procedure is proposed to find the artefact free point for any amount of the two components. Instead of varying the composition of the system, the *layers* are shifted over the interface, while keeping the composition of the system constant. This is accomplished by varying the width of the first ($z = 1$) and last ($z = M$) layer of the system, in such a way that the total volume of the system remains constant. This requires a special treatment of the first and last layer of the system to which we return later. Since the composition of the system is constant, we now have a n, V, T ensemble.

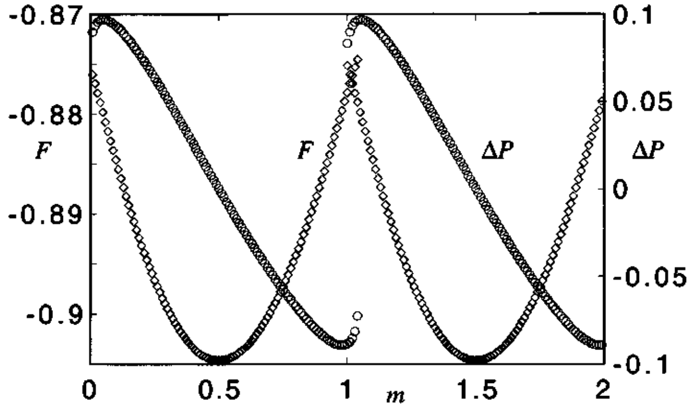

FIGURE B.4: The Helmholtz energy F (diamonds) and the bulk pressure difference ΔP (circles) as a function of the width of the first layer m for the same system as in fig. B.2, here with constant $\theta_A = 25$. Lines are drawn for comparison.

Its characteristic function is the Helmholtz energy F.

Figure B.4 shows the Helmholtz energy F and the pressure difference ΔP as a function of the width m of the first layer of the system for the same system as studied in fig. B.2 but now for constant $\theta_A = 25$. It can be seen that the free energy F passes through a minimum at two points ($m = 0.505$ and $m = 1.505$). At these points the pressure difference is zero. The values for m at both minima differ exactly unity, which shows the consistency of the method. The chemical potentials of A_3 and B (not shown) are also a function of m. Their values in both minima equal the chemical potentials predicted from the Flory-Huggins theory. We conclude that minimising the characteristic function F as a function of the width of the first layer yields the lattice artefact free point for a planar lattice. Such a minimum is readily found numerically.

In fig. B.4 two values for the Helmholtz energy F are found for several values of m in the neighbourhood of $m = 1$. The points in fig. B.4 have been computed by varying m from 0 to 2 and vice-versa. When varying a parameter (in this case m) between two subsequent calculations it is customary to use the result of the first calculation as an initial guess for the second calculation. This illustrates that solving the SCF equations may lead to convergence towards a local minimum (as opposed to a global minimum) in the Helmholtz energy. This case is comparable to the two solutions that were earlier found in fig. B.2. In fig. B.2 the two solutions also differ in Helmholtz energy.

One could wonder about the boundary conditions and the chain propagator in this method. A chain propagator working on only a fraction of a layer seems problematic. However, when there are no gradients in volume fractions at the boundaries of the system, the problem is easily solved. When computing the unnormalised volume fractions, the change in the width of the first and last layer is not taken into account. Also the field is computed without considering the shift of the lattice. When the normalisation (eq. 4.5) is computed the change in width is taken into account. For a planar system $L(1)$ equals m, the width of the first layer, $L(M) = 2-m$ and $L(z) = 1$ otherwise. The Helmholtz energy is computed from the Helmholtz energy density profile also by weighting with $L(z)$.

B.5.3 Two component curved interfaces

In the previous section it was shown that shifting the lattice, while retaining the total volume and composition, until a minimum in the Helmholtz energy F is reached, guarantees that the lattice artefact was eliminated. This could be checked by comparing the obtained chemical potentials with the analytical Flory-Huggins theory and by noting that the pressure difference between the two phases becomes zero. For curved lattices these checks cannot be made. The Flory-Huggins theory cannot deal with a drop of oil in water. No analytical theory exists that predicts the artefact free chemical potentials for our model. Furthermore a physically real pressure difference between the two phases exists, as is demanded by the generalised Laplace equation[56].

$$\Delta P = \gamma J + \left[\frac{\partial \gamma}{\partial R_s}\right] \tag{B.22}$$

Here, J is the curvature defined by $J = 1/R_s$ for a cylindrical surface and by $J = 2/R_s$ for a spherical surface. The square brackets denote a notional differential; the choice for the position of the dividing plane is changed, while the entire system, including the lattice, remains the same. It is purely a mathematical procedure.

Investigation of a two-phase equilibrium as done in the previous section, but now for a curved geometry, shows that the generalised Laplace equation B.22 holds at all times, also when a discretisation artefact is present. However, ΔP does show the characteric oscillation as discussed in the previous section, which indicates an artefact. This means that an artefact is present in both the left and right hand side of this equation.

The same procedure, as was used for a planar lattice, is also applied for a curved geometry. The radius of the first layer and last layer of the system is changed, while both the total volume and the composition of the system remain constant until we reach the minimum of the Helmholtz energy F. However, the check that could be made in a planar geometry ($\Delta P = 0$) cannot be used in a curved geometry. We simply have to assume the proposed procedure is generally valid. An example calculation for a cylindrical geometry is given in in fig. B.5, where the free energy F and the position of the interface R_s are plotted against the radius of the first layer, while retaining constant total volume and composition. The free energy F passes trough two minima, of equal depth, the distance between the minima corresponds exactly with a difference of unity in radius of the first layer. This shows the consistency of the procedure.

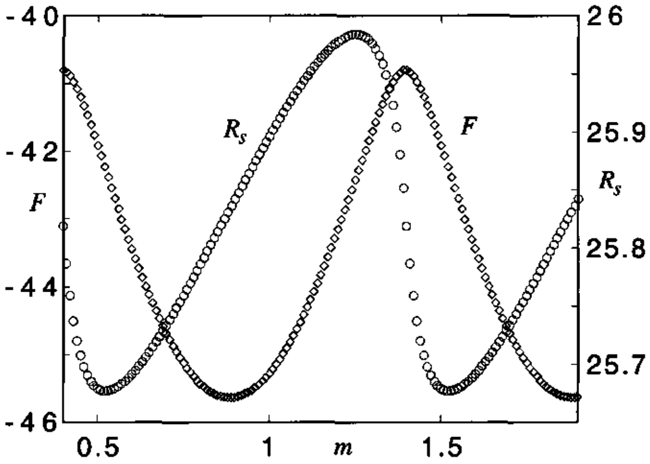

FIGURE B.5: The Helmholtz free energy F (diamonds) and the position of the interface R_s (circles) as a function of the width of the first layer m, in a cylindrical geometry, $\theta_A = 2500$, other parameters equal to fig. B.4.

For phase separating monomers a different procedure has been used in the past.[55] Here, the surface tension from a planar lattice γ_0 was calculated first. This surface tension was then used to predict the resulting pressure difference for a given curvature

$$\Delta P = \gamma J \simeq \gamma_0 J \tag{B.23}$$

Then, material was added until the predicted pressure difference was obtained. However, this procedure does not guarantee that any lattice artefact free point can be found, it could even result in more than one artefact free point. The prediction for the pressure difference ΔP from eq. B.23 suffers from two problems. The curvature J should be placed at the surface of tension where the term $\left[\frac{\partial \gamma}{\partial R_s}\right]$ vanishes. However, this was not done. Furthermore, as was remarked earlier [89], the assumption is made that the surface tension γ changes negligibly when bending the interface, which may not be true in general. For these reasons it is concluded that the previously used method cannot be exact. However, it should be remarked that the results obtained in ref. [55] cannot be graphically distinguished from the results obtained by our new method.

B.5.4 Multicomponent systems

In the previous two sections simple binary systems where considered. In these systems we can eliminate the discretisation artefact by adjusting the discretisation so that the Helmholtz energy is minimised. The situation is complicated considerably by considering block copolymers and multi component systems. In these systems generally one may have more than one interface. Therefore, it is not expected that the methods of the previous section can be applied. Nevertheless we will investigate whether our method can at least reduce the artefact for vesicles. Firstly, however, we should mention another approach that has been used to reduce the discretisation artefact in multicomponent systems.

Adjusting the contact interactions

It turns out that calculations with one gradient and $\lambda = 1/3$ suffer only a little from artefacts due to the position of the interface. For example, in fig. B.3 the oscillations of ΔP are reduced by a factor of 100 if $\lambda = 1/3$. The position of the Gibbs dividing plane R_s in fig. B.2 graphically becomes a straight line when $\lambda = 1/3$. When relatively diffuse surfaces are considered, we end up with an acceptable solution for many cases. Upon increasing the repulsion between the monomers, the interface becomes more narrow and the artefact becomes more pronounced again.

The reduction of the discretisation artefacts for calculations with $\lambda = 1/3$ stems from the layer average, eq. 3.26 used in eq. 4.2, *not* its application in computing the end-segment weighting factors $G(z, s, |1)$. When we use $\lambda = 1/3$ the oscillation of the contact energy upon shifting the interface is damped considerably.

For symmetrical interfaces, e.g. between two molecules A and B with an equal chain length, a calculation with $\lambda = 1/2$ completely eliminates the artefact. It can be analytically verified that the total contact energy does not change upon changing the amount of one of the components in this case. For non-symmetrical interfaces, the optimal value for λ depends on the problem at hand but turns out to be closer to 1/2 than 1/3. However, the choice of $\lambda = 1/2$ has the consequence that the contact interactions within the same layer are no longer accounted for, which seems physically unrealistic.

For some systems, the method of adjusting λ may be the only way to reduce the discretisation artefact. This is because the methods to reduce the artefact that were described in the previous sections are not generally applicable. Consider for example a system where two interfaces are present. Here, one cannot eliminate the artefact for both interfaces at the same time by changing the width of the first layer. Another example is when a gradient in the volume fraction exists at the boundary of the system. Changing the width of the first layer in this case should be accompanied by a rewrite to the chain propagators, which complicates the method considerably.

Shifting the layers in multicomponent systems

In the two component systems that were considered in sec. B.5.2 the total amount θ of one of the components was chosen, the amount for the other component is then also fixed. In multicomponent systems often one or more of the components has a fixed bulk volume fraction. This means the system is no longer an n, V, T ensemble and the Helmholtz energy is not the characteristic function which needs to be minimised with respect to m. There are two possible solutions. Instead of the Helmholtz energy a different characteristic function X can be chosen. Another solution is to change the calculation towards an n, V, T ensemble. The latter method is the preferred method for most calculations, as will be shown.

For the first solution we need a new characteristic X function to minimise:

$$X = F - \sum_{\varphi_i^b = \text{fixed}} \frac{\theta_i}{N_i} \mu_i \tag{B.24}$$

here the sum runs over all components with a fixed bulk volume fraction. This is the right approach when the μ_i values in the sum are constant upon changing m. However, generally this is not the case. When the amount of one of the components is fixed, its bulk volume fraction will vary upon varying m. This means that the activity coefficient of the components with fixed bulk volume fraction may vary and therefore also their chemical potential. In this case X is no longer the characteristic function of the system, which renders this method invalid on thermodynamical grounds.

The second possible solution is to do a 'normal' SCF calculation, i.e. a calculation where the bulk volume fraction of certain components is fixed. This SCF calculation results in a certain total amount for each molecule. Then these amounts are taken as the fixed values and F is minimised as a function of m. Upon changing m all bulk volume fractions φ_i^b will change. This means that the artefact free solution does not have the exact bulk volume fractions that we set out to calculate. It turns out that these changes are usually relatively very small, and the results are hardly affected, whereas in the method of optimising X one easily obtains physically unrealistic results.

Vesicles with diffuse interfaces

In the previous sections it was shown how a lattice artefact can be eliminated when only one interface is present. However, when multiple interfaces are considered some extra problems may arise. A common example where two interfaces are present is a vesicle. For vesicles, the pressure difference ΔP should be zero at all times, since full equilibrium exists over the membrane. This is indeed the case in the numerical calculations, also when a lattice artefact is present. Previously, it was suggested to iterate the zero-th moment of the pressure profile to zero[89]. As is shown elsewhere [56] this procedure is physically unjustified. Therefore it is of interest to investigate whether the newly proposed procedure that finds the minimum in the characteristic function F upon the change of the width of the first layer m is also valid for vesicles. Some complications may be expected. A membrane is not a single liquid-liquid interface, rather it can be viewed as consisting of two liquid-vesicle interfaces. It seems our method would minimize the artefact of one liquid-vesicle interface only. Some physical features of vesicles are available to test our method. The test relies on the Helfrich equation eq. 4.6

Upon decreasing the curvature J of a vesicle it's surface tension should become zero ($\gamma_0 = 0$). Since J_0 equals zero for a symmetrical membrane, a plot of γ

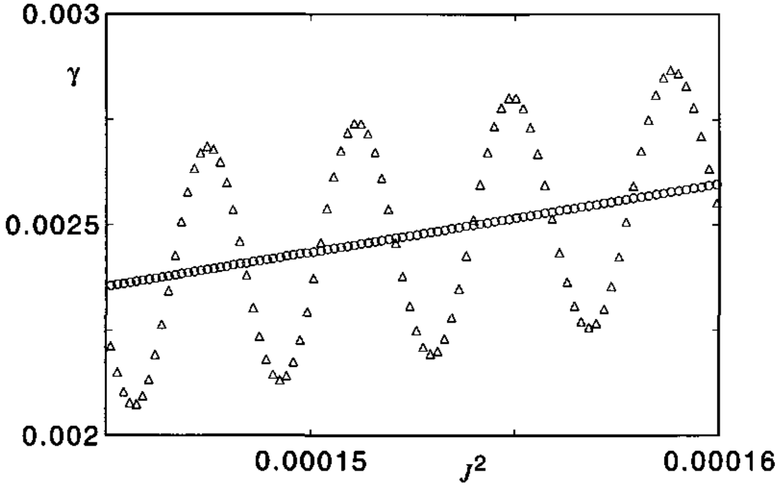

FIGURE B.6: The surface tension γ of a $\mathtt{C_{12}E_5}$ surfactant vesicle in solvent W as a function of J^2, $\lambda = 1/6$, $\chi_{\mathtt{CW}} = \chi_{\mathtt{CO}} = 1.6$ and $\chi_{\mathtt{CO}} = -0.3$. Circles and triangles denote the calculation with and without reduction of the lattice artefact, respectively.

versus J^2 should yield a straight line. This is indeed the case for weakly structured bilayers as is shown in fig. B.6 for a $\mathtt{C_{12}E_5}$ surfactant in a solvent W. The surfactant is modelled as $\mathtt{C_{12}(OC_2)_5O}$, $\chi_{\mathtt{CW}} = \chi_{\mathtt{CO}} = 1.6$, $\chi_{\mathtt{CO}} = -0.3$. The figure shows only a small lattice artefact, which is easily iterated away by minimising F. In fact the artefact is so small that averaging over it gives a good estimate of $(k_c + \bar{k}/2)/2$. The new procedure to remove the artefact has the added advantage that far less evaluations of different vesicle radii are necessary to come up with a good estimate for the bending moduli. Evaluating at a few radii without removal of the artefact may lead to aliasing in γ, resulting in bad averaging.

Rigid vesicles

As expected, when considering more rigid vesicles some troubles appear as is shown in fig. B.7, where the same system as in fig. B.6 is used except that $\chi_{\mathtt{CW}} = \chi_{\mathtt{CO}} = 2.2$ and $\chi_{\mathtt{CO}} = -0.8$ In this figure the width of the first layer is first increased and then decreased again, always using the result of a former calculation as an initial guess for the current calculation. Clearly, we see that two different SCF solutions to the same problem are found, the one with the higher free energy F corresponds to a local minimum. The acceptance of the local minimum of F is triggered by the use of the initial guess and becomes more likely as the membrane becomes more rigid. In fact, 3 or more local SCF minima for a given m have been observed. We first will discuss a work-around for these local minima followed by a discussion of their origin.

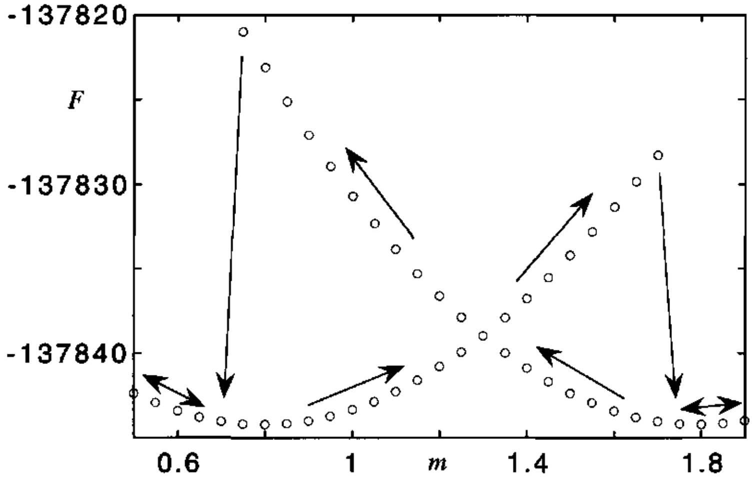

FIGURE B.7: The Helmholtz free energy F as a function of increasing m followed by decreasing m, in a spherical geometry for the same system as in fig. B.6, only now $\chi_{\mathtt{CW}} = \chi_{\mathtt{CO}} = 2.2$ and $\chi_{\mathtt{CD}} = -0.8$ The arrows indicate the order of the computations.

A workaround for the unwanted acceptance of local minima is as follows. The interest is in the minimum of the characteristic function F. This is found by calculating $\frac{\partial F}{\partial m}$, say for $m = 1$. When this derivative is positive m is increased, m is decreased if the derivative is negative and the subsequent derivative is computed. This is done until the derivative changes sign. This leaves us with a good estimate of the global minimum of F, which then can be computed using standard techniques [49]. When m becomes too large, say $m = 1.9$ or to small, say $m = 0.5$, we subtract or add unity to m, respectively.

The procedure described above makes sure that the global minimum of F is found. Checking eq. 4.6 for a number of different vesicles showed that it indeed holds at all times and that γ_0 is zero in the limit of $J \to \infty$. This may lead to the conclusion that our procedure to eliminate the lattice artefact is valid for vesicles also but we need to be careful. To explain our concern we consider planar membranes in fig. B.8. We calculate a $\mathtt{A}_n\mathtt{B}_3$ lipid bilayer on a planar lattice for varying values of n $\chi_{AB} = \chi_{AW} = 2$, $\chi_{BW} = -1$. Molecules are added to the membrane until the physically relevant condition of $\gamma = 0$ is reached. The resulting thickness of the membrane is computed as the first moment over the excess volume fraction profile of the outer B segment defined by eq. B.21. Since the bilayer is symmetric, we can make use of the mirror boundary condition (see sec. B.2.2) and calculated only half of the bilayer, eq. B.21 then yields half the thickness of the bilayer $d/2$.

In fig. B.8 half the thickness of the bilayer $d/2$ is shown as a function of n, the length of the A-block. For $\lambda = 1/6$ the bilayer 'snaps' onto the lattice, showing a

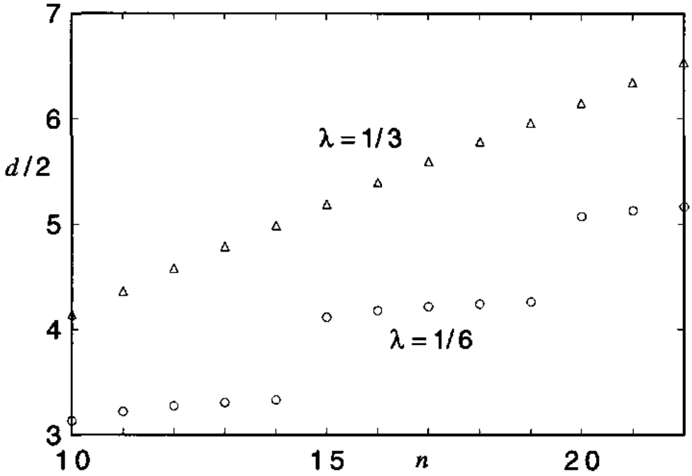

FIGURE B.8: The influence of the length of the A-block of the A_nB_3 lipid on the thickness of the resulting planar bilayer for $\lambda = 1/6$ and $\lambda = 1/3$. $\chi_{AB} = \chi_{AW} = 2$, $\chi_{BW} = -1$.

preference for $d/2$ to become an integer value. This clearly shows the presence of an artefact for the surfactant under consideration. In contrast, for $\lambda = 1/3$, $d/2$ varies smoothly with the chain length of the surfactant, illustrating the effectiveness of this 'artefact poor' lattice as discussed in sec. B.5.4.

The SCF equations do not *demand* that $\gamma = 0$ for a planar bilayer. We add this condition as an extra constraint to the calculations, as explained before. The multiple SCF solutions we saw in fig. B.7 correspond to different vesicle radii. When the radius is changed, the number of surfactants per unit area is changed. The global minima of F in fig. B.7 all correspond to $\gamma_0 = 0$. In fig. B.8 it is shown that these points are not guaranteed to be free of a lattice artefact when using $\lambda = 1/6$. Instead, a combination of the artefact poor value for λ and the our new method to eliminate the artefact can be used.

B.6 Anisotropy artefacts

Lattices with two or more gradients may suffer from an undesired anisotropy of the chains. A standard 'cubic' lattice does not meet the requirement that a Gaussian chain has the same shape in all directions. The shape of the volume fraction profile in the x direction is different from that in a diagonal direction. Maurits et al.[35] have corrected this deficiency for Gaussian chains by equating the lattice propagator to the continuous differential equation for a Gaussian chain. The values for λ and the lattice spacing ℓ for Gaussian chains are then found from the resulting equalities.

As was discussed in sec. B.2.4 some different walks on the lattice may be allowed, e.g. diagonal walks. As more types of discrete steps are allowed the similarity between the continuous and lattice equations generally improves. However, the CPU time needed to perform the calculations also increases [35].

We would like to stress two particular points about this method. Firstly, other lattice artefacts, for example due to the position of the interface (section B.5) are not removed by this procedure. Furthermore, their proposed values for λ and ℓ are fitted to a Gaussian chain in the absence of a field. The procedure of Maurits et al. is used in the calculations of Fraaije et al. [90] where local phase separation of block copolymer melts is studied, which results in chains which will remain Gaussian. Other values for λ and ℓ might be more appropriate when studying brushes in a monomer solvent. We do not agree with the claim of Maurits et al. that the introduction of clever values for λ results in a theory that is 'off-lattice'. We would rather say they use a clever lattice. Nevertheless, their scheme overcomes an important deficiency of the standard 'cubic' lattice. Without the new values for λ actual calculations on lattices with 3 gradients do not even converge [35].

B.7 Comparing different lattices

When comparing results obtained from calculations in one gradient we see that at first sight the results depend on the parameter λ, the lattice constant. The way to deal with this depends on the problem at hand.

When we want to compare the radius of gyration found for a chain grafted on a planar lattice for different values of λ, it should not depend on λ. From the Edwards diffusion equation for general λ it follows that for a planar geometry with one gradient

$$b\sqrt{N/6} = \ell\sqrt{\lambda N} \tag{B.25}$$

where b is the bond length or bead size, ℓ is the lattice spacing and N is the chain length. The left hand side is the analytical expression for the radius of gyration R_g of an isolated Gaussian chain and the right hand side is the lattice analogon. From this equation we can calculate the appropriate value for the lattice spacing ℓ as $b/\sqrt{6\lambda}$. This equality also appears successful when applied for adsorbing polymers [60].

However, when our interest is in brushes above the overlap concentration, we know that the brush height should scale linearly with N. To compare the brush height obtained from different lattices it is sufficient to set ℓ equal to b. The same applies for an isolated chain that is collapsed.

However, if we consider an isolated Gaussian chain in a spherical geometry, the expression for the radius of gyration R_g becomes

$$R_g = b\sqrt{N/2} \tag{B.26}$$

and therefore the relation between the lattice spacing ℓ and λ now reads $\ell = b/\sqrt{2\lambda}$.

We conclude that no general procedure can be given to eliminate the difference in results between different lattices and that comparing results between different calculations is most safely done by using the same λ values.

B.8 Translating experimental parameters to model parameters

Volume fractions are dimensionless concentrations. When comparing volume fractions with actual concentrations, some care need to be taken. For example, in the modelling of chemical reactions like acid-base or redox equilibria, as discussed in chapter 2 we need to determine the appropriate equilibrium constants. Furthermore, it is important to set the spacing between layers ℓ to a realistic value when doing computations with charged molecules.

The translation of experimental quantities to model parameters is best explained by using an example. In many cases, the interest is in calculations in aqueous solutions so we will use the example of acetic acid in water

$$\mathtt{HA} + \mathtt{H_2O} \rightleftarrows \mathtt{A^-} + \mathtt{H_3O^+} \tag{B.27}$$

and the autoprotolysis equilibrium

$$2\mathtt{H_2O} \rightleftarrows \mathtt{OH^-} + \mathtt{H_3O^+} \tag{B.28}$$

at 298 K. Suppose we want to model a 1 mM solution of acetic acid in water. In our model the volumes of all segments are equal, which is obviously an approximation. Pure water has a molarity of 55.5 mol/l. Water is the abundant species so the natural choice is to set the molarity of all segments in their pure form to 55.5 mol/l. When we use the natural assumption that each 'cell' of a layer can contain one segment, this yields a layer spacing of $\ell = 0.31$ nm, the volume of one water molecule. Note that the distinction between different 'cells' within a layer is not explicitly made.

A solution of 1 mM is modelled by setting the volume fraction to $10^{-3}/55.5 \approx 1.8 \cdot 10^{-5}$. The acidity constant found from standard literature is $pK_a = 4.75$ for the first equilibrium and the autoprotolysis constant of water is $pK_w = 14$. We need to recalculate those in volume fractions. Note that the volume fraction of $\mathtt{H_2O}$ is about unity. It follows that the two equilibrium constants for our model are $10^{-6.5}$ and $10^{-17.5}$, respectively.

The layer spacing ℓ can also set unequal to 0.31 nm, for example $\ell = 0.62$ nm. The change in the discretisation of space affects the translation of volume fractions to concentrations. Now each 'cell' within a layer contains 8 times as much material. Therefore, a solution of 1 mM is now modelled by setting the volume fraction to $8 \cdot 10^{-3}/55.5 \approx 1.44 \cdot 10^{-4}$. At first sight this may seem a bit unnatural: the bulk volume fraction changes as the lattice spacing is changed. However, doubling the lattice spacing also effects the size of the salt ions: their volume is augmented by a factor of 2^3. This reflects an unphysical change. A way to interpret this is to say that each ion is surrounded by 7 water molecules. The 7 water molecules are 'incorporated' in the ion with a double radius. We checked that the Debye screening length resulting from our theory for a planar electric double layer corresponds to the prediction of the DLVO theory and remains unaffected when the lattice spacing is changed, as long as the transformation of concentrations to volume fractions is done as described here.

B.9 The Stern layer

The Gouy-Chapman theory of electric double layers is known to suffer from some imperfections. One of those is the point charge approximation where it is neglected that ions have a finite size. For the diffuse double layer, this gives no problems. However, one of the consequences is that the concentration of ions near the surface is predicted to be much higher that the space that is available. Stern therefore came up with a correction that treats the region near the surface differently. In this treatment ions have a finite size directly next to the surface, the outer part of the double layer is again treated as consisting of point charges.

If our theory is applied to an electric double layer, it is effectively a multi layer Stern model. In each layer the finite size of the ions is taken into account. Outside the first layer the multi layer nature is hardly noted: lattice results for an electric double layer are virtually identical to the original Stern model, where the diffuse layer is continuous.

In polymer adsorption from solution a similar problem arises: the segments next to the surface have a finite volume. The lattice theory obviously takes care of this physical feature. In analytical theories however, some problems may emerge, in dealing with high packing densities near the surface.

We illustrate this by considering polymer adsorption to a solid surface from semi-dilute solution in a good solvent. In the GSA theory the volume fraction profile $\varphi(z)$ of polymers is related to the order parameter ψ as [44, 91]

$$\varphi(z) = \psi^2 = \varphi^b \coth^2 x \tag{B.29}$$

where $x = (z+p)/d$ is a dimensionless distance, $d = \sqrt{2\lambda/\varphi^b}$ is the correlation length, and p is the proximal length which is found from a boundary condition. The boundary condition reads

$$\frac{1}{2}\sinh\frac{2p}{d} = \frac{1}{6d(\chi_s + \ln 5/6)} \tag{B.30}$$

which for strong adsorption ($p \ll d$) is simplified to

$$p = \frac{1}{6(\chi_s + \ln 5/6)} \tag{B.31}$$

The volume fraction profiles of the adsorbing polymers resulting from these analytical equations show good agreement with the numerical SCF results[44]. For

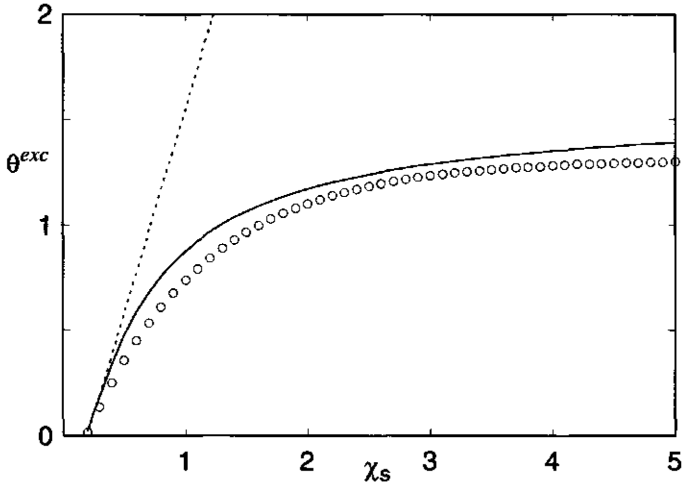

FIGURE B.9: Excess amount of polymer as a function of the Silberberg adsorption parameter χ_s, for a polymer chain length $N = 10000$, good solvent, and a bulk volume fraction $\varphi^b = 0.01$. Symbols: SF-theory (symbols), dotted curve: GSA-theory, solid curve: GSA theory with special treatment of layer $z = 1$ (see text).

the calculation of the excess adsorbed amount we split up the integral as was done before[60].

$$\theta^{exc} = \int_0^\infty (\varphi(z) - \varphi^b)\mathrm{d}z = \varphi(0.5) - \varphi^b + \int_1^\infty (\varphi(z) - \varphi^b)\mathrm{d}z \tag{B.32}$$

As can be seen, the first layer is treated separately from the rest of the integral, reflecting the notion of the 'Stern' layer. In ref. [44], this separation was not made, consistent with the analytical nature of the equations.

In fig. B.9 the data of van der Linden [44] are reproduced. The dashed straight line represents θ^{exc} as computed by the left hand side integral of eq. B.32, the solid line corresponds to the right hand side of eq. B.32, the symbols denote numerical results. If we do not split up the integral as done in eq. B.32, the excess amount of polymer continues to grow linearly with χ_s. The SF data show a plateau where the surface is saturated, which seems more likely from a physical point of view.

We conclude that a simple modification of the original GSA equations, in the form of a different treatment near the surface, improves the agreement with the results from the SF-theory. Our modification is not consistent within the model, instead we should have rewritten the boundary condition as done in Fleer et al. [60] as well. Our example does show a system where the lattice variant of equations may be physically more realistic.

B.10 Possible future improvements

The discussion of the lattice artefact in section B.5, was restricted to lattices with one gradient. When lattices with more gradients are used, extra complications arise. Firstly, the shape of the interface may be irregular; the curvature may vary along the interface. This makes shifting the lattice over the interface a difficult, if not impossible, procedure. Therefore, different techniques should be investigated.

One approach would be to find an 'artefact poor' lattice as was done in the lattice with one gradient. However, when this lattice does not suffer from artefacts due to the position of the interface, it could very well introduce the anisotropy artefacts, as were discussed in section B.6. The solution is to assign different values for λ for both the contact interactions and the chain propagators as has been done before [92, 93]. There seems to be no reason why the λ values should be equal for both operations, other than the (unjustified) view of a lattice where packing constraints govern the values of λ, as was discussed in section B.3.

Another possible approach would be to use more lattice layers in the vicinity of the interface, decreasing the spacing in this area as more accuracy is desired. This could be viewed upon as 'zooming in' on interfaces. A method common in fluid dynamics. This method would require rewriting the discrete propagators.

The discussion of the influence on the results of the *a priori* transition probability λ was limited to the volume fraction profiles. A remaining challenge is to find similar expressions for thermodynamical properties. Systems with more gradients also represent an open problem here.

C Numerical solver for SCF calculations

ABSTRACT

The numerical method for solving the system of Self-Consistent-Field (SCF) equations as used in this thesis is explained. The method is based on a quasi-Newton algorithm for which a short general mathematical description is given. The implementation details of the method used at our laboratory are described. In some cases a justification for the details is given. Some tricks, mostly resulting from empirical findings during this research, are described that ensure convergence of the equations or speed up convergence by one or two orders of magnitude. We conclude by giving some ideas for improvements of the method.

C.1 Introduction

The equations of the SCF theory described in this thesis have no general analytical solution. To obtain numerically accurate results we have to resort to a numerical method. The equations of the mean-field theory have been written in terms of segment potentials $u(\vec{r})$ and volume fractions $\varphi(\vec{r})$. These two quantities $u(\vec{r})$ and $\varphi(\vec{r})$ should be self-consistent. This means that computing $\varphi(\vec{r})$ from $u(\vec{r})$ or vice-versa should yield the same two distributions. We can write this self-consistency demand in a set of equations with corresponding iteration variables. The self-consistent solution is found when all equations are zero. However, these equations are non-linear and ill-behaved. As there is a wide variety of problems that can be dealt with by a Scheutjens-Fleer like theory, the demands on a numerical routine that solves the equations are high.

Solving a set of equations with an equal amount of variables has been the topic of investigation for decades, although there seems less progress in recent years [94]. Here, we will not try to give an overview of all methods that have been or are currently in use. This appendix is primarily meant to describe the method that is now routinely used at our laboratory. Most of this method is based on mathematical optimisation literature which has been implemented in a computer program by the late Jan Scheutjens, who dedicated much of his work to efficiently solving the SCF equations. Unfortunately, details of the inner workings of his computer program have never been documented.

It should be noted that Jan Scheutjens' program is not dedicated solely to solve SCF equations. Also curve fitting (more unknowns than equations) and function minimisation can be dealt with. Explicit information about first and/or second derivatives can be used. When this information is not available analytically, numerical derivatives are used instead. Furthermore, constrained optimisation can also be dealt with. These generalisations clearly have their merits but will not be discussed here.

The methods described in this appendix were partly found in literature and partly through 'reverse engineering' Jan Scheutjens' computer program. Sec. C.2 outlines the main features of the numerical method used to solve the SCF equations. Sec. C.3 gives the implementation details. It turns out that these details differ considerably from the methods used in standard optimisation texts like Dennis and Schnabel[94]. Often, the literature cited in the source code of Jan Scheutjens' program described methods different from those actually present. Nevertheless, we attempted to give justifications for the numerical methods used in the computer program. Sec. C.4 gives details about solving the SCF equations. In sec. C.5 some tricks are presented that were empirically developed, mostly during this investigation. These tricks deal with common problems or speed up the convergence. This appendix may serve as a starting point for those who would like to improve on the method described here, using more recent optimisation theory. In the last section of this appendix some suggestions for such improvements are given that exploit the special structure of the SCF equations.

C.2 Solving nonlinear equations

Our interest is in finding the solution $\vec{x}^*$ of the following system of equations:

$$g_i(\vec{x}) \equiv g(x_1, x_2, \ldots, x_n) = 0 \qquad i = 1, 2, \ldots n \tag{C.1}$$

In the remainder we will mostly drop the subscript i and use the shorthand notation

$$\vec{g}(\vec{x}) = \vec{0} \tag{C.2}$$

where $\vec{0}$ is a vector with n elements equal to zero. Note that the number of equations is equal to the number of variables. *A priori* we cannot be sure that a solution in real space exists. On the other hand, there could also be more than one solution.

Only Newton and quasi-Newton methods will be discussed. The popular steepest-descent and conjugated gradient methods have their merits, such as a very low computer memory consumption, but they are mostly unsuitable due to slow or no convergence of the highly non-linear SCF equations, especially when a high accuracy is desired.

Dennis and Schnabel[94] prefer to call the method described in sec. C.2.1 'quasi-Newton' and refer to the method of sec. C.2.3 as a secant method. While their arguments are sound, in practice almost no one shares their preference, therefore we have also not used their nomenclature.

C.2.1 Newton's method

Expanding eq. C.2 around a given $\vec{x}_0$ we find

$$\vec{g}(\vec{x}) \approx \vec{g}(\vec{x}_0) + J(\vec{x}_0)(\vec{x} - \vec{x}_0) \tag{C.3}$$

where J is the Jacobian defined by

$$J_{ij} = \frac{\partial g_i}{\partial x_j} \tag{C.4}$$

We equate the expansion of $\vec{g}(\vec{x})$ to $\vec{0}$ and solve it

$$\vec{x}_1 = \vec{x}_0 - J(\vec{x}_0)^{-1}\vec{g}(\vec{x}_0) \tag{C.5}$$

If the inverse of J_0 exists, then the (unique) solution $\vec{x}_1$ exists as well. When the system given by eq. C.2 is a linear combination of $\vec{x}$ then $\vec{x}_1$ is the solution to eq. C.2.

Generally, eq. C.2 is non-linear and we need to iterate

$$\vec{x}_{k+1} = \vec{x}_k - J(\vec{x}_k)^{-1}\vec{g}(\vec{x}_k) \tag{C.6}$$

where k denotes the number of the iteration step. It can be shown that $\lim_{k\to\infty} \vec{x}_k = \vec{x}^*$ when $\vec{x}_0$ is in the neighbourhood of $\vec{x}^*$ and $J(\vec{x}^*)$ is non-singular (see e.g. Dennis and Schnabel [94]). The convergence is quadratic in this case.

In Newton's method either the Jacobian J is explictly calculated when an algebraic form of J is known, or J is approximated by finite differences

$$J_{ij} = \frac{g_i(x_1, \ldots, x_j + \epsilon, \ldots, x_n) - g_i(x_1, \ldots, x_j, \ldots, x_n)}{\epsilon} \tag{C.7}$$

where only the variable x_j is changed by a sufficiently small amount ϵ. With a proper choice of ϵ it can be proven that the quadratic convergence property of Newton's method is retained. In fact, iterations using a numerical Jacobian are virtually indistinguishable from those using an analytical Jacobian [94].

Note that a numerical Jacobian requires n evaluations of the functions $\vec{g}$. Therefore, when an algebraic form of J is not known, it is common to resort to the quasi-Newton method discussed in sec. C.2.3, which requires only one evaluation of $\vec{g}$ for each iteration.

C.2.2 Line-search

As stated in the previous section, if the first guess $\vec{x}_0$ is sufficiently close to the solution $\vec{x}^*$ the Newton method converges. When $\vec{x}_0$ is not in the neighbourhood of $\vec{x}^*$, a number of problems may arise:

- $J(\vec{x}_k)$ may be singular. Solutions to this problem exist (see e.g. Dennis and Schnabel[94]) but they will not be discussed here, except in the context of the quasi-Newton method (sec. C.2.3).

- If we define

$$f(\vec{x}) = |\vec{g}(\vec{x})|^2 \equiv \sum_i^n (g_i(\vec{x}))^2 \tag{C.8}$$

  f_{k+1} may be larger than f_k. This means we are too far away from the solution and the proposed change in $\vec{x}$ is not downhill.

The latter problem can be solved with a line-search. It is useful to define the direction vector $\vec{p}_k$

$$\vec{p}_k = -J_k^{-1}\vec{g}_k \tag{C.9}$$

We can now obtain $\vec{x}_{k+1}$ from

$$\vec{x}_{k+1} = \vec{x}_k + \alpha_k\vec{p}_k \tag{C.10}$$

which reduces to eq. C.6 for $\alpha_k = 1$. An exact line-search minimises $f_{k+1} = f(\vec{x}_k + \alpha_k\vec{p}_k)$ as a function of α_k. Obviously, an exact line-search only pays off in terms of computational demand when the evaluation of $f(\vec{x}_k + \alpha_k\vec{p}_k)$ is relatively inexpensive. Approximate line-searches can therefore be advantageous. We will discuss the approximate line-search routine that we use in sec. C.3.4.

C.2.3 Quasi-Newton method

The biggest disadvantage of the Newton method is that it involves the computation of the Jacobian J (eq. C.4) at each iteration. When no (simple) algebraic form of the Jacobian is present and the function evaluation is computationally very demanding it is more favourable to make use of a quasi-Newton method. In this method an approximation A to the Jacobian is used instead of the 'exact' Jacobian J. The estimate A_k is updated to A_{k+1} using information readily available at iteration step $k+1$.

The update procedure for the Jacobian is based on the following update procedure, proposed by Broyden[95]

$$A_{k+1} = A_k + \frac{(\vec{y}_k - A_k\vec{\delta}_k)\vec{\delta}_k^{\,T}}{|\vec{\delta}_k|^2} \tag{C.11}$$

where

$$\vec{y}_k = \vec{g}_{k+1} - \vec{g}_k \tag{C.12}$$

$$\vec{\delta}_k = \vec{x}_{k+1} - \vec{x}_k = \alpha_k\vec{p}_k \tag{C.13}$$

Broyden's update stems from trying to find the matrix A_{k+1} which satisfies the secant equation

$$A_{k+1}\vec{\delta}_k = \vec{y}_k \tag{C.14}$$

A possible solution for A_{k+1} is

$$A_{k+1,i,j} = \frac{g_{k+1,i} - g_{k,i}}{x_{k+1,j} - x_{k,j}} \tag{C.15}$$

so that A_{k+1} is the secant approximation to the Jacobian. However, eq. C.14 does not have a unique solution, in fact it has many. Broyden's update corresponds to the minimal update to A_k that is needed to let A_{k+1} satisfy eq. C.14. The idea behind this is to retain as much of the information from previous iterations as possible. Note that there is no guarantee that A_k will converge to the true Jacobian even for an infinite number of iterations, in fact it rarely does for nonlinear equations [94].

The estimate A of the Jacobian is not needed directly anywhere in the quasi-Newton scheme, instead an estimate of the *inverse* Jacobian A^{-1} is needed, cf. eq. C.9 for the Newton method:

$$\vec{p}_k = -A_k^{-1}\vec{g}_k \tag{C.16}$$

Inverting a matrix of size $n \times n$ takes order n^3 operations. Therefore it may seem that it is more advantageous to update the inverse directly. An equivalent of eq. C.11 for the estimate of J^{-1} exists [94, 96]. This equivalent takes order n^2 operations. However, factorising A as done below results in an algorithm that is order n^2 as well. Furthermore, A may be ill-conditioned, which is easier to check in the factorised form.

Following a suggestion by Gill et al. [97, 98], the estimate A of the Jacobian is decomposed in the following way:

$$A = LDU \tag{C.17}$$

where L is a lower-triangular matrix with a unit diagonal, D is a diagonal matrix and U is an upper-triangular matrix with a unit diagonal. This means that the solution of $\vec{p}_k$ from the equations

$$L_k D_k U_k \vec{p}_k = -\vec{g}_k \tag{C.18}$$

may be found in order n^2 operations by solving $L\vec{y} = \vec{g}_k$ (forward elimination), $D\vec{z} = \vec{y}$, and $U\vec{p}_k = \vec{z}$ (back substitution). This compares favourable to the order n^3 operations needed for the matrix inversion in eq. C.16 [99]. If A has no special structure, the decomposition in LDU factors requires order n^3 operations. However, this decomposition has to be performed only once. In the subsequent iterations the decomposition only needs an update. Since eq. C.11 is a rank 1 modification of A, the LDU factorisation can be updated in order n^2 operations [97].

The implementation of the update procedure that is actually used in this thesis is more complicated than eq. C.11 and is discussed in sec. C.3.3. Line-searches are typically expensive in SCF calculations. Therefore, the step length α is estimated from previous calculations. This approximate scheme is discussed in sec. C.3.4.

C.3 Details of the algorithm

In the previous section a rough outline was given of the procedure to solve systems of nonlinear equations. In this section we discuss the details of the quasi-Newton method.

C.3.1 The first iterations

The standard initial guess of $\vec{x}_0$ is set to zero, unless the user supplies a different vector. From the initial guess $\vec{x}_0$ the function values $\vec{g}_0$ are computed. The starting value for the estimate A_0 of the Jacobian is the diagonal matrix

$$A_{ii} = 1 + |\vec{g}|^2 \tag{C.19}$$

which is trivially factorised in LDU. The first direction vector $\vec{p}_0$ becomes

$$\vec{p}_0 = -\frac{\vec{g}_0}{1 + |\vec{g}_0|^2} \tag{C.20}$$

which has the same direction as a steepest-descent step where $\vec{p}_0$ equals $-\vec{g}_0/|\vec{g}_0|$. The formulation of eq. C.20 reduces the step $\vec{p}_0$, as compared to the steepest-descent method. We have been unable to find a justification for this method in the literature. However, as will be shown shortly, any drawbacks from a (too) small step size $\vec{p}_0$ are eliminated in the second iteration where the diagonal is scaled prior to the update routine.

From $\vec{p}_0$ the new variables $\vec{x}_1$ are calculated using eq. C.10 with α_0 set to unity. Subsequently, the new function values $\vec{g}_1$ are calculated. Then using the criteria of sec. C.3.4 it is decided whether a line-search is necessary or not. In any case we end up with values for $\vec{x}_1$ and $\vec{g}_1$ and the first iteration is finished. We may now update A_0 to A_1 using the methods described in sec. C.3.3 and compute the new direction vector $\vec{p}_1$. Except for the special starting value for A_0 and the possible reversal of $\vec{p}$ (sec. C.3.2), all subsequent iterations will be performed this way until the stop criterion is met (sec. C.3.5) or the user-defined maximum number of iterations is performed.

For the second iteration we need A_1. However, before updating A_0 to A_1 according to the scheme in sec. C.3.3 we can rescale A_0 by using a weakened variant of eq. C.14, where A_{k+1} is replaced by A_k. We seek $A'_0 = \gamma_0 A_0$ such that

$$\vec{\delta}_0^T A'_0 \vec{\delta}_0 = \vec{\delta}_0^T \vec{y}_0 \tag{C.21}$$

This immediately yields

$$\gamma_0 = \frac{\vec{\delta}_0^T \vec{y}_0}{\vec{\delta}_0^T A_0 \vec{\delta}_0} \tag{C.22}$$

The rescaling of A_0 with γ_0 ensures that the diagonal of A'_0 is of the same order of magnitude as that of J_0. The scaling is not performed when γ_0 turns out to be negative. This would mean that $\vec{\delta}_0^T \vec{y}_0$ is negative since $\vec{\delta}_0^T A_0 \vec{\delta}_0$ is always positive because A_0 is positive definite [99].

The scaling given by eq. C.22 is not only performed on A_0 but also when A is reset during the iterations as described in sec. C.3.2. This rescaling has first been proposed in the context of function minimisation [100]. Here it is used to solve nonlinear equations. Numerical experiments on several SCF problems have shown an overall improvement in convergence when this scaling routine is used.

C.3.2 Reversing the direction vector

As was explained in sec. C.2.3 the estimate A of the Jacobian is available as the factors LDU. Ideally, A is positive definite, then the direction $\vec{p}$ is down-hill, which means that for an infinitesimal small step size α eq. C.8 is decreasing [96]. A positive definite matrix always has a positive determinant, the reverse is not necessarily true. Furthermore, if A is positive definite then all elements of D are positive [99]. The determinants of L and U are unity [101]. Since $\det(A) = \det(L)\det(D)\det(U)$, this means that the determinant of A is equal to the determinant of D, which is trivial to evaluate.

This feature is exploited in the following way. When $\det(A)$ is positive a Newton step is taken. Conversely, when $\det(A)$ is negative, the sign of all elements of $\vec{p}_k$ as computed from eq. C.16 is reversed. If the direction vector has to be reversed for three consecutive iterations, the third Jacobian is reset using eq. C.19 before it is used. Note that a positive determinant of A does not guarantee that A is positive definite.

It is useful to introduce the following definitions

$$\vec{v}_k = -\vec{g}_k \qquad \text{normal step} \tag{C.23a}$$

$$\vec{v}_k = A_k\vec{p}_k \qquad \text{reversed direction} \tag{C.23b}$$

The vector $\vec{v}_k$ will be used as an replacement for $A_k\vec{p}_k$ where appropriate. For a normal step eq. C.16 holds, so $A_k\vec{p}_k = -\vec{g}_k$. However, if the sign of $\vec{p}$ is inverted one would naively say that $\vec{v}_k = \vec{g}_k$. It is unknown why this latter equality is not used in the computer program since this simplification would save order n^2 operations. The reason may be numerical instability. At present it is also unclear why this numerical instability would not be present when the number of negative diagonal elements is, for example, two.

C.3.3 Updating the Jacobian

The update procedure given by eq. C.11 does not guarantee that the new estimate for the Jacobian A_{k+1} can be inverted. Therefore, the following update is used

$$A_{k+1} = A_k + \beta\frac{(\vec{y}_k - \vec{v}_k)\vec{\delta}_k^T}{|\vec{\delta}_k|^2} \tag{C.24}$$

where v_k is defined by eq. C.23. If $(A_{k+1})^{-1}$ does not exist, i.e. when A_{k+1} is singular, the decomposition LDU can also not be performed. To avoid singularity in A_{k+1} Powell[102] suggests to compute

$$\theta_1 = \left|\frac{\vec{\delta}_k^{\,T} J_k^{-1}\vec{y}_k}{|\vec{\delta}_k|}\right| \tag{C.25}$$

If θ_1 smaller than 0.1 then $\beta = 0.8$ is used, otherwise β is set equal to unity. In the case that a normal step was taken (see eq. C.23) eq. C.11 is recovered.

However, we use a slightly different approach here. The following values for β are used

$$
\begin{aligned}
|\gamma_k| &< 0.01 && \text{then} \quad \beta = 0.8 && \text{(C.26a)}\\
0.01 \leq |\gamma_k| &\leq 100 && \text{then} \quad \beta = 1 && \text{(C.26b)}\\
|\gamma_k| &> 100 && \text{then} \quad \beta = \gamma_k/50 && \text{(C.26c)}
\end{aligned}
$$

where γ_k is computed from eq. C.22. So, although the source code of the program refers to Powell [102], different values for β are used.

C.3.4 Trust region and line-search

It would be desirable if each iteration resulted in an improvement towards the solution of the system of equations. This can be accomplished by performing e.g. an exact line search (sec. C.2.2). However, the number of function evaluations needed in the line search iteration is relatively large. The computational cost of the function evaluation in the SCF equations is about as expensive or even more expensive than the generation of a search direction. This means that line-search steps should only be performed as a last resort, when the relative improvement (or worsening) is deemed unacceptable. This is even more so since numerical experience has shown that quasi-Newton methods have very good convergence properties when the step length α is unity as often as possible [94].

Performing a line-search to find an optimal value for α is rather expensive. Therefore, a better procedure is to predict a new value for α from the previous calculation. Of course, such predictions are not always perfect, so we resort to a line-search when this is the case. In this section first the line-search method is described, and then the method to estimate α from previous iterations is described. We have been unable to find literature that describes the following routines, which is not to say that they are undocumented. It is known that within our laboratory at least the values of the various constants have been tuned through trial and error [103].

The normalised inner-product

$$B = \frac{(\vec{g}_{k+1}, \vec{g}_k)}{(\vec{g}_k, \vec{g}_k)} \tag{C.27}$$

will be negative when $\vec{g}$ oscillates around zero. This is good as long as it is not diverging. This divergence is tested by computing

$$C = \frac{(\vec{g}_{k+1}, \vec{g}_{k+1})}{(\vec{g}_k, \vec{g}_k)} = \frac{f_{k+1}}{f_k} \tag{C.28}$$

A large value of C indicates that the iteration step is leading to larger values of f. Note that the exact line-search as described in sec. C.2.2 demands $C < 1$. Here a very liberal criterion is used: only when C exceeds 10 a line-search is always performed. When, on the other hand, B is negative and C does not exceed 2 no line iteration is performed.

For the remaining conditions (e.g. positive B) the following inequality is tested

$$D = 0.4\frac{1 + 0.75 * C}{C - B|B| + 0.1} < 0.35 \tag{C.29}$$

and when it holds a line-search step is performed, when it doesn't hold not no line-search is done. One detail remains: an additional fine-tuning of the above algorithm is performed. If $C - B|B| < 0.2$ and either $B > 1$ or $C > 1$ then C is multiplied by 1.5 prior to testing the criteria of eqs. C.27–C.29.

In each line-search step the step length α_k is divided by 4. The line-search iteration continues until one of the above criteria indicates that no further line-search is needed or the user defined maximum number of line-search iterations is performed.

Apart from explicit line-searches, α_k is adjusted according to information obtained from previous calculations. This is done to prevent the computationally expensive line-search. To this end, $\alpha_{k,\mathrm{bound}}$ gives the first value of α_k that is attempted. The actual step taken can only be smaller due to one or more line searches. The upper bound of α_k is given by

$$\alpha_{k,\mathrm{bound}} = \frac{T_k}{|\vec{p_k}| + \epsilon} \tag{C.30}$$

where ϵ is a tiny number which prevents an overflow if $|\vec{p_k}|$ should ever be (very close to) zero. When α_{bound} exceeds unity it is set equal to unity. The parameter T_k denotes the trust region. Its value is positive and bounded by user input. The user may both specify the minimum and maximum value of T_k. Common values are zero for the minimum and 0.5 for the maximum value. The value of T_0 is equal to the user specified maximum. The value T_k is computed as follows. First it is checked whether the previous value T_{k-1} exceeds $2\alpha_{k-1}|\vec{p_{k-1}}|$, if so then T_{k-1} is set equal to this value. Then the trust region T_k for the current iteration is computed:

$$T_k = T_{k-1} D_{k-1} \frac{\alpha_{k-1}}{\alpha_{k-1,\mathrm{bound}}} \left(\frac{4}{(\gamma_{k-1} - 1)^2 + 1} + 0.5 \right) \tag{C.31}$$

The factor D_{k-1} is computed from eq. C.29 in the previous iteration. However, when a line-search has been performed it is set equal to unity. The step size α_{k-1} only differs from $\alpha_{k-1,\mathrm{bound}}$ when one or more line-search steps have been taken in the previous iteration. The value for γ_{k-1} is computed from eq. C.22. The term in between brackets ensures that T_k is increased when the weak secant eq. C.21 is (approximately) obeyed, since then γ_{k-1} will be about unity. When eq. C.21 is seriously violated T_k is small.

In practice, these criteria lead to very few iterations in which a line-search is performed. It is quite common to not encounter any line-search at all when solving

SCF equations. When a line-search is performed it is rarely seen that two line-search steps are needed. This observation is exploited by the algorithm to do an additional check. Before performing the 4th line search step, the function values of $\vec{g_k}$ are recomputed using $\vec{x_k}$. Then the new computation of $\vec{g_k}$ is compared to the result obtained from the previous calculation. Of course, the results should be exactly identical, even the rounding errors should be equal. If this is not the case the user is warned that the functions are time dependent. This means that the molecular fields do not unambiguously result in volume fractions, which indicates a programming error in the SCF equations.

C.3.5 Stop criterion

One could stop the iterations when eq. C.8 results in less than some user-supplied value, say 10^{-7}. However, in practice the following equation is used

$$f = \sqrt{\frac{|\vec{p}_k||\vec{g}_k|}{1 + |\vec{x}_k|}} \qquad \text{(C.32)}$$

This form was shown to work well in numerical experiments performed in our group, most notably in the area of function minimalisation or curve fitting [103]. However, we are not aware of any theoretical justification for it.

C.4 Solving self-consistent-field equations

A solution to the self-consistent-field equations corresponds to a local extremum of the ‘free energy’. Note that we use the term ‘free energy’ loosely here: the thermodynamical quantity that actually needs to be minimised depends on the problem at hand. It could be, for example, the Helmholtz energy for a closed system, or the surface tension for an open system.

Note, however, that some boundary conditions have to be taken in to account. Firstly, the volume in each layer needs to be filled up with segments. Other boundary conditions may be that the total adsorbed amount of polymer is fixed, or even that some volume fraction profiles have a fixed value. Whatever boundary conditions are used, we are interested in the minimum of the free energy. As far as we know, no equation has been derived that gives a measure for the ‘free energy’ when the SCF solution is not reached yet. Therefore, function minimisation cannot be used for the SCF theory.

C.4.1 Uncharged copolymers

First, the SCF equations of uncharged copolymers are given. The modifications needed for charged multistate systems are given in sec. C.4.2. From the equilibrium theory it follows that the 'volume-filling' potential (or Lagrange multiplier) $u'(\vec{r})$ is independent of the segment type. This is the basis of the equations used for finding the SCF solution. The elements of the potential fields $u_A(\vec{r})$, which *do* depend on the segment type are used as the iteration variables. From this estimate of $u_A(\vec{r})$ the volume fractions $\varphi_A(\vec{r})$ are computed, using the equations described in sec. 2.2.4. With these volume fractions we can compute a kind of segment-type dependent volume-filling potential $\beta_A(\vec{r})$.

$$\beta_A(\vec{r}) = u_A(\vec{r}) - \sum_B \chi_{AB} \left(\frac{\langle \varphi_B(\vec{r}) \rangle}{\sum_B \varphi_B(\vec{r})} - \varphi_B^b \right) \tag{C.33}$$

The division by $\sum_B \varphi_B(\vec{r})$ damps the influence of fluctuations in $\varphi_B(\vec{r})$ during the iteration, when the boundary condition $\sum_B \varphi_B(\vec{r}) = 1$ is not yet satisfied. This division leads to a more stable iteration and generally a faster convergence [22].

We iterate until all $\beta_A(\vec{r})$ are independent of the segment type A and the volume is completely filled, $\sum_B \varphi_B(\vec{r}) = 1$. The functions $g_A(\vec{r})$ are zero when the SCF solution is found, where $g_A(\vec{r})$ is defined by

$$g_A(\vec{r}) = \beta_A(\vec{r}) - \frac{\sum_A \beta_A(\vec{r})}{\sum_A 1} - 1 + \frac{1}{\sum_A \varphi_A(\vec{r})} \tag{C.34}$$

A large number of alternatives have been proposed in the past for this equation [6, 22]. However, we are not aware of a general way to predict the convergence behaviour of a particular alternative. One has to resort to empirical findings of the type mentioned below eq. C.33. Alternatives to eq. C.34 have been constructed by trail and error. In general, the proposed alternatives are more complex and only give a marginal speed-up of convergence for specialised problems. Therefore we will not discuss these methods and merely conclude that the above equations have passed the test of time.

C.4.2 Charged multistate copolymers

Several modifications to the above scheme need to be made to apply it to the SCF equations described in chapter 2. Firstly, the potentials are no longer dependent on the segment type but on the type of state. Furthermore, the effects of charge and polarisation need to be taken into account. The generalisation of eq. C.33 reads

$$\begin{aligned}\beta_{Ak}(\vec{r}) = u_{Ak}(\vec{r}) - \sum_{Bl} \chi_{Ak,Bl} \left(\frac{\langle \varphi_{Bl}(\vec{r}) \rangle}{\sum_{Bl} \varphi_{Bl}(\vec{r})} - \varphi_{Bl}^b \right) \\ - v_{Ak} e \frac{\Psi(\vec{r})}{k_B T} + \frac{1}{2} \epsilon_0 (\epsilon_{r,Ak} - 1) \frac{P(\vec{r})}{k_B T}\end{aligned} \tag{C.35}$$

which follows from eq. 2.83, when $\beta(z) - \beta^b$ is set equal to $\beta_{Ak}(\vec{r})$. Instead of using the state potentials $u_{Ak}(\vec{r})$ as iteration variables, the iteration variables for the different states are defined by

$$x_{Ak}(\vec{r}) = u_{Ak}(\vec{r}) - v_{Ak} e \frac{\Psi(\vec{r})}{k_B T} + \frac{1}{2} \epsilon_0 (\epsilon_{r,Ak} - 1) \frac{P(\vec{r})}{k_B T} \tag{C.36}$$

The electric potential $\Psi(\vec{r})$ and the vector associated with the polarisation $P(\vec{r})$ are iteration variables as well. This enables us to use the same iteration variables $x_{Ak}(\vec{r})$ for states that only differ in valence (v_{Ak}) or relative dielectric constant ($\epsilon_{r,Ak}$), a common situation.

Eq. C.34 also needs to be modified. Instead of one type of equation, we use three different equations:

$$g_{Ak}(\vec{r}) = \beta_{Ak}(\vec{r}) - \frac{\sum_{Ak}\beta_{Ak}(\vec{r})}{\sum_{Ak}1} - 1 + \frac{1}{\sum_{Ak}\varphi_{Ak}(\vec{r})} \tag{C.37a}$$

$$g_{\Psi}(\vec{r}) = \Psi(\vec{r}) - \widetilde{\Psi}(\vec{r}) \tag{C.37b}$$

$$g_P(\vec{r}) = P(\vec{r}) - \widetilde{P}(\vec{r}) \tag{C.37c}$$

where the first equation is a straightforward generalisation of eq. C.34 and the latter two are new. When these latter two are zero, the electro-static interactions are self-consistent. $\widetilde{\Psi}(\vec{r})$ is calculated from the Poisson equation, as described in detail in ref. [41]. For a given set of iteration variables the volume fractions $\varphi_{Ak}(\vec{r})$ are calculated. Then we calculate the charge density from eq. 2.43 and use the discrete variant of the Poisson equation to calculate $\widetilde{\Psi}(r_i)$ for a given coordinate r_i from the charge density at r_i and the potentials Ψ in the adjacent layers.

A similar procedure is followed to calculate $\widetilde{P}(\vec{r})$. Once the volume fractions φ_{Ak} are calculated we can compute the average dielectric permittivity $\epsilon_r(\vec{r})$ using eq. 2.39. Then $\widetilde{P}(\vec{r})$ is calculated from eqs. 2.62, 2.68, or 2.73.

C.5 Speeding up convergence of SCF equations

In this section some tricks are described that may help finding a solution to the SCF equations. The ideas given here are not justified by a mathematical proof, rather they are the result of empirical findings. Some tricks are necessary to get convergence. Others merely speed up the process, sometimes by as much as two orders of magnitude.

C.5.1 Homogeneous solutions

The procedure described in sec. C.4 is suitable to find a (sometimes local) minimum of the 'free energy'. When the iteration is started in a local maximum of the 'free energy', the routine will also claim to have found a solution. This is mostly notable when computing separating phases. If all the fields $u_A(z)$ are zero in the initial guess $\vec{x}_0$, this results in a homogeneous phase, which is the maximum of the 'free energy'. The way around this is to use a different starting condition. Preferably, one that is close to the real solution of the SCF equations. The method of sec. C.4 does not walk 'up-hill', so even a relatively small distortion from the homogeneous solution results in phase separation.

C.5.2 Initial guess

Several problems encountered regularly in practice do not converge to a solution, especially so when the solution $\vec{x}^*$ differs largely from the initial guess $\vec{x}_0$. This is often the case when large positive values for χ_{AB} are used. These values lead to phase separation or to high adsorption with $\vec{x}^*$ significantly different from zero. The solution is as simple as effective: first a calculation is done with lower values for χ_{AB} then this solution is used as the initial guess for the original problem, with the higher χ_{AB}

C.5.3 Local minima

It is sometimes encountered that the SCF solution depends on the initial guess. This means that the quasi-Newton routine has converged to a local minimum of the 'free energy', starting from at least one of the initial guesses. This situation is not easy to detect, even by experienced users, so automating the detection seems pretty hopeless. However, once the two (or more) local minima are determined we may inspect the computed value for the partition function relevant for the system. The solution which has the smallest 'free energy' is then identified as the global minimum. A similar situation is present in chapter 4 where vesicles are computed. Here several solutions to the SCF equations are explored to find an artefact free point which corresponds to the minimum in the 'free energy'.

C.5.4 Small step sizes

The trust region approach described in sec. C.3.4 may result in a step size that is relatively small. When the step size is (very) small for many iterations the direction in which the variables are changed is usually wrong. This may even lead to a step size that is decreasing at each iteration so that the variables $\vec{x}$ effectively do not change any more. For example: we have encountered SCF problems that lead to a step size $\alpha < 10^{-10}$ for over 100 consecutive iterations. As can be seen from eq. C.11, a small step size does not lead to a significant change in the Jacobian. It proved helpful to reset the matrix using eq. C.19 as soon as $\alpha < 10^{-5}$ for 50 consecutive iterations.

C.5.5 Mixing the Newton and quasi-Newton method

The big advantage of the quasi-Newton method over the Newton method is that we do not need to evaluate J using eq. C.7. Computing eq. C.7 takes n function evaluations for each iteration in the Newton method. In contrast, in the quasi-Newton method each iteration takes only one function evaluation (except in the case of a line-search). The evaluation of the SCF equations C.34 generally is computationally demanding: a typical function evaluation takes order n^2 operations.

When $\vec{x}$ is sufficiently close to the solution $\vec{x}^*$, it can be proven that Newton's method converges quadratically. It turned out to be favourable to do one Newton step sufficiently 'near' the solution, to obtain a very good estimate of the Jacobian J. After this one step, the quasi-Newton method continues. The remaining (small) differences in J will be ironed out by the update procedure [94]. In a typical application the quasi-Newton method is used until $f < 0.1$, followed by one Newton step. After this convergence is usually reached within 10 iterations, even for problems where the number n of iteration variables exceeds 10^3.

The above procedure is not suitable for an arbitrary type of problem. Obviously, when the number of iterations in the quasi-Newton method is smaller than the number of iteration variables n, which luckily is often the case, the method does not pay off. This is due to the fact that one Newton step requires n function evaluations.

The problems that are most suitable to employ the above procedure can be subdivided in three classes. The first typically features high potential fields of a relatively long range, like for example found in weak polyelectrolyte brushes with a low salt concentration. Another class of problems are those that require a high accuracy of the solution, where the relative error in the computed potential fields and volume fraction profiles should be $O(10^{-9})$ or less. Adding more and more precision during the calculation might take a lot of iterations in the quasi-Newton procedure. One full Newton step may speed up the calculations by an order of magnitude. The type of problems where our method has proven to be the most successful is described in sec. C.5.6.

C.5.6 Re-using the Jacobian

In most practical applications of the SCF theory one is interested in a series of computations that compute the dependence of a certain result on a given parameter. For example the height of a brush as a function of the grafting density. When varying the control parameter only slightly it proved useful to re-use the Jacobian as was obtained in the previous calculation. Especially when this former Jacobian was computed explicitly with a full Newton step, the observed speed-up of convergence of the new calculation is one or (often) two orders of magnitude. When re-using the Jacobian, we should not perform the scaling of the diagonal elements of the Jacobian given by eq. C.22.

C.5.7 Reverse directions

One may encounter series of iterations in which the direction vector is reversed for one iteration and subsequently accepted for the next iteration and again reversed for the iteration following it. Once we have three reversals of direction in a row, the Jacobian is reset. However, when a series of iterations arise as described, convergence is usually extremely slow. It was found that resetting the Jacobian after about 50 iterations which contain 40% or more reversals of direction speeded up convergence.

C.6 Possible future improvements

In this appendix, we have discussed a rather general solver which is routinely applied to the special case of SCF equations. The solver has been optimised carefully to minimise the number of function evaluations. This general solver is useful since the SCF theory is not static. New molecular fields are regularly introduced in the theory and testing these variants of the theory then 'only' requires the introduction of new variants of the SCF equations. The reader experienced in SCF methods will immediately recognize the irony in the previous sentence: the construction of new functions which show good convergence behaviour is far from trivial and almost no general guidelines seem to be available.

However, a great deal of the SCF theory has matured. It is expected that convergence of this subclass of SCF equations would benefit from inserting information from the theory directly into the numerical method.

The solver discussed here is very suitable to solve SCF problems with only one spatial gradient in the molecular fields and volume fractions. In this case, the storage requirement needed to store the Jacobian is less than the memory requirement to store the end-segment weighting factors, needed to compute the volume fractions. As soon as the memory reduction method of sec. A.4 is used this is no longer the case. When we turn to computations using two gradients in the volume fractions, the memory requirement of the of the computations is dominated by the storage of the Jacobian. For example, if we have A different segments in a system with M^2 different spatial coordinates then the storage of the Jacobian requires A^2M^4 floating point numbers. Values for M of order 100 are usually desired and any non-trivial computation will have a number of different segments A amounting to 3, so that the Jacobian has order 10^9 floating point numbers. While it is certainly possible to store a Jacobian which is slightly smaller on modern hardware, it should be clear that a generalisation towards three gradients in volume fractions is out of the question using Newton's method directly.

A solution to this problem actually exists for the special case of homopolymer adsorption onto a solid wall using only one gradient. The computer program `polad` [85], does not store the full Jacobian. Instead, a band-diagonal estimate of the Jacobian is computed directly using an approximate partition function. The convergence of this algorithm is very fast, especially compared to solving the same problem with the more general method described in this appendix.

Another method to solve the SCF equations would be to minimise the Helmholtz energy in a closed system. One of the immediate advantages would be the use of a (symmetrical) Hessian instead of a Jacobian, resulting in less memory consumption. As far as we know, no attempt has been made to pursue this route in SCF theory. One would need a measure for the 'free energy' when the SCF solution is not reached yet, which is not available as far as we are aware.

A related method, used for quantum-chemical density functional theory calculations, uses perturbation theory to find an approximation of the Hessian times $\vec{p}$ [104]. This means that the Hessian itself is never evaluated. It could be that a similar approach can be used for the SCF equations. This may result in a speed-up of convergence but, more importantly, this method could avoid the necessity of storing the estimate of the Jacobian.

Bibliography

[1] P. W. Atkins. *Energie en entropie. De tweede hoofdwet van de thermodynamica.* Natuur en Techniek, Maastricht/Brussel, 1988. Translated from English.

[2] R. P. Feynman, R. B. Leighton, and M. Sands. *The Feynman Lectures on Physics*, volume 1. Addinson-Wesley Publishing Company, Reading, Massachusetts, first edition, 1964.

[3] T. L. Hill. *An introduction to statistical thermodynamics.* Addison Wesley, Reading, Massachhusetts, 1960.

[4] D. C. Rapaport. *The Art of Molecular Dynamics Simululations.* Cambridge University Press, Cambridge, first edition, 1995.

[5] P. J. HoogerBrugge and J. M. V. A. Koelman. Simulating microscopic hydrodynamic phenomena with dissipative particle dynamics. *Europhys. Lett.*, 19: 155–160, 1992.

[6] J. M. H. M. Scheutjens and G. J. Fleer. Statistical theory of the adsorption of interacting chain molecules. 1. Partition function, segment density distribution, and adsorption isotherms. *J. Phys. Chem.*, 83:1619–1635, 1979.

[7] S. F. Edwards. The statistical mechanics of polymers with excluded volume. *Proc. Phys. Soc.*, 85:613–624, 1965.

[8] E. Helfand and Y. Tagami. Theory of the interface between immiscible polymers. II. *J. Chem. Phys.*, 56:3592–3601, 1972.

[9] E. A. DiMarzio and R. J. Rubin. Adsorption of a chain polymer between two plates. *J. Chem. Phys.*, 55:4318–4336, 1971.

[10] J. G. E. M. Fraaije. Dynamic density-functional theory for microphase separation kinetics of block-copolymer melts. *J. Chem. Phys.*, 99:9202–9212, 1993.

[11] G. H. Fredrickson, V. Ganesan, and F. Drolet. Field-theoretic computer simulation methods for polymers and complex fluids. *Macromolecules*, 35:16–39, 2002.

[12] P.-G. de Gennes. *Scaling Concepts in Polymer Physics.* Cornell University Press, first edition, 1979.

[13] A. Ben-Shaul, I. Szleifer, and W. M. Gelbart. Chain organization and thermodynamics in micelles and bilayers. I. Theory. *J. Chem. Phys.*, 83:3597–3611, 1985.

[14] M. A. Carignano and I. Szleifer. On the structure and pressure of tethered polymer layers in good solvent. *Macromolecules*, 28:3197–3204, 1995.

[15] M. A. Carignano and I. Szleifer. Pressure isotherms, phase transition, instability, and structure of tethered polymers in good, θ, and poor solvents. *J. Chem. Phys.*, 100:3210–3223, 1994.

[16] J. van Male. sfbox, 2000. Computer program.

[17] F. Clement and J.-F. Joanny. Curvature elasticity of an adsorbed polymer layer. *J. Phys. II France*, 7:973–980, 1997.

[18] S. P. F. M. Roefs, J. M. H. M. Scheutjens, and F. A. M. Leermakers. Adsorption theory for polydisperse polymers. *Macromolecules*, 27:4810–4816, 1994.

[19] M. Hara, editor. *Polyelectrolytes*. Marcel Dekker, New York, 1993.

[20] M. A. Carignano and I. Szleifer. Statistical thermodynamic theory of grafted polymeric layers. *J. Chem. Phys.*, 98:5006–5018, 1992.

[21] E. Helfand and Z. R. Wasserman. Block copolymer theory. 4. Narrow interphase approximation. *Macromolecules*, 9:879–888, 1976.

[22] O. A. Evers, J. M. H. M. Scheutjens, and G. J. Fleer. Statistical thermodynamics of block copolymer adsorption. 1. Formulation of the model and results for the adsorbed layer structure. *Macromolecules*, 23:5221–5233, 1990.

[23] F. A. M. Leermakers and J. M. H. M. Scheutjens. Statistical thermodynamics of association colloids. I. Lipid bilayer membranes. *J. Chem. Phys.*, 89:3264–3274, 1988.

[24] F. A. M. Leermakers and J. M. H. M. Scheutjens. Statistical thermodynamics of association colloids. V. Critical micelle concentration, micellar size and shape. *J. Colloid Interface Sci.*, 136:231–241, 1990.

[25] F. A. M. Leermakers and J. M. H. M. Scheutjens. Statistical thermodynamics of association colloids. II. Lipid vesicles. *J. Chem. Phys.*, 93:7417–7426, 1989.

[26] F. A. M. Leermakers and J. M. H. M. Scheutjens. Statistical thermodynamics of association colloids. III. The gel to liquid phase transition of lipid bilayer membranes. *J. Chem. Phys.*, 89:6912–6924, 1988.

[27] P. Linse and M. Björling. Lattice theory for multicomponent mixtures of copolymers with internal degrees of freedom in heterogeneous systems. *Macromolecules*, 24:6700–6711, 1991.

[28] R. Israëls, F. A. M. Leermakers, and G. J. Fleer. On the theory of grafted weak polyacids. *Macromolecules*, 27:3087–3093, 1994.

[29] A. Vincze, G. Horvai, and F. A. M. Leermakers. Multistate self-consistent field theory for the calculation of the interface of two imiscible electrolyte solutions. *J. Phys. Chem*, 100:8946–8953, 1996.

[30] A.-C. Shi and J. Noolandi. Theory of inhomogeneous weakly charged polyelectrolytes. *Macromol. Theory Simul.*, 8:214–229, 1999.

[31] K. M. Hong and J. Noolandi. Theory of inhomogeneous multicomponent polymer systems. *Macromolecules*, 14:727–736, 1981.

[32] C. J. F. Böttcher, O. C. van Belle, P. Bordewijk, and A. Rip. *Theory of Electric Polarization*, volume 1. Elsevier Scientific Publishing Company, second edition, 1973.

[33] M. R. Böhmer, O. A. Evers, and J. M. H. M. Scheutjens. Weak polyelectrolytes between two surfaces: adsorption and stabilization. *Macromolecules*, 23:2288, 1990.

[34] M. Borkovec, B. Jönsson, and G. J. M. Koper. Ionization processes and proton binding in polyprotic systems: Small molecules, proteins, interfaces and polyelectrolytes. *Surface and Colloid Science*, 16:99–339, 2001.

[35] N. M. Maurits, P. Altevogt, O. A. Evers, and J. G. E. M. Fraaije. Simple numerical quadrature rules for gaussian chain polymer density functional calculations in 3d and inplementation on parallel platforms. *Comp. Pol. Sci.*, 6: 1–8, 1996.

[36] H. Fröhlich. *Theory of Dielectrics.* Clarendon Press, Oxford, second edition, 1958.

[37] I. C. Sanchez and R. H. Lacombe. Statistical thermodynamics of polymer solutions. *Macromolecules*, 11:1145, 1978.

[38] D. N. Theodorou. Variable-density model of polymer melt surfaces: structure and surface tension. *Macromolecules*, 22:4578–4589, 1989.

[39] S. M. Oversteegen, P. A. Barneveld, F. A. M. Leermakers, and J. Lyklema. On the pressure in mean-field lattice models. *Langmuir*, 15:8609–8617, 1999.

[40] R. Israëls, J. M. H. M. Scheutjens, and G. J. Fleer. Adsorption of ionic diblock copolymers: self-consistent-field predictions and scaling analysis. *Macromolecules*, 26:5404–5413, 1993.

[41] P. A. Barneveld, D. E. Hesselink, F. A. M. Leermakers, J. Lyklema, and J. M. H. M. Scheutjens. Bending moduli and spontaneous curvature. II. Bilayers and monolayers of pure and mixed ionic surfactants. *Langmuir*, 10:1084–1092, 1994.

[42] P. N. Hurter, J. M. H. M. Scheutjens, and T. A. Hatton. Molecular modeling of micelle formation and solubilisation in block copolymer micelles. 2. Lattice theory for monomers with internal degrees of freedom. *Macromolecules*, 26: 5030–5040, 1993.

[43] G. J. Fleer, J. M. H. M. Scheutjens, M. A. Cohen Stuart, T. Cosgrove, and B. Vincent. *Polymers at interfaces.* Chapman and Hall, London, 1998.

[44] C. C. van der Linden. *Polymer Adsorption Theory: Universal Aspects and Intricacies.* PhD thesis, Wageningen Agricultural University, 1995.

[45] N. A. M. Besseling and M. A. Cohen Stuart. Self-consistent field theory for the nucleation of micelles. *J. Phys. Chem.*, 110:5432–5436, 1999.

[46] R. P. Feynman, R. B. Leighton, and M. Sands. *The Feynman Lectures on Physics*, volume 2. Addinson-Wesley Publishing Company, Reading, Massachusetts, first edition, 1964.

[47] E. P. K. Currie, F. A. M. Leermakers, M. A. Cohen Stuart, and G. J. Fleer. Grafted adsorbing polymers: scaling behaviour and phase transitions. *Macromolecules*, 32:487–498, 1999.

[48] J. Lyklema. *Fundamentals of Interface and Colloid Science, Volume I: Fundamentals.* Academic press, London, first edition, 1991.

[49] W. H. Press, S. A. Teukolsky, W. T. Vetterling, and B. P. Flannery. *Numerical Recipes in C, the art of scientific computing.* Cambridge university press, Cambridge, Australia, second edition, 1992.

[50] J. Klein Wolterink, F. A. M. Leermakers, G. J. Fleer, L. K. Koopal, E. B. Zhulina, and O. V. Borisov. Screening in solutions of star-branched polyelectrolytes. *Macromolecules*, 32:2365–2377, 1999.

[51] P.-G. de Gennes. Interactions between polymers and surfactants. *J. Phys. Chem.*, 94:8407–8413, 1990.

[52] C. G. Brooks, C. M. Marques, and M. E. Cates. Role of adsorbed polymer in bilayer elasticity. *Europhys. Lett.*, 14:713–718, 1991.

[53] W. Helfrich. Elastic properties of lipid bilayers: theory and possible experiments. *Z. Naturforsch*, 28c:693–703, 1973.

[54] R. C. Tolman. The effect of droplet size on surface tension. *J. Chem. Phys.*, 17:333–337, 1949.

[55] S. M. Oversteegen and E. M. Blokhuis. Rigidity constants from mean-field models. *J. Chem. Phys.*, 112:2980–2986, 2000.

[56] S. M. Oversteegen, P. A. Barneveld, J. van Male, F. A. M. Leermakers, and J. Lyklema. Thermodynamic derivation of mechanical expressions for interfacial parameters. *Phys. Chem. Chem. Phys.*, 1:4987–4994, 1999.

[57] C. L. Murphy. *Thermodynamics of Low Tensions and Highly Curved Interfaces.* PhD thesis, University of Minnesota, Minneapolis, USA, 1966.

[58] V. S. Markin, M. M. Kozlov, and S. L. Leikin. Definition of surface tension at a non-spherical interface. *J. Chem. Soc. Faraday Trans. 2*, 84:1149–1162, 1988.

[59] J. M. H. M. Scheutjens and G. J. Fleer. Statistical theory of the adsorption of interacting chain molecules. 2. Train, loop, and tail size distribution. *J. Phys. Chem.*, 84:178–190, 1980.

[60] G. J. Fleer, J. van Male, and A. Johner. Analytical approximations to the Scheutjens-Fleer theory for polymer adsorption from dilute solution. 1. Trains, loops, and tails in terms of two parameters: the proximal and distal lenghts. *Macromolecules*, 32:825–844, 1999.

[61] A. Gorbunov, A. M. Skvortsov, J. van Male, and G. J. Fleer. Mapping of continuum and lattice models for describing the adsorption of an ideal chain anchored to a planar surface. *J. Chem. Phys.*, 114:5366–5375, 2001.

[62] W. M. Gelbart, A. Ben-Shaul, and D. Roux. *Micelles, Membranes, Microemulsions, and Monolayers.* Springer-Verlag, New York, 1994.

[63] S. A. Safran. *Statistical thermodynamics of surfaces, interfaces, and membranes.* Addison-Wesley, 1994.

[64] S. M. Oversteegen and F. A. M. Leermakers. Thermodynamics and mechanics of bilayer membranes. *Phys. Rev. E*, 62:8453–8461, 2000.

[65] F. A. M. Leermakers. unpublished results.

[66] H. N. W. Lekkerkerker. The electric contribution to the curvature elastic-moduli of charged fluid interfaces. *Physica A*, 167:384–394, 1990.

[67] H. N. W. Lekkerkerker. Contribution of the electric double-layer to the curvature elasticity of charged amphiphilic monolayers. *Physica A*, 159:319–328, 1989.

[68] C. Hiergeist and R. Lipowsky. Elastic properties of polymer-decorated membranes. *J. Phys. II France*, 6:1465–1481, 1996.

[69] J. de Joannis, R. K. Ballamudi, C. W. Park, J. Thomatos, and I. A. Bitsanis. Scaling of homopolymers next to adsorbing surfaces: A monte carlo study. *Europhys. Lett.*, 17:69–77, 2001.

[70] A. N. Semenov, J. Bonet-Avalos, A. Johner, and J-F. Joanny. Adsorption of polymer solutions onto a flat surface. *Macromolecules*, 29:2179–2196, 1996.

[71] A. N. Semenov and J.-F. Joanny. Structure of adsorbed polymer layers - loops and tails. *Europhys Lett.*, 29:279–284, 1995.

[72] M. A. Cohen Stuart. In F. M. S. El-Aasser, editor, *Future directions in polymer colloids*, volume E138 of *NATO Advanced Study Institute Series.* Dordrecht, the Netherlands, 1987.

[73] C. C. van der Linden and F. A. M. Leermakers. On the self-similar structure of adsorbed polymer layers: the dependence of the density profile on molecular weight and solution concentration. *Macromolecules*, 25:3449–3453, 1992.

[74] J. des Cloizeaux and G. Jannink. *Polymers in Solution.* Clarendon Press, Oxford, 1990.

[75] P. J. Flory. *Principles of polymer chemistry.* Cornell University Press, Ithaca, N. Y., 1953.

[76] M. Doi and S. F. Edwards. *The Theory of Polymer Dynamics.* Clarendon Press, Oxford, 1986.

[77] K. Binder. *Monte Carlo and Molecular Dynamics Simulations in Polymer Science.* Oxford University Press, New York, 1995.

[78] A. Yu. Grosberg and A. R. Khokhlov. *Statistical Physics of Macromolecules.* AIP Press, 1994.

[79] M. Daoud, J. P. Cotton, B. Farnoux, G. Jannink, G. Sarma, H. Benoit, R. Duplessix, C. Picot, and P. G. de Gennes. *Macromolecules*, 8:804, 1975.

[80] J. van der Gucht, N. A. M. Besseling, J. van Male, and M. A. Cohen Stuart. Coil size oscillatory packing in polymer solutions near a surface. *J. Chem. Phys.*, 113:2886–2893, 2000.

[81] E. Helfand. Block copolymer theory. III. Statistical mechanics of the microdomain structure. *Macromolecules*, 8:552–556, 1975.

[82] R. Israels, D. Jasnow, A. C. Balazs, L. Guo, G. Krausch, J. Sokolov, and M. Rafailovich. Compatibilizing A/B blends with AB diblock copolymeres: Effect of copolymer molecular weight. *J. Chem. Phys.*, 102:8149–8157, 1995.

[83] C. M. Wijmans, J. M. H. M. Scheutjens, and E. B. Zhulina. Self-consistent field theories for polymer brushes. *Macromolecules*, 25:2657–2665, 1992.

[84] R. Israëls. copel, 1994. Computer program.

[85] J. M. H. M. Scheutjens. polad, 1988. Computer program, available on request.

[86] A. Johner, J. Bonet-Avalos, C. C. van der Linden, A. N. Semenov, and J.-F. Joanny. Adsorption of neutral polymers: Interpretation of the numerical self-consistent field results. *Macromolecules*, 29:3629–3638, 1996.

[87] A. A. Mercurieva, F. A. M. Leermakers, T. M. Birshtein, G. J. Fleer, and E. B. Zhulina. Amphiphilic brush in a mixture of incompatible liquids. numerical self-consistent-field calculations. *Macromolecules*, 33:1072–1081, 2000.

[88] F. A. M. Leermakers, J. M. H. M. Scheutjens, and J. Lyklema. Statistical thermodynamics of association colloids. IV. Inhomogeneous membrane systems. *Biochim. Biophys. Acta*, 1024:139–151, 1990.

[89] P. A. Barneveld, J. M. H. M. Scheutjens, and J. Lyklema. Bending moduli and spontaneous curvature. I. Bilayers and monolayers of pure and mixed nonionic surfactants. *Langmuir*, 8:3122–3130, 1992.

[90] J. G. E. M. Fraaije, B. A. C. van Vlimmeren, N. M. Maurits, M. Postma, O. A. Evers, C. Hoffmann, P. Altevogt, and G. Goldbeck-Wood. The dynamic mean-field density functional method and its applications to the mesoscopic dynamics of quenched block copolymer melts. *J. Phys. Chem.*, 106:4260–4269, 1997.

[91] A. Johner, J.-F. Joanny, and M. Rubinstein. Chain statistics in adsorbed polymer solutions. *Europhys. Lett.*, 22:591–596, 1993.

[92] L. A. Meijer, F. A. M. Leermakers, and J. Lyklema. Modelling the interactions between phospholipid bilayers membranes with and without additives. *J. Phys. Chem.*, 99:17282–17293, 1995.

[93] L. A. Meijer, F. A. M. Leermakers, and J. Lyklema. Self-consistent-field modeling of complex molecules with united atom detail in inhomogeneous systems. Cyclic and branched foreign molecules in dimyristoylphosphatidylcholine membranes. *J. Chem. Phys.*, 110:6560–6579, 1999.

[94] J. E. Dennis, Jr. and R. B. Schnabel. *Numerical methods for unconstrained optimization and nonlinear equations*. the Society for Industrial and Applied Mathematics, first edition, 1996.

[95] C. G. Broyden. A class of methods for solving nonlinear simultaneous equations. *Math. Comp.*, 19:577–593, 1965.

[96] M. J. D. Powell. A hybrid method for nonlinear equations. In P. Rabinowitz, editor, *Numerical methods for nonlinear algebraic equations*, chapter 6, pages 87–114. Gordon and Breach science publishers, London, 1970.

[97] P. E. Gill, W. Murray, and M. A. Saunders. Methods for computing and modifying the LDV factors of a matrix. *Math. Comp.*, 29:1051–1077, 1975.

[98] P. E. Gill and W. Murray. Modification of matrix factorizations after a rank-one change. In D. Jacobs, editor, *The State of the Art in Numerical Analysis*, chapter 2, pages 55–83. Academic Press, first edition, 1977.

[99] G. H. Golub and C. F. Van Loan. *Matrix Computations.* The Johns Hopkins University Press, Baltimore and London, second edition, 1989.

[100] D. F. Shanno and K. H. Phua. Matrix conditioning and nolinear optimization. *Math. Prog.*, 14:149–160, 1978.

[101] R. Bronson. *Linear Algebra: an introduction.* Academic Press, London, 1995.

[102] M. J. D. Powell. A FORTRAN subroutine for solving systems of nonlinear algebraic equations. In P. Rabinowitz, editor, *Numerical methods for nonlinear algebraic equations*, chapter 7, pages 115–162. Gordon and Breach science publishers, London, 1970.

[103] F. A. M. Leermakers. personal communication, 2002.

[104] F. Filippone, S. Meloni, and M. Parrinello. A novel implicit Newton-Raphson geometry optimization method for density functional theory calculations. *J. Chem. Phys.*, 115:636–642, 2001.

Summary

This thesis deals with several aspects of the self-consistent-field (SCF) theory for chain molecules. The SCF theory can calculate the equilibrium density distribution of chain molecules in inhomogeneous system at a mean-field level. The treatment is restricted to molecules in the liquid phase. The chains are in solution, in a melt, or near solid or liquid interfaces.

Chapter 2 serves as a review of the SCF method: it gives a detailed derivation of quantities used in the remainder of this thesis. A statistical thermodynamical analysis, starting from the partition function, leads to expressions for the spatial distribution of the molecules and several thermodynamical quantities: the surface tension, the Helmholtz energy, and the chemical potentials of the molecules.

Additionally, the Scheutjens-Fleer formalism is extended to chain segments with multiple states. The different states of segments are related to each other by reaction equilibria. This work is a generalisation of the multistate theory of Linse and Björling [27], who considered polymer segments that may have one or more internal states. In this thesis an explicit coupling between the internal states of different segments is made. This coupling is expressed in an equilibrium reaction constant. Common examples of these coupled reactions are acid-base equilibria, redox equilibria, and complexation of ions. It is shown that the thermodynamical quantities of these coupled reaction equilibria are significantly different from the original theory by Linse and Björling.

Another topic covered in chapter 2 is the electrostatic description of segments with different dielectric constants. A derivation of the segment potential starting from the free energy is given. It is shown how the equations for thermodynamical quantities are affected when segments may have a different permittivity.

In chapter 3 the SCF theory is used to analyse the influence of adsorbing homopolymers on the bending moduli of surfactant membranes. In this chapter, an impenetrable surface is used as a model for the membrane. In agreement with earlier findings of Brooks et al. [52] and Clement and Joanny [17] it is found that adsorbing polymers *decrease* the rigidity k_c of the interface when the deformation of the interface so slow that the polymers at the interface are in equilibrium with the bulk solution. Homopolymer adsorption and, especially, polymer desorption is known to be a relatively slow process. When the deformation of the interface is so fast that there is no time for the polymer to enter or leave the surface, then the influence of the adsorbing polymers on the bending rigidity is less negative or may be even positive. There is no difference in the influence on the Tolman length k_cJ_0/γ_0 and saddle-splay modulus $\bar{k}$ between reversibly and irreversibly adsorbed polymers. This latter point is proven from thermodynamical arguments, without assuming any molecular model.

In the numerical SCF theory, two adsorption mechanisms are considered. The first one is called 'adsorption on sites'. Here the adsorption energy *per segment* is constant upon bending. The second one is adsorption through contact interactions, where the adsorption energy per segment is constant *per unit accessible area*; then the adsorption energy per segment changes upon curving the interface. Both adsorption mechanisms give qualitatively different results: the sign of the polymer contribution to the bending constants may depend on the molecular detail of the adsorption interaction. The numerical results are compared to an existing analytical mean-field theory by Clement and Joanny, based on a ground-state approximation, and qualitative agreement is found for the case of adsorption through contact interactions.

In chapter 4 the bending moduli for vesicles with a homopolymer layer adsorbed onto the head groups of the surfactants are calculated. Now the membrane is not modelled as a mathematical surface but molecular detail, which may be affected by adsorbing polymer, is taken into account.In our calculations the self-assembly of $C_{12}E_5$ and $C_{12}A_nC_{12}$ surfactants into vesicles is explicitly considered. When adsorbing polymers are introduced the bending moduli of the membranes change. The magnitude and the sign of the change in bending moduli is shown to depend on the size of the head groups. As the head-group increases in size, the polymer contribution Δk_c to the bending rigidity increases. The increment $\Delta \bar{k}$ of the saddle-splay modulus is shown to have a maximum as a function of the size of the head groups and becomes negative for large head groups. The bending moduli of adsorbed polymer layers onto a solid surface containing short hairs are used as a model for a fully inert membrane (where the packing of the head groups is not affected). The results for Δk_c largely follow the same trends as for polymers adsorbing onto vesicles. In contrast, the maximum in $\Delta \bar{k}$ cannot be reproduced: as the hairs become longer $\Delta \bar{k}$ continues to increase.

From chapters 3 and 4 it can be concluded that the contribution of adsorbing polymers to the bending moduli depend largely on the molecular details of the interactions. It would be useful to predict the influence of these molecular details without performing the actual numerical calculations. It is known that mean-field theory has its deficiencies for describing the adsorption of polymers. Chapters 3 and 4 show that the influence of adsorbing polymers on the bending moduli of interfaces depend to a large extend on details. It can therefore be questioned to what extent our calculations are valid. However, we feel that it is safe to conclude that using a solid wall as a model for membrane interfaces is clearly inappropriate when one wants to know the influence of adsorbing polymers on the bending moduli of these membranes.

Chapter 5 describes an efficient computational scheme to evaluate the volume fractions of polydisperse block copolymers in a grand canonical ensemble. For polydisperse homopolymers, Roefs et al. [18] divised such a scheme, but this is not applicable to block copolymers. Traditionally, polydisperse block copolymers had to be described as a mixture of all the different block length compositions, where the volume fraction is computed separately for each block length composition of the chains. This chapter presents a method that computes the total volume fraction profile of polydisperse block copolymers more efficiently, while the results remain exactly the same. The computational time for a polydisperse block copolymer is only twice that of a homodisperse block copolymer. The application of the scheme has two restrictions. Firstly, the length distributions of different blocks within the polymer should be uncorrelated. While this may not be mathematically strict for experimental systems, this approximation is commonly used. Secondly, the polymers have to be in equilibrium with an infinitely large bulk phase. This poses a more serious restriction on the applicability of our computational scheme.

In chapter 6 an attempt is made to incorporate intramolecular excluded volume within the SCF theory, retaining the mean-field level of the description. It is similar to the technique introduced by Edwards [7], where a chain is end-grafted onto the centre of a spherical coordinate system. Instead of end-grafting the polymer, the polymer is grafted with a random segment. Due to the accumulation of mass near the centre, the polymer will swell in good solvent conditions and collapse in a bad solvent. The theory gives predictions for the properties of a single chain in solution which are in good agreement with known mean-field and scaling results. The Flory swelling exponent is recovered for arbitrary dimensionality of space, both in a good and theta solvent.

Satisfactory agreement with known results is obtained for a solution with a finite concentration of chains. For semi-dilute polymer solutions, the theory breaks down, much like Edwards theory. The polymers surrounding the central chain screen the intramolecular excluded volume of the central chain. The interpenetrated part of the chain does not swell anymore. Upon increasing the volume fraction of surrounding polymers even further, the bulk solution shows relatively small oscillations in the density profile, which are analysed in detail. Rather surprisingly, the dominant length scale in these oscillations is the chain length.

In the standard SCF theory the intramolecular excluded volume for chains in the bulk is neglected. For homopolymers in good solution this results is a systematic overestimation of the entropy of the bulk chains. This leads a systematic underestimation of the adsorbed amount for homopolymer adsorption. When we equate the chemical potential of a chain with excluded volume in solution to the chemical potential of adsorbed chains, we find indeed a slight increase in the adsorbed amount. Furthermore, we analyse the density profile of the adsorbed polymers. It is found that in the central region of the adsorbed layer, the volume fraction profile follows more or less a power-law: $\varphi \sim z^{\alpha}$. For standard SCF theory α is known to approach the limiting value of -2 from below for infinitely long chains and infinitely dilute solutions. Here, we find a value that is notably higher than -2; it seems to be consistent with the value found from a scaling analysis: $\alpha = -4/3$. However, if we match the chemical potentials of the adsorbed and bulk chains we see that for relatively high concentrations the volume fraction profiles become unrealistic. This is probably due to the fact that the chains at the surface need to be treated individually instead of as a laterally smeared out layer to be consistent with the bulk calculation.

It is expected that this theory may be generalised to study more complex systems as copolymer and polyelectrolyte adsorption, where the neglect of intramolecular excluded volume in the bulk phase of in the standard SCF theory may have more serious consequences.

In appendix A two numerical procedures are described that solve common problems in the numerical evaluation of Green functions. Their discrete version is used in the SCF theory to evaluate the volume fractions. The first procedure prevents over- and underflows. The main principle of the method is to rewrite the equations that compute the volume fraction distribution of the polymers in a logarithmic form. The second procedure deals with extremely long chains. Both the memory consumption and the CPU time needed to compute the volume fractions of a polymer chain from a given potential field normally scale as MN, where M is the number of space coordinates and N is the chain length. We present an algorithm for which the memory consumption scales as $MN^{1/3}$ while the CPU time increases by at most a factor of two.

In appendix B the discretisation of space within the SCF theory is considered. The discrete space co-ordinates are often called a lattice. Different geometries are discussed that can be used to discretise the equations. The different boundary conditions and their implementation is reviewed. The frequently used geometrical packing view of the lattice is critically examined. The discretisation of equations may lead problems. Firstly, the discretisation of derivatives can be done in a number of different ways. It is shown how physical arguments may favor one way over the other. Secondly, a discretisation artefact may arise when the width of the interface is of the order of the lattice spacing. An overview of the methods that have been used in the past to correct for this type of artefact is given and a new method to eliminate it is proposed. The central idea is to shift the lattice with respect to the interface at fixed molecular composition and system volume until the free energy is minimised. Furthermore, it is shown how the results of calculations with different lattice constants can be compared and how experimental data should be translated to parameters common in the lattice theory. Finally, a Stern layer concept is used to show how a lattice theory may lead to more realistic results than a continuum model without such a Stern layer.

In appendix C the numerical method for solving the system of SCF equations as described in this thesis is explained. The method is based on a quasi-Newton algorithm for which a short general mathematical description is given. The implementation details of the method used at our laboratory are described. Where possible a justification for the details is given. Some tricks, mostly resulting from empirical findings during this research, are described that ensure convergence of the equations or speed up convergence by one or two orders of magnitude. We conclude by giving some ideas for improvements of the method.

Samenvatting

Vloeistoffen, gassen en vaste stoffen bestaan uit moleculen. Op hun beurt bestaan moleculen weer uit atomen. In de natuur komen zo'n 90 verschillende atomen voor. Atomen kunnen onderling aan elkaar verbonden zijn en zo een enorme hoeveelheid verschillende moleculen vormen. In de scheikunde worden de veranderingen van onderlinge bindingen tussen atomen bestudeerd. Er zijn miljoenen verschillende moleculen bekend. De chemische reacties die moleculen vormen blijven in dit proefschrift onbesproken. In plaats daarvan wordt het gedrag van moleculen beschreven.

Dit proefschrift gaat over ketenmoleculen, ook wel polymeren genoemd. Er bestaan industriële polymeren (bijv. plastics) en biopolymeren zoals zetmeel en eiwit. Een polymeermolecuul is een grote aaneenschakeling van atomen tot een lange keten, zoals in een kralenketting. De kralen in de ketting worden monomeren genoemd. Eventueel kunnen deze ketens vertakt zijn, maar vertakte ketens blijven hier onbesproken. De ketenmoleculen in dit proefschrift bevinden zich steeds in een vloeistof. Zoals suiker oplosbaar is in water, zo kunnen ook verschillende polymeren opgelost worden in water of andere vloeistoffen.

Het gedrag van polymeren in oplossing laat zich vaak voorspellen uit relatief eenvoudige eigenschappen als ketenlengte, oplosbaarheid en concentratie. Het is dan niet noodzakelijk om het detail-gedrag van alle monomeren afzonderlijk te betrekken in de analyse. Dit maakt polymeren tot een dankbaar studie-object. Met relatief eenvoudige theorie kunnen behoorlijk nauwkeurige voorspellingen gedaan worden over het gedrag van polymeren. Zo kunnen twee polymeren die alleen verschillen in het type monomeer waaruit ze bestaan toch min of meer hetzelfde gedrag vertonen. Dit in tegenstelling tot kleine moleculen, waar de moleculaire details veelal belangrijk zijn.

Dit proefschrift gaat over een theorie die geschikt is om het gedrag van ketenmoleculen in vloeistoffen en nabij grensvlakken te beschrijven. Met een grensvlak wordt hier de overgang tussen twee verschillende fasen bedoeld. In een glas water is de overgang van een glaswand naar het water een grensvlak, maar ook de overgang van water naar lucht is een grensvlak. Dit zijn twee voorbeelden van oppervlakken die zo groot zijn dat ze met het blote oog zichtbaar zijn. De grensvlakken kunnen ook veel kleiner zijn. Pigmentdeeltjes in verf bijvoorbeeld zijn zeer kleine korreltjes, mayonaise bestaat uit zeer kleine druppeltjes olie in water.

Deze grensvlakken hebben verschillende eigenschappen die in dit proefschrift aan bod komen. Polymeren kunnen zich bijvoorbeeld ophopen in zo'n grensvlak, we spreken dan van adsorptie. Dit kan bijvoorbeeld als een glaswand de polymeren aantrekt. Met de theorie uit dit proefschrift kan voorspeld worden hoeveel polymeer er zich ophoopt in het grensvlak en hoe die polymeren zich in dit grensvlak gedragen.

Vloeibare grensvlakken kunnen ook vervormen, de vraag is dan hoe makkelijk dit gaat. Het bekendste voorbeeld van een dergelijke vervorming is het groter maken van het grensvlak, zoals bij het blazen van bellen. Een ander soort vervorming is het buigen van een grensvlak.

De theorie die in dit proefschrift gebruikt wordt om bovenstaande eigenschappen van grensvlakken te beschrijven komt voort uit de thermodynamica. De thermodynamica dateert uit de 19de eeuw en geeft twee algemene wetmatigheden waar alle processen die tot nu toe zijn bestudeerd zich aan houden. De eerste wet stelt dat in een gesloten systeem energie altijd behouden blijft. De tweede wet stelt dat bij een gegeven energie een proces alleen spontaan verloopt als daarbij de totale wanorde (entropie) toeneemt. Deze wetmatigheden zijn eerst geformuleerd zonder dat daarbij het bestaan van moleculen werd aangenomen. Later zijn deze wetmatigheden beschreven in wiskundige vergelijkingen die het gedrag van moleculen beschrijven. Het zijn deze wiskundige vergelijkingen die als uitgangspunt dienen voor dit proefschrift.

Een exacte thermodynamische beschrijving van polymeren in oplossing en nabij grensvlakken kan niet zonder meer gemaakt worden: de resulterende wiskundige vergelijkingen zijn te ingewikkeld om direct op te lossen. Er bestaan verschillende methoden om de vergelijkingen te vereenvoudigen zodat ze wel op te lossen zijn. In dit proefschrift wordt gebruik gemaakt van de gemiddeld-veld benadering die in de tweede helft van de 20e eeuw is ontwikkeld voor polymeren. In deze benadering wordt het gedrag van een molecuul niet gedicteerd door alle andere moleculen afzonderlijk, maar door een gemiddelde van die andere moleculen. Deze benadering heeft tot gevolg dat bepaalde eigenschappen van moleculen niet precies of in sommige gevallen volkomen verkeerd worden beschreven. Door de jaren heen is echter gebleken dat deze benadering goed voldoet voor het beschrijven van vele eigenschappen van polymeren in oplossing en nabij grensvlakken.

Zoals in de verschillende hoofdstukken is te zien, bestaat de beschreven theorie uit nogal wat vergelijkingen. Deze vergelijkingen kunnen niet handmatig (analytisch) worden opgelost zodat de hulp van een computer nodig is. Daarom is tijdens dit onderzoek een computerprogramma geschreven waarmee de resultaten zijn berekend. Dit programma is algemeen van opzet zodat een grote verscheidenheid van problemen kan worden doorgerekend die lang niet allemaal in dit proefschrift aan bod komen.

De theorie uit dit proefschrift kan meestal niet direct in de praktijk worden ingezet. Dit komt omdat de meeste toepassingen van polymeren bestaan uit complexe mengsels van vele ingrediënten. Polymeren vinden bijvoorbeeld toepassingen in levensmiddelen, in verf en in pesticiden. Deze mengsels bestaan echter niet uit polymeren alleen. Alle ingrediënten oefenen invloed op elkaar uit. Om wat orde in deze chaos te scheppen houdt de fysische chemie zich bezig met de fundamentele eigenschappen van de ingrediënten. Hiertoe worden experimenten gedaan met sterk vereenvoudigde mengsels van moleculen. De theorie uit dit proefschrift kan gebruikt worden om een beter inzicht te verkrijgen in de resultaten van een deel van deze experimenten. Voorbeelden zijn de adsorptie van humuszuren aan kleideeltjes, de zelf-associatie van biologische membranen, of de stabiliserende werking van polymeren op pigmentdeeltjes in verf.

In hoofdstuk 2 wordt een overzicht gegeven van de gemiddeld-veld theorie zoals die in dit proefschrift wordt gebruikt. Getracht is om de statistisch thermodynamische afleiding van de bestaande theorie zo volledig mogelijk weer te geven. Verder wordt de bestaande theorie uitgebreid op twee onderdelen. De eerste uitbreiding betreft het beschrijven van evenwichtsreacties. Zuren en basen in oplossing laten zich bijvoorbeeld beschrijven met evenwichtsreacties. De meest bekende zuren en basen zijn kleine moleculen. Polymeren kunnen ook zure en basische eigenschappen bezitten. De theorie zoals die in hoofdstuk 2 wordt beschreven maakt het mogelijk om deze eigenschappen te bestuderen. De theorie in hoofdstuk 2 is zo opgezet dat iedere reactie die de ketens intact laat in principe kan worden beschreven.

Reacties van zuren en basen maken de polymeren in meer of mindere mate electrisch geladen. Dit brengt ons bij de tweede uitbreiding die op de theorie wordt gemaakt. Gelijke ladingen stoten elkaar af. Die afstoting is echter minder sterk in water dan in lucht. De precieze mate van afstoting hangt op een tamelijk complexe manier af van de hoeveelheden en de typen van de moleculen in de buurt van de ladingen. Wederom wordt hier een benadering toegepast: de precieze mate van afstoting wordt benaderd door een gemiddelde van de afzonderlijke moleculen. De mate van afstoting tussen twee ladingen laat zich goed beschrijven door een eigenschap die de relatieve diëlectrische permittiviteit heet. Dit is een eigenschap die gemeten kan worden. Hoe groter de relatieve diëlectrische permittiviteit, hoe kleiner de afstoting tussen de moleculen. De systemen waarin we geïnteresseerd zijn hebben echter geen constante diëlectrische permittiviteit: deze is op elke plaats in de ruimte verschillend. Dit heeft invloed op de precieze formulering van de thermodynamische grootheden. De vergelijkingen die nodig zijn om de thermodynamische grootheden uit te rekenen worden afgeleid in hoofdstuk 2.

Hoofstuk 3 gaat over het buigen van een geadsorbeerde polymeerlaag. Polymeren in oplossing kunnen adsorberen aan bijvoorbeeld een metalen plaatje. Dit gebeurt als de monomeren voldoende sterk worden aangetrokken door zo'n plaatje. Er ontstaat dan een ophoping (adsorptie) van polymeren. Als we een metalen plaatje buigen kost dit een bepaalde arbeid. Als polymeren adsorberen op een ultradun plaatje is het voorstelbaar dat die arbeid niet meer hetzelfde is. In hoofdstuk 3 wordt de verandering in de benodigde arbeid uitgerekend. Er wordt aangetoond dat het moleculaire mechanisme waarmee de polymeren adsorberen van grote invloed is op de verandering in de arbeid die nodig is om het plaatje te buigen. In het ene geval wordt die benodigde arbeid kleiner, in een ander geval juist groter.

Het maakt verschil of de polymeren aan een kant of juist aan beide kanten van het plaatje adsorberen. Verder kan een plaatje verbogen worden in twee richtingen die loodrecht op elkaar staan. Deze aspecten worden beschreven met de Helfrich vergelijking. Deze vergelijking heeft drie parameters die de buigingsarbeid kwantificeren. Deze parameters worden de Tolman-lengte $k_c J_0/\gamma_0$, de buigingselasticiteit k_c en de zadelvlakmodulus $\bar{k}$ genoemd.

Als het plaatje oneindig langzaam wordt vervormd dan krijgen de polymeren op het oppervlak de gelegenheid om steeds de meest gunstige posities in de ruimte in te nemen, bijvoorbeeld door van het plaatje naar de oplossing te gaan. Een andere limiet is een zodanig snelle vervorming van het plaatje dat geen enkel polymeermolecuul van het oppervlak kan vertrekken of er bij kan komen. Meer wetenschappelijke benamingen voor beide extremen zijn respectievelijk reversibele en irreversibele adsorptie. Er wordt aangetoond dat beide extremen dezelfde waarden opleveren voor de Tolman-lengte en de zadelvlakmodulus. Verder is de buigingselasticiteit altijd hoger voor een irreversibel geadsorbeerde laag dan voor een reversibel geadsorbeerde laag. Voor deze uitkomsten van de theorie wordt een thermodynamische verklaring gegeven die onafhankelijk is van de numerieke theorie.

Het moleculaire mechanisme van de aantrekking van het polymeer door het oppervlak speelt ook een rol in de benodigde krommingsarbeid. Twee verschillende interacties worden beschouwd. Ten eerste adsorptie op specifieke plekjes van het oppervlak, bijvoorbeeld door de vorming van waterstofbruggen. De aantrekking tussen de monomeren en het oppervlak hangt dan niet af van de kromming. Ten tweede wordt de situatie berekend waarbij de aantrekking van de monomeren juist wel afhangt van de kromming, zoals bij Van der Waals-krachten. Beide adsorptiemechanismen leiden tot zeer verschillende resultaten. De tekens van de bijdragen die de polymeerlaag heeft aan de verschillende buigingsparameters kunnen van deze moleculaire interacties afhangen. Dat betekent dat de buigingsarbeid als gevolg van adsorberende polymeren toe of af kan nemen. De uitkomst hangt af van het adsorptiemechanisme.

Het vervormen van het vlakke, vaste oppervlak in hoofdstuk 3 is een tamelijk academisch probleem: de elasticiteit van een plaatje is zo hoog dat de invloed van polymeer daarop te verwaarlozen is. Dit vlakke plaatje wordt daarom gebruikt als een model voor een vloeibaar oppervlak dat oneindig dun is. Vloeibare oppervlakken hebben echter een meetbare dikte. In het oppervlak tussen water en olie treedt een geleidelijke overgang van de waterfase naar de oliefase op: in het grensvlak mengen de vloeistoffen. Een vloeibaar oppervlak is over het algemeen veel minder stijf dan een vast plaatje. Adsorberende polymeren kunnen dan wel belangrijke invloed hebben op de krommingsarbeid. Een voorbeeld van zo'n vloeibaar oppervlak is een celmembraan, dat bestaat uit vele losse moleculen die elke levende cel omgeven. Zo'n celmembraan bestaat uit een mengsel van relatief ingewikkelde moleculen. Om de analyse eenvoudig te houden is gerekend aan een membraan dat bestaat uit slechts één type moleculen. Ook dit molecuul wordt beschreven als een ketenmolecuul. Het bestaat uit een deel dat goed oplost in water en een deel dat juist slecht oplost. Deze slecht oplosbare delen gaan bij elkaar zitten en vormen een vlak membraan, waarbij de goed oplosbare delen in het water uitsteken. Zoals bij olie en water zijn de grensvlakken van deze membranen enigszins diffuus. In hoofdstuk 4 wordt de invloed uitgerekend van polymeren die aan de buitenkant adsorberen van dit modelmembraan. Er wordt aangetoond dat de buigingsparameters van de membranen inderdaad veranderen als daar polymeren op adsorberen. Deze veranderingen in de buigingsparameters hangen sterk af van de mate waarin de membraanoppervlakken diffuus zijn. Zoals verwacht zijn de bijdragen van de polymeerlaag voor zeer dunne grensvlakken ongeveer gelijk aan de bijdragen die gevonden zijn voor een vlakke wand. Voor meer diffuse grensvlakken veranderen die bijdragen van teken.

Polymeren zijn meestal niet allemaal even lang. Sterker nog, het is erg lastig om polymeren te maken die allemaal dezelfde lengte hebben. Blokcopolymeren bestaan uit blokken van identieke monomeren. Een voorbeeld van een blok copolymeer is $A_{100}B_{100}$: 100 monomeren A gevolgd door 100 monomeren B. Als nu de lengte van het A-blok in werkelijkheid variëert tussen 91 en 110 dan hebben we al 20 verschillende lengtes van A-blokken. Als hetzelfde geldt voor het B-blok dan resulteert een mengsel van $20 \times 20 = 400$ verschillende ketenmoleculen. Als we nu nog een C blok hieraan vastzetten dan wordt de hoeveelheid verschillende blokcopolymeren nog veel groter.

De theorie zoals die in hoofdstuk 2 is beschreven is prima in staat om een mengsel van moleculen met een verschillende lengte door te rekenen. De benodigde rekentijd is echter evenredig met het aantal verschillende lengtes. In hoofdstuk 5 wordt een truc beschreven om mengsels van verschillende blok copolymeren efficiënt uit te rekenen. Met deze truc is de benodigde rekentijd slechts marginaal hoger dan de rekentijd voor een oplossing met één component, terwijl de uitkomsten van de berekening precies identiek blijven. Deze truc kent twee beperkingen. De blokken moeten willekeurig aan elkaar verbonden zijn. Het mag dus bijvoorbeeld niet zo zijn dat kleine A-blokken vaker aan korte B-blokken dan aan lange B-blokken vast zitten. Deze benadering kan in de praktijk vaak gemaakt worden. De tweede beperking is dat het systeem in evenwicht moet zijn met een oneindig groot reservoir van moleculen. Als de polymeren bijvoorbeeld op een oppervlak adsorberen dan moet de omringende oplossing erg groot zijn. Dit is een wat serieuzere beperking.

De theorie uit de voorgaande hoofdstukken kent een aantal beperkingen die voortkomen uit de benaderingen die gemaakt zijn. Een tamelijk drastische benadering is dat de ketens beschreven worden als een zogenaamde 'random walk': een dronkemanswandeling. Dit wil zeggen dat twee (of meer) monomeren van dezelfde keten dezelfde positie in de ruimte kunnen innemen. Dit is uiteraard niet juist. Toch is deze benadering erg populair onder theoretici omdat de berekeningen er veel eenvoudiger door worden. Binnen de gemiddeld-veld benadering wordt alleen gekeken naar de totale hoeveelheid materiaal op een bepaalde positie in de ruimte. De totale hoeveelheid moleculen in een deel van de ruimte is aan een maximum gebonden. Simpel gezegd: vol is vol. De wetenschappelijke benaming van dit principe is uitgesloten volume. Het volume dat een gegeven molecuul inneemt is uitgesloten voor de andere moleculen.

Voor polymeren in oplossing kan het uitgesloten volume onderverdeeld worden in twee bijdragen. Zo zijn de ketens in een verdunde oplossing te ver van elkaar verwijderd om elkaar sterk te 'voelen'. Wetenschappelijker gezegd: het *inter*moleculair uitgesloten volume is dan verwaarloosbaar. De monomeren van een gegeven keten concurreren wel met elkaar om een plaatsje in de ruimte en voelen elkaar dus wel sterk, ze zitten immers aan elkaar vast en kunnen elkaar daarom niet ontlopen. Anders gezegd: het *intra*moleculair uitgesloten volume is juist wel belangrijk in een verdunde oplossing.

In de voorgaande hoofdstukken werd het inter- en intramoleculair uitgesloten volume op één hoop gegooid. In hoofdstuk 6 wordt een scheiding aangebracht in het inter- en intramoleculair uitgesloten volume. Het effect van het intramoleculair uitgesloten volume wordt op een eenvoudige manier benaderd en uit een vergelijking met bestaande, meer exacte, theorie kan geconcludeerd worden dat deze benadering zeer goed voldoet voor geïsoleerde ketens in oplossing. Als de concentratie polymeren wordt opgevoerd vertoont de benadering kleine gebreken. Tenslotte wordt het effect van het intramoleculair volume op de adsorptie van polymeren bekeken. Aangetoond wordt dat de totale hoeveelheid geadsorbeerd polymeer groter wordt, zoals ook verwacht werd. De toename is echter gering. Uit andere, meer exacte, theoretische overwegingen is bekend dat de geadsorbeerde hoeveelheid nog groter zou moeten zijn. Nadere inspectie van de geadsorbeerde laag brengt andere onvolkomenheden naar voren zodat verder onderzoek nodig is om deze binnen de zelf-consistente veldtheorie te verhelpen.

Appendix A beschrijft twee speciale rekenschema's voor ketenmoleculen die de (altijd aanwezige) grenzen aan de capaciteit van computers weet te omzeilen. Het eerste schema is speciaal geschikt voor zeer lange ketens. In het standaardrekenschema is het benodigde computergeheugen voor ketens is evenredig met de lengte van die ketens. Het schema dat hier wordt beschreven reduceert dit tot een evenredigheid met de derde-machtswortel uit de ketenlengte. Dit maakt het mogelijk om ook eigenschappen van ketens die bestaan uit meer dan 100000 monomeren uit te rekenen. Het tweede schema is speciaal voor ketens die sterke interacties met hun omgeving hebben. De getallen waar een computer standaard mee overweg kan zijn aan grenzen gebonden. Getallen kleiner dan 10^{-300} of groter dan 10^{300} zijn vaak niet door een computer te verwerken. De tussenuitkomsten die gegenereerd worden in het standaardrekenschema kunnen echter vele malen kleiner of groter zijn dan deze grenzen, in het bijzonder als de interacties tussen de moleculen erg sterk zijn. Dit komt regelmatig voor als de polymeren geladen zijn. Door het rekenschema te herschrijven in een logaritmische vorm kunnen ook deze systemen succesvol worden doorgerekend.

Appendix B behandelt het opdelen van de ruimte in de theorie. Om de berekeningen met de theorie mogelijk te maken moet de ruimte opgedeeld worden in een soort hokjes. De moleculen bevinden zich dan alleen op vaste posities in de ruimte. In werkelijkheid zijn moleculen vrij om ook alle ruimte tussen die vaste posities in te nemen. Dit is te vergelijken met het verschil tussen gehele getallen en breuken, waarbij breuken de waarden weergeven tussen de gehele getallen. Slordig gezegd maken we bij het doorrekenen van de theorie alleen gebruik van de gehele getallen, terwijl breuken ook mogelijk zijn. Het opdelen van de ruimte in vaste posities is een benadering van de werkelijkheid. Wetenschappelijk wordt gezegd dat de ruimte wordt gediscretiseerd. Deze benadering leidt tot verschillende complicaties en misvattingen. Deze technische details worden uitgebreid behandeld in appendix B. De discretisering van de ruimte kan leiden tot foute uitkomsten (artefacten genoemd) van de berekeningen. Deze artefacten zijn in veel gevallen niet belangrijk. De artefacten worden wel merkbaar in de berekeningen van de krommingsarbeid in hoofdstuk 4. Deze berekeningen kunnen zo ernstig verstoord worden door de discretisatie dat er geen zinnige uitspraak meer gedaan kan worden over de krommingsarbeid. Dit wordt verholpen door een nieuwe truc waarbij de discretisatie op een zodanige manier aangepast wordt dat de uitkomsten van de berekeningen wel betrouwbaar worden.

De vergelijkingen die uit de theorie volgen moeten numeriek worden opgelost. Om een idee te geven: we zijn geïnteresseerd in het oplossen van bijvoorbeeld 1000 vergelijkingen met 1000 variabelen. We willen de waarden weten van die 1000 variabelen die zorgen dat de uitkomst van alle 1000 vergelijkingen gelijk wordt aan nul. Dergelijke problemen komen in meerdere vakgebieden voor, hetgeen geleid heeft tot het ontstaan van een apart onderdeel binnen de numerieke wiskunde waarin geprobeerd wordt om deze vergelijkingen zo efficiënt mogelijk op te lossen. Veelal is het voldoende om de variabelen te kennen in twee of drie decimalen nauwkeurig maar voor de toepassingen in dit proefschrift is het regelmatig nodig om de variabelen kennen met een nauwkeurigheid van bijvoorbeeld zeven of twaalf cijfers. Het rekenschema dat gebruikt is om dit probleem op te lossen wordt beschreven in appendix C. Verder worden daar een aantal trucs behandeld die het mogelijk maken om bepaalde ingewikkelde problemen toch tot een oplossing te brengen, of om dit vele malen sneller dan gebruikelijk te doen.

Publications

- G. J. Fleer, J. van Male, and A. Johner, Analytical approximations to the Scheutjens-Fleer theory for polymer adsorption from dilute solution. 1. Trains, loops, and tails in terms of two parameters: the proximal and distal lengths. *Macromolecules*, **32**, 825–844, 1999.

- G. J. Fleer, J. van Male, and A. Johner, Analytical approximations to the Scheutjens-Fleer theory for polymer adsorption from dilute solution. 2. Adsorbed amounts and structure of the adsorbed layer. *Macromolecules*, **32**, 845–862, 1999.

- S. M. Oversteegen, P. A. Barneveld, J. van Male, F. A. M. Leermakers, and J. Lyklema, Thermodynamic derivation of mechanical expressions for interfacial parameters. *Phys. Chem. Chem. Phys.*, **1**, 4987–4994, 1999.

- A. M. Skvortsov, L. I. Klushin, J. van Male, and F. A. M. Leermakers. The rolling transition of a Gaussian chain end-grafted at a penetrable surface. *J. Chem. Phys.*, **112**, 7238 - 7246, 2000.

- J. van der Gucht, N. A. M. Besseling, J. van Male, and M. A. Cohen Stuart. Coil size oscillatory packing in polymer solutions near a surface. *J. Chem. Phys.*, **113**, 2886–2893, 2000.

- F. A. M. Leermakers, E. B. Zhulina, J. van Male, A. A. Mercurieva, G. J. Fleer, and T. M. Birshtein. Wetting of a polymer brush, a system with pronounced critical wetting. *Langmuir*, **16**, 7082–7087, 2001.

- A. M. Skvortsov, J. van Male, and F. A. M. Leermakers. Exactly solvable model with a first-order phase transition: The rolling transition of a pinned Gaussian chain. *Physica A*, **290**, 445 – 452, 2001.

- E. B. Zhulina, O. V. Borisov, J. van Male, and F. A. M. Leermakers. Adsorption of tethered polyelectrolytes onto oppositely charged solid-liquid interfaces. *Langmuir*, **17**, 1277–1293, 2001.

- A. A. Gorbunov, A. M. Skvortsov, J. van Male, and G. J. Fleer. Mapping of continuum and lattice models for describing the adsorption of an ideal chain anchored to a planar surface. *J. Chem. Phys.*, **114**, 5366–5375, 2001.

- A. M. Skvortsov, L. I. Klushin, J. van Male, and F. A. M. Leermakers. First-order coil-to-flower transition of a polymer chain pinned near a stepwise external potential: Numerical, analytical, and scaling analysis. *J. Chem. Phys.*, **115**, 1586 – 1595, 2001.
- F. A. M. Leermakers, E. B. Zhulina, J. van Male, A. A. Mercurieva, G. J. Fleer, and T. M. Birshtein. Effect of a polymer brush on capillary condensation. *Langmuir*, **17**, 4459–4466, 2001.
- F. A. M. Leermakers, J. van Male, and A. M. Skvortsov. Coil-to-flower transition of a polymer chain pinned near a stepwise external potential: Finite size effects. *J. Chem. Phys.*, **115**, 8294 – 8302, 2001.
- A. A. Mercurieva, T. M. Birshtein, E. B. Zhulina, P. Iakovlev, J. van Male, and F. A. M. Leermakers. An annealed polyelectrolyte brush in a polar-nonpolar binary solvent: Effect of pH and ionic strength. *Macromolecules*, **35**, 4739 – 4752, 2002.
- J. Klein Wolterink, J. van Male, M. A. Cohen Stuart, L. K. Koopal, E. B. Zhulina, and O. V. Borisov. Annealed Star-Branched Polyelectrolytes in Solution. *Macromolecules*, **35**, 9176–9190, 2002.
- J. van Male, F. A. M. Leermakers, and G. J. Fleer Computation of chain propagators in inhomogeneous systems: over- and underflow protection and reducing computer memory requirements. *Comp. Pol. Sci.*, accepted for publication, 2001.

Levensloop

Jan van Male werd op 25 november 1972 geboren in Knokke-Heist, België. In 1991 behaalde hij het VWO diploma aan scholengemeenschap "Het Zwin" te Oostburg. In 1995 voltooide hij met lof de studie Moleculaire Wetenschappen aan de Landbouwuniversiteit Wageningen. Zijn afstudeervak Fysische Chemie werd bekroond met de C.T. de Wit scriptieprijs en de Unilever research prijs. Van juni 1995 tot juni 1999 was hij in dienst van het NWO als Onderzoeker In Opleiding, gedetacheerd bij de vakgroep Fysische en Kolloïdchemie van de Landbouwuniversiteit Wageningen. Hieruit is dit proefschrift voortgekomen. Vanaf 1 november 2001 is hij werkzaam als postdoc aan de Universiteit Leiden bij de werkgroep Soft Condensed Matter.

Dankwoord

Het boekje is eindelijk af! Graag maak hier ik van de gelegenheid gebruik om een aantal mensen te bedanken voor hun bijdrage. Mijn directe begeleider Frans Leermakers heeft zonder twijfel de grootste inhoudelijke bijdrage geleverd. Zijn deur stond letterlijk altijd open voor allerlei discussies. De hoeveelheid ideeën die Frans weet te spuien is werkelijk enorm, het enthousiasme waarmee dit gebeurt is zo mogelijk nog groter. Regelmatig vergaten we ieder besef van tijd terwijl de plannen steeds woester werden. Frans, hartelijk bedankt voor een fijne periode.

Verder dank ik m'n promotor Gerard Fleer die altijd veel vertrouwen in me gehad heeft, ook op momenten waar daar wat minder reden toe was. Tijdens het werken aan de eerste gezamelijke artikelen maakte ik kennis met zijn enorme werktempo. Ik kan me nog goed herinneren dat hij eens binnen stapte met de vraag of ik een paar numerieke berekeningetjes kon doen. Binnen de korste keren lagen er twee grote manuscripten. Ook mijn hoofdstukken werden in hoog tempo en zeer zorgvuldig becommentariëerd. Zijn kritische opmerkingen hebben de kwaliteit van dit proefschrift duidelijk verbeterd.

De 'multi-state' theorie die in hoofdstuk 2 staat beschreven kwam voort uit kritiek van Edwin Currie op de implementatie van de theorie tot dan toe. Dat zou ik wel even opknappen: mooi niet dus. Het resulteerde in een project van twee jaar. Het werk aan gekromde oppervlakken zoals dat beschreven wordt in hoofdstukken 3 en 4 komt voort uit een samenwerking met Martijn Oversteegen in wiens proefschrift de fundamenten voor dit werk werden gelegd. Discussies met Edgar Blokhuis hebben ook bijgedragen aan mijn kennis over het krommen van oppervlakken.

Jos van den Oever leerde ik als m'n afstudeerstudent kennen. Zijn afstudeerwerk sluit aan op hoofstuk 6 maar staat tot mijn spijt niet in dit proefschrift. Tijdens zijn afstudeervak leerde ik mede door hem een aantal essentiële concepten van de programmeertaal C++. Deze concepten maakten het eenvoudiger om het handvol losse computer programmaatjes waar ik tot dan toe mee werkte samen te bundelen in een groter, algemener programma. Later kwam Jos in dienst als collega waar hij dit algemene programma op een aantal belangrijke punten wist uit te breiden. Verder zorgde hij voor een enorme sprong voorwaarts in de hoeveelheid lokaal beschikbare rekentijd door alle desktop PCs buiten werktijden in te zetten.

During my years at the lab many guests from abroad have visited for a short or longer period. I had the pleasure of sharing a room with Victor Pryamitsyn, whose views on polymer physics were inspiring. Johannes Lützenkirchen tested the initial implementation of the multi-state theory and found many limitations or bugs. Anna Mercurieva visited several times to do some numerical calculations and the observations she made with Frans Leermakers urged me to carefully re-examine the thermodynamical fundamentals of the multi-state theory. During several summers Alexei Gorbunov and Alexander Skvortsov visited, which has resulted in several joint papers and a lot of fun.

Peter Barneveld heeft me geholpen met mijn eerste schreden in C++ en UNIX. Daarnaast was het erg plezierig om met hem van gedachten te wisselen over allerlei aspecten van de theorie. Ook discussies met Klaas Besseling en Jasper van der Gucht hebben mijn inzicht vergroot. In de eindfase hebben de bordsessies met Hans Fraaije mijn ideeën verder aangescherpt.

Naast de wetenschap was er ook voldoende afleiding op het lab te vinden. De vele kamergenoten die ik in de loop der jaren gehad heb waren altijd wel in voor een praatje en als zij niet zo gesteld waren op sigaretten kon ik altijd bij Ben of Ab terecht. Regelmatig werd er op vrijdagavond stoom afgeblazen in de kroeg met de theoretici en enkele (verdwaalde?) experimentalisten. Verder denk ik met plezier terug aan de zeilweekenden. Wat me het meest zal bijblijven is de prettige sfeer op de vakgroep. Ik heb het hier al die tijd prima naar m'n zin gehad.

Ook buiten de vakgroep was aan afleiding geen gebrek. Regelmatig bracht ik een avond door in m'n stamkroeg Beneden waar ik vele zinnige en onzinnige gesprekken gevoerd heb met de 'Rijnsteeg-clan' waarvan ik met name Leo, Peter en Wim wil noemen. De 'mannuh van de FC' waren en zijn legendarisch. Tom, je wordt gemist.

Mijn ouders hebben me altijd aangemoedigd om te studeren. Het is voor een groot deel aan hen te danken dat dit proefschrift er nu ligt. Pa en ma, bedankt voor het vertrouwen en de steun die jullie me gegeven hebben.

De laatste woorden zijn uiteraard voor Joanne. Zij heeft alle ups en downs van de afgelopen periode van dichtbij meegemaakt, zelfs als collega! Joanne, bedankt voor vele fijne jaren, ik hoop dat er nog veel meer volgen.